

A CONCEPTUAL EVALUATION OF FREQUENCY DIVERSE ARRAYS AND  
NOVEL UTILIZATION OF LFMCW

A THESIS SUBMITTED TO  
THE GRADUATE SCHOOL OF NATURAL AND APPLIED SCIENCES  
OF  
MIDDLE EAST TECHNICAL UNIVERSITY

BY

TAYLAN EKER

IN PARTIAL FULFILLMENT OF THE REQUIREMENTS  
FOR  
THE DEGREE OF DOCTOR OF PHILOSOPHY  
IN  
ELECTRICAL AND ELECTRONICS ENGINEERING

SEPTEMBER 2011

Approval of the thesis:

**A CONCEPTUAL EVALUATION OF FREQUENCY DIVERSE ARRAYS  
AND NOVEL UTILIZATION OF LFM CW**

submitted by **TAYLAN EKER** in partial fulfillment of the requirements for the degree of **Doctor of Philosophy in Electrical and Electronics Engineering Department, Middle East Technical University** by,

Prof. Dr. Canan ÖZGEN \_\_\_\_\_  
Dean, Graduate School of **Natural and Applied Sciences**

Prof. Dr. İsmet ERKMEN \_\_\_\_\_  
Head of Department, **Electrical and Electronics Engineering**

Assoc. Prof. Dr. Şimşek DEMİR \_\_\_\_\_  
Supervisor, **Electrical and Electronics Engineering Dept., METU**

Prof. Dr. Altuncan HIZAL \_\_\_\_\_  
Co-Supervisor, **Electrical and Electronics Engineering Dept., METU**

**Examining Committee Members:**

Prof. Dr. Sencer KOÇ \_\_\_\_\_  
Electrical and Electronics Engineering Dept., METU

Assoc. Prof. Dr. Şimşek DEMİR \_\_\_\_\_  
Electrical and Electronics Engineering Dept., METU

Prof. Dr. Ayhan ALTINTAŞ \_\_\_\_\_  
Electrical and Electronics Engineering Dept., BİLKENT

Prof. Dr. Özlem Aydın ÇİVİ \_\_\_\_\_  
Electrical and Electronics Engineering Dept., METU

Assoc. Prof. Dr. Ali Özgür YILMAZ \_\_\_\_\_  
Electrical and Electronics Engineering Dept., METU

Date: 16.09.2011

**I hereby declare that all information in this document has been obtained and presented in accordance with academic rules and ethical conduct. I also declare that, as required by these rules and conduct, I have fully cited and referenced all material and results that are not original to this work.**

Name, Last name : Taylan EKER

Signature :

# ABSTRACT

## A CONCEPTUAL EVALUATION OF FREQUENCY DIVERSE ARRAYS AND NOVEL UTILIZATION OF LFMCW

EKER, Taylan

Ph.D., Department of Electrical and Electronics Engineering

Supervisor: Assoc. Prof. Dr. Şimşek DEMİR

September 2011, 191 pages

Phased array based systems have extending applications in electronic warfare, radio astronomy, civilian applications with technological advancements. The main virtue offered by these systems is the creation of agile beams with utilization of phase shifting or delay elements. In fact, the desire for flexible steering comes with a cost.

Frequency Diverse Array (FDA) concept is another approach to beam steering problem. In this context, the subsequent antenna elements are fed with stepped discrete frequencies causing continuous scanning of space in time. So a range-angle dependent scanning is made possible. Also the diversity of waveforms between the antennas is another area of research especially in Moving Target Indicator (MTI) applications. Although several implementation schemes were proposed, the costs and the non-ideal behavior of building blocks make the schemes hard to implement. During this study, a new implementation scheme is proposed where a Linear Frequency Modulated Continuous Wave (LFMCW, Linear FMCW) source is used for feeding a special beam forming network, where the subsequent outputs of the beam forming network have uniform delays. The

dynamic behavior of the source and the uniform (or non-uniform) delay provided by the beam forming network create the required frequency steps between antenna elements as described in conventional FDA. So, the implementation of FDA concept requires just the design of the source, beam forming network and the antenna array.

Throughout the study, mathematical analysis of both conventional FDA and the LFMCW based FDA is made and various implementations are realized. Justification of the mathematical derivations is made by the results of the measurements with the implemented structures. Besides, analysis and simulation of the array in a radar environment with various scenarios are performed. The drawbacks and the proposals for overcoming these drawbacks are also reported during the analysis, which will be useful for future studies on the subject.

Keywords: FMCW, Linear FMCW, LFMCW, FDA, Frequency Diverse Array, Linear Frequency Modulation

# ÖZ

## AYRIK FREKANSLI DİZİLERİN KAVRAMSAL DEĞERLENDİRMESİ VE LFMCW YÖNTEMİNİN ÖZGÜN KULLANIMI

EKER, Taylan

Doktora, Elektrik ve Elektronik Mühendisliği Bölümü

Tez Yöneticisi: Doç. Dr. Şimşek DEMİR

Eylül 2011, 191 sayfa

Teknolojik gelişmeler sayesinde, Faz Dizili Sistemler, elektronik harp, radyo-astronomi ve günlük uygulamalarda genişleyen kullanıma erişmektedirler. Bu sistemlerin sunmuş olduğu asıl özellik, yapılarında yer alan faz kaydırıcı ya da geciktirme elemanları sayesinde yaratılan bağımsız huzmelerdir.

Ayrık Frekanslı Dizi (AFD) kavramı huzme oluşturma sorununa başka bir yaklaşım getirmiştir. Bu bağlamda, ardışık dizi anten elemanları birbirinden ayrık adımlı frekansta işaretlerle sürülürler ve bu sayede uzayın sürekli taranması sağlanır. Böylece, menzil-açı bağımlı tarama şablonu gerçekleştirilebilir. Bununla birlikte, anten elemanlarını besleyen işaretler arasındaki ayrım, özellikle Hareketli Hedef Belirleyici (HHB) uygulamalarında, farklı bir araştırma alanının konusu olmuştur. Literatürde çeşitli kurulum şemalarının var olmasına rağmen, kurulum fiyatları ve ideal olmayan malzeme davranışları kurulumu zorlaştırmaktadır. Bu çalışmada, Doğrusal Frekans Şekillendirmeli Sürekli Dalga (LFMCW, Doğrusal FMCW) kaynağı ve ardışık çıkışları arasında düzgün gecikme olan huzme

oluřturma ađı kullanımı ile yeni bir AFD kurulum yntemi nerilmiřtir. Bu yapıda, kaynađın dinamik davranıřı ve huzme oluřturma ađının anten ıkıřları arasındaki dzgn gecikme, geleneksel AFD yapılarında belirtilen ardıřık antenler arasındaki dzenli frekans kayması gereksinimini karřılamaktadır. Bu sayede, AFD kurulumu, sadece kaynađın, huzme oluřturma ađının ve anten dizisinin tasarımı gerektir.

Bu alıřmada, geleneksel ve LFMCW tabanlı AFD yapılarının matematiksel analizleri ve kurulumları gerekleřtirilmiřtir. Analitik sonuların dođrulaması, yapılan lmler ile teyit edilmiřtir. Bunlarla birlikte, AFD yapısının bir radar ortamında, eřitli senaryolar iin analiz ve benzetimleri de yapılmıřtır. Analizler boyunca, AFD yapısının sorunlu noktaları ve bu sorunların ařılmasına ynelik nermeler de gelecekte yapılacak alıřmalar iin aktarılmıřtır.

Anahtar Kelimeler: FMCW, Dođrusal FMCW, LFMCW, AFD, Ayrık Frekanslı Dizi, Dzgn Frekans Őekillendirmesi

To the *one*

## ACKNOWLEDGMENTS

First of all I want to express my gratitude towards my family for their patience and endless aid throughout this study.

I am so grateful to Şimşek DEMİR, Altuncan HIZAL, Sencer KOÇ, Ayhan ALTINTAŞ, Mustafa AKKUL, Şebnem SAYGINER, Tuncay ERDÖL, and Kadir ERALTAY for their valuable efforts in mathematical developments and in implementation and measurement recommendations.

I want to thank Ömer ÖÇAL, Tahsin İşeri, Kenan GÜNEŞ, Erkan KÖK, Mehmet AKYER, Tülay CAN, Murat MUTLUOL, Hayati TAN for their technical assistance during the implementation phase of the structures.

I also want to express my special thanks to Keziban AKKAYA, Kutlay GÜZEL, Mustafa İNCEBACAK, Zafer TANÇ, Deniz AKGÖR, Erkan KUDAY, Rıdvan SÜRBAHANLI, Dilek BAYSAL, Cenk ATALAN for their support during this study.

# TABLE OF CONTENTS

ABSTRACT .....	iv
ÖZ .....	vi
ACKNOWLEDGMENTS.....	ix
TABLE OF CONTENTS .....	x
LIST OF FIGURES.....	xv
LIST OF TABLES .....	xxii
LIST OF ABBREVIATIONS .....	xxiv
CHAPTERS	
1. INTRODUCTION.....	1
2. PHASED ARRAY LITERATURE AND MOTIVATION .....	5
2.1 PHASED ARRAYS .....	5
2.1.1 A Description of Phased Arrays in General Terms.....	5
2.1.2 Applications and Offerings of Phased Arrays.....	6
2.1.3 Phased Array as a part of a RADAR System.....	8
2.2 ARRAY STEERING.....	9
2.2.1 Mechanical Steering.....	9
2.2.2 Electronic Steering in One and Two Dimensions .....	10
2.3 FREQUENCY DIVERSE ARRAY (FDA) .....	12
2.3.1 General Remarks on FDA .....	12
2.3.2 Research on FDA .....	13
2.3.3 Typical Implementation Schemes .....	16
2.4 FREQUENCY DIVERSE ARRAYS USING LINEAR FREQUENCY MODULATED CONTINUOUS WAVE (LFMCW) TECHNIQUE .....	18

2.4.1	Introduction .....	18
2.4.2	Main Differences between FDA using LFMCW and Frequency Scanning.....	20
2.4.3	A General Summary of Work Done.....	20
2.5	ORGANIZATION OF THE THESIS .....	22
3.	ANALYSIS OF FREQUENCY DIVERSE ARRAYS (FDA) AND LINEAR FREQUENCY MODULATED CONTINUOUS WAVE (LFMCW) BASED FDA.....	23
3.1	CONVENTIONAL FDA ANALYSIS .....	23
3.1.1	Problem Definition.....	23
3.1.2	Analysis of Array Pattern.....	25
3.1.3	Extraction of Design Parameters.....	27
3.1.4	Physical Explanation of the Mechanism.....	30
3.2	LFMCW BASED FDA ANALYSIS .....	33
3.2.1	Problem Definition.....	33
3.2.2	Mathematical Analysis of Array Pattern.....	36
3.2.3	Extraction of Design Parameters.....	41
3.2.4	Comparison with Conventional FDA in terms of Design.....	46
3.2.5	Physical Explanation of the Mechanism.....	47
3.3	DIFFERENCES BETWEEN LFMCW BASED FDA AND FREQUENCY SCANNING .....	50
3.3.1	Analysis of Frequency Scanning.....	50
3.3.2	Differences between the Techniques.....	52
4.	FIRST IMPLEMENTATION OF LFMCW BASED FDA .....	55
4.1	REQUIREMENTS FOR THE IMPLEMENTATION.....	55
4.2	HARDWARE FOR MEASUREMENT .....	56
4.2.1	Beam former- Divider/Combiner.....	56
4.2.2	LFMCW Waveform Generator .....	60

4.2.3	Vivaldi Antenna and Vivaldi Array .....	62
4.2.4	Detector .....	71
4.2.5	Other Hardware .....	72
4.3	TEST CONFIGURATIONS AND MEASUREMENTS .....	73
4.3.1	Test Configuration – 1 .....	73
4.3.2	Measurements with Configuration – 1 .....	75
4.3.3	Test Configuration – 2 .....	77
4.3.4	Measurements with Configuration – 2 .....	79
4.4	RESULTS AND DISCUSSIONS .....	89
5.	ANALYSIS OF LFMCW BASED FDA IN A TRANSCEIVER CONFIGURATION .....	92
5.1	TRANSMITTING FDA – RECEIVING FDA CASE .....	92
5.1.1	Problem Definition .....	92
5.1.2	Analysis of the Array .....	95
5.1.3	Physical Explanation of the Mechanism .....	101
5.1.4	Discussion on the Array Design .....	102
5.2	ANALYSIS OF A SPECIAL CASE: TRANSMITTING FDA – RECEIVING OMNI DIRECTIONAL ANTENNA .....	103
5.2.1	Problem Definition .....	104
5.2.2	Analysis of the Fields .....	104
5.2.3	Analysis of the Case in RADAR Context and Extraction of Design Parameters .....	105
5.2.4	A Typical Example .....	117
5.3	FREQUENCY DIVERSITY ASPECT OF LFMCW BASED FDA ....	121
5.3.1	How to Benefit from Frequency Diversity – Proposal 1 .....	122
5.3.2	How to Benefit from Frequency Diversity – Proposal 2 .....	123
5.3.3	How to Benefit from Frequency Diversity – Proposal 3 .....	124
6.	SECOND IMPLEMENTATION OF LFMCW BASED FDA .....	125

6.1	MOTIVATION AND REQUIREMENTS.....	125
6.2	NEW HARDWARE FOR IMPLEMENTATION .....	126
6.2.1	Proposed Structure .....	126
6.2.2	2-way Divider.....	127
6.2.3	Four-Way Beam-former .....	129
6.2.4	Antenna Array .....	132
6.2.5	Cables as tuners.....	133
6.2.6	Other Parts.....	133
6.3	FULL STRUCTURE AND MEASUREMENTS .....	135
6.4	DISCUSSIONS ON IMPLEMENTATION .....	138
6.5	MEASUREMENT SETUPS AND TESTS .....	139
6.5.1	Measurement Configuration – 1.....	139
6.5.2	Sample Measurements with Configuration – 1 .....	140
6.5.3	Measurement Configuration – 2.....	146
7.	SIMULATIONS OF LFMCW BASED FDA STRUCTURE .....	149
7.1	BASIC INFORMATION ABOUT THE SIMULATION ENVIRONMENTS .....	149
7.2	INFRASTRUCTURES OF SIMULATION .....	150
7.2.1	LFMCW Source .....	150
7.2.2	FDA and an Approach to Propagation Implementation.....	151
7.2.3	Processing on Incoming Waveform .....	153
7.2.4	Further Processing.....	154
7.2.5	Discussion on the simulations.....	155
7.3	WAVEFORMS AT DISTINCT POINTS AND DISCUSSIONS .....	156
7.4	SIMULATION OF A RADAR.....	161
7.4.1	Requirements.....	161
7.4.2	Sample Target Returns and Multiple Target Cases.....	163

7.4.3 Discussions on the Performance of the Structure – Proposals for Better Performance.....	171
8. CONCLUSIONS AND FUTURE STUDIES .....	174
REFERENCES.....	177
APPENDICES	
A. SPECIFICATIONS OF HARDWARE .....	182
B. SIN(X)/X TABLE .....	188
CURRICULUM VITAE .....	190

## LIST OF FIGURES

### FIGURES

Figure 2.1: A diagrammatic display of a typical phased array.....	6
Figure 2.2: Mechanical beam steering is achieved by means of drive motors controlling the direction of the antenna. Note that, the effective area of the antenna does not change with physical rotation. ....	9
Figure 2.3: Electronic Beam Steering by means of phase shifters. Note that the effective aperture is shortened by the cosine of steering direction .....	11
Figure 2.4: Schematic view of the FDA concept .....	13
Figure 2.5: An implementation scheme using mixers for stepped frequencies over the aperture of the array. The amplitude control and phase control are also shown in the sketch all of which are commanded from a waveform controller.....	16
Figure 2.6: FDA implementation for discrete sources at each antenna element. Waveform generators, not only create discrete waveforms for each antenna element, but also provide antenna elements with discrete center frequencies, enabling frequency diversity .....	17
Figure 2.7: An implementation proposal in [18]. Note that power is sampled at each port and combined to create a time reference .....	18
Figure 2.8: LFMCW fed FDA structure using delay lines for frequency steps between the antenna elements .....	19
Figure 3.1: Conventional Frequency Diverse Array with parameters .....	24
Figure 3.2: $ M(\varphi) $ vs $\varphi/\pi$ sketch for an 16 element FDA. Note that the pattern has peaks at $\varphi = 2m\pi$ and the nulls are at $\varphi = \frac{2m\pi}{16}$ .....	28

Figure 3.3: Periodicity in time and range for an FDA array with 16 elements (uniform weighting) and $\Delta\omega = 2\pi 10^4 \text{ Hz}$ .....	29
Figure 3.4: Interference of 4 waves having frequencies 100Hz, 150Hz, 200Hz, 250Hz. Note the interference points in time. ....	31
Figure 3.5: 2-D simulation of an FDA. FDA starting frequency is 10GHz with inter-element frequency spacing of 15 kHz. There are 10 antennas in the array with uniform weighting on the antennas. Note that there is a beam bending in 2-D space .....	32
Figure 3.6: FDA far field array pattern plots for various time instants. The simulation instants are taken to be in one period, so the first and last plots are the same ones although they are taken at different times.....	33
Figure 3.7: LFMCW source frequency regime .....	34
Figure 3.8: Problem Definition for LFMCW based FDA concept. Note that each antenna has a different amount of delay to the source, and this delay will cause a frequency shift of excitation between the antenna elements.....	35
Figure 3.9: Periodicity in range and time is shown for two different simulations. The parameters of the simulation are shown on the plots. The slope of the frequency regime is selected to be $2\pi 10^{13} \text{ Hz}^2$ .....	44
Figure 3.10: LFMCW frequency regime in one period of scanning.....	45
Figure 3.11: A sample radiation pattern in 2D for an LFMCW based FDA. Details are in the text .....	48
Figure 3.12: LFMCW based FDA far field array pattern plots for various time instants. The simulation instants are taken to be in one period, so the first and last plots are the same ones although they are taken at different times.....	49
Figure 3.13: Problem definition for Frequency Scanning Formulation.....	51
Figure 3.14: Turning LFMCW based FDA into frequency scanned antenna by controlling the LFMCW source digitally, whose clock period is larger than the total delay in the array.....	53

Figure 4.1 Corporate division and the delay sections. T-junctions are used for power division between the sections of divider and meandered lines accomplish the required delay between the antenna elements. ....	56
Figure 4.2: A photograph of the final beam former with connectors and applied tuning.....	58
Figure 4.3: $S_{n1}$ measurements of the beam-former .....	58
Figure 4.4: $S_{11}$ measurements of the beam-former .....	59
Figure 4.5: At 0.55ns delay, the phases coincide (approximately) .....	59
Figure 4.6: Schematic of LFMCW waveform generator .....	61
Figure 4.7: LFMCW generator PCB .....	61
Figure 4.8: Output Power and control voltage vs frequency measurement .....	62
Figure 4.9: Antipodal Vivaldi Antenna.....	63
Figure 4.10: Antipodal Vivaldi Antenna in array form, with 25 mm inter-element distance.....	63
Figure 4.11: $S_{11}$ (dB) measurement of each antenna in Figure 4.10.....	64
Figure 4.12: Inter-element coupling.....	65
Figure 4.13: CST simulation result for E-plane pattern of the vivaldi antenna radiation at 7GHz. ....	65
Figure 4.14: Measured E-plane antenna pattern of a Vivaldi antenna in the array.....	66
Figure 4.15: CST simulation result for H-plane pattern of the vivaldi antenna radiation at 7GHz. ....	66
Figure 4.16: Measured H-plane antenna pattern of a Vivaldi antenna in the array. ....	67
Figure 4.17: AutoCAD output of the beam-former and antenna array .....	68
Figure 4.18: Implemented beamformer and antenna assembly – front side of the board.....	68
Figure 4.19: Implemented beamformer and antenna assembly – back side of the board.....	69

Figure 4.20: Return Loss measurements at the common port of the array and the fill antenna.....	70
Figure 4.21: S-parameter measurement between the array input and the fill antenna .....	70
Figure 4.22: Input Power vs Output Voltage for various frequencies .....	71
Figure 4.23 Output Voltage vs Frequency for various input powers.....	72
Figure 4.24: Configuration for the first experiment.....	73
Figure 4.25: A photograph of the first measurement setup.....	74
Figure 4.26: First observation of the amplitude modulation effect on the oscilloscope screen.....	75
Figure 4.27: The output waveform for the parameters in Table 4.1. ....	77
Figure 4.28: Configuration for the next tests .....	78
Figure 4.29: Resulting waveform for measurement 1 .....	81
Figure 4.30: Resulting waveform for measurement 2.....	82
Figure 4.31: Resulting waveform for measurement 3 .....	83
Figure 4.32 Resulting waveform for measurement 4.....	84
Figure 4.33: Effect of center frequency on beam shift.....	86
Figure 4.34: Effect of frequency slope on the time scaling .....	89
Figure 5.1: Transmitter Configuration .....	93
Figure 5.2: Receiver Configuration.....	94
Figure 5.3: LFMCW source frequency regime .....	94
Figure 5.4: The placement of transmitter and the receiver sites in the space .....	95
Figure 5.5: Problem sketch for Transmitting FDA-Receiving Omni-directional antenna .....	104
Figure 5.6: A realistic LFMCW frequency regime plot.....	109
Figure 5.7: Fourier Transform of (5.54) with unity amplitude assumption .....	112
Figure 5.8: Incoming pulses in time domain and 3dB points. The simulation is made for an 32 element antenna array with inter-element spacing of 25mm and delay of 0.55ns. Also the starting frequency is 6GHz with 2GHz scan in 1ms...	113

Figure 5.9: The placement of targets at three different angles.....	116
Figure 5.10: A proposal for FDA processing. Pipelined structure is used where the FFT at each step would provide possible target ranges. Using the time reference from the transmitter, other information about the target can be collected. ....	117
Figure 5.11: Dependency of time-of-arrival on the target angle, $\varphi = 2p\pi, p = 1$	119
Figure 5.12: Adding a phase shifter can be beneficial for frequency diversity ...	123
Figure 6.1: General structure of the FDA .....	127
Figure 6.2: 2-way equal amplitude/ equal phase divider .....	128
Figure 6.3: Measurements of 2-way divider .....	129
Figure 6.4: A Wilkinson divider junction on a 25 mil RO6010 substrate .....	130
Figure 6.5: Drawing of the beam former from CAD software.....	130
Figure 6.6: Photograph of the divider during production.....	131
Figure 6.7: S21 (dB) measurements at all arms of the divider.....	131
Figure 6.8: Phase measurement at each arm with 0.5ns inter-arm delay .....	132
Figure 6.9: Photograph of 10 element Antipodal Vivaldi Array.....	133
Figure 6.10: Lumped equalizer structure. The equalizer in the line-up use distributed version where the resonators are replaced with stubs and bond-wires. ....	134
Figure 6.11: Schematic view of the built FDA structure .....	135
Figure 6.12: Photograph of the built FDA structure .....	136
Figure 6.13: S21 (dB) measurement at all ports of the beam former.....	137
Figure 6.14: S21 Phase measurement with added inter-element delay (0.5ns)....	137
Figure 6.15: First trial of implementation .....	138
Figure 6.16: First Configuration- same as the configuration of Figure 4.28. ....	139
Figure 6.17: Resulting waveforms for measurement 1 - effect of slope change on the time domain waveforms .....	142
Figure 6.18: Measurement 2 results .....	143
Figure 6.19: Demonstration of effect of look angle on the positioning of beam peaks.....	145

Figure 6.20: FDA transmitter - FDA receiver configuration .....	146
Figure 6.21: A sample measurement for FDA transmitter – FDA receiver case. ....	148
Figure 7.1: LFMCW source and the constituting parts.....	151
Figure 7.2: FDA part of the simulation.....	152
Figure 7.3: Lossless delay element as propagation environment.....	153
Figure 7.4: Mixing the original LFM waveform and the target return .....	154
Figure 7.5: All structure arranged for the basic simulations .....	155
Figure 7.6: Controlling waveform (left) and output frequency (right) as a function of time .....	157
Figure 7.7: Time domain waveform at the output of the FDA .....	158
Figure 7.8: Transmitted and received waveforms, assuming no amplitude change during propagation and return.....	159
Figure 7.9: Instantaneous frequency of the source and the returned waveform ..	160
Figure 7.10: Demonstration of waveform after mixer .....	160
Figure 7.11: The returning waveform from a target at 90 m and 30 degrees and the Fourier transform of the waveform.....	164
Figure 7.12: The returning waveform from a target at 90 m and 20 degrees and the Fourier transform of the waveform.....	165
Figure 7.13 The returning waveform from targets at 90 m and 20 degrees and 30 degrees and the Fourier transform of the waveform .....	167
Figure 7.14: The returning waveform from targets at 90 m and 50m with 30 degrees of angular bearing and the Fourier transform of the waveform.....	168
Figure 7.15: Two targets at $50m,10^\circ$ and $80m,30^\circ$ .....	169
Figure 7.16: Two targets at $50m,10^\circ$ and $80m,15^\circ$ .....	170
Figure 7.17: Two targets at $50m,5^\circ$ and $80m,15^\circ$ .....	170
Figure 7.18: Adding a dummy element to the array and using interferometry principles can help in solving angular resolution problems.....	172
Figure A.1: TGA2513 chip photograph.....	182

Figure A.2: Photograph of the NARDA divider (33 series) .....	183
Figure A.3: Pin functions of HMC487LC4B .....	185
Figure B.1: SIN(X)/X plot .....	188

## LIST OF TABLES

### TABLES

Table 4.1: Parameters for a sample measurement using the configuration in Figure 4.24.....	76
Table 4.2: FDA constants.....	79
Table 4.3: Parameters of measurement 1 .....	80
Table 4.4: Parameters for second measurement.....	81
Table 4.5: Parameters for third measurement .....	83
Table 4.6: Parameters for fourth measurement .....	84
Table 4.7: Test variables for effect of center frequency on the positioning of beam peaks.....	86
Table 4.8: Test variables for effect of frequency span.....	88
Table 5.1: An example for a radar structure using FDA for transmit and Omni-directional antenna for receive .....	118
Table 5.2: Time of arrivals and angular resolution for a target at 250m range and various angles for $\varphi = 2p\pi, p = 1$ .....	120
Table 5.3: Time of arrivals and angular resolution for a target at 250m range and various angles for $\varphi = 2p\pi, p = 1$ .....	121
Table 6.1: Measurement Constants .....	140
Table 6.2: Measurement 1 parameters .....	141
Table 6.3: Measurement 2 Parameters .....	143
Table 6.4: Measurement 3 variables .....	144
Table 6.5: Parameters for FDA Transmitter – FDA Receiver sample measurements .....	147

Table 7.1: Parameters of simulation.....	156
Table 7.2: The variables of structure used for the simulation.....	162
Table 7.3: Time of arrival and angular resolution calculations for $\varphi = 2p\pi, p = 1$ .....	162
Table A.1: Specifications for TGA2513 .....	182
Table A.2: Specifications of NARDA 3326B-2.....	183
Table A.3: Specifications of the detector .....	184
Table A.4: Specifications for HMC487LC4B.....	185
Table A.5: Some electrical properties of RO6010 .....	186
Table A.6: Properties of alumina .....	186
Table A.7: Specifications of a 4" minibend cable.....	187
Table A.8: RG316 Specifications.....	187
Table B.1: SIN(X) / X values.....	189

## LIST OF ABBREVIATIONS

<b>AM-PM</b>	:	Amplitude Modulation – Phase Modulation
<b>CW</b>	:	Continuous Wave
<b>DAC</b>	:	Digital to Analog Converter
<b>DC</b>	:	Direct Current
<b>DDS</b>	:	Direct Digital Synthesis
<b>ECCM</b>	:	Electronic Counter-Counter Measure
<b>ECM</b>	:	Electronic Counter Measure
<b>EM</b>	:	Electromagnetic
<b>ESM</b>	:	Electronic Support Measure
<b>FDDBS</b>	:	Frequency Diverse Bistatic System
<b>FDA</b>	:	Frequency Diverse Array
<b>FFT</b>	:	Fast Fourier Transform
<b>FOV</b>	:	Field Of View
<b>GMTI</b>	:	Ground Moving Target Indicator
<b>IF</b>	:	Intermediate Frequency
<b>ISAR</b>	:	Inverse Synthetic Aperture Radar
<b>LFMCW</b>	:	Linear Frequency Modulated Continuous Wave
<b>LO</b>	:	Local Oscillator
<b>MIMO</b>	:	Multiple Input Multiple Output
<b>MMIC</b>	:	Microwave Monolithic Integrated Circuit
<b>MSA</b>	:	Mechanically Steered Antenna
<b>MTI</b>	:	Moving Target Indicator
<b>PCB</b>	:	Printed Circuit Board

<b>PLL</b>	:	Phase Locked Loop
<b>PRI</b>	:	Pulse Repetition Interval
<b>RCS</b>	:	Radar Cross Section
<b>RF</b>	:	Radio Frequency
<b>SAR</b>	:	Synthetic Aperture Radar
<b>SMA</b>	:	Sub-Miniature Assembly
<b>TEM</b>	:	Transverse Electric Magnetic
<b>T/R</b>	:	Transmit/Receive
<b>VCO</b>	:	Voltage Controlled Oscillator

# CHAPTER 1

## INTRODUCTION

Phased arrays have been utilized in many applications such as radar, electronic warfare systems, radio astronomy, airport safety and even medicine. Due to the flexibility of the design, the huge benefits of efficient aperture utilization in terms of amplitude and phase control and the long life times in active arrays, they are invaluable to most of the designed systems. Especially, the technological advancements in MMIC and hybrid design led to miniature front-ends up to millimeter wave frequencies, assisting compact front-end structures. Wide-band arrays are another aspect of the phased array concept where aperture can be shared among several tasks presenting multi-tasking opportunities to the system designers [1].

The division of the antenna aperture to fine element apertures and controlling the attributes of each aperture is not an easy task and come with increased system cost. This is the main drawback of the phased array structure and directs the designers through cheaper alternatives like semi-active arrays or constant beam arrays where steering is achieved by means of complex servo systems [1]. Although the technological advancements seem to decrease the cost of requirements, increased demand from the engineers for tighter specifications of front end systems seem to continually increase the cost of building phased array based systems.

In all mentioned systems, electronic steering is an important task for the operation of the systems and directs the designers through various solutions of phased array structures. Although various techniques are available for steering the

main beam of the antenna (photonic techniques, true delay lines, phase shifters, vector modulators etc.), the main drawback, the cost, is again an important limit in the implementation. In this study, another technique for steering, namely frequency diverse array (FDA) is researched.

FDA can be defined to be an antenna aperture where the frequency of each element aperture can be controlled individually to steer the main beam of the array in the space, relying on the time domain relations of each frequency component in the far field. By applying step frequency difference between each subsequent aperture or subsequent antenna element, the beam can be made to scan the space in a periodic manner whose properties are dictated by the inter-element frequency difference, the amplitude distribution among the antenna apertures and the inter-element distance [18, 22]. This powerful method also lends itself to the application of waveform diversity which is beneficial in imaging systems [21, 23, 25]. Also, various implementation schemes are proposed by various researchers in the literature [18, 28, and 33] where some of the studies are resulted in patent. Although, the proposals solve the implementation issues, they have remarkable drawbacks due to non-ideal characteristics of utilized devices (decreasing the performance of array in operation) or increased costs of implementation.

In this study, a novel method of solving the implementation issue is proposed, where the difference between the antenna elements is mainly accomplished by the utilization of a Linear Frequency Modulated Continuous Wave (LFMCW) source and a special beam former before the antenna array. In this technique, the beam-former is supposed to be designed such that each progressive output of the beam-former is delayed by a stepped amount. Due to the dynamic scanning property of the LFMCW source, each antenna in the array receives a unique frequency during a period of the source. In this manner, the requirements mentioned in the FDA operation are fulfilled. The ease of implementation and test makes it a novel method for the task.

At a first glance the technique resembles frequency scanning technique accomplished in conventional antenna arrays. In frequency scanning, the antenna elements are supposed to receive the same (frequency-wise) but delayed waveform and it is the delay responsible for the beam scanning. In the applications, the

antenna beam is tilted with frequency scanning during operation to track the target. In LFMCW based FDA technique the frequency is scanned continually and each antenna element in the array radiates distinct time points of the waveform. This dynamic property of the LFMCW based FDA technique constitutes the main distinction between the aforementioned scanning methods. Note that the frequency scanning is continuous which should be taken into account during implementation. Otherwise, stepping the source in discrete steps would cause frequency scanning if the step periods are not taken into account. More information and detailed mathematical treatment of the case will be presented at appropriate sections of this thesis.

Literature survey is the first part of this thesis, where the studies realized by various researchers and research groups will be quoted. As will be seen during the literature survey section, the concept is analyzed not only in the array scanning concept, but also in the signal processing context, where the FDA antenna elements can create effective waveform diversity if each antenna element can be fed by a distinct waveform. Especially in imaging tasks, this property of the array promises a great future.

The mathematical treatment of FDA concept is performed using primer knowledge of antenna array concept. The LFMCW based FDA concept is similarly analyzed mathematically and comparisons between the two is presented with graphical demonstrations and simulations. LFMCW based FDA concept is also simulated in radar concept to demonstrate the critical waveforms and proposals for processing. During the research, two sample structures were implemented and various measurements were performed. In the thesis, important results and discussions can be found with graphical results.

In the thesis, some proposals about the improvement of the technique are also presented. The drawbacks and inadequate aspects of the technique are shown (during simulations and measurements) and proposals for the solutions are shown. Besides, during research, valuable foresights are gained for the future of the study and they will be presented in this thesis also.

In the simulations, MATLAB and Microwave Office (MWO) software from Advanced Wave Research (AWR) is used extensively. Especially MWO is utilized for the implementation in the computer making it easy to tune and manipulate the FDA.

## **CHAPTER 2**

### **PHASED ARRAY LITERATURE AND MOTIVATION**

#### **2.1 PHASED ARRAYS**

##### **2.1.1 A Description of Phased Arrays in General Terms**

Phased array is composed of a group of antennas whose excitation parameters (amplitude, relative phase or relative delay) and physical placement are arranged in such a way that the radiation pattern of the antenna structure is forced through desired direction(s) and suppressed in undesired directions [1], [2]. In Figure 2.1, a diagrammatic display of a typical phased array is shown with some important control parameters. Antenna elements can be of various types such as dipoles, patch antennas or slotted waveguides with any desired sense of polarization according to the application of interest [1]. Physical arrangement of antenna elements can be determined according to the beam properties or application environment. Combiner, attenuators and phase shifters (in the figure a phase shifter is shown but delay lines or even frequency scanning in the source can be used) can be utilized for any desired beam weighting, with which a shaped radiation pattern in a desired direction can be created in the far field of the phased array antenna system.

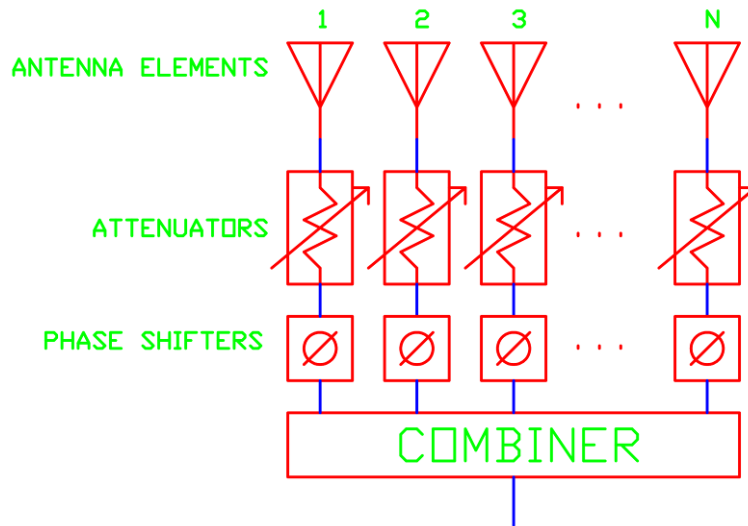


**Figure 2.1: A diagrammatic display of a typical phased array**

The flexibility in control has made phased array systems an invaluable solution in radar applications with the disadvantage of high implementation costs [3]. The advancements in the technology (advances in MMIC technology, dense packaging, new SSPA technologies...) tend to decrease the costs but the desire for much better beam and radar performances still keeps the costs high [1,4]. The costs of phased array systems are also affected by the type of phased array system (passive, active or semi-active) but in the context of this thesis, these subjects will not be explored. The reader is referred to [1] for more information on the phased array based systems.

Nevertheless, as described in the next subsection, phased array antenna systems have found numerous applications with the invaluable offerings according to the field of application [1].

### **2.1.2 Applications and Offerings of Phased Arrays**

In the phased array literature, there are many sources describing the applications of the phased arrays together with the offerings that suit the type of application. In this subsection, the virtues presented by the phased arrays will be summarized.

The main virtue gained by the phased arrays is the synthesis of an agile, inertialess and shaped beam(s) in any desired direction in the field of view (FOV)

with a careful arrangement of the parameters shown in Figure 2.1 [1]. Rapid and accurate arrangement of weighting of each antenna element permits implementation of multi-function radar systems which can track, search, monitor, fire control and even be used as a communication system [1,4]. The beam parameters (beam width, beam shape etc.) can be changed according to the scenario [1,4]. Frequency diversity is also possible which increases signal-to-noise ratio (SNR) [1,4].

Another important offering of the phased arrays is the power combination from the amplifiers distributed across the active area of the array [3]. The power requirement of a radio-astronomy or a radar system is mainly dictated by the target at maximum range of interest with minimum radar cross section (RCS) and the receiver properties [3]. The power combination property of the phased array system can be benefited in these application areas.

Third, phased array antenna deployment is a flexible matter. Arrays may conform to curved surfaces like aircrafts or missiles [4]. So, the existence of a phased array does not affect the aerodynamic properties of these vehicles [1]. In this case, the physical placement of antennas should be taken into account in the synthesis of beams [4].

In radio-astronomy applications, phased array based telescopes led to tiny spatial resolutions with affordable costs [1].

Apart from these applications, the phased arrays are also used in Electronic Support Measures (ESM), Electronic Counter Measure (ECM), Electronic Counter-Counter Measure (ECCM), Synthetic Aperture Radar (SAR), inverse SAR (ISAR), and some communications systems [1]. Also, some phased array based systems utilize 2-3 octave bandwidths to utilize all aperture of the array for various functions like radar functions, airport management etc [1].

The properties of phased arrays listed in this subsection are some of the important ones which helped scientists and engineers meet various requirements of research and design. New technological advances will definitely increase the demand for phased arrays in new systems.

### **2.1.3 Phased Array as a part of a RADAR System**

In section 2.1.2, some of the important properties of phased arrays were listed and some of the applications in radar systems were defined. In this subsection, details about the phased arrays in radar applications will be presented.

As described before, agile and inertia-less beam synthesis property of a phased array is the most influential property. Mechanically steered antennas rely on the speed of the gimbal drive motors, which is far behind that of a phased array [5]. With this property of the phased arrays, tracking after detection of a target, multiple target tracking, dwell selections during tracking, track while scan, hemispherical search, adaptive track and search rates, target illumination for missile guidance, sequential detection methods, digital clutter map generation are possible and most of these capabilities can be utilized on a single radar [1, 3, 5].

Reliability is also another concern in the radar systems, where radars with mechanically steered antennas (MSA) also rely on the life cycle of mechanical parts like gimbals structure, drivers, rotary joints etc. On the contrary, degradation times of typical solid state transmit/receive (T/R) modules can be made considerably high [5]. It should be noted that for the phased array system degradation, at least five percent of the modules should fail, making the phased array life time comparable to the lifetime of the platform it is mounted on [5]. Moreover, for a passive phased array (in which antenna elements are not populated with any transmit (T), receive (R) or T/R module) with only phase shifting elements behind the antenna elements, the MTBF (mean time between failure) rates of phased arrays become considerably higher than MSA [5].

The high power requirement of a radar system can be eased by distributing the power among T/R modules over the aperture and utilizing the power combination property of the phased array system [1]. So, together with the weightings associated with the antenna elements, the required power would be focused through the desired direction [1].

In literature, one can find many examples of radar systems using phased array (passive or active) systems. In [4] and [5], many examples of these radars can be found together with their operational characteristics.

In the next section, an important property of phased arrays, steering, will be discussed literally and the progress towards the main workhorse of the current work will be presented.

## 2.2 ARRAY STEERING

### 2.2.1 Mechanical Steering

Mechanical steering is the simplest way of steering the antenna beam in the desired direction. In this case, the antenna beam is fixed with respect to the antenna platform and the steering of the beam is provided by means of driver motors as shown in Figure 2.2. The effective area of the antenna does not change with the rotation, so the beam-width and side-lobe performance of the antenna is not affected by steering [5]. Besides, using mechanical steering, the antenna can be steered in any direction as far as the mechanical limitations permit.

One of the limitations of mechanically steered arrays is the high failure rates [1, 6]. This case makes the lifetime cost of a mechanically steered array a few times the initial cost of the system.

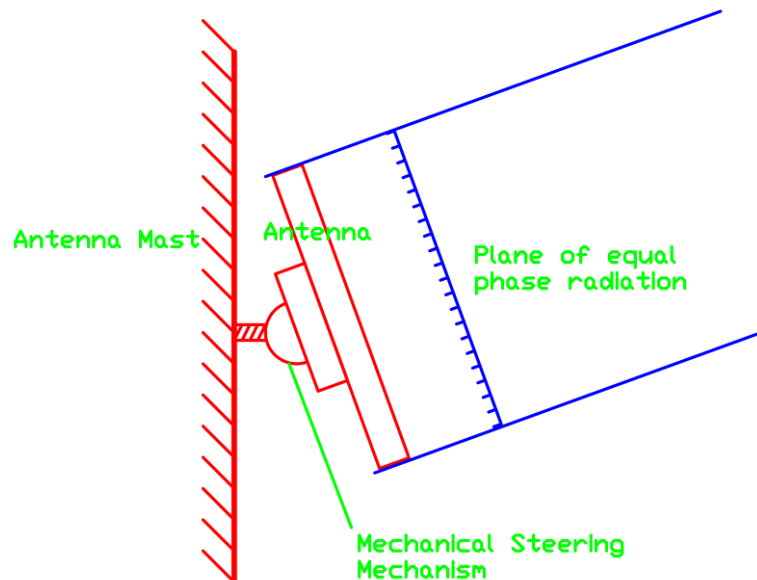


**Figure 2.2: Mechanical beam steering is achieved by means of drive motors controlling the direction of the antenna. Note that, the effective area of the antenna does not change with physical rotation.**

The main drawback of the mechanical steering is the steering delay. The parameters of servo system controlling the antenna direction should be taken into account during search and tracking [7]. The concept of mechanical steering will not be detailed here, but readers are referred to [3], [5] and [7] for more information about the effect of servo bandwidth on tracking error and optimum servo bandwidth. Nevertheless, mechanical steering limits the capabilities of radar in terms of multi-functionality.

### **2.2.2 Electronic Steering in One and Two Dimensions**

As mentioned in 2.1.1, steering in one dimension can be achieved by using the phase shifters at each antenna channel. Antenna beam steering is achieved by simply phasing each consecutive channel by a phase shift value, which is a function of desired beam look angle, inter-element spacing and frequency of operation (in real life, the AM-PM, PM-AM and inter-element coupling should be taken into account for true steering of the beam, also the amplitude distribution across the aperture of the array is important in the beam shape formation) [1, 2, 8].

The fast switching times and the high reliability offered by the manufacturers of phase shifters, agile beam creation is possible permitting multi-functional array implementation.

One of the drawbacks of electronic steering is the foreshortening of the effective aperture [5]. In Figure 2.3, this case is depicted schematically (In the aforementioned figure, the effect is shown in a one dimensional array but the effect is more pronounced in the planar array context). The phase shifters are arranged to steer the beam to an angle of  $\theta$ , and the effective aperture of the antenna is shortened to  $W \cos(\theta)$ . This effect limits the maximum practical steering to +/-60 degrees off broadside [1, 5].

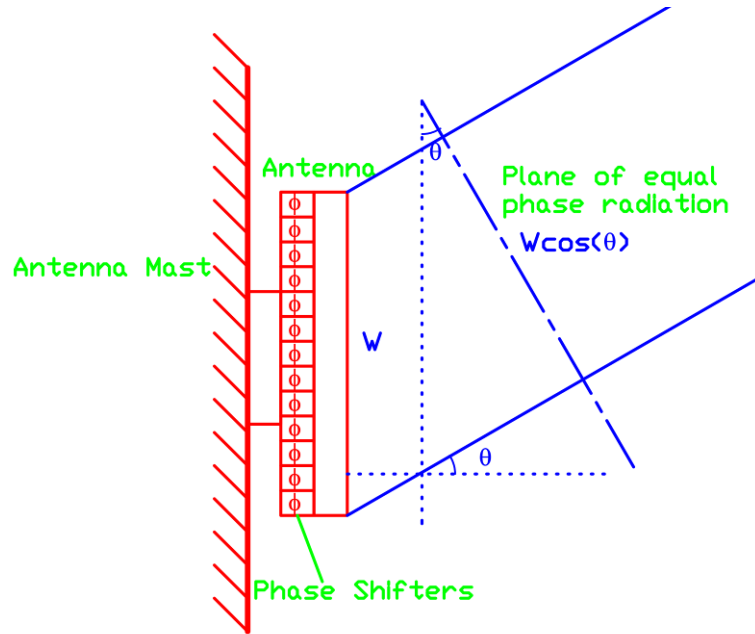


**Figure 2.3: Electronic Beam Steering by means of phase shifters. Note that the effective aperture is shortened by the cosine of steering direction**

Besides the phase shifters, there are other means of steering. True time-delay is an applicable solution to the problem of steering. Usage of optical techniques for the true time-delay steering has been reported in various studies [9-13], where the array bandwidths can be increased up to 3 octaves [1, 9-13]. The phase shifters can also be realized at the IF frequencies with lower errors in the beam forming, but the local oscillator requirement for each antenna channel limits the practical number of antenna elements in terms of cost [1]. Another, and more effective, technique is digital beam-forming. Implementing the required dynamic range by the front-end receivers, the beam synthesis and beam steering can be handled in digital signal processors together with some advanced techniques like adaptive nulling, multiple beam generation, pattern correction, automated calibration and effective timing [14-16]. Despite the high costs required for implementation, digital beam-forming is being more wide-spread with the advancements in packaging and integrated circuit technologies [1].

Another technique for beam steering is attained by using the frequency diversity between antenna elements. This technique also forms the basis of this work. In Frequency Diverse Array (FDA) concept, the antenna elements of the

array are fed by sources of discrete frequencies, where the frequency of each subsequent antenna is offset by a small amount of frequency. The progressive frequency shift between the antenna elements is the main factor in continuous steering in space [17, 18]. In the next sub-section primary information about the Frequency Diverse Array (FDA) concept will be presented. Also, in Chapter 3, detailed mathematical derivations will be supplied.

For more information on beam-steering, the reader is referred to [1] and [4].

## **2.3 FREQUENCY DIVERSE ARRAY (FDA)**

### **2.3.1 General Remarks on FDA**

In the previous sub-section, general comments about the beam steering were presented with various references. In this section some preliminary information about the FDA concept will be explained.

As explained before, FDA concept relies on the instantaneous frequency of each antenna element. Each antenna element is fed with CW signals and there is progressive frequency shift between the consecutive antenna elements, which is the main idea of FDA technique. The discrete CW signals fed to each antenna element interfere in space in a way that the resulting waveform has amplitude modulation in time, range and look-angle. The parameters of the so said amplitude modulation (in fact pulsed waveform is created) is determined mainly by the progressive frequency shifts together with the central frequency, inter-element spacing and the complex weighting of each antenna element [18]. In Figure 2.4, a schematic view of the array is shown with important critical parameters. This figure is a bare version of the FDA concept, but addition of phase shifters to each antenna element also provides more flexibility in steering in space [17, 18]. The origin is taken to be on the first antenna element on the leftmost and throughout all derivations in this thesis; this coordinate system will be used.

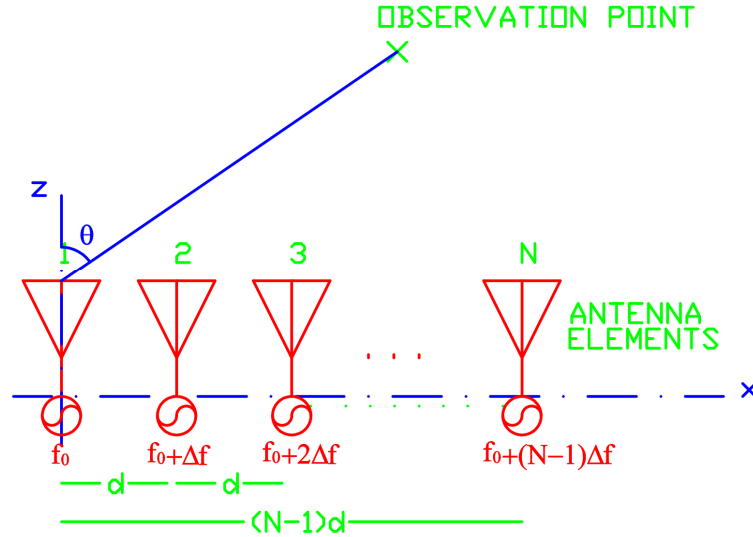


**Figure 2.4: Schematic view of the FDA concept**

As a radar array, besides the steering feature, FDA concept introduces resistance to multi-path interferences [17] and the inherent bent-beam can be utilized in increasing the cross-range resolution of Synthetic Aperture Radars (SAR) [23, 31]. Possible waveform diversity at each antenna element is also another concern where especially in SAR and telecommunications applications, potential benefits are reported by various researchers [21, 27].

One problem with the FDA is the implementation issue. Various studies have been employed on the implementation issues. Also, some methods were published and patented by the researchers[21, 33].

In the next sub-section, a brief timeline of FDA research and patent progress will be presented.

### **2.3.2 Research on FDA**

In this sub-section, research on time modulated arrays will not be presented with all details, but [19] is an important publication about the understanding of the potential of time modulation in side-lobe reduction. In the publication, time modulation is mainly attributed to the weightings of each antenna (using on/off switching of antenna elements sequentially) in the array, and by careful timing of on times of antennae, the static far-field radiation pattern of the array can be synthesized.

In [17], the modulation logic is extended to the Frequency Diverse Array concept, where the frequency of each radiator is sequentially increased to create a time modulated radiation pattern. [17] also points to the range-angle-time dependent far field array pattern creation, which is the core to the understanding of the concept. [17] states the resistance of the technique to the multi-path interferences and the availability of flexible beam scanning options.

Another publication on FDA concept focuses on the waveform diversity where each antenna radiates a diverse LFM chirp at diverse center frequencies [21]. This structure is especially beneficial in SAR and MTI applications [21].

In [18], FDA concept is presented analytically indicating the periodicity of far field array pattern with respect to time, range and angle. The same modulation pattern in time, range and angle is stressed and various simulations are presented in the publication. In the same publication, an implementation strategy is also shown (which will be analyzed in the next subsection) with a technique to determine the position of a target.

Reference [20] is another publication where utilization of range-angle dependent pattern of the FDA is proposed for detection improvement in GMTI processing.

EM simulation of the FDA concept is carried out in [22], where radiation properties of the FDA are analyzed using electromagnetic tools. Various simulations with controlled inter-element frequency steps, the dynamics of beam scanning feature is observed in the aforesaid paper.

[23] is an essential publication in the area of FDA, where the improvement in cross-range resolution in SAR using the bent-beam property in FDA is proposed by the authors. Also, the same publication proposes FDA concept for improvement in range resolution.

Reference [24] analyzes FDA and rearranges the radiating elements to break the radiation dependency between the range and angle, terming the new array as “Wavelength Array” (WA). The same paper also introduces “Frequency Diverse Bistatic System” (FDBS) where at a calculated reference point, the FDA

waveform can be observed as angle independent. A receiver at reference point receives the pulse modulated waveforms of FDA with no angular dependency.

Another publication focusing on the utilization of waveform diversity is [24]. In this paper, the antenna elements of FDA receive LFM chirps with slightly different frequencies and the associated range-angle dependent pattern is analyzed. Also ambiguity diagram is formulated in the same paper.

[26] is an extension of [24] with derivations of important parameters of FDDBS is presented. An accurate formulation of array pattern taking the bistatic geometry into account is shown in the aforementioned publication.

M. C. Wicks review the waveform diversity concept in [27]. This paper is beneficial for the understanding of the waveform diversity concepts and developments.

Reference [28] is an extension of [22] with an implementation of the concept using PLL frequency synthesizers. In this publication the results of measurements are not presented, but in the next subsection implementation will be analyzed.

MIMO and FDA concepts are combined in [29]. The authors discuss the transmission of pseudo-noise codes at different frequencies from each antenna element of FDA and recovery of information at receivers. Here, the angle-changing characteristics are provided by MIMO while range changing characteristics are provided by FDA.

Authors of [30] re-analyze FDA and make various simulations with a proposed T/R configuration.

[31] is a continuation over [23] with cross range resolution improvement in focus.

Finally in [32], authors analyze the FDA formulation and mainly worked on the frequency offset of the FDA, rather than the inter-element frequency steps. So, it is proposed that precise beam steering toward a desired range with a desired angle is possible.

### 2.3.3 Typical Implementation Schemes

In this part several techniques of implementation will be analyzed and virtues and drawbacks will be presented. Some of the implementations are already patented, and some are published as described in the previous subsection.

[33] is a patent describing a basic implementation scheme as shown in Figure 2.5. A waveform generator creates a predetermined frequency and this waveform is mixed with multiples of step frequency,  $\Delta f$ , with which the step frequency change over the aperture of the array is provided. Besides, the authors add extra phase control and amplitude control at each channel for extra beam scanning flexibility. Note that, a separate waveform control unit is required for the FDA beam shaping.

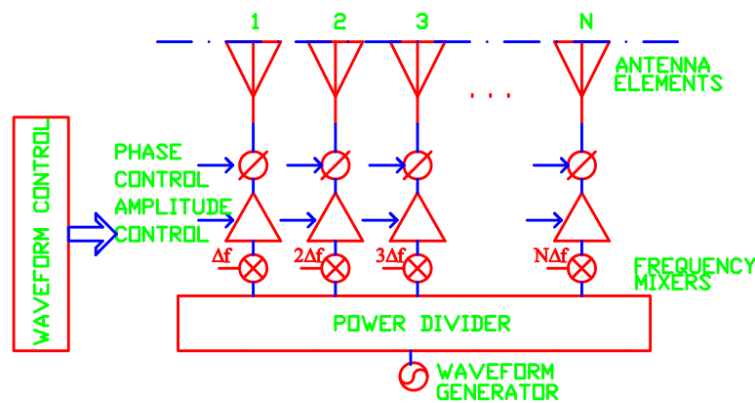


**Figure 2.5: An implementation scheme using mixers for stepped frequencies over the aperture of the array. The amplitude control and phase control are also shown in the sketch all of which are commanded from a waveform controller**

The main drawback of Figure 2.5 is the poor spectral purity, since the frequency mixers also create components at image frequencies as well as some multiples of RF and LO frequencies. Especially low step frequencies between the antenna elements, put hard filtering filter requirements after mixer element. Intermodulation products created by the mixers would certainly cause ambiguous results during processing.

In the same patent, there is also another scheme, in which the waveform of each antenna element is supplied from a discrete source. In this case, waveform diversity together with the stepped frequency change is handled at these discrete sources. Figure 2.6 shows this configuration.

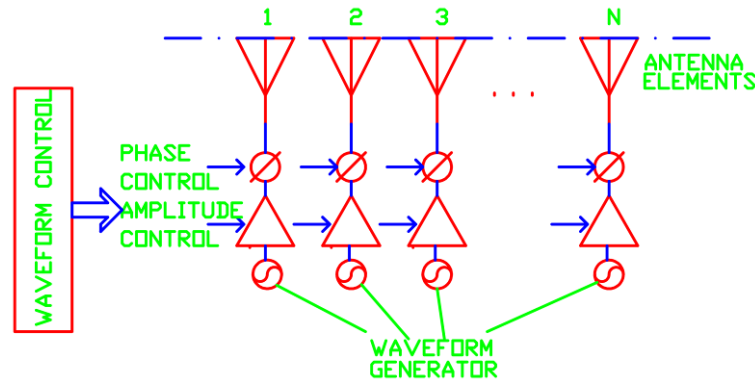


**Figure 2.6: FDA implementation for discrete sources at each antenna element. Waveform generators, not only create discrete waveforms for each antenna element, but also provide antenna elements with discrete center frequencies, enabling frequency diversity**

The configuration in Figure 2.6 is an expandable implementation scheme, since the waveform generators at each antenna channel can be used for stepped frequency changes as well as discrete waveform generations for waveform diversity. Direct Digital Synthesizers (DDS) or programmable PLL Synthesizers [28] can be utilized for waveform generators, but at the expense of possible clock jitters or phase errors. Configurations in Figure 2.5 and Figure 2.6 can also be combined for easier and spectrally cleaner output waveforms, but the cost increases due to the added hardware to the system.

Another implementation is presented in [18], which is very similar to the one shown in Figure 2.5, but a clearer sketch. This scheme is shown in Figure 2.7. This structure also suffers from the intermodulation products and image products created by the mixers, but reliable timing information is fetched by the couplers and power combiner. Since the radiation is time-range and angle dependent, timing information is crucial to the operation of FDA.

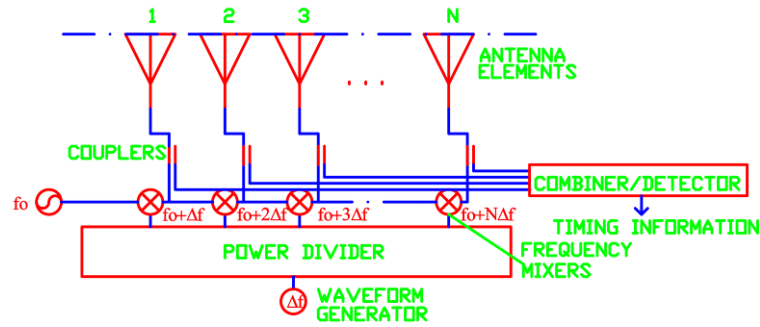


**Figure 2.7: An implementation proposal in [18]. Note that power is sampled at each port and combined to create a time reference**

In this study, an implementation method for FDA concept is introduced and analyzed which is using Linear Frequency Modulated Continuous Wave (LFMCW) source with delay lines between the antenna elements. In the next section, an introduction to the concept will be made.

## 2.4 FREQUENCY DIVERSE ARRAYS USING LINEAR FREQUENCY MODULATED CONTINUOUS WAVE (LFMCW) TECHNIQUE

### 2.4.1 Introduction

Up to this point, a brief perspective of phased array systems and steering concept of phased array based systems are presented. Various steering architectures and finally FDA are shown literally and schematically. Especially, implementation side of the concept creates a challenge in terms of the design. In this study, an easier implementation method than the proposed ones ([18], [28], [33]) is analyzed and formulated mathematically. Several important design equations are derived for the implementation. Besides, several implementations are performed and measurements are recorded as will be given in the following chapters.

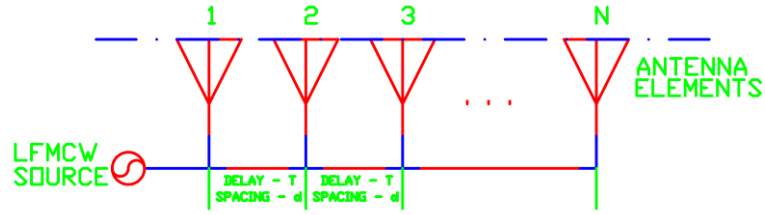


**Figure 2.8: LFM CW fed FDA structure using delay lines for frequency steps between the antenna elements**

Figure 2.8 shows a sketch of the basic structure. According to this figure, for basic FDA functionality, what is required is just a linear frequency modulated source and the delay lines between the antenna elements. The linear frequency modulation in time and the uniform delay between the antenna elements constitute the required frequency diversity between the antenna elements. The frequency sweep implemented at the source is the source of dynamic beam scanning feature. Due to the range-angle-time dependent radiation pattern of the structure, every point in space is scanned with different frequency components which can be altered by use of programmable delay lines or phase shifters at each antenna. This property of the array is an important virtue for radar applications requiring frequency diversity in detection improvement.

FDA using LFM CW has a clearer spectrum than the proposed structures using frequency mixers or discrete sources at each antenna element. A drawback of FDA using LFM CW is the analog control requirement for the frequency shift because the technique relies on the continuous frequency shift over the real aperture of the array and digital control of frequency steps would cause same frequencies to be supplied to several consecutive antennas. In this case, beam scanning would again be observed but it will turn into a frequency scanned antenna (the frequency will be static during a period of the clock) which will be analyzed in the next subsection. During the thesis, all of the derivations and calculations will assume perfect control of frequency with an analog control. Nevertheless, with advancements in digital technologies, higher clock frequencies will become available and simple Digital-to-Analog Converters (DAC) may be adapted for precise control of LFM CW source frequencies with time.

## **2.4.2 Main Differences between FDA using LFMCW and Frequency Scanning**

Frequency scanning is a technique used in antenna arrays, where the inter-element delay mechanism is used for tilting the direction of look. The inter-element delay creates different phase shifts between the antenna elements causing the main beam direction to be tilted [4]. The beam scanning feature encountered in frequency scanning concept is not dynamic since each antenna element receives a phase shifted but equal frequency waveform and array pattern is steered to different directions for each frequency. Range-angle-time dependent waveform normally encountered in LFMCW fed FDA is not present in frequency scanning. This distinction is important in the understanding of the concept.

Detailed analysis of the case is shown in [4] but also in this thesis, mathematical derivations for the case will be shown in subsequent chapters.

## **2.4.3 A General Summary of Work Done**

This study started with general mathematical derivations of FDA concept based on [17] and [21]. Especially amplitude (or pulse) modulated waveform and periodicity of waveform in space, time and angle was perceived [18]. At this point, the challenge in the implementation was realized and the study was focused on realization of the structure. During research, several structures were analyzed taking engineering design constraints into account. LFMCW based FDA concept were noticed then.

The mathematical derivations and comparison of findings with conventional FDA was the first step towards the research. In these mathematical derivations, far field array pattern of FDA was derived and critical parameters of array were found through equations. Several MATLAB simulations were performed to check the results of analytical calculations. During simulations realizable values are selected for the problem variables at hand, since the aim was to implement the structure in real life. The difference between the LFMCW based FDA and Frequency Scanning was a core point in the research in terms of novelty and this point was always emphasized.

After initial analytical findings, a small antenna beam-former with inter-arm delays and an LFMCW source is built for initial tests. Initial tests were successful and during these tests the calculated waveforms were generated in the laboratory.

In the next step antennas were designed, built for the application and integrated with the pre-designed beam-former. Several measurements were performed in the anechoic chamber using the first FDA. The parameters of the concept were justified in this step, but the array was not acceptable in terms of transmission (magnitude and inter-element delay) parameters.

In the following step, the formulations were renewed for transmission and reception, where both the transmitter and the receiver were FDA. The mathematical results of this step were not justified with measurements but focusing effect of the array was an important result. During derivations, a new, better and larger antenna array were built. Using this array the previous measurements were repeated. Also FDA-FDA measurements were made using the two arrays in hand.

After measurements, the radar properties of FDA were focused on. In this context, waveforms for transmitter FDA – receiver omni-directional antenna was derived. As a radar application, and using appropriate references, heuristic methods of target detection techniques were analyzed on the derivations. Besides, the frequency diversity techniques for radar applications were shown. As mentioned before, realizable system parameters were selected for calculations.

In the last step, LFMCW based FDA is simulated on the computer. As an extension of these simulations, the concept was also simulated for the transmitter FDA – receiver omni-directional antenna case and conceptual radar was created. Previously derived equations were also checked during these simulations. Finally, angular resolution properties of LFMCW based FDA were analyzed and some mathematical relations regarding the angular resolution were found.

## **2.5 ORGANIZATION OF THE THESIS**

Organization of thesis will follow the steps in section 2.4.3. In Chapter 3, mathematical derivations of conventional FDA are repeated. In the same chapter, LFMCW based FDA concept will be analyzed and detailed equations will be presented.

Next chapter will focus on the first implementation and the reported measurements. The measured findings will be compared to the theoretical findings.

Chapter 5 is devoted to the mathematical derivations again where equations on transmitting FDA – receiving FDA will be presented. Then the focus will turn toward transmitting FDA – receiving omni-antenna derivations and results. The application of this latter scenario in a radar application and derivation of radar parameters will be shown in this chapter also.

In Chapter 6, measurements using the new FDA are presented with design constraints on all parts of the beam former. Transmitting FDA - receiving FDA results are also shown in this chapter but these results are not used for the justification of derivations of Chapter 5 due to the problems explained in this chapter.

Next, in Chapter 7, simulations of LFMCW based FDA as a radar antenna will be presented. The discussions on the simulation results and proposals will be shared here.

Chapter 8 will conclude the thesis with general remarks about the proposals.

References and appendices are placed at the end of this thesis.

## **CHAPTER 3**

# **ANALYSIS OF FREQUENCY DIVERSE ARRAYS (FDA) AND LINEAR FREQUENCY MODULATED CONTINUOUS WAVE (LFMCW) BASED FDA**

In this chapter, first, conventional FDA analysis will be presented with critical design parameters extracted. Similar analysis will also be made for LFMCW based FDA, with comparisons between the techniques. Lastly, frequency scanning concept will be examined and differences between frequency scanning and LFMCW based FDA will be discussed.

### **3.1 CONVENTIONAL FDA ANALYSIS**

In this section, far field array pattern of a conventional FDA will be derived in time domain. First, a problem definition will be supplied and derivations will be done. Next, key equations (in terms of design) will be derived and physical explanations of the equations will be discussed.

#### **3.1.1 Problem Definition**

Previously, in Figure 2.4, properties of the array were presented. Here the sketch is redrawn with the reference origin and the observation point for analytical derivations. Figure 3.1 shows the sketch with parameters at respective points. A contribution of Figure 3.1 is the addition of the phase shifters at each antenna element. The phase shifters are added for mathematical convenience here and the benefits of phase shifters will be explained in following sections.

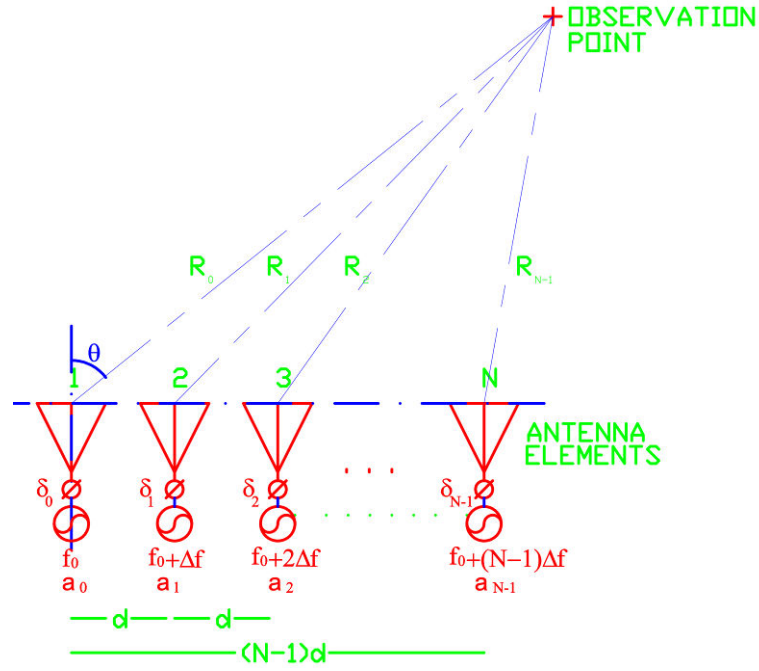


**Figure 3.1: Conventional Frequency Diverse Array with parameters**

According to Figure 3.1,  $n^{\text{th}}$  antenna element is excited with a frequency of  $f_n = f_0 + (n-1)\Delta f$  or  $\omega_n = \omega_0 + (n-1)\Delta\omega$  for radial frequencies. It is assumed that the problem origin stays at the first antenna of the array, which will cause extra phase terms in the far field radiation pattern. Also, in the formulation, we will be interested in the array factor in elevation only; so the electric fields of antenna elements should be understood in elevation plane only. The variables of the problem are as follows:

- $\theta$ : Angular position of observation point in elevation.
- $d$ : Inter-element spacing.
- $R_n$ : Range of observation point to the  $n^{\text{th}}$  antenna ( $n = 0$  to  $N-1$ ).
- $\delta_n$ : Excitation phase of  $n^{\text{th}}$  antenna.
- $a_n$ : Amplitude weighting of  $n^{\text{th}}$  antenna element.
- $f_e(\omega)$ : Element pattern of  $n^{\text{th}}$  antenna in the elevation.

### 3.1.2 Analysis of Array Pattern

The far field array pattern can be written as follows [2]:

$$E_A = \sum_{n=0}^{N-1} \frac{a_n}{R_n} f_e(\omega_0 + n\Delta\omega) e^{j(\omega_0 + n\Delta\omega)t} e^{-jk(n)R_n} e^{-jn\delta} \quad (3.1)$$

In (3.1);

$$R_n = R_0 - nd \sin(\theta) \quad (3.2)$$

$$k(n) = k_0 + n\Delta k \quad (3.3)$$

$$k_0 = \frac{\omega_0}{c} \quad (3.4)$$

$$\Delta k = \frac{\Delta\omega}{c}$$

The phase of the term in summation is

$$\psi_n = (\omega_0 + n\Delta\omega)t - (k_0 + n\Delta k)R_n - n\delta \quad (3.5)$$

Expanding all terms in (3.5)

$$\psi_n = (\omega_0 + n\Delta\omega)t - (k_0 + n\Delta k)(R_0 - nd \sin(\theta)) - n\delta \quad (3.6)$$

Now, we need to find all products in (3.6) to distinguish the equation elements depending on the antenna indices and the others.

$$\psi_n = \omega_0 t + n\Delta\omega t - k_0 R_0 + k_0 nd \sin(\theta) - n\Delta k R_0 + n^2 \Delta k d \sin(\theta) - n\delta \quad (3.7)$$

$$\psi_n = \omega_0 t - k_0 R_0 + n(\Delta\omega t + k_0 d \sin(\theta) - \Delta k R_0 + n\Delta k d \sin(\theta) - \delta) \quad (3.8)$$

Now, assume that the inter-element frequency shift is much smaller than the center frequency of the array, or

$$(N-1)\Delta\omega \ll \omega_0 \quad (3.9)$$

So (3.9) can be rewritten as

$$\psi_n = \omega_0 t - k_0 R_0 + n(\Delta\omega t + k_0 d \sin(\theta) - \Delta k R_0 - \delta) \quad (3.10)$$

or

$$\psi_n = \omega_0 t - k_0 R_0 + n(\varphi) \quad (3.11)$$

$$\varphi = \Delta\omega t + k_0 d \sin(\theta) - \Delta k R_0 - \delta \quad (3.12)$$

Now, (3.12) can be used in (3.1) to get

$$E_A = \sum_{n=0}^{N-1} \frac{a_n}{R_n} f_e(\omega_0 + n\Delta\omega) e^{j(\omega_0 t - k_0 R_0)} e^{j(n\varphi)} \quad (3.13)$$

Now, assume that  $f_e(\omega_0 + n\Delta\omega) \approx f_e(\omega_0)$ ,  $R_n \approx R_0$  in amplitude sense, (3.13) becomes

$$E_A = \frac{f_e(\omega_0) e^{j(\omega_0 t - k_0 R_0)}}{R_0} \sum_{n=0}^{N-1} a_n e^{j(n\varphi)} \quad (3.14)$$

Equation (3.14) is important in the understanding of FDA concept. Here the element pattern  $f_e(\omega_0)$  is multiplied with the array pattern which has clear dependence on time, angular bearing of observation point, and range of observation point and the complex weighting of each channel. At this point for the ease of mathematical expressions, assume that the amplitude weighting of each channel is unity,  $a_n = 1$  for all elements. Here (3.14) becomes

$$E_A = \frac{f_e(\omega_0) e^{j(\omega_0 t - k_0 R_0)}}{R_0} \sum_{n=0}^{N-1} e^{j(n\varphi)} \quad (3.15)$$

In (3.14), the summation term can be rewritten as [2]

$$\sum_{n=0}^{N-1} e^{j(n\varphi)} = e^{j\left(\frac{N-1}{2}\right)\varphi} \frac{\sin\left(N\frac{\varphi}{2}\right)}{\sin\left(\frac{\varphi}{2}\right)} \quad (3.16)$$

Using (3.16) in (3.15),

$$E_A = \frac{f_e(\omega_0) e^{j(\omega_0 t - k_0 R_0)}}{R_0} e^{j\left(\frac{N-1}{2}\right)\varphi} \frac{\sin\left(N\frac{\varphi}{2}\right)}{\sin\left(\frac{\varphi}{2}\right)} \quad (3.17)$$

And the real physical elevation field becomes (ignoring the element pattern);

$$\text{Re}\{E_A\} = \frac{\cos(\omega_0 t - k_0 R_0 + \frac{N-1}{2}\varphi) \sin\left(N\frac{\varphi}{2}\right)}{R_0 \sin\left(\frac{\varphi}{2}\right)} \quad (3.18)$$

Since  $\varphi$  has time dependent terms, we can expand (3.18) using (3.12).

$$\begin{aligned} \text{Re}\{E_A\} = & \frac{1}{R_0} \cos(\omega_0 t - k_0 R_0 + \frac{N-1}{2} \Delta\omega t + \\ & \frac{N-1}{2} k_0 d \sin(\theta) - \frac{N-1}{2} \Delta k R_0 - \frac{N-1}{2} \delta) \frac{\sin\left(N \frac{\varphi}{2}\right)}{\sin\left(\frac{\varphi}{2}\right)} \end{aligned} \quad (3.19)$$

Grouping the terms in (3.19);

$$\begin{aligned} \text{Re}\{E_A\} = & \frac{1}{R_0} \cos\left(\left(\omega_0 + \frac{N-1}{2} \Delta\omega\right)t - \left(k_0 + \frac{N-1}{2} \Delta k\right)R_0\right. \\ & \left. + \frac{N-1}{2} (k_0 d \sin(\theta) - \delta)\right) \frac{\sin\left(N \frac{\varphi}{2}\right)}{\sin\left(\frac{\varphi}{2}\right)} \end{aligned} \quad (3.20)$$

Equation (3.20) indicates the amplitude modulation of a continuous wave signal at frequency  $\omega_0 + \frac{N-1}{2} \Delta\omega$  by the parameters of the last term in (3.20) time, range and observation angle. The design equations for the array operation can be extracted from the modulation term, which is accomplished in the next subsection.

### 3.1.3 Extraction of Design Parameters

For the design parameters, modulation term in (3.20) can be analyzed. The amplitude modulation term is rewritten in (3.21) for convenience.

$$M(\varphi) = \frac{\sin\left(N \frac{\varphi}{2}\right)}{\sin\left(\frac{\varphi}{2}\right)} \quad (3.21)$$

In this equation, for  $\frac{\varphi}{2} = m\pi$ ,  $m \in N$ , the modulation has periods. Similarly for  $\frac{N\varphi}{2} = m\pi$ ,  $m \in N, m \neq 0$ , the modulation has nulls. The properties of the modulating waveform are visible in Figure 3.2. This figure is produced for an FDA

with 16 antenna elements and the pattern nulls are arranged at  $\varphi = \frac{2m\pi}{16}$  while the peaks are at  $\varphi = 2m\pi$ .

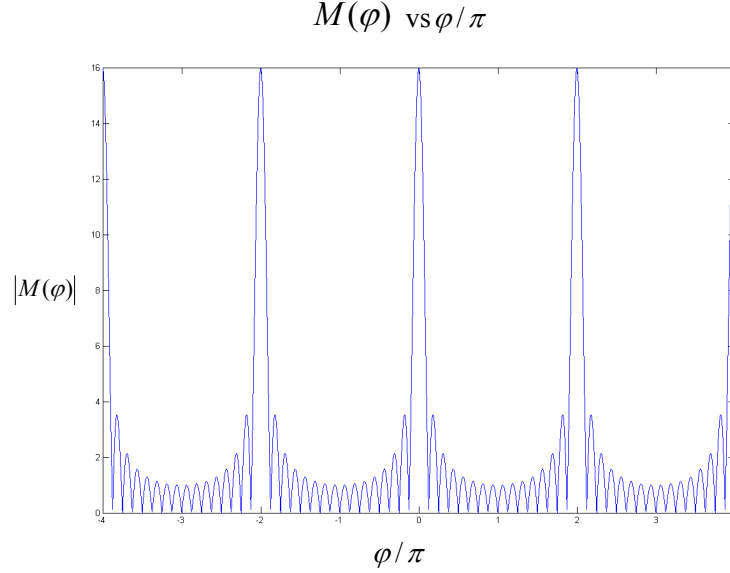


**Figure 3.2:**  $|M(\varphi)|$  vs  $\varphi/\pi$  sketch for an 16 element FDA. Note that the pattern has peaks

$$\text{at } \varphi = 2m\pi \text{ and the nulls are at } \varphi = \frac{2m\pi}{16}$$

Here we can look at (3.22) for the peak points shown in Figure 3.2. According to this equation,  $\varphi$  term has time, look angle and range dependence and there are infinitely many solutions of this equation. Also, the flexibility provided by the phase term is clearly visible in (3.22), the dependence can be manipulated by changing phase values of each antenna element.

$$\varphi = \Delta\omega t + k_0 d \sin(\theta) - \Delta k R_0 - \delta = 2m\pi \quad (3.22)$$

For a point in space, the periodicity in time (or pulse repetition interval - PRI) can be calculated from (3.22) for consecutive values of  $m$ .

$$\Delta\omega t_0 + k_0 d \sin(\theta) - \Delta k R_0 - \delta = 2\pi * 0$$

$$\Delta\omega t_1 + k_0 d \sin(\theta) - \Delta k R_0 - \delta = 2\pi * 1$$

$$\Delta t = t_1 - t_0 = \frac{1}{\Delta f} \quad (3.23)$$

Similarly for a fixed angular bearing and time, the periodicity in range (or unambiguous range) can be calculated as:

$$\Delta \omega t + k_0 d \sin(\theta) - \Delta k R_{00} - \delta = 2\pi * 0$$

$$\Delta \omega t + k_0 d \sin(\theta) - \Delta k R_{01} - \delta = 2\pi * 1$$

$$\Delta R = R_1 - R_0 = \frac{c}{\Delta f} \quad (3.24)$$

The periodicity in  $\sin(\theta)$  can be found as

$$\Delta \sin(\theta) = \frac{2\pi}{k_0 d} \quad (3.25)$$

The periodicity in time and range is also shown graphically in Figure 3.3 for 16-element FDA with 10 kHz inter-element frequency step.

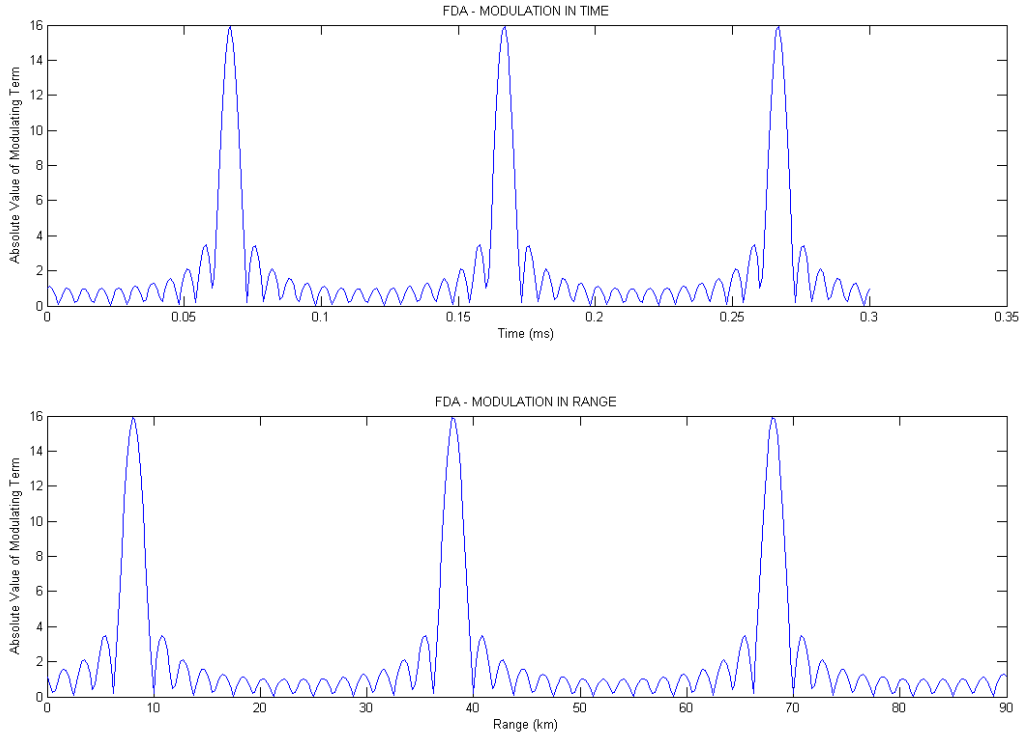


**Figure 3.3: Periodicity in time and range for an FDA array with 16 elements (uniform weighting) and  $\Delta \omega = 2\pi 10^4$  Hz**

The null-to-null interval of the pulses is another parameter of interest especially in radar calculations. Using  $\frac{N\varphi}{2} = m\pi$ , the null-to-null interval of the pulse is found to be

$$\Delta t_{null-to-null} = \frac{4\pi}{N\Delta\omega} = \frac{2\pi}{N\Delta f} \quad (3.26)$$

Up to this point, the array amplitude weightings were assumed to be uniform and the simulations and calculations resulted in beam patterns shown in Figure 3.3, having -13dBc side lobes. In fact, the weightings associated with the antennas can be arranged to decrease the side lobes with the cost of increased beam widths (as in the beam shaping techniques of conventional phased arrays [1]). Some simulations throughout the thesis will be using weighted antennas having low side lobes and the reader will be acknowledged during demonstrations.

### 3.1.4 Physical Explanation of the Mechanism

The FDA concept utilizes the fact that each antenna element in the array is excited with different frequencies and the time periodicity and range periodicity has a direct relation with the frequency difference between consecutive antennas in the array. Also, during derivations, it was assumed implicitly that at  $t = 0$  all frequency components over the aperture of the array are in-phase but due to differences in frequencies, the points where the frequency components become in-phase will depend on the position in space and the time of travel of wave components from the antenna to the aforementioned point in space. The points where the frequency components are in phase which other, (3.22) is satisfied, the beam peaks are observed in space. The interference is an easy-to-understand phenomenon with a basic example as shown in Figure 3.4, where 4 waves with frequencies of 100Hz, 150Hz, 200Hz and 250 Hz are superimposed on the same graph. Note that  $\Delta\omega = 2\pi 50\text{Hz}$  requiring 0.02 seconds of beam periodicity in time according to (3.23), is visible also in Figure 3.4.

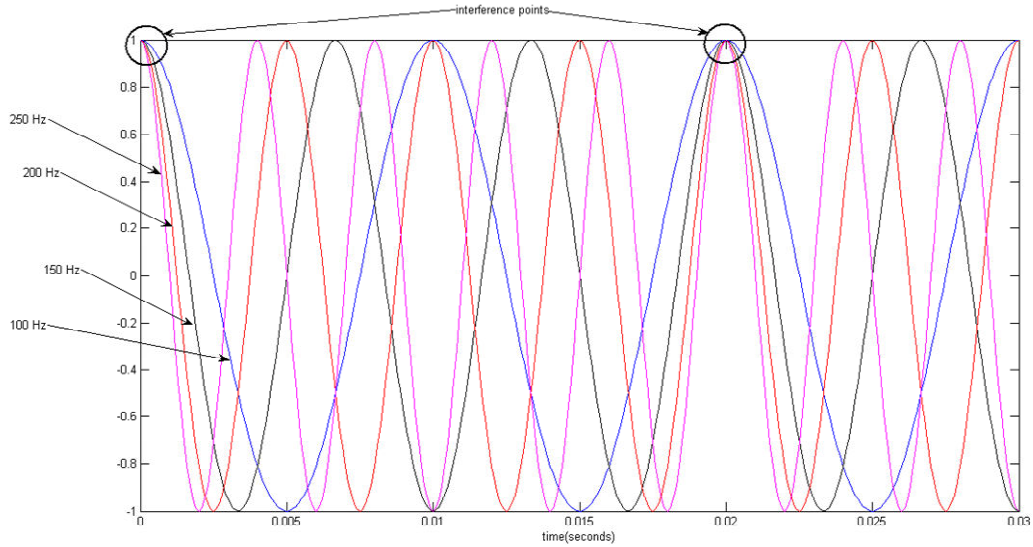


**Figure 3.4: Interference of 4 waves having frequencies 100Hz, 150Hz, 200Hz, 250Hz. Note the interference points in time.**

The modulation in time also requires modulation in range since the wave components travel in space with velocity of light. Because of this, periodicity in range is just the product of velocity of wave components,  $c$ , with the periodicity in time as apparent from (3.23) and (3.24).

The angle dependency is mainly due to the inter-element spacing. For different observation point angles, points of interference should shift since, for each angle of interest, the wave components from each antenna element would experience different delays (from (3.1), (3.2) and (3.3),  $k(n)R_n$ ) and the time of interference will shift in such a way to compensate for the extra delay.

So what is going on in 2-D space during radiation? The answer is beam-bending or spiral-like radiation pattern at any time instant. In the thesis, it is impossible to show the video of array patterns in time, but simulation of the mechanism at some time instants is still possible. Figure 3.5 shows an array pattern simulation result of FDA at a specified instant ( $t=181$  us) for 0-50 km broadside range and in cross-sides -25 to 25km (The  $1/R_0$  term in (3.19) is ignored). The array has 10 elements and the starting frequency of the array is 10GHz with inter-element frequency steps of 15 kHz. The interference points are shaded in the figure and note the beam bending.

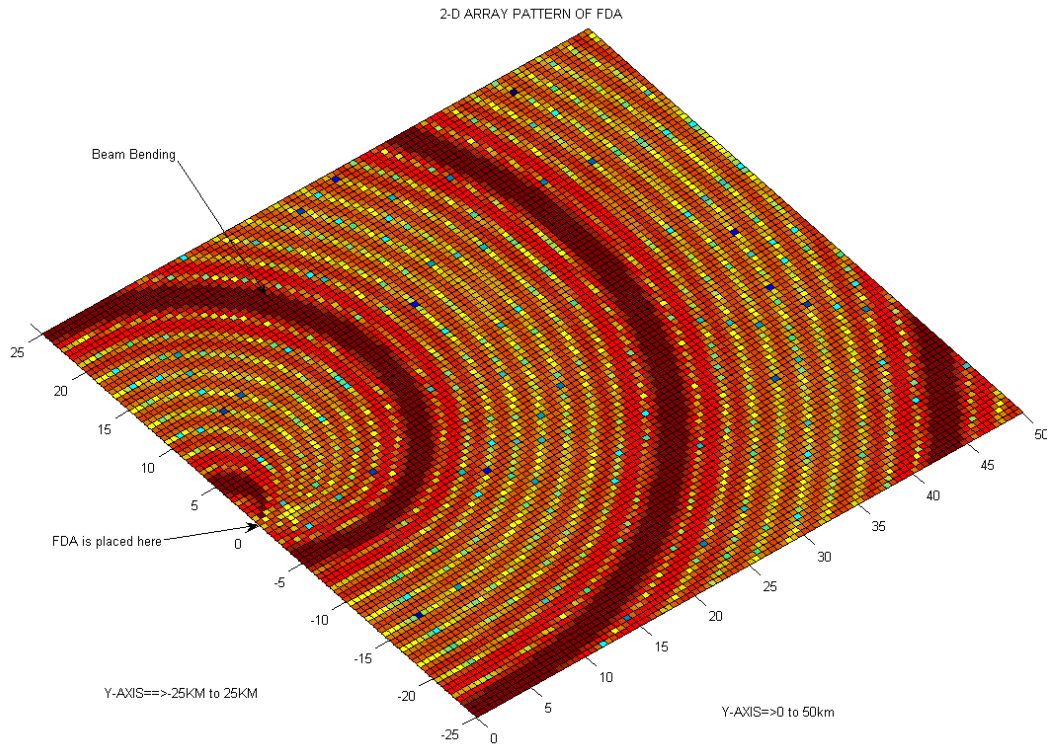


**Figure 3.5: 2-D simulation of an FDA. FDA starting frequency is 10GHz with inter-element frequency spacing of 15 kHz. There are 10 antennas in the array with uniform weighting on the antennas. Note that there is a beam bending in 2-D space**

In Figure 3.6, the simulation of the same FDA at various time instants are shown. In this simulation a beam period is sampled at 6 time points and the propagation of beam peaks can be viewed as time passes. The far field pattern at  $t = 670 \text{ us}$  and  $t = 737 \text{ us}$  are the same since  $67 \text{ us}$  is one period of the main beam.

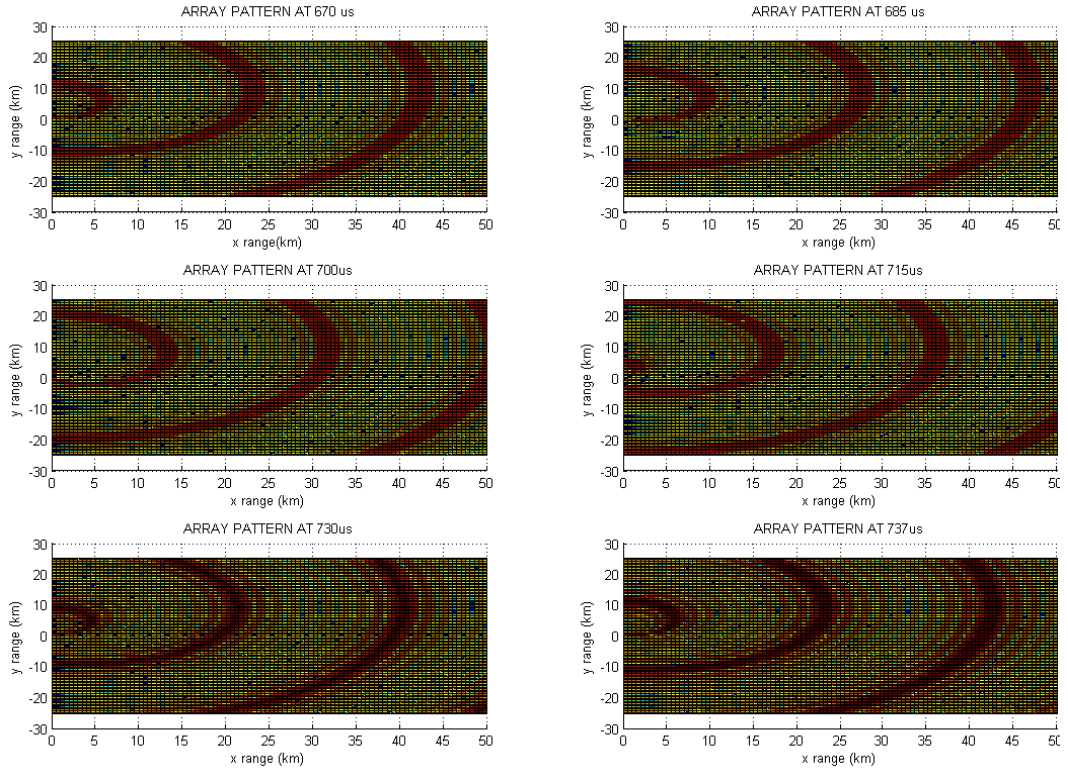


**Figure 3.6: FDA far field array pattern plots for various time instants. The simulation instants are taken to be in one period, so the first and last plots are the same ones although they are taken at different times.**

## 3.2 LFM CW BASED FDA ANALYSIS

In this section, far field array pattern of a LFM CW based FDA will be derived in time domain. First, a problem definition will be supplied and derivations will be done. The analysis of the problem will be similar to the ones performed for the conventional FDA.

### 3.2.1 Problem Definition

In LFM CW based FDA concept, the main aim is to supply the antennas with the stepped frequency changes. The technique gets its roots from the fact that the LFM CW source frequency changes as time advances, but at the same time as time advances, the wave from the sources propagates on a TEM line. If proper sampling points on the TEM line are chosen, periodic step frequencies can be provided to all antennas in the array. The main difference is the continual change

of the center frequency of operation in the array, but even this property of the array can be very beneficial in terms of frequency diversity of radars (which will be discussed in subsequent chapters).

First step is the explanation of the LFMCW source frequency dynamics. It is assumed to be linear with time as shown in Figure 3.7. Here the instantaneous frequency of the waveform is:

$$\omega = \omega_0 + mt \quad (3.27)$$

where  $\omega_0$  is the starting frequency of the waveform and  $m$  is the slope of the frequency line. So the phase of the waveform will be [34]:

$$\varphi = \int \omega dt = \omega_0 t + \frac{m}{2} t^2 + \varphi_0 \quad (3.28)$$

and the output of the source in phasor form becomes

$$W = ae^{j\left(\omega_0 t + \frac{m}{2} t^2 + \varphi_0\right)} \quad (3.29)$$

where  $a$  is the amplitude of the waveform and  $\varphi_0$  is a constant phase term.

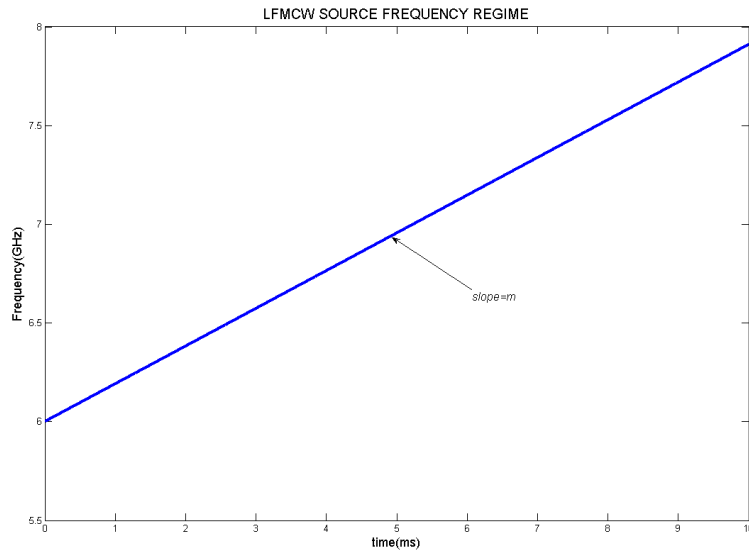


**Figure 3.7: LFMCW source frequency regime**

In Figure 3.8, the FDA configuration for the solution is shown. The radiation part of the plot is similar to the one for conventional FDA, but the setup of the array is different. The source is LFM CW as explained in (3.29), and each antenna in the array has a different delay from the source. Equation (3.28) defines the frequency dynamics of the LFM CW source and the delay to each antenna element also defines a unique instantaneous frequency at each antenna element. Using (3.29), the instantaneous waveform at each antenna can be defined as:

$$W_n = a_n e^{j\left(\omega_0(t-t_n) + \frac{m}{2}(t-t_n)^2\right)} \quad (3.30)$$

where in this equation the constant phase term is assumed to be zero ( $\varphi_0 = 0$ ). The delay to each antenna is defined to be  $t_n$ , where  $n$  is the index of the antenna starting from 0 increasing up to  $N-1$ . The delay elements are defined to be ideal with no losses or distortion (in practice the losses or unequal power divisions between the antenna elements may be utilized for lowered side-lobe in far-field patterns). Also, Figure 3.8 does not show the phase shifters in the line but in the formulation of array patterns, a stepped phase shift between the antenna elements will be assumed to exist (included in the beam-former of Figure 3.8). In the subsequent chapters the benefits of these phase shifting elements will be discussed.

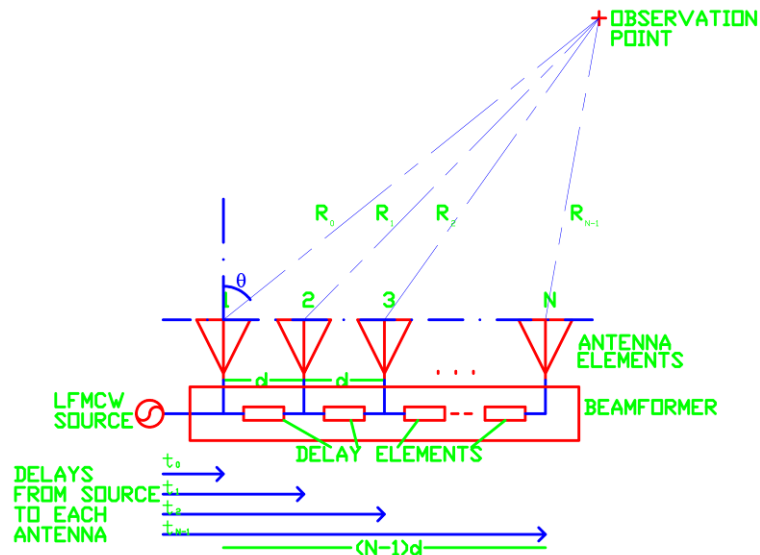


**Figure 3.8: Problem Definition for LFM CW based FDA concept. Note that each antenna has a different amount of delay to the source, and this delay will cause a frequency shift of excitation between the antenna elements**

### 3.2.2 Mathematical Analysis of Array Pattern

For the mathematical analysis, the weights of each antenna are taken as (3.30) and (3.1) is rewritten for the new scenario.

$$E_A = \sum_{n=0}^{N-1} \left( \frac{a_n}{R_n} e^{j\left(\omega_0(t-t_n) + \frac{m}{2}(t-t_n)^2\right)} f_e(\omega_0 + m(t-t_n)) \right) e^{-j(k_n(t)R_n)} e^{-jn\delta} \quad (3.31)$$

In this equation;

$a_n$  : Weight of each antenna element

$R_n$  : As defined in (3.2), but take as  $R_0$  in amplitude sense

$\theta$  : As defined in Figure 3.8

$\omega_0$  : Starting frequency

$m$  : Frequency Regime Slope

$t_n$  : delay to the  $n^{\text{th}}$  antenna

$$k_n(t) = \frac{\omega_0 + m(t-t_n)}{c} : \text{Wave-number at antenna } n \text{ and at } t \quad (3.32)$$

$\delta$  : The phase difference between consequent antennas

$f_e(\omega_0 + m(t-t_n))$ : Element pattern at antenna  $n$  and at frequency  $\omega_0 + m(t-t_n)$

Now, for the ease of derivations assume that  $a_n = 1$  for all antenna elements. Also,  $f_e(\omega_0 + m(t-t_n))$  is same for all frequencies and equal to 1 (so the last equation that will be reached will be the array factor of FDA). Next, assume that the delay between the source and antenna  $n$  is  $nT$ .

$$t_n = nT \quad (3.33)$$

So in this case, the inter-element delay is defined to be  $T$ , which is in fact a critical design parameter of the system. Now (3.31) can be rewritten as follows:

$$E_A = \frac{1}{R_0} \sum_{n=0}^{N-1} e^{j\left(\omega_0(t-nT) + \frac{m}{2}(t-nT)^2\right)} e^{-j\left(\left(\frac{\omega_0 + m(t-nT)}{c}\right)(R_0 - nd \sin(\theta))\right)} e^{-jn\delta} \quad (3.34)$$

The phase term in (3.34) is

$$\phi = \omega_0(t-nT) + \frac{m}{2}(t-nT)^2 - \left(\frac{\omega_0 + m(t-nT)}{c}\right)(R_0 - nd \sin(\theta)) - n\delta \quad (3.35)$$

Expanding (3.35)

$$\phi = \omega_0 t - n\omega_0 T + \frac{m}{2}t^2 + \frac{m}{2}n^2 T^2 - mnTt - \left(\frac{\omega_0 R_0}{c} - \frac{\omega_0 nd \sin(\theta)}{c} + \frac{mR_0 t}{c} - \frac{mR_0 nT}{c} - \frac{mntd \sin(\theta)}{c} + \frac{mn^2 Td \sin(\theta)}{c}\right) - n\delta \quad (3.36)$$

Now we can group the terms in (3.36) according to dependency on n. So, the terms in the summation will have the n-dependency while the other terms can be moved out of the summation.

$$\phi = \omega_0 t + \frac{m}{2}t^2 - \frac{\omega_0 R_0}{c} - \frac{mR_0 t}{c} + n \left( -\omega_0 T + \frac{m}{2}nT^2 - mTt + \frac{\omega_0 d \sin(\theta)}{c} + \frac{mR_0 T}{c} + \frac{mtd \sin(\theta)}{c} - \frac{mnTd \sin(\theta)}{c} - \delta \right) \quad (3.37)$$

Rewriting (3.34) and rearranging the terms, we will get the expression shown in (3.38). The term outside the summation is the CW signal at the observation point. Note that the instantaneous frequency of this CW signal is also affected by the time advance while traveling  $\frac{R_0}{c}$ . The terms inside the summation forms the amplitude modulation effect as will be analyzed in this text.

$$E_A = \frac{1}{R_0} e^{j\left(\omega_0 t + \frac{m}{2} t^2 - \frac{\omega_0 R_0}{c} - \frac{m R_0 t}{c}\right)} \sum_{n=0}^{N-1} e^{jn\left(\frac{-\omega_0 T - mtT + \frac{m}{2} nT^2 + \frac{\omega_0 d \sin(\theta)}{c} + \frac{mTR_0}{c} + \frac{md \sin(\theta)t}{c} - \frac{mnTd \sin(\theta)}{c} - \delta\right)} \quad (3.38)$$

To clarify this last equation, let's produce some more variables. So we can go on analysis over these new variables.

$$U(t) = \frac{1}{R_0} e^{j\left(\omega_0 t + \frac{m}{2} t^2 - \frac{\omega_0 R_0}{c} - \frac{m R_0 t}{c}\right)} \quad (3.39)$$

$$\varphi(n, t) = -\omega_0 T - mtT + \frac{m}{2} nT^2 + \frac{\omega_0 d \sin(\theta)}{c} + \frac{mTR_0}{c} + \frac{md \sin(\theta)t}{c} - \frac{mnTd \sin(\theta)}{c} - \delta \quad (3.40)$$

In (3.39) and (3.40), the new variables are shown to be functions of only n or t. It is clear that there are other variables of interest in these equations, but for this time only indexes of antennas and the time will be our concern. Using (3.39) and (3.40) in (3.38);

$$E_A = U(t) \sum_{n=0}^{N-1} e^{jn\varphi(n,t)} \quad (3.41)$$

Now we can focus on (3.40);

$$\varphi(n, t) = \frac{mT}{c} (R_0 - nd \sin(\theta)) + \left(\frac{\omega_0 + mt}{c}\right) (d \sin(\theta) - cT) + \frac{m}{2} nT^2 - \delta \quad (3.42)$$

$$\varphi(n, t) = \frac{mT}{c} \left(R_0 - nd \sin(\theta) + \frac{cnT}{2}\right) + \left(\frac{\omega_0 + mt}{c}\right) (d \sin(\theta) - cT) - \delta \quad (3.43)$$

In (3.43), some assumptions need to be made to ease the remaining equations. (3.43) is the phase part in (3.41) and while making the assumptions, some cautions should be taken. The phase part of the expression is  $2\pi$  periodic, so any term in the exponent have effect on the result. Here some assumptions are used with possible results of these assumptions.

Firstly, assume that, in (3.43),  $R_0 \gg \frac{ncT}{2}$ . The consequence of this assumption is a deviation from the expected amplitude modulated waveform. But, note that  $\frac{ncT}{2}$  is a constant term, that is, the inter-element delay is a constant term which is designed according to beam scanning parameters.

Another, and more critical, assumption can be reached as follows. In (3.43), gather the terms depending on  $\sin(\theta)$  together to get:

$$\begin{aligned}\varphi(n, t)_\theta &= \sin(\theta) \frac{d}{c} (-mnT + \omega_0 + mt) \\ &= \sin(\theta) \frac{d}{c} (\omega_0 + m(t - nT))\end{aligned}\quad (3.44)$$

In the last equation both the  $\theta$  dependent term and time dependent term are being multiplied indicating a cross relation in between. Here  $nT$  term is a constant and the time is the variable and time is delayed by  $nT$ , for each antenna element. Ignoring  $nT$  in the derivations will definitely cause deformation in the pulse shapes at larger observation point angles. Especially the position of nulls and side lobe peak values may change due to this assumption, but the deformation is minimal considering simulations.

Utilizing the last two assumptions, (3.43) can be rewritten as follows (in this equation, there is no  $n$  dependence but as a continuum for (3.43), this variable is added to the definition):

$$\varphi(n, t) = \frac{mT}{c} R_0 + \left( \frac{\omega_0 + mt}{c} \right) (d \sin(\theta) - cT) - \delta \quad (3.45)$$

Now, (3.41) can be rewritten;

$$E_A = U(t) \sum_{n=0}^{N-1} e^{jn\varphi(t)} \quad (3.46)$$

At this point, it can be said that (3.46) resembles (3.15), providing similar results to the conventional FDA case. Expanding (3.46);

$$E_A \cong \frac{1}{R_0} e^{j\left(\omega_0 t + \frac{m}{2} t^2 - \frac{\omega_0 R_0}{c} - \frac{m R_0 t}{c}\right)} \sum_{n=0}^{N-1} e^{jn\left(\left(\frac{\omega_0 + mt}{c}\right)(d \sin(\theta) - cT) + \frac{m T R_0}{c} - \delta\right)} \quad (3.47)$$

Rearranging (3.47) an equation similar to (3.17) can be reached.

$$E_A \cong \frac{1}{R_0} e^{j\left(\omega_0 t + \frac{m}{2} t^2 - \frac{\omega_0 R_0}{c} - \frac{m R_0 t}{c} + \frac{N-1}{2} \varphi\right)} \frac{\sin\left(\frac{N\varphi}{2}\right)}{\sin\left(\frac{\varphi}{2}\right)} \quad (3.48)$$

The phase of the carrier is:

$$\phi_c = \omega_0 t + \frac{m}{2} t^2 - \frac{\omega_0 R_0}{c} - \frac{m R_0 t}{c} + \frac{N-1}{2} \left( \left( \frac{\omega_0 + mt}{c} \right) (d \sin(\theta) - cT) + \frac{m T R_0}{c} - \delta \right) \quad (3.49)$$

According to (3.49), the resulting carrier signal is again a linear frequency modulated wave, but this wave is also amplitude modulated in time as evident in

(3.48). The frequency of modulation is  $\omega_0 + mt - \frac{m R_0}{c} + \frac{N-1}{2} \frac{m}{c} (d \sin(\theta) - cT)$ .

In this expression, the last term comes from the modulation part of (3.48), since the array reference point is taken to be on the first antenna of the array instead of middle point, this term can be ignored. Also, note that this last term is very small when compared to  $\frac{m R_0}{c}$  term. The result is similar to FM chirps, where the envelope here is mainly determined by the arrangement of antennas (physical placement, inter-element spacing and delay) and parameters of LFMCW feed (starting frequency of excitation and slope of the frequency regime) all of which are clear in (3.45).

In the next subsection, the amplitude modulation term of (3.48) will be at the focus of the derivations, since beam scanning parameters of the FDA are mainly contained in this modulation part of the expression. The carrier part is in fact a replica of the source wave as shown in (3.49).

### 3.2.3 Extraction of Design Parameters

Equation (3.45) is rewritten below for convenience.

$$\varphi(n, t) = \frac{mT}{c} R_0 + \left( \frac{\omega_0 + mt}{c} \right) (d \sin(\theta) - cT) - \delta$$

In this equation, for  $\frac{\varphi}{2} = p\pi$ ,  $p \in \mathbb{N}$ , the modulation is periodic. Similarly for  $\frac{N\varphi}{2} = p\pi$ ,  $p \in \mathbb{N}$ ,  $p \neq 0$ , the modulation has nulls, but this time, the dependency is affected by other parameters of FDA. The points in space and time where (3.45) is equal to  $m\pi$ , the pulse peaks can be observed similar to the conventional FDA case, and there are infinite possible solutions at a given time.

The period in time can be found by equating (3.45) to  $p\pi$  and solving the two equations for consecutive values of  $p$ . The period in time can be found to be:

$$\Delta t = \frac{2\pi c}{m(d \sin(\theta) - cT)} \quad (3.50)$$

In (3.50), the inter-element delay,  $T$ , is a system parameter and in this study, the implementations of the delay are performed with micro-strip lines between the antenna elements. In this case, the effective dielectric constant and length of the interconnect lines are effective in the designation of the delay between the antenna elements. For the derivations, assume that:

$$cT = sd \quad (3.51)$$

Using (3.51) in (3.50);

$$\Delta t = \frac{2\pi c}{msd \left( \frac{\sin(\theta)}{s} - 1 \right)} \quad (3.52)$$

or

$$\Delta t = \frac{2\pi}{mT \left( \frac{\sin(\theta)}{s} - 1 \right)} \quad (3.53)$$

Equation (3.53) is a negative number, and the right way to treat the delay is to treat it as a positive number. A better way to show (3.53) is to write it as in (3.54).

$$\Delta t = \left| \frac{2\pi}{mT \left( \frac{\sin(\theta)}{s} - 1 \right)} \right| \quad (3.54)$$

In (3.54), remembering T to be the inter-element delay and  $\Delta\omega = mT$ , this equation can be modified as:

$$\Delta t = \left| \frac{1}{\Delta f \left( \frac{\sin(\theta)}{s} - 1 \right)} \right| \quad (3.55)$$

Further assume that

$$\hat{k}(\theta, s) = \left| \left( \frac{\sin(\theta)}{s} - 1 \right) \right| \quad (3.56)$$

And (3.55) becomes

$$\Delta t = \frac{1}{\Delta f \hat{k}(\theta, s)} \quad (3.57)$$

The inter-element delay can be made large compared to the inter-element distance.

So,  $\hat{k}(\theta, s)$  can be made equal to approximately unity ( $\hat{k}(\theta, s) \approx 1$ ). In this case, (3.57) turns into the known formula from (3.23):

$$\Delta t \cong \frac{1}{\Delta f} \quad (3.58)$$

Using similar arguments, the periodicity in range would be found similar to (3.24).

$$\Delta R = \frac{c}{\Delta f} \quad (3.59)$$

The periodicity in  $\sin(\theta)$  has important properties. It depends on the time of arrival of frequency components to the observation point and can be written as in (3.60). This result is similar to (3.25) but this time the operating frequency changes dynamically causing the wave-number expression in (3.25) to change continuously. This is an important property of the structure, since discrete angles of observation (and ranges) are scanned by discrete frequency components which can be changed by careful utilization of stepped phase change between the antenna elements,  $\delta$  between the antenna elements.

$$\Delta \sin(\theta) = \frac{2\pi c}{d(\omega_0 + mt)} \quad (3.60)$$

The null-to-null interval of the pulse can be found by equating (3.45) to  $\frac{2p\pi}{N}$ ,  $p \in \mathbb{N}$ ,  $p \neq 0$ .

$$\Delta t_{null-to-null} = \left| \frac{4\pi c}{mN(d \sin(\theta) - cT)} \right| \quad (3.61)$$

Using (3.51) and (3.56) in (3.61),

$$\Delta t_{null-to-null} = \frac{4\pi c}{mNs d \hat{k}(\theta, s)} \quad (3.62)$$

Since  $\Delta\omega = mT$  (inter-element frequency steps) and  $sd = cT$ , (3.62) can be further simplified by making the appropriate modifications:

$$\Delta t_{null-to-null} = \frac{2}{N\Delta f \hat{k}(\theta, s)} \quad (3.63)$$

Finally, noting (3.56) and assuming that the inter-element delay is large, ( $s \gg 1$ ), a handy rule of thumb can be derived for calculations:

$$\Delta t_{null-to-null} \cong \frac{2}{N\Delta f} \quad (3.64)$$

In Figure 3.9, the periodicity in range and time are shown. Note that, since the elements are uniformly weighted, the waveforms have high side lobes following the sinc-pattern as shown in Figure 3.3. For the simulation 10 antennas are used at 10GHz. The inter-element spacing is 25 mm and inter-element delay is

0,83 ns. The slope of the LFM CW source frequency regime is  $2\pi 10^{13} \text{ Hz}^2$  causing the inter-element frequency to be 10,472 KHz. The observation angle for both cases is selected as  $-5^\circ$  off broad-side. The first plot is generated at 6,1 us for 0 to 50km range, while the second plot for 0 to 16ms at 24,75km. The results of these simulations are in harmony with (3.58), (3.59) and (3.64).

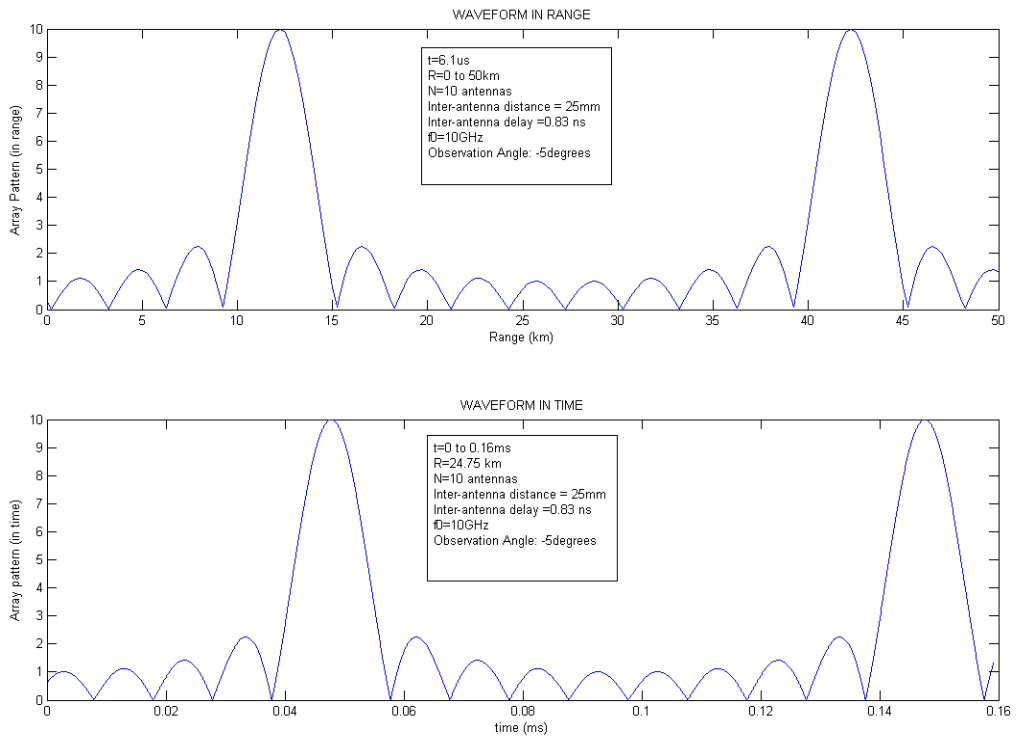


**Figure 3.9: Periodicity in range and time is shown for two different simulations. The parameters of the simulation are shown on the plots. The slope of the frequency regime is selected to be  $2\pi 10^{13} \text{ Hz}^2$ .**

So what will be the total frequency shift experienced by the LFM CW source? To answer this question, Figure 3.7 can be plotted in Figure 3.10 again.

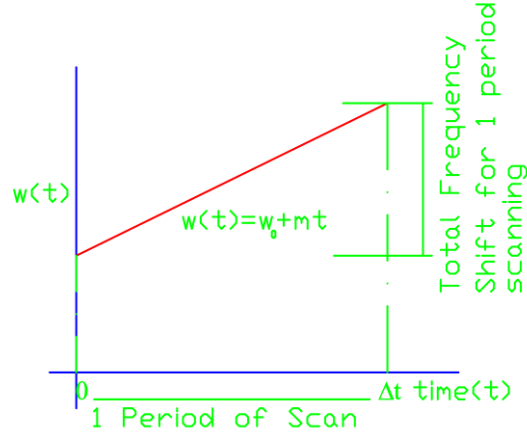


**Figure 3.10: LFM CW frequency regime in one period of scanning**

According to Figure 3.10, for a full scanning of 360 degrees, one period of scan should be achieved and for one scan the total frequency shift from the LFM CW source will be (using (3.57)):

$$\Delta W = m\Delta t = \frac{m}{\Delta f \hat{k}(\theta, s)} \quad (3.65)$$

Also,  $\Delta f = mT$ , the inter-element frequency difference due to the inter-element delay. Using this equation in (3.61):

$$\Delta W = \frac{2\pi}{T \hat{k}(\theta, s)} \quad (3.66)$$

Equation (3.62) states that, for each angle of observation in space, we need to specify a distinct frequency shift at LFM CW source for one period of scan through that direction. As mentioned before,  $\hat{k}(\theta, s)$  can be made close to unity by selecting longer delay with respect to inter-element delay, thus (3.62) would be approximately as shown in (3.63) and (3.64). This result is useful in terms of engineering design.

$$\Delta W \cong \frac{2\pi}{T} \quad (3.67)$$

$$\Delta F \cong \frac{1}{T} \quad (3.68)$$

If the total frequency shift of LFMCW is increased over the value in (3.64), some points in space will be scanned by more than one frequency component, which is also a beneficial property in terms of frequency diversity. Especially, the phase shifters at each antenna can be used for selective scanning of space with more than one frequency.

### **3.2.4 Comparison with Conventional FDA in terms of Design**

Up to this point, during derivations some comparisons are made, but here a summary of these will be repeated. The periodicity derivations found for LFMCW based FDA were reported in (3.58) - (3.60). These equations are similar to the equations found for conventional FDA, (3.23), (3.24) and (3.25). The important thing here is that, although the periodicity parameters hold mathematically, physically every point in space is scanned with a discrete frequency from LFMCW source and this result is a great advantage of the LFMCW based FDA concept. The scanning properties can be easily adapted for a new scenario by adapting a different frequency regime at the source, or by just changing phase shifter settings at each antenna. Focusing (selecting an angular sector) in space is also possible by selecting unique frequency intervals and unique phase settings at each antenna element. In a radar application, by adapting different FDA at transmitter site and receiver site, focusing at space is also possible (details can be found in Chapters 5, 6 and 7). The selection of inter-element delay is also a design constraint where this parameter specifies the total frequency shift at the source for a full scan through any angular portion of space, but reasonable values can be possible by conventional microwave elements. By increasing the total frequency shift, some points in space can be scanned with more than one frequency component and this diversity increases the resistance to multi-path interferences (in subsequent chapters, this notion will be encountered again). Note that only the excitation properties of LFMCW source and phase settings of all phase shifters at each antenna channel are altered to accomplished the so-said properties of the array.

In conventional FDA, similar features presented by LFMCW based FDA can be reached by altering center frequency of operation and  $\Delta f$  between the

antenna elements, but at a higher cost. Besides, the resistance to multi-path effects would be limited in conventional FDA unless expensive hardware (wideband synthesizers or frequency converters) are used.

The easiness presented by LFMCW based FDA is attractive in implementation sense. A draw-back of the technique is the requirement of control of time and instantaneous frequency of the LFMCW source and a careful calibration of the system, but with advancing digital technologies, control of system at high clock frequencies is possible (in this study, basic measurement techniques are applied in laboratory tests, and some sketches are reported for demonstration purposes.).

### **3.2.5 Physical Explanation of the Mechanism**

The delay experienced by the waves when traveling from the source to each antenna, and stepped delays from the source to consequent antennas causes each antenna to radiate stepped frequency waves as aimed at the conventional FDA design. As mentioned earlier, the points where (3.45) is equal to  $m\pi, m \in \mathbb{Z}$ , the wave has its peaks similar to Figure 3.3. This mechanism is mainly responsible for the amplitude modulation effect. So, similar arguments encountered in conventional FDA is also true for LFMCW based FDA but the continuous change of frequency from LFMCW source implements the dynamic feature of the scanning technique.

The amplitude modulated LFM waveform is what is seen at the observation point according to (3.48). The instantaneous time, range and angle of observation are the main factors determining the instantaneous amplitude of the modulated waveform and the instantaneous time of observation at this point specifies the instantaneous frequency. The main lobes of the waveform shown in Figure 3.9 are the pulses at the observation point. Besides, the side lobes in the so-said figure can be decreased more by selecting specialized amplitude weightings at the antenna elements (Chebyshev, Taylor One Parameter or Taylor #...).

The final demonstration for this subsection is about the 2-D array radiation pattern at specific times, showing the beam bending effect similar to that observed in conventional FDA (Figure 3.11).

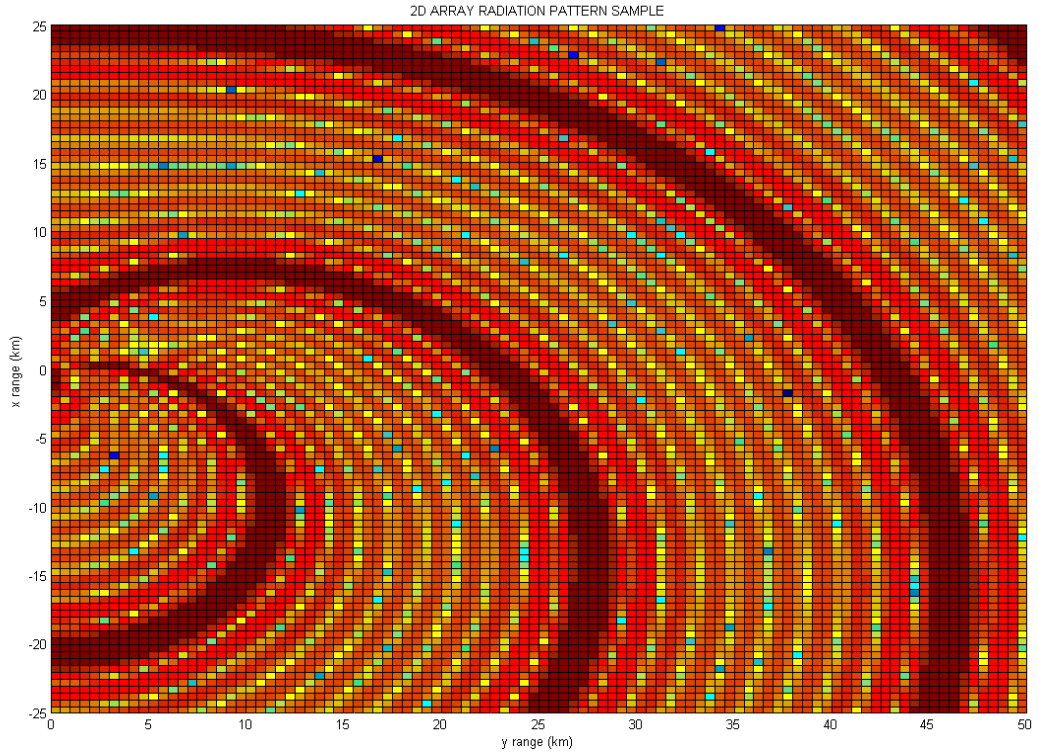


**Figure 3.11: A sample radiation pattern in 2D for an LFMCW based FDA. Details are in the text**

The plot in Figure 3.11 is generated with an LFMCW based FDA simulation where there are 10 antenna elements with 25mm of inter-element spacings. The inter-element delay is 0.83ns and the slope of the LFMCW frequency line regime is selected such that inter-element frequency difference becomes 15 kHz. In the simulation, the antenna array is placed at the origin and the simulation is performed for 0-50 km broadside range -25 to 25km cross-side range (The  $1/R_0$  term in (3.19) is ignored in the simulation for demonstration purposes). Starting frequency of the sweep is 10GHz and the time of generation of the plot is 348.3us.

Below, Figure 3.12 is another plot from the same simulation showing the propagation of waves at 6 time instants. The time instants are selected such that all of them are in one period defined by (3.58), so the last plot and the first plot are the same. Also, note that the beam bending phenomena encountered in

conventional FDA system is also a characteristic property of LFMCW based FDA concept and is readily visible in Figure 3.12.

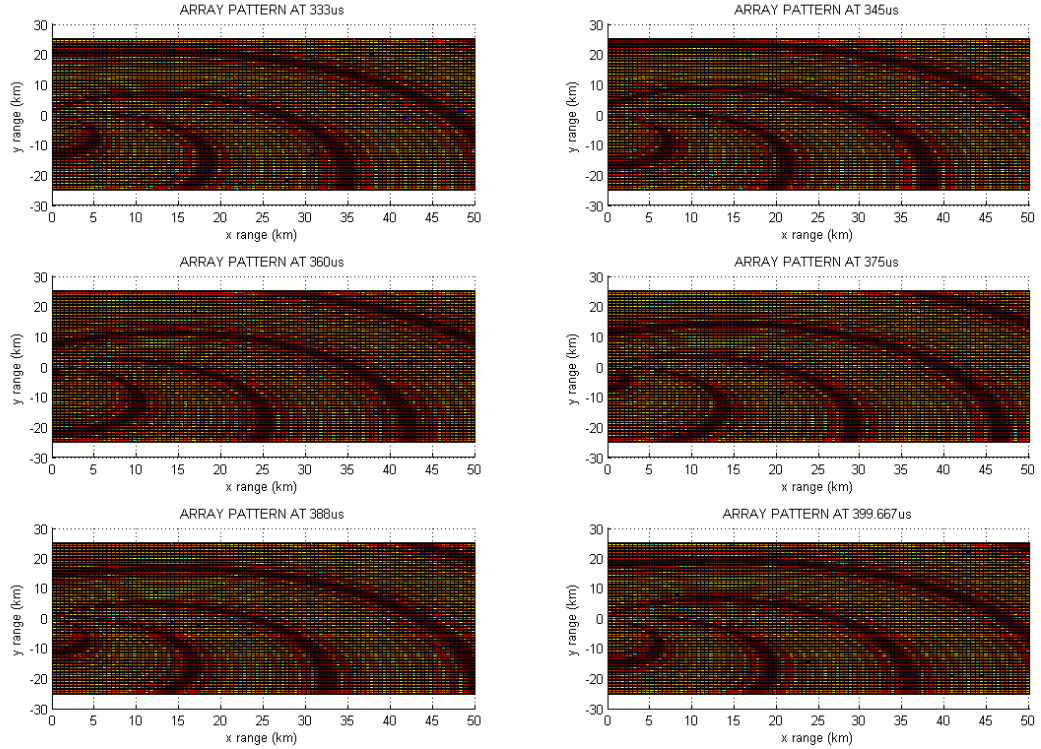


**Figure 3.12: LFMCW based FDA far field array pattern plots for various time instants. The simulation instants are taken to be in one period, so the first and last plots are the same ones although they are taken at different times.**

Up to this point, the mathematical derivations of FDA and LFMCW based FDA are shown and qualitative descriptions for the underlying mechanisms are presented. A point of confusion about the LFMCW based FDA arises from the frequency scanning required at the LFMCW source; which resembles the frequency scanned antenna concept, but the dynamic frequency character in LFMCW based FDA constitutes the main difference between these two techniques as shown qualitatively in the next section.

### **3.3 DIFFERENCES BETWEEN LFMCW BASED FDA AND FREQUENCY SCANNING**

In this section, frequency scanning concept will be mathematically treated and the governing equations regarding the concept will be presented. Afterwards, a qualitative description on differences between the frequency scanning concept and LFMCW based FDA will be demonstrated.

#### **3.3.1 Analysis of Frequency Scanning**

Frequency scanning is another steering mechanism as described in 2.2 and 2.4.2. The main aim is to steer the antenna main beam by changing the frequency of excitation of the source. There is no time domain relation, all antennas are excited by the same wave (at the determined frequency) but at shifted phase due to frequency change (due to inter-element delay or a phase shift at a specific frequency). In the following subsections, this notion will be analyzed mathematically.

##### **3.3.1.1 Problem Definition**

In Figure 3.13, a case for the mathematical derivation of frequency scanning is shown schematically [1], [4]. According to the figure two antennas are placed on a line with inter-element spacing of  $d$ . One of the antennas has a phase shifter (any kind of phase control element) as a control element before the combiner. In the structure three points are defined for the derivation of the incoming wave and it is assumed that the phase shift provided by the phase shifter is defined at a single frequency (like a delay element, whose phase shift is dependent on the frequency of excitation) [4]. Point P1 is just after the first antenna at left, point P2 is after the phase shifter and finally point P3 is at the terminals of the second antenna on the right side. In this problem the interference of incoming waves from both antennas will be analyzed and the beam tilting will be formulated.

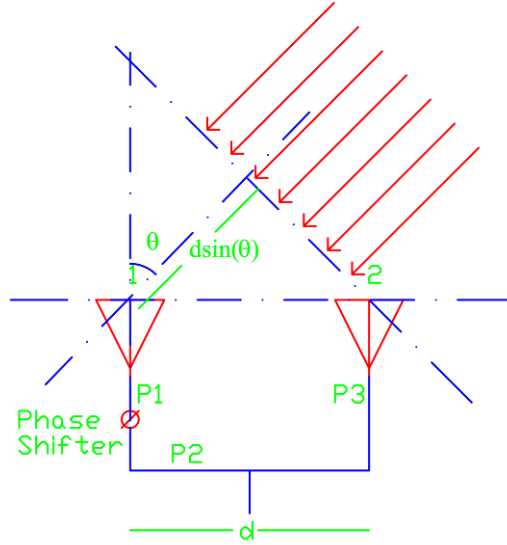


Figure 3.13: Problem definition for Frequency Scanning Formulation

### 3.3.1.2 Analysis

From Figure 3.13, it should be noted first that the incoming wave from observation angle  $\theta$  (off broadside); will be delayed by a length of  $d \sin(\theta)$  at the first antenna [4]. So the wave at the terminals of the first antenna becomes (using  $j\omega t$  convention):

$$P1 = e^{j\left(\omega t - \frac{2\pi}{\lambda} d \sin(\theta)\right)} \quad (3.69)$$

while at P3, the incoming wave is;

$$P3 = e^{j(\omega t)} \quad (3.70)$$

assuming the other phase terms at the exponents are all zero and the same amplitude is received at both antenna terminals (for the ease of mathematics).

Besides, the wave at point P2 is:

$$P2 = e^{j\left(\omega t - \frac{2\pi}{\lambda} d \sin(\theta) + \beta_0\right)} \quad (3.71)$$

For in-phase combination of waves at points P2 and P3, the exponents of the fields at these points should be the same requiring [4];

$$-\frac{2\pi}{\lambda} d \sin(\theta) + \beta_0 = 2p\pi, p \in \mathbb{N} \quad (3.72)$$

For  $x = 0$ ,  $\theta = \theta_o$  and  $f = f_o$  (a predetermined frequency), (3.72) can be solved.

So,

$$\beta_0 = \frac{2\pi}{\lambda_o} d \sin(\theta_o) \quad (3.73)$$

Now, using (3.73) in (3.72),

$$\frac{\sin(\theta)}{\sin(\theta_o)} = \frac{f_o}{f} \quad (3.74)$$

can be reached. Differentiating (3.74) [4],

$$\frac{\partial f}{\partial \theta} = -\frac{f_o \sin(\theta_o) \cos(\theta)}{\sin^2(\theta)} \quad (3.75)$$

is found. At  $\theta \approx \theta_o$  and (3.75) becomes

$$\frac{\partial f}{\partial \theta} = -\frac{f_o \cos(\theta_o)}{\sin(\theta_o)} \quad (3.76)$$

or (3.76) can be rearranged to notice the beam tilt as shown in (3.77) [4].

$$\partial \theta = -\frac{\partial f}{f_o} \tan(\theta_o) \quad (3.77)$$

So according to (3.77), a small amount of operating frequency shift would cause a shift in the observation angle proportional to the tangent of instantaneous look angle [4]. In the derivations, no dynamic frequency relations at the antenna elements were used.

### 3.3.2 Differences between the Techniques

As evidenced by (3.69) through (3.77), frequency scanning concept makes use of the static properties of wave and spectral properties of a phase shifting element and do not utilize frequency difference between the antenna elements due to inter-element delay and linear frequency regime of an LFMCW source as encountered in LFMCW based FDA. This dynamic scanning property (in time) of LFMCW based FDA is the main difference between these two techniques.

LFMCW based FDA can be turned into frequency scanned antenna if a digitally controlled source is used whose clock period is much larger than the total delay experienced on a FDA. Figure 3.14 sketches the case.

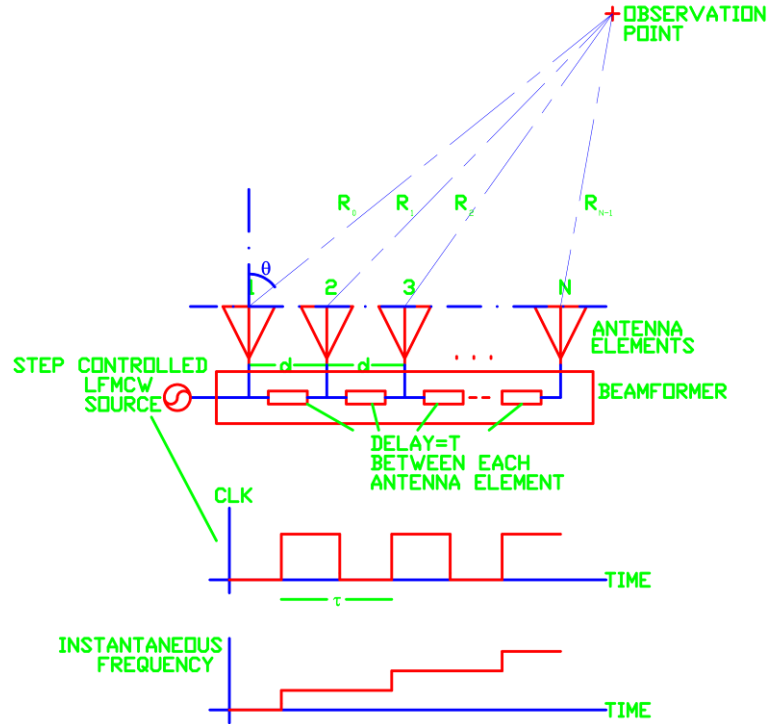


**Figure 3.14: Turning LFMCW based FDA into frequency scanned antenna by controlling the LFMCW source digitally, whose clock period is larger than the total delay in the array.**

According to Figure 3.14, at each period of the clock, the frequency output of the LFMCW source is stepped to a new frequency and if the period of the clock is selected to be longer than the total delay experienced by the wave out of the source, the array is turned into a frequency scanned array. At an instant, all antennas in the array receive the same frequency with the shifted phases due to delay elements in the array. To formulate, the inter-element phase shift due to scanning the antenna towards a predetermined direction can be written as shown in (3.78).

$$\Delta\varphi = kd \sin(\theta) \quad (3.78)$$

and the inter-element phase-shift on the array is

$$\Delta\varphi_{array} = 2\pi fT \quad (3.79)$$

At a frequency of  $f_0$  and a look direction of  $\theta_0$ , (3.78) and (3.79) should be equal to each other for scanning through  $\theta_0$ . But since this is a phase relation and for the requirements of FDA,  $cT \gg d \sin(\theta)$ , (3.57) and (3.58), we should take the phase wrapping into account due to  $2\pi$  periodicity.

$$\text{mod}(2\pi f_0 T, 2\pi) = \frac{2\pi f_0}{c} d \sin(\theta) \quad (3.80)$$

or

$$\text{mod}(f_0 T, 1) = \frac{f_0}{c} d \sin(\theta) \quad (3.81)$$

So for a two element FDA,

$$kd \sin(\theta) - \text{mod}(2\pi f_0 T, 2\pi) = 0 \quad (3.82)$$

And similar to (3.81), (3.82) can be rearranged to find

$$f = \frac{c}{d \sin(\theta)} \text{mod}(f_0 T, 1) \quad (3.83)$$

taking the derivative similar to (3.75)

$$\frac{\partial f}{\partial \theta} = \frac{c}{d} \text{mod}(f_0 T, 1) \left( \frac{-\cos(\theta)}{\sin^2(\theta)} \right) \quad (3.83)$$

and at  $\theta_0$ ;

$$\partial\theta = -\partial f \frac{d}{c} \frac{1}{\text{mod}(f_0 T, 1)} \frac{\sin^2(\theta_0)}{\cos(\theta_0)} \quad (3.84)$$

can be found. This result is found based on Figure 3.14 and uses the fact that at an instant all antennas receive the same frequency from the source, different from LFMCW based FDA notion.

## CHAPTER 4

### FIRST IMPLEMENTATION OF LFMCW BASED FDA

The implementation of the concept stems from Figure 3.8, the hardware required in the so-said figure is implemented for the measurements. According to the figure, a beam former, LFMCW generator, antenna array and a detector would be adequate for the measurements (no phase shifter will be used for all implementations in this thesis). In this chapter, the hardware and the test configuration are explained and the measurements are presented. Lastly, the discussions on the results of the measurements are given.

#### 4.1 REQUIREMENTS FOR THE IMPLEMENTATION

A basic LFMCW based FDA structure is implemented for the justification of mathematical derivations and the demonstration of ease of implementation. The requirements for the implementation are as follows:

- Array size is 4x1. This size is adequate for the first tests.
- The total frequency band of operation is at least 6GHz to 10GHz. The band of interest is important especially in selecting the inter-element delay.
- The inter-element delay is larger than 0.4ns. This corresponds to 2GHz frequency span and smaller than the bandwidth of the array.
- The frequency band of source should cover the total frequency band of interest.

- A wideband detector capable of detecting power values higher than -40dBm.
- The designed antenna and antenna array should cover the frequency band of operation.

The inter-element delay parameter is an important parameter since it limits the total frequency scan limit of the LFMCW source according to (3.68). Besides, the limit found from this equation specifies the total frequency band of the oscillator and the other hardware. Note that the frequency bands should be at least twice the limit set by (3.68), so the frequency diversity can be benefited from in applications.

In the following sections, details about the hardware of the LFMCW based FDA system are presented.

## 4.2 HARDWARE FOR MEASUREMENT

### 4.2.1 Beam former- Divider/Combiner

The beam former circuit is just a divider with 4 output ports. The power division is accomplished with a corporate division and each subsequent arm has an extra delay from the corporate division as shown in Figure 4.1.

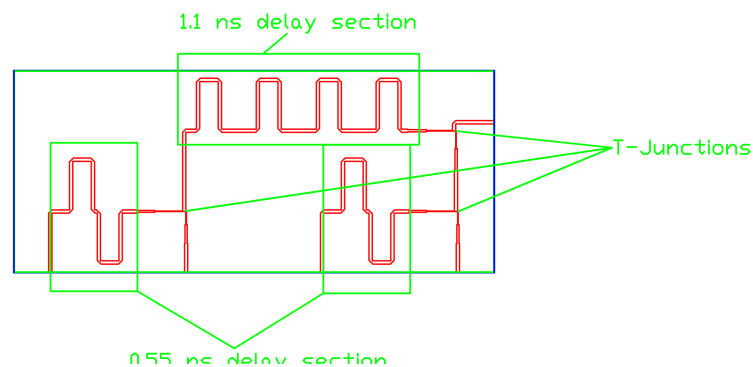


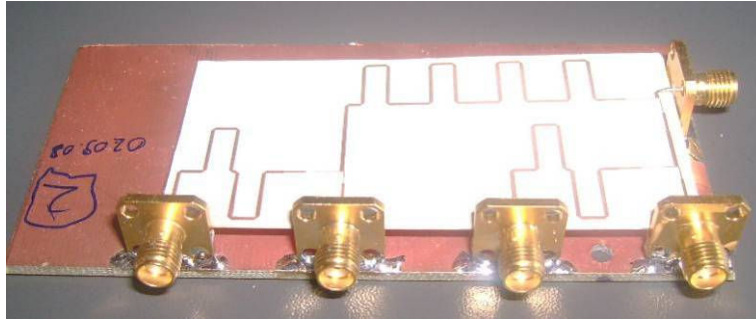
**Figure 4.1 Corporate division and the delay sections. T-junctions are used for power division between the sections of divider and meandered lines accomplish the required delay between the antenna elements.**

For the design of the divider RO6010 is used as the substrate whose dielectric constant is 10.2 with  $\tan(\delta)$  of 0.0023 (at 10GHz) and 25 mil thickness. This dielectric constant is required for the delay of between the antenna elements just by using realizable meandered lines as shown in Figure 4.1. Also, the thickness of the substrate is high for the ability to realize high impedance lines. But note that  $\tan(\delta)$  of the substrate is high causing high loss in the transmission parameters.

There are three two-way dividers (T-junctions [35]) in the structure with each having two sections of matching to the common port, so the bandwidth of operation can be increased to 6GHz-10GHz frequency bandwidth. The junctions are not Wilkinson type dividers, so the output isolation is not so good and the in-band ripple of the divider with respect to frequency is somewhat high. Between the dividers there are meandered sections of line achieving 0.55ns inter-element delay (after some tuning on the board). The so-said T-junctions in the divider are not equal type divider, since  $\tan(\delta)$  of the substrate is high and the leftmost arm in Figure 4.1 receives lower power than the other arms in equal divider case, requiring the dividers to be unequal type. Changing the division ratio at the t-junctions also changes the delays to each antenna and the tuning requires careful inspection of parameters at each stage of design and implementation.

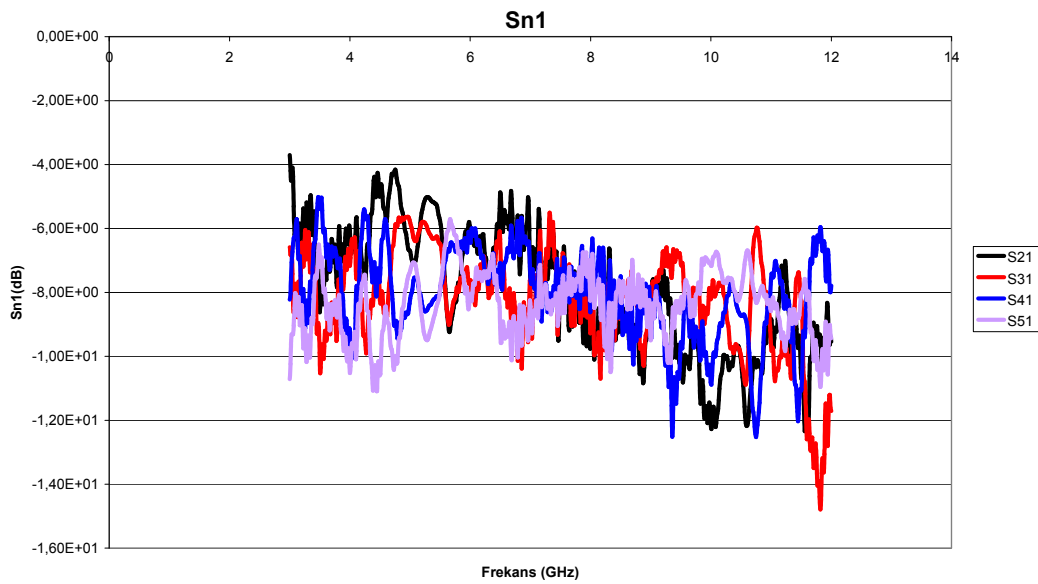
The inter-arm spacing is selected as 25mm, half-wave length at 6GHz (this inter-arm distance is also inter-element spacing as explained in following sections).

Figure 4.2 shows a photograph of the implemented final beam-former. SMA connectors are used at the common and output ports and the board is stiffened with a FR4 substrate below (this supplementary substrate is also useful in decreasing the ground impedance between the SMA connectors). Some of the micro-strip lines on the board are tuned to reach the required group delay requirements.



**Figure 4.2: A photograph of the final beam former with connectors and applied tuning.**

S-parameters of the implemented beam-former are measured with 8510C Network analyzer. The  $S_{n1}(dB)$  and  $S_{11}(dB)$  measurements are shown in Figure 4.3 and Figure 4.4.



**Figure 4.3:  $S_{n1}$  measurements of the beam-former**

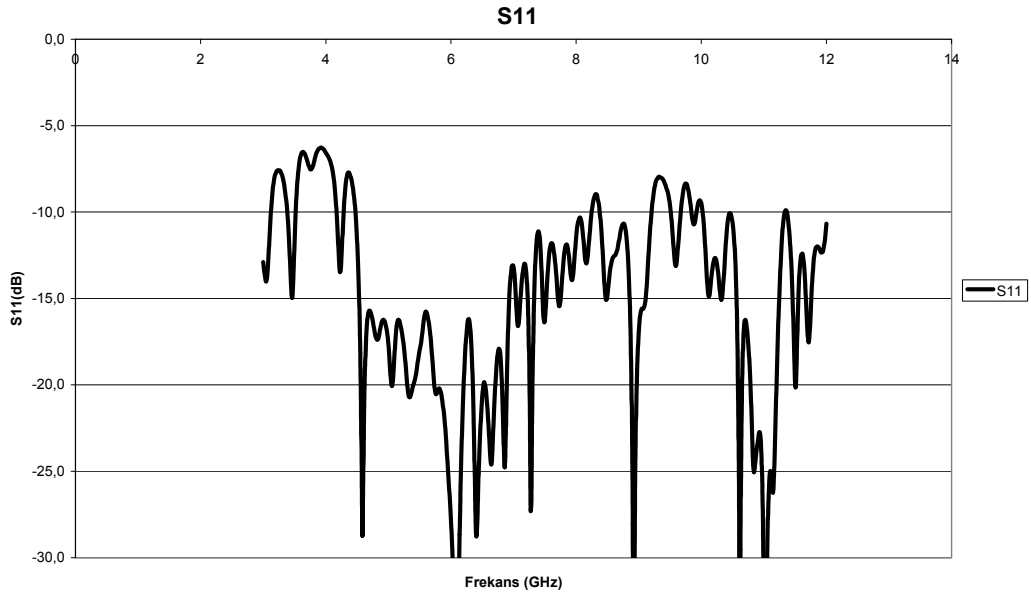


**Figure 4.4:  $S_{11}$  measurements of the beam-former**

The group delay of the beam-former can be calculated by adding  $\omega T$ ,  $2\omega T$ ,  $3\omega T$  and  $4\omega T$  phases to the phase measurements and changing  $T$  to check the point where the phase measurements of all arms coincide. Around 0.55ns (the best point), the phase measurements coincide as shown in Figure 4.5.

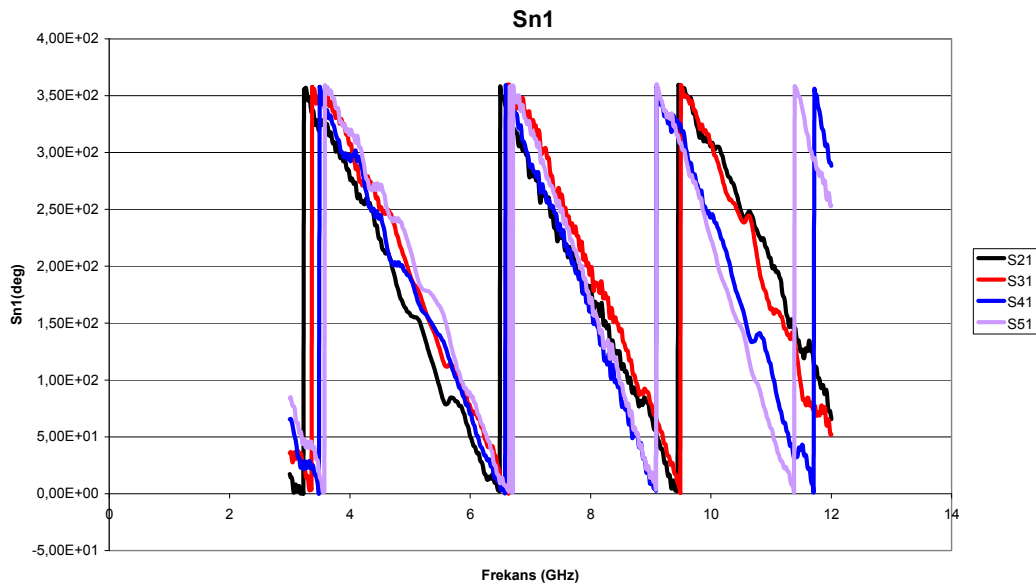


**Figure 4.5: At 0.55ns delay, the phases coincide (approximately)**

According to (3.68), 0.55ns inter-element delay corresponds to 1.818GHz span in LFMCW waveform generator for a full scan (360 degree) of space. So, the oscillator for LFMCW waveform generator should be selected with this value in mind, as shown in the next subsection.

#### **4.2.2 LFMCW Waveform Generator**

HMC587LC4B from Hittite Microwave Corp. is used as the VCO of the waveform generator. This VCO has a wide tuning range (5GHz-10GHz) and 3dBm output power on average. The tuning voltage can be varied over 0 to 18 V and supply voltage is only 5V, consuming 55mA. It has an approximately linear tuning voltage versus frequency curve. More information about the properties of this VCO can be found at [36] or Appendix 1.

A PCB has been built as shown in Figure 4.7 whose schematic is included in Figure 4.6. The PCB has an SMA input for controlling waveform and an RF output. The DC controls are also shown in Figure 4.6 and Figure 4.7. Note that the bias of the VCO is cleaned with a regulator. In Figure 4.8, the measurements on the VCO are shown. The power is stable with frequency and the relation between the control voltage and the output frequency is approximately linear as required in the measurements.

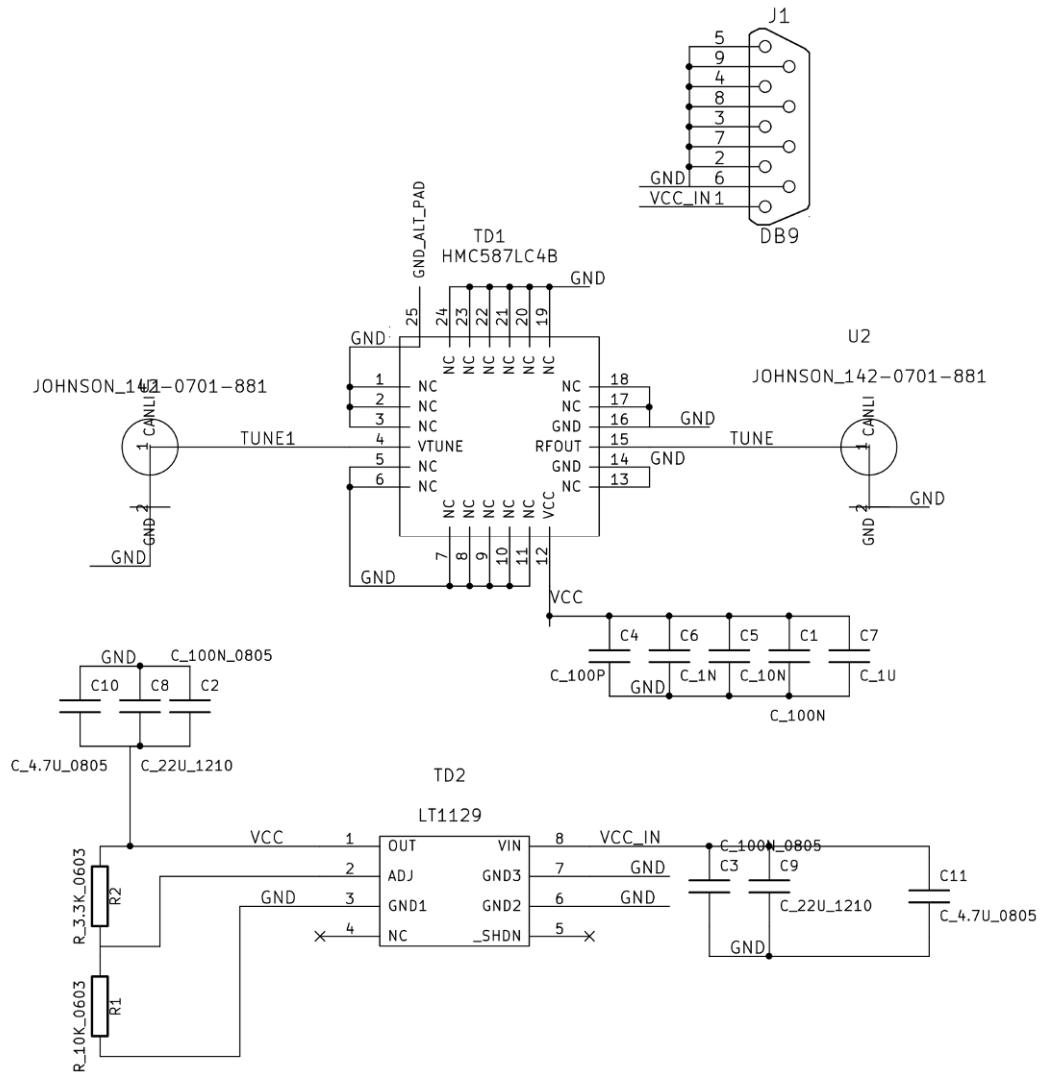


**Figure 4.6: Schematic of LFM CW waveform generator**

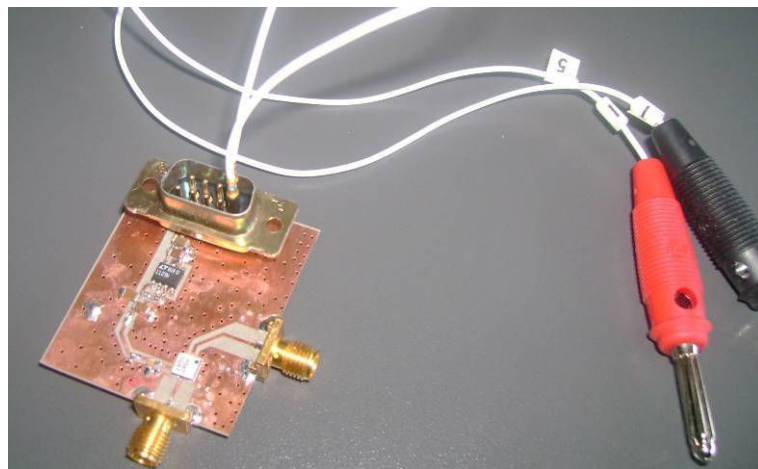


**Figure 4.7: LFM CW generator PCB**

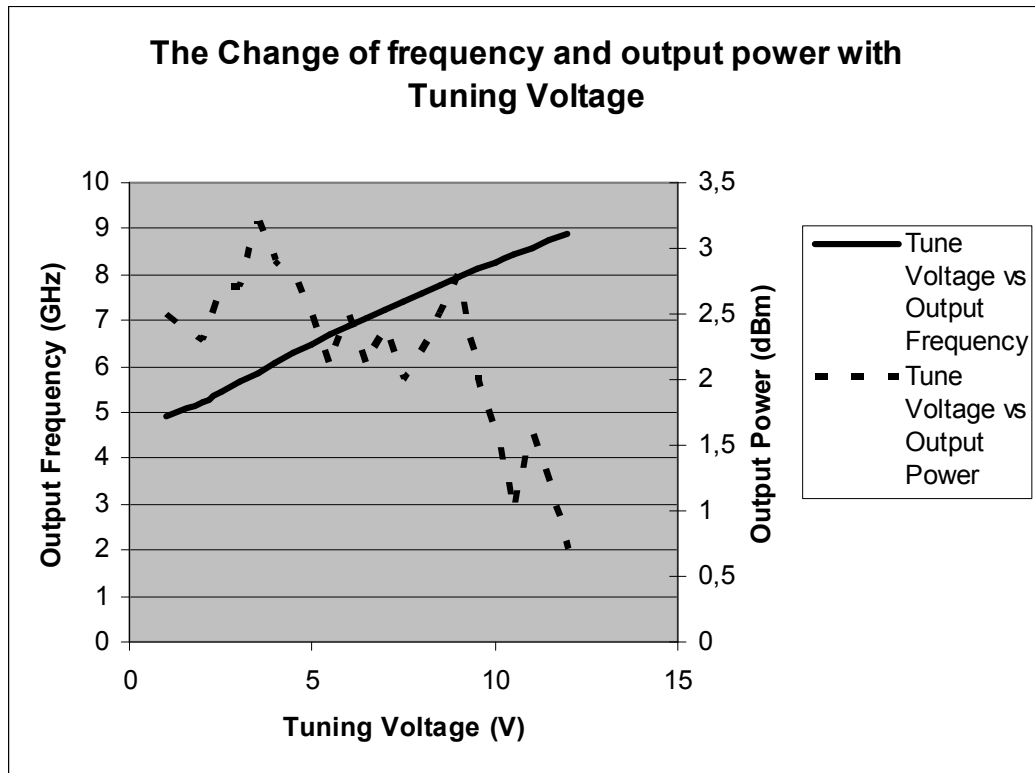


Figure 4.8: Output Power and control voltage vs frequency measurement

The frequency controlling waveform (saw-tooth waveform) of the VCO is supplied from a waveform generator; no specific circuit for the task is designed, since the trigger from the waveform generator is also used for time reference in the measurements.

### 4.2.3 Vivaldi Antenna and Vivaldi Array

The antenna of the array is also another important concern in the design of the FDA. The frequency bandwidth of the array is 6-10GHz and the antenna should cover this band for proper operation of the system. There are many types of wideband antennas in the literature but in this work Vivaldi type is selected for the implementation.

The selected antenna is antipodal type Vivaldi antenna [37-43]. The antenna is manufactured on RO6010 with 25 mil thickness as in beamformer. The sketch of the antenna is shown in Figure 4.9. The antenna is formed by two sections, namely the balun and the antenna section. Balun section is basically a

tapered transition from microstrip to symmetric double sided slot line [41]. The slot width between the antenna arms is exponentially tapered for wideband operation of the antenna.

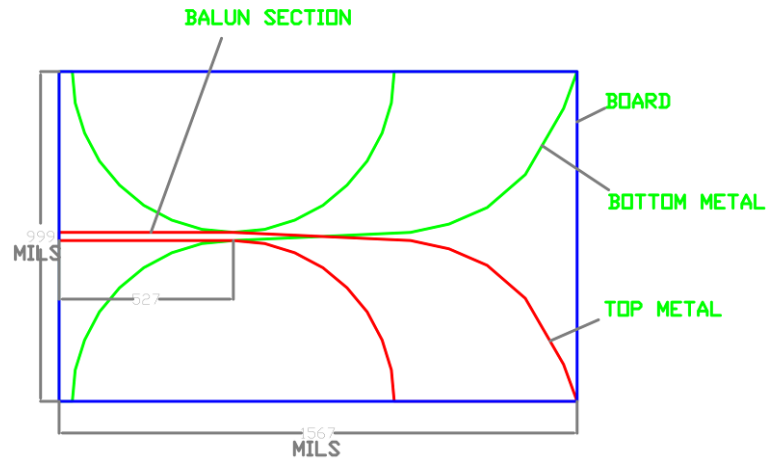


**Figure 4.9: Antipodal Vivaldi Antenna**

The simulation of the antenna is performed in CST. The antenna performance is tuned in the array using CST. The tapering properties and the balun are the main tuning parameters of the antenna. The array form of the antenna is also shown in Figure 4.10. The antenna elements are placed 25 mm apart on one axis. In the sketch, the uppermost part of the antenna is selected to be PEC in the simulation assuming no radiation through that side.

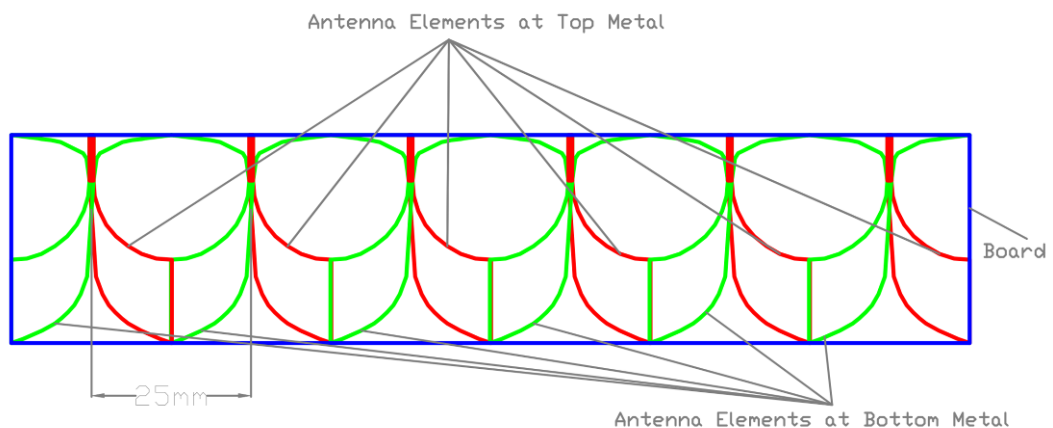


**Figure 4.10: Antipodal Vivaldi Antenna in array form, with 25 mm inter-element distance**

Note that in Figure 4.10, there are 6 antennas in the array. The left most and right most antennas are only fill-antennas and they are not responsible for the main radiation. They are loaded with system impedance and only the middle four antennas are concerned for the radiation properties. The  $S_{11}$  measurements of each antenna in the middle of the array are shown in Figure 4.11. Return losses of the leftmost and the rightmost antennas in the array are different from the middle antennas, and this is why fill-antennas are used in the array.

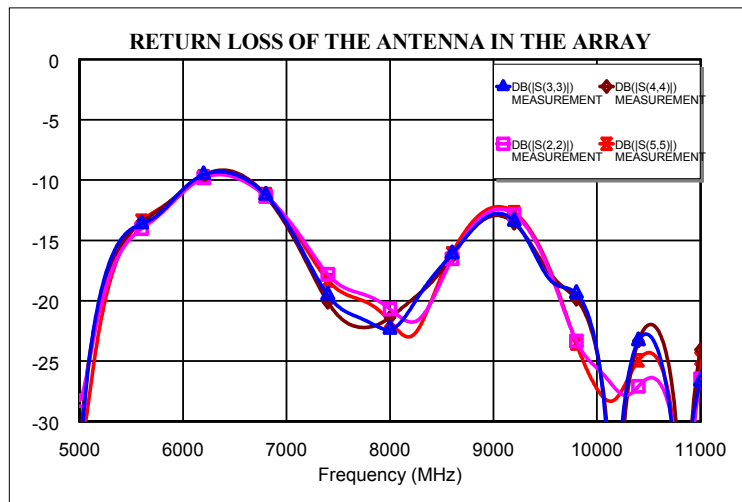
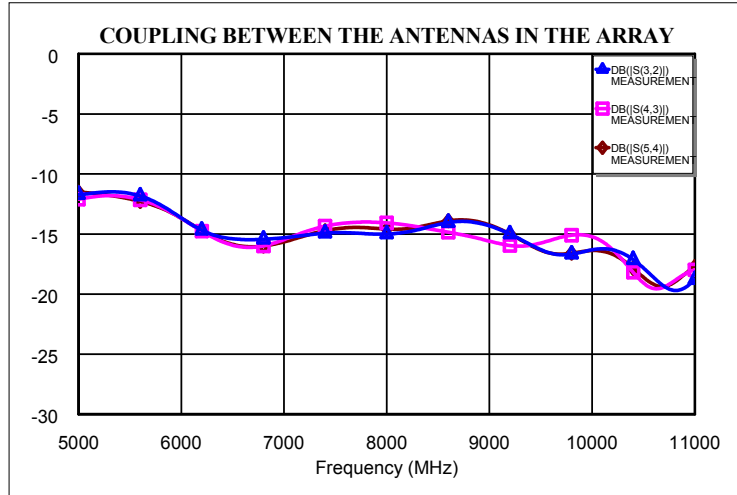


Figure 4.11:  $S_{11}$  (dB) measurement of each antenna in Figure 4.10.

In Figure 4.12, the inter-element coupling is also shown, and it is measured to be around 15 dB, which is an expected value for Vivaldi type antenna arrays. In [37-43], various techniques for decreasing the inter-element coupling are explained in detail. In this thesis, the inter-element coupling is also effective in the formation of the beams but it is ignored during measurements.



**Figure 4.12: Inter-element coupling**

The antenna radiation pattern measurements are performed in METU EEE anechoic chamber. For the measurement of antenna pattern, all antennas in the array are loaded with the system impedance, and only the pattern of one antenna is measured in the chamber (similarly in CST, same calculations are made). The theoretical E-plane pattern calculated by the CST is shown in Figure 4.13 and the measurement is shown in Figure 4.14 at 7GHz.

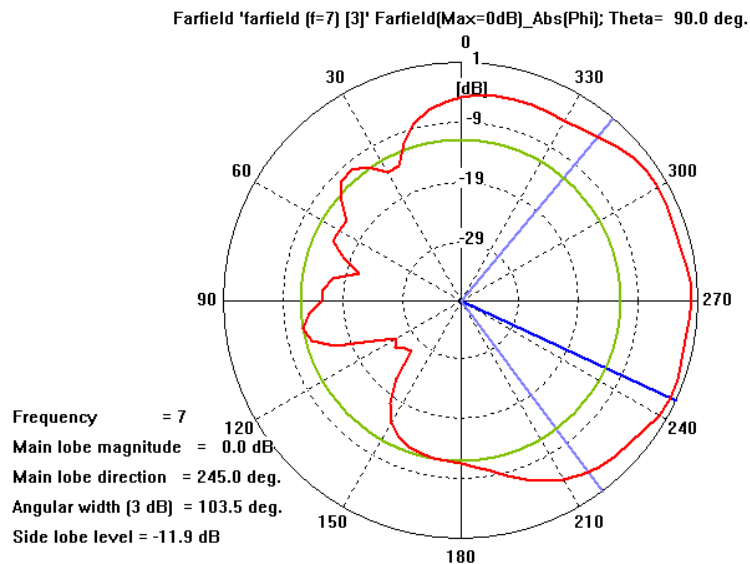


**Figure 4.13: CST simulation result for E-plane pattern of the vivaldi antenna radiation at 7GHz.**

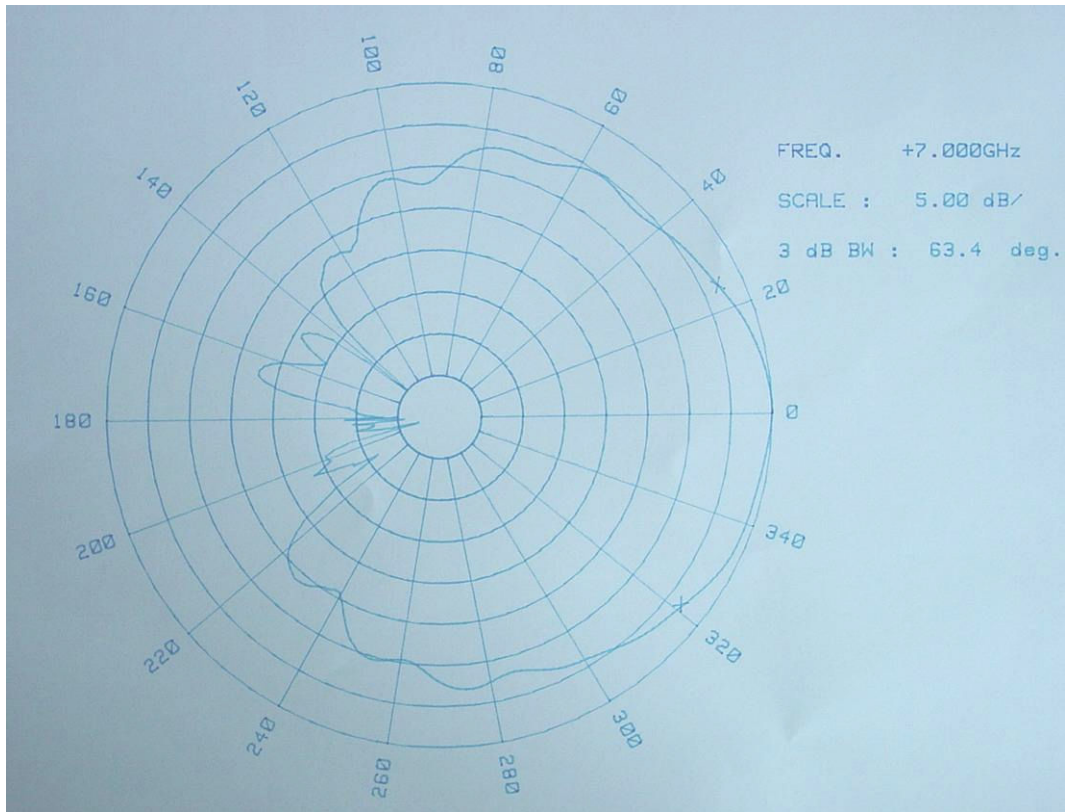


Figure 4.14: Measured E-plane antenna pattern of a Vivaldi antenna in the array.

In following figures, the calculated and measured H-plane patterns are shown.

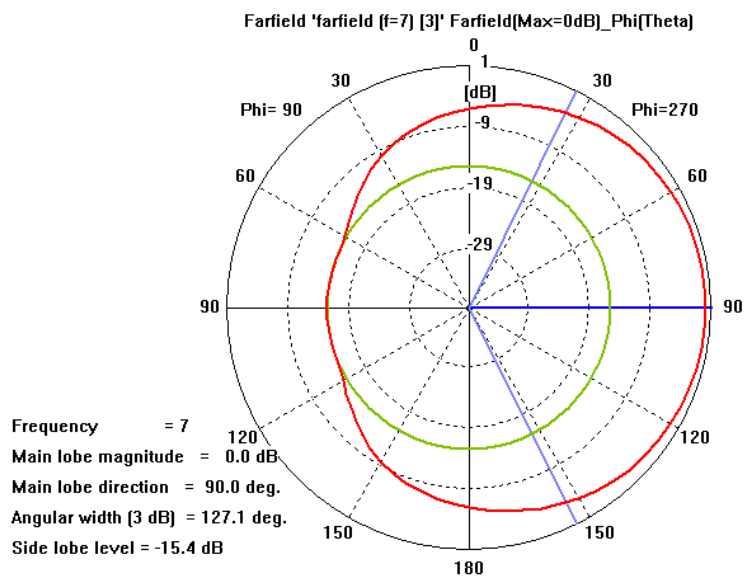
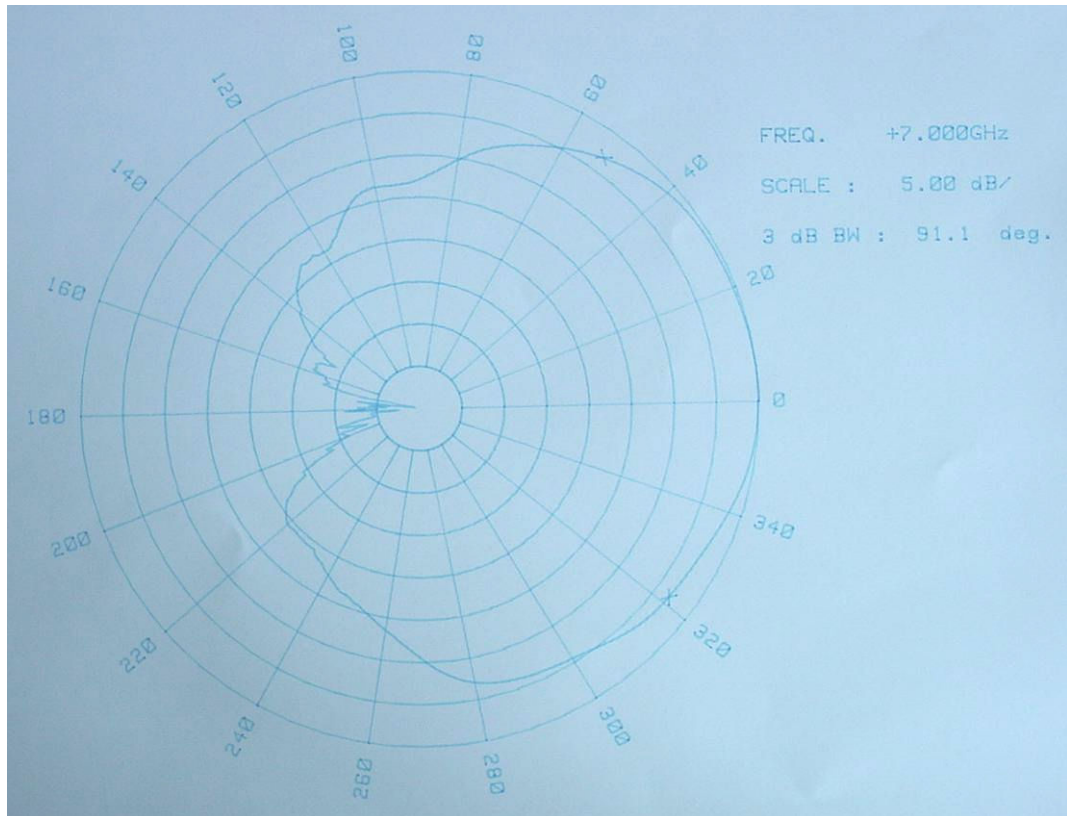
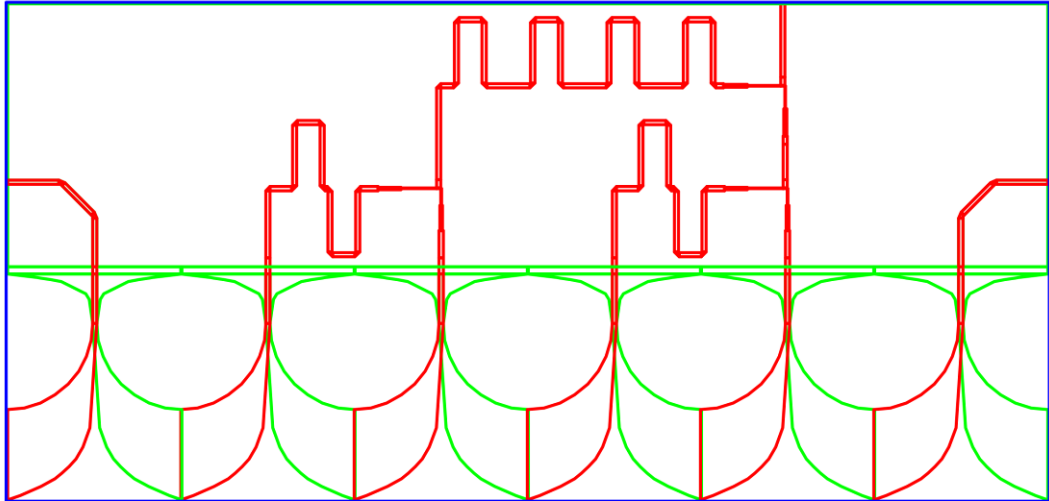


Figure 4.15: CST simulation result for H-plane pattern of the vivaldi antenna radiation at 7GHz.



**Figure 4.16: Measured H-plane antenna pattern of a Vivaldi antenna in the array.**

The next step in the implementation is the integration of the beam former in Figure 4.2 with the antenna array in Figure 4.10. Since both parts are on the same substrate, the integration is easy as shown in Figure 4.17. Also, in Figure 4.18 and Figure 4.19 the photographs of the implemented array are demonstrated. The array is manufactured with LPKF H-100.



**Figure 4.17: AutoCAD output of the beam-former and antenna array**

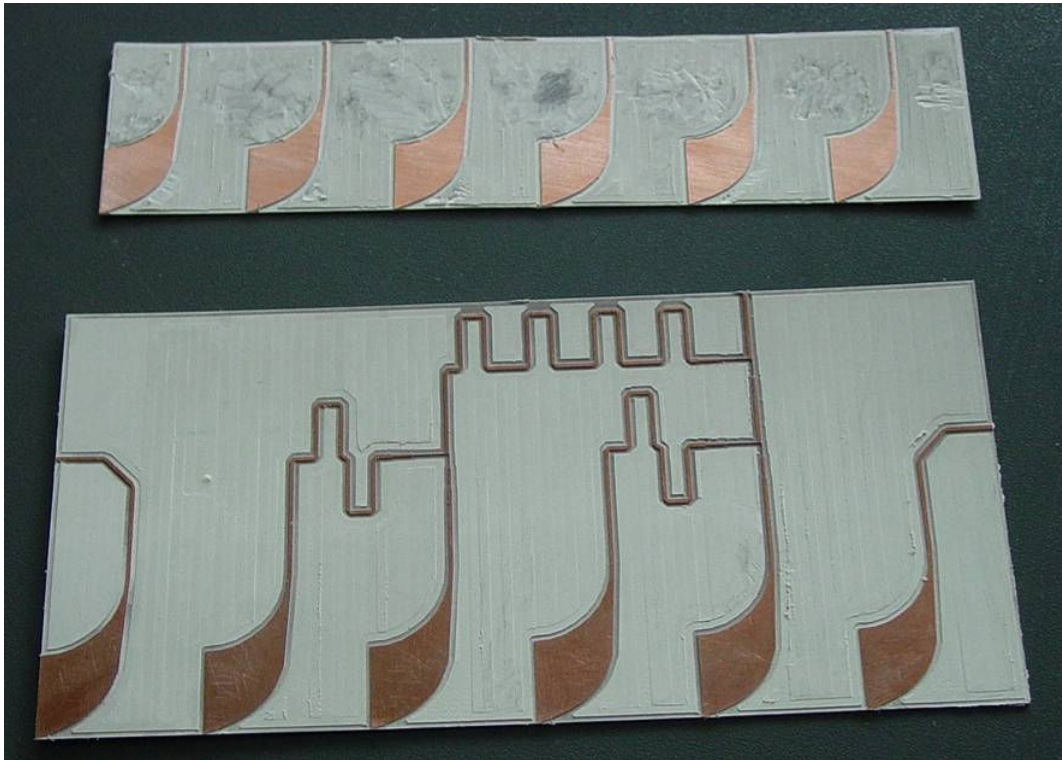


**Figure 4.18: Implemented beamformer and antenna assembly – front side of the board**

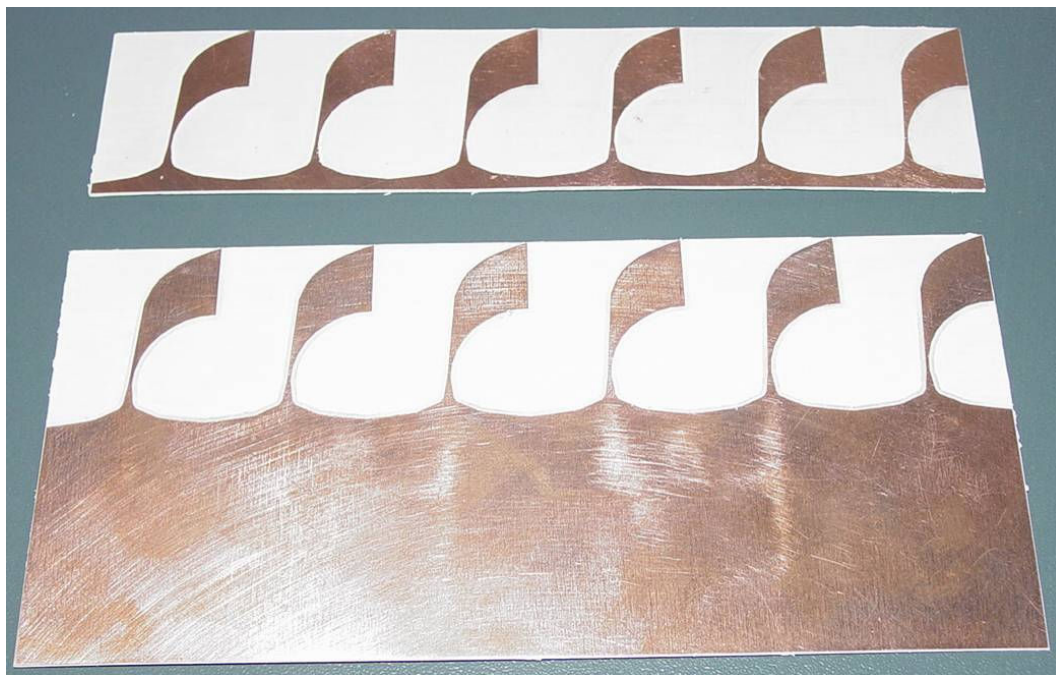


**Figure 4.19: Implemented beamformer and antenna assembly – back side of the board**

The return loss measurements of the array are shown in Figure 4.20. According to the measurements, the return loss is somewhat higher than 10dB in the band of operation but it is acceptable for the tests. Note also that, return loss is better at the fill-antennas; explaining the effect of beam former and the cross coupling between the antennas on the return loss performance of the array. Figure 4.21 also explains the coupling between the array input and the fill-antenna output.

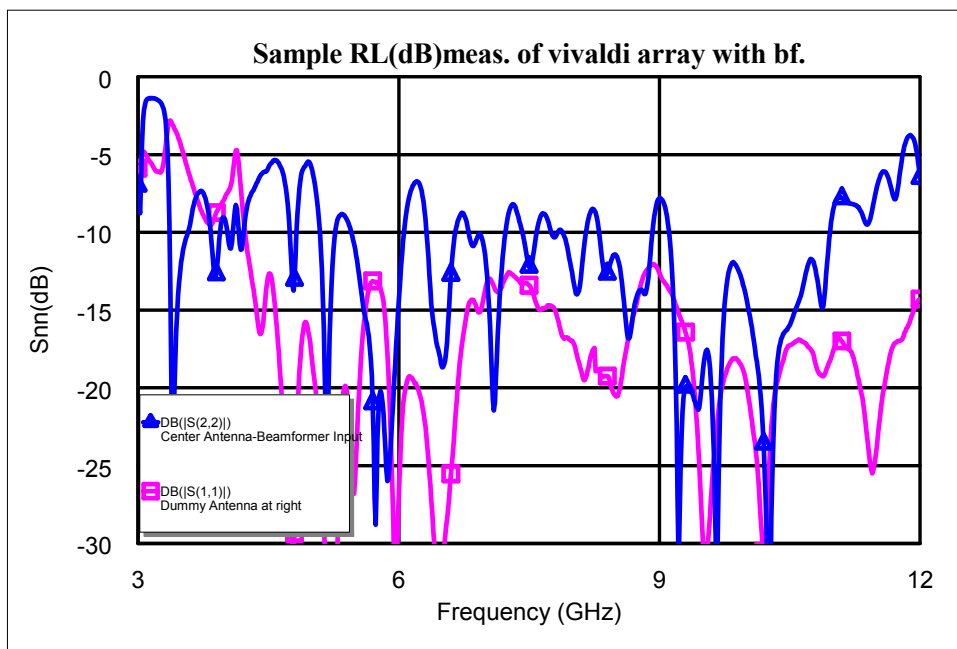


Figure 4.20: Return Loss measurements at the common port of the array and the fill antenna.

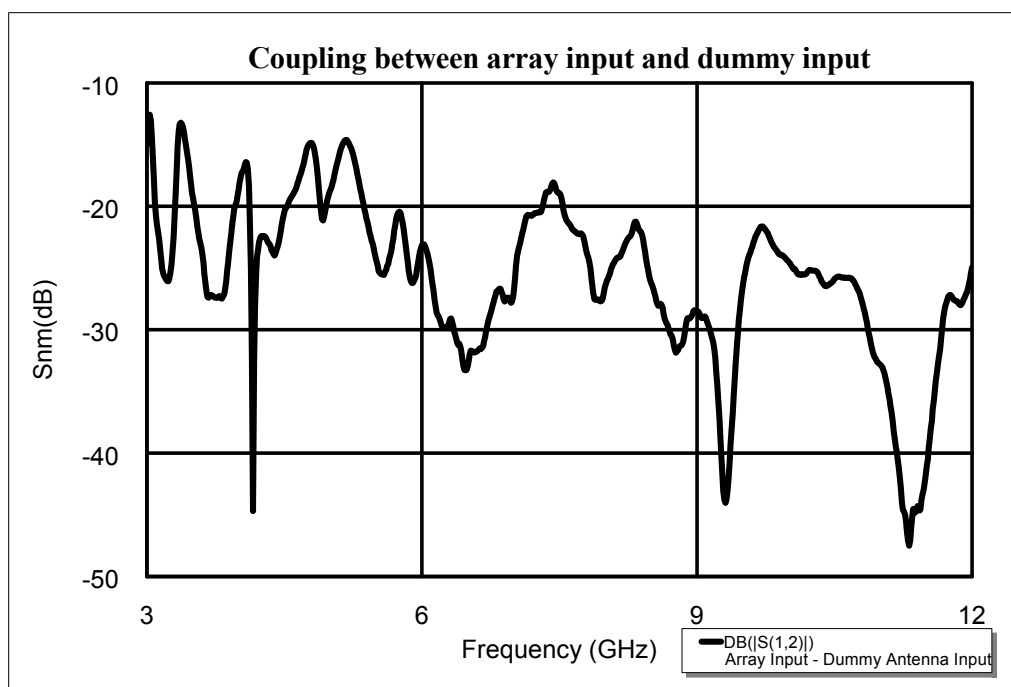
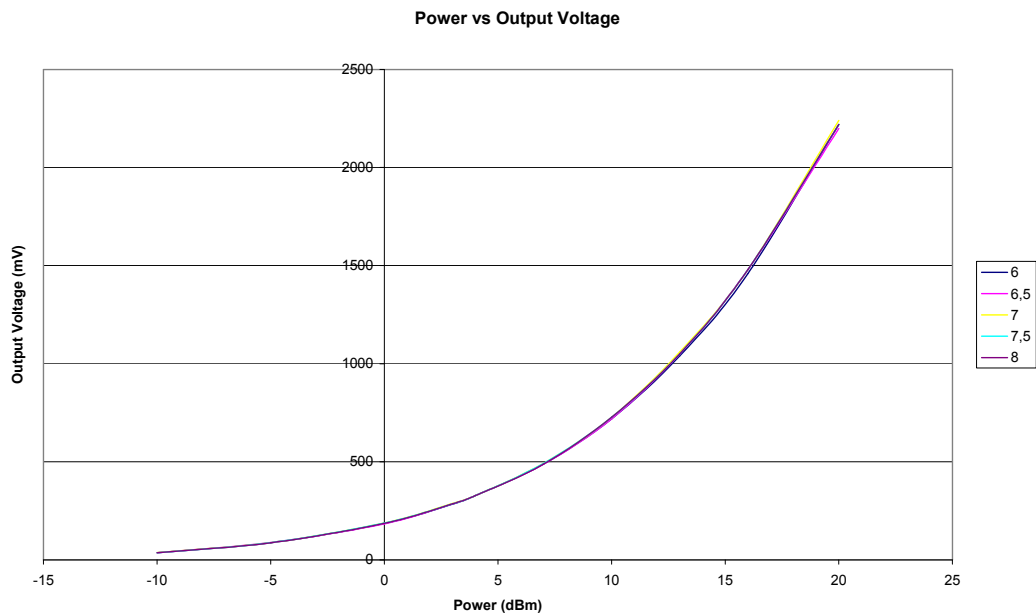


Figure 4.21: S-parameter measurement between the array input and the fill antenna

## 4.2.4 Detector

Throughout measurements, a detector is utilized at each setup to monitor the envelope on the oscilloscope. The detector used in the experiments is from NARDA, whose specifications are presented in Appendix 1. Some measurements are performed with the detector to check its linearity and frequency response.

The first measurement for the detector is shown in Figure 4.22. In this figure, the output voltage of detector for input power is shown for various frequencies. Note that below 0 dBm, the relation is approximately square-law as required for the application. Through out the measurements, the power in front of detector should not exceed 0dBm. This would require a gain control or source power control throughout the measurements.



**Figure 4.22: Input Power vs Output Voltage for various frequencies**

Another point to note about Figure 4.22 is that the spectral response of the detector is acceptable especially below 0 dBm. Although not clear in this figure, Figure 4.23 shows the spectral results clearly. As the input power is increased, rectification is pronounced more in the diode detector, whose spectral properties become effective on the output voltage. For lower powers at the input port of the detector, spectral dependencies reduce as shown in the aforementioned figure (the

junction capacitance of Schottky detectors heavily depends on the input power. The diode behavior under various input power excitations can be investigated using Harmonic Balance Analysis or Volterra methods [32, 44, 45]).

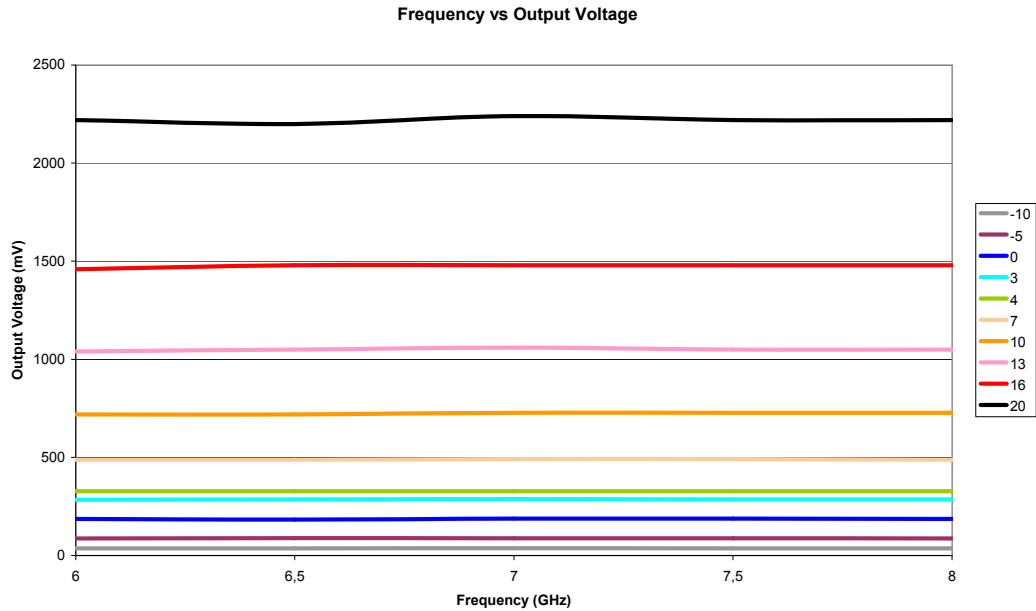


**Figure 4.23 Output Voltage vs Frequency for various input powers**

#### 4.2.5 Other Hardware

Up to this point, critical hardware for the implementation of the LFMCW based FDA is demonstrated. There are also other parts that are used throughout the measurements. Detailed information will not be presented here but datasheet regarding these parts are supplied in Appendix 1.

A 4-way uniform divider from NARDA is used as supplementary hardware. The amplitude imbalance of this divider is +/-0,1dB and phase imbalance is +/- 1 degree throughout the band of interest. Input and output return losses and the output isolation of this divider is better than -15dB through 6-10GHz band.

Cables from ASTROLABS (MINIBEND-4, MINIBEND-6) are used for the interconnections in some tests. The cables are all standard length (4", 6") and the phase imbalance between the cables is better than +/-1degrees.

The other parts that are used in the experiments will be pronounced as general parts and no specific information will be supplied about them.

### 4.3 TEST CONFIGURATIONS AND MEASUREMENTS

At the first step of the measurements two basic tests are performed. The first experiment is performed in the laboratory without the antenna in the arrangement while the second test is performed in the anechoic chamber. In the following subsections details about the tests are presented with the results.

#### 4.3.1 Test Configuration – 1

In this test, main aim is to check the concept using basic laboratory tools and designed hardware. Neither any antenna is utilized, nor the experiment is performed in the anechoic chamber. The setup is shown in Figure 4.24.

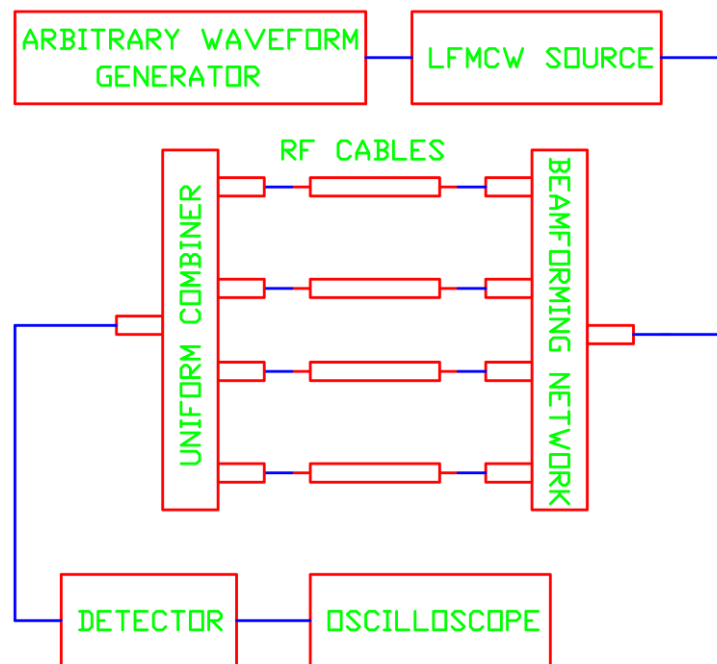


Figure 4.24: Configuration for the first experiment

In this setup, the waveform (saw tooth waveform is commonly used throughout all experiments) from the arbitrary waveform generator is fed to the oscillator, or LFMCW source. The amplitude range of the saw-tooth waveform

specifies the total extent of frequencies that the LFM CW source generates. According to Figure 4.8, the LFM CW source is fairly linear in the frequency range of interest, but the frequency output from the source is calibrated for each measurement. The output of the source is fed to designed FDA beam forming network as shown in Figure 4.24. The four output of the beam forming network is transferred to the equal combiner and summed at the common port of the equal combiner. Finally, summed waves are fed to detector, output of which is coupled to an oscilloscope for inspection of the pulses.

In this configuration, the aim is to make the beam-former behave like an FDA looking broadside only. The waves propagate in the cables and interference is observed at the common port of the combiner. The range of interference point to the array origin is very small but since the array is simulated to look through broadside direction, the results are expected to be consistent.

A photograph of the setup is shown in Figure 4.25. The connections between the devices are not very clear due to cable harnesses but the configuration in Figure 4.25 is an exact application of the configuration in Figure 4.24.

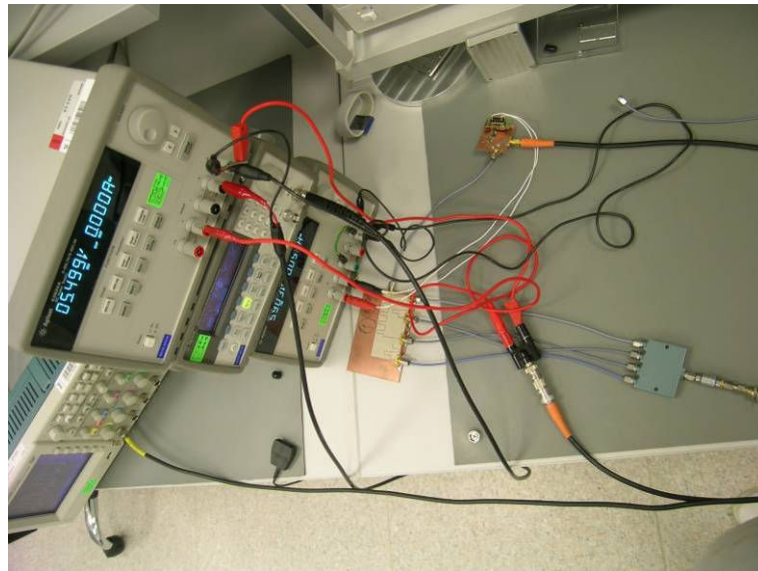


**Figure 4.25: A photograph of the first measurement setup**

### 4.3.2 Measurements with Configuration – 1

In the measurements of the first configuration, the aim is to get a feel of amplitude modulation at the output of the combiner. In fact, the results are satisfying in terms of the modulation. The first result is shown in Figure 4.26 as a demonstration. Although the waveform is not a perfect  $\frac{\sin(N\varphi)}{\sin(\varphi)}$  due to imperfections in the utilized devices, the amplitude modulation in time (at an imaginary point in space) is clearly visible.

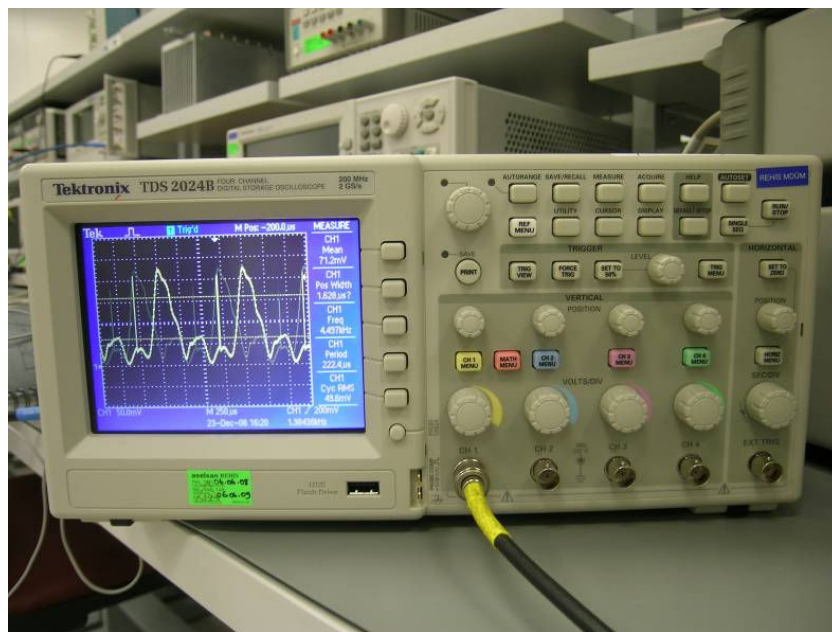


Figure 4.26: First observation of the amplitude modulation effect on the oscilloscope screen

A sample test for the first configuration can be defined as in Table 4.1. According to the table, the arbitrary waveform generator outputs a saw-tooth waveform with a period of 10ms. The minimum voltage output of the waveform is 5V, while the maximum is at 11V. The voltage range of the waveform output corresponds to a frequency sweep at LFMCW source between 6.31GHz and 8.61GHz (These values are measured at spectrum analyzer using the max hold feature of the spectrum analyzer.). The slope of the frequency regime is calculated to be  $1.445 \cdot 10^{12}$  or  $2\pi \cdot 2.3 \cdot 10^{11}$ , corresponding to 2.3GHz total frequency shift in

10ms.  $s$  constant is calculated to be 6,6 from (3.51) and the instantaneous frequency difference between the antenna elements is predicted to be 123 Hz, corresponding to 7.9ms beam period in time (3.58). Corresponding range period becomes 2371541.5km and the null to null interval of the pulses is calculated to be 3.95 ms (3.64). Since all measurements are assumed to be performed for  $\theta = 0^\circ$ , (3.56) would result in 1, regardless of the value of  $s$ . So, equations 3.58 and 3.64 can be used with no assumption requirement.

The result of the measurement is shown in Figure 4.27. Since the period of the waveform generator output is 10ms, the period in this measurement is also found to be 10ms.

**Table 4.1: Parameters for a sample measurement using the configuration in Figure 4.24.**

Voltage Start (V)	5V
Voltage End (V)	11V
Frequency Start (GHz)	6,31
Frequency End (GHz)	8,61
Sweep Time (ms)	10,00
$m$ (2piHz/s)	1,445E+12
Total Frequency Shift (GHz)	2,3
$s$ constant	6,6
Inter-element distance(mm)	25
Inter- element delay (ns)	0,55
Frequency Difference Between Antennas (Hz)	126,5
Beam Period (ms)	7,9
Range Period(km)	2371541,5
Null to Null interval (ms)	3,95

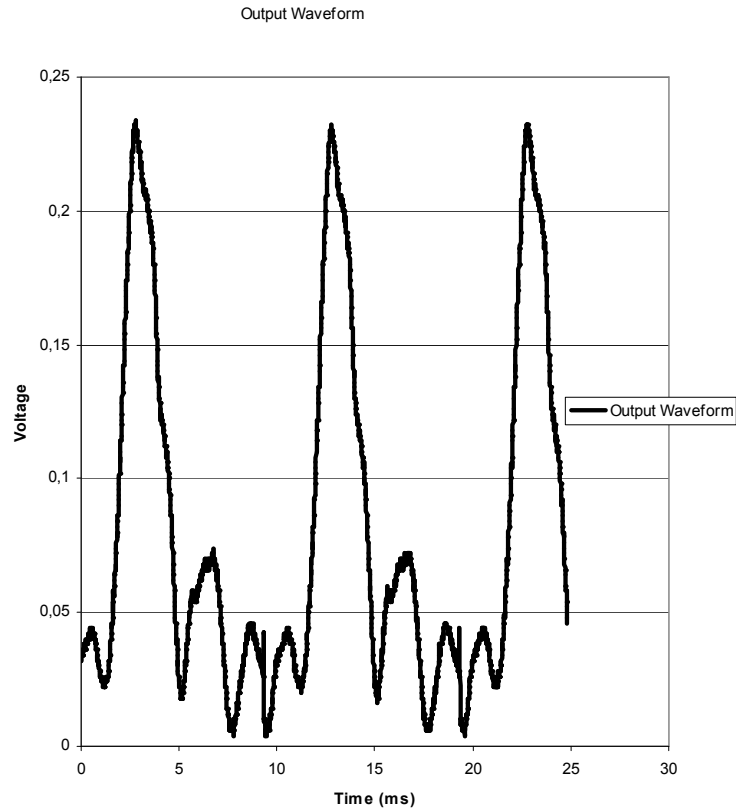


**Figure 4.27: The output waveform for the parameters in Table 4.1.**

The null-to-null interval of the measurement result is found to be 3.94ms, consistent with the value found in Table 4.1. Besides, in Table 4.1, the beam period is calculated to be 7,9ms, but in the figure the second beam is not visible since the second beam corresponds to the next period of scan. In this set of measurements, the beam period is not checked but in following subsections, in anechoic chamber this parameter is also justified.

In this setup various measurements similar to the one in Figure 4.27 are performed but they will not be presented here. This part is a preparation for the measurement of the LFMCW based FDA concept in anechoic chamber. In the following subsections, the next setup and measurements will be demonstrated.

### **4.3.3 Test Configuration – 2**

In the second test, the array is aimed to be used in the anechoic chamber. The devices used in Figure 4.24 and Figure 4.25 are benefited in the new

configuration together with the new devices. The configuration for this setup is shown in Figure 4.28.

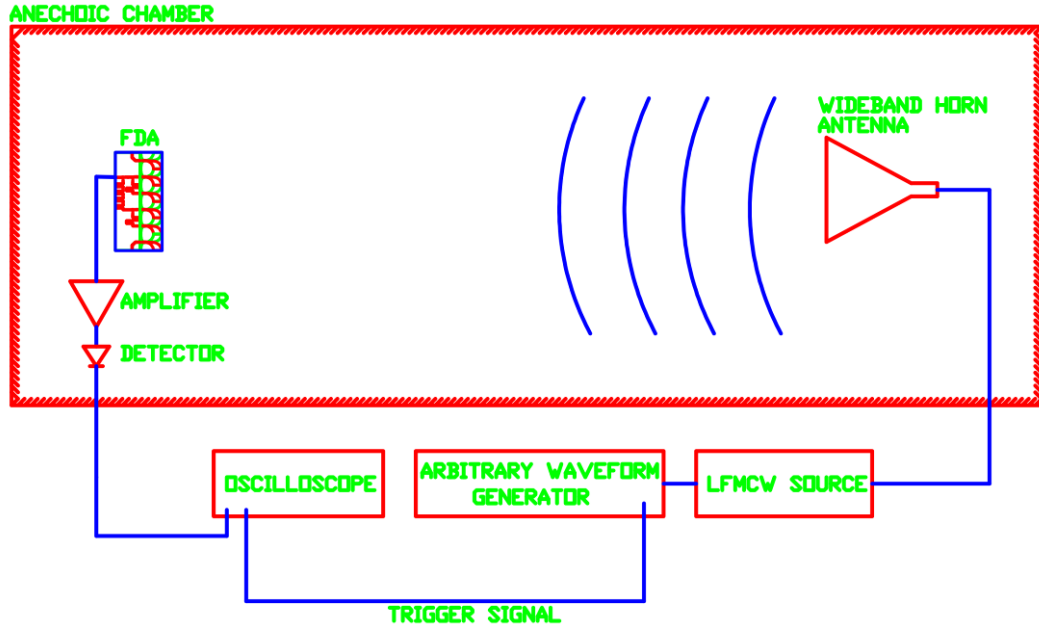


Figure 4.28: Configuration for the next tests

In this setup, FDA is configured to receive the incoming waves while a wide band horn antenna is used as the transmitter. Both antennas are placed in the anechoic chamber. Besides the antennas, an amplifier with a medium power gain and detector are placed just after the receiving FDA. Other devices such as oscillator, arbitrary waveform generator and LFMCW source are placed outside the anechoic chamber. The interconnections are made using long 50 Ohm cables.

The mechanism is as follows: The waveform generated by the arbitrary waveform generator is a saw-tooth waveform feeding the LFMCW source. Besides the saw-tooth, a trigger signal is generated by the arbitrary waveform generator which is used to trigger the oscilloscope (This trigger signal can also be used as a shifter time reference for professional applications). The LFMCW output of the source is fed directly to a wideband horn antenna. Radiated waves from the wideband horn antenna is gathered at the FDA and amplified. Next, detector is used after amplifier to detect the total instantaneous power at the output of the

amplifier. Finally, the waveform output from the detector is fed to the oscilloscope.

In this configuration various measurements are picked experimenting with the FDA look angle and LFMCW waveform generator characteristics. Especially, as mentioned before, The LFMCW waveform frequency extent is checked on the spectrum analyzer and linear frequency ramp is assumed at the output of the generator.

Another point to note about this configuration is that the array is always at the same range but the angle of direction can be altered. So, what will be observed on the oscilloscope is the time domain dynamics of scanning properties of the array. The scanning beam samples collected by the array are analyzed based on the calculations using formulations of Chapter 1.

#### 4.3.4 Measurements with Configuration – 2

In this section six measurements will be presented for the justification of findings. Most of the measurements are used for demonstration of the LFMCW based FDA concept, so they will not be presented with details, in this thesis.

The FDA constants regarding the FDA are demonstrated in Table 4.2. The inter element distance is 25mm, while the inter element delay is  $T = 0,55ns$  making  $s = 6,6$ . In the measurements and calculations these values are constants.

**Table 4.2: FDA constants**

Inter-element distance (mm)	25
Inter-element delay (ns)	0.55
s	6.6

##### 4.3.4.1 Measurement 1

Measurement 1 is a general demonstration of the theory with the second measurement setup. The parameters of the setup are shown in Table 4.3.

**Table 4.3: Parameters of measurement 1**

Voltage Offset (V)	2,35V
Voltage Amplitude (V)	3V
Frequency Start (GHz)	5,20
Frequency End (GHz)	7,64
Sweep Time (ms)	10,00
m (2piHz/s)	1,53812E+12
Total Frequency Shift (GHz)	2,448
Frequency Difference Between Antennas (Hz)	134,64
Calculated Beam Period (ms)	7,06
Calculated Range Period(km)	2118386,59
Calculated Null to Null interval (ms)	3,71

In this measurement, the starting frequency of measurement is 5,2GHz and all of the devices work well at this frequency. The frequency scan range is from 5,2GHz to 7,64GHz, over a 2GHz range. So, it will be possible to see the secondary beam at the point of FDA (and it will be seen). The total sweep time is 10 ms and the slope of the curve is  $1,538 \cdot 10^{12} \cdot 2\pi Hz^2$ . The resulting waveform is shown in Figure 4.29.

According to Figure 4.29, there are two beams in one period each 7,12ms apart from each other and the calculation requires this value to be 7,06ms very close to the measured value. Due to 10ms period of the saw-tooth waveform, the output waveforms will also be observed with 10ms delay. The null to null beam width is calculated to be 3,71 ms but in the measurement this value is found to be around 3ms. This difference is mainly due to the spectral properties of the elements and nonlinearity of FM waveform. Similarly the second beam also has a narrower beam-width than the first one since the nonlinearity is more pronounced at this point. Also note that there are two more beams at the end of each period. These beams are due to down ramping of saw-tooth waveform from waveform generator at the end of each period (in one period, 95% for up ramping and 5% for down ramping), but these beams will not be analyzed in the thesis.

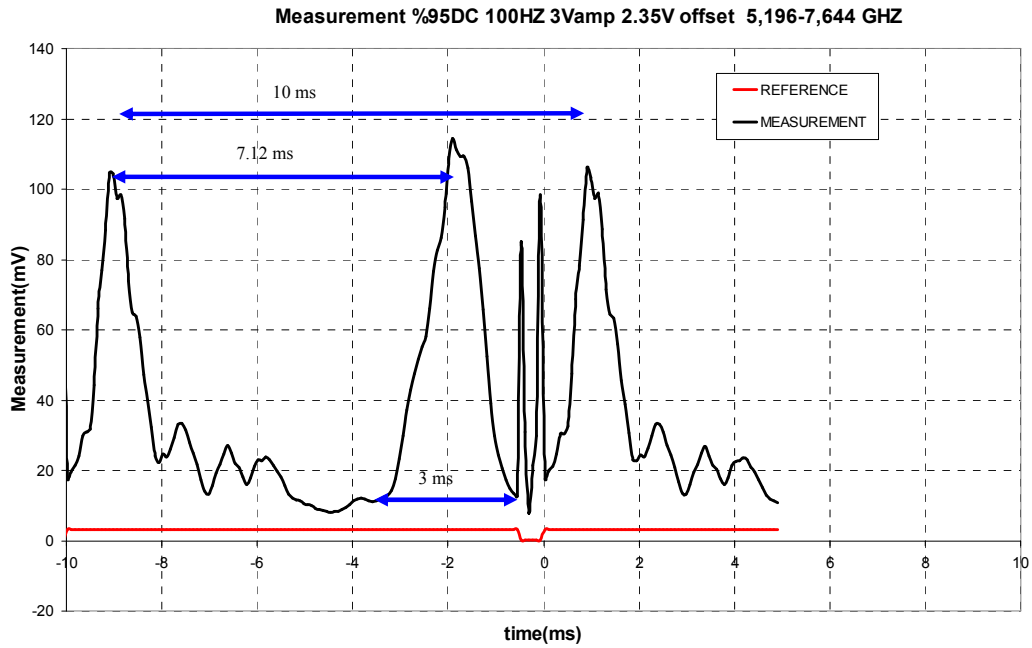


Figure 4.29: Resulting waveform for measurement 1

#### 4.3.4.2 Measurement 2

The parameters for this measurement are shown in Table 4.4.

Table 4.4: Parameters for second measurement

Voltage Offset (V)	4V
Voltage Amplitude (V)	2,7V
Frequency Start (GHz)	6,73
Frequency End (GHz)	8,63
Sweep Time (ms)	10,00
m (2piHz/s)	1,19758E+12
Total Frequency Shift (GHz)	1,906
Frequency Difference Between Antennas (Hz)	104,83
Calculated Beam Period (ms)	-9,07
Calculated Range Period(km)	-2720781,93
Calculated Null to Null interval (ms)	4,77

Here, the frequency scan is around 1,818GHz and not all space is scanned more than one with this beam. The resulting scanning waveform can be observed in Figure 4.30.

Here the beam width is found to be approximately 4 ms again lower than the predicted value due to the reasons mentioned before. In this measurement the beam period is predicted to be 9,02 ms but the second beam is not visible in the plot, since after 9,02ms, secondary beam will be at the second period. This is equivalent to saying that the frequency span is around 1,818GHz (3.68) not adequate for scanning the space more than once.

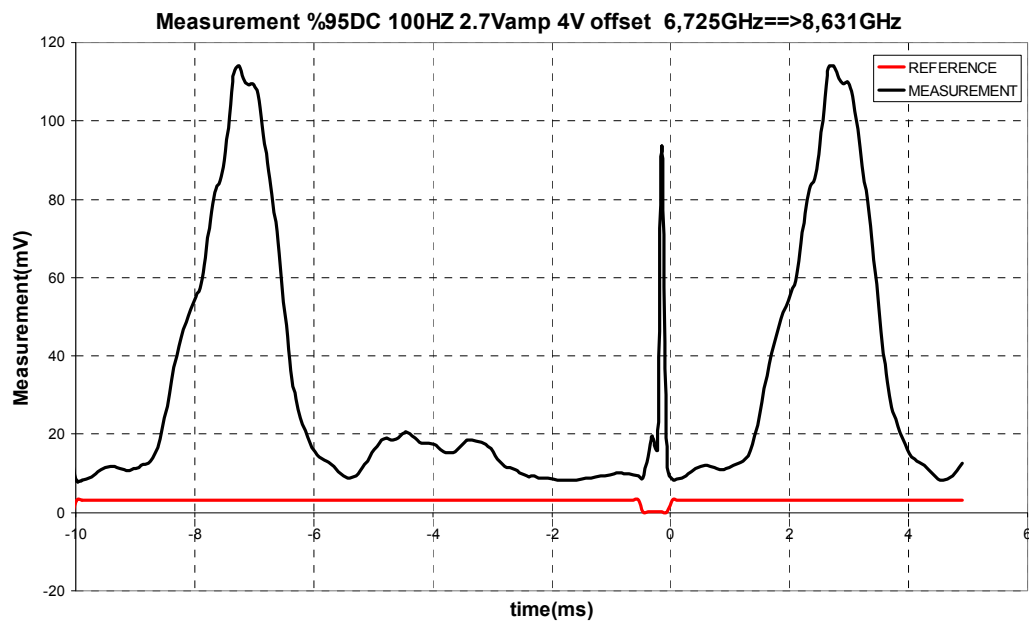


Figure 4.30: Resulting waveform for measurement 2

#### 4.3.4.3 Measurement 3

Measurement 3 is just a repetition of Measurement 2 with the scanning range altered as shown in Table 4.5. Note that the total frequency shift is increased above 2GHz, and the starting frequency is lowered to 5,21GHz. So, the secondary beam is squeezed into one period in this case. The resulting waveform at the output is shown in Figure 4.31. Note that the beam periodicity predicted by the derivations is again justified but the null-to-null beam width calculations have discrepancies due to spectral properties of the utilized devices and the nonlinear scanning regime of LFMCW source.

**Table 4.5: Parameters for third measurement**

Voltage Offset (V)	2,21V
Voltage Amplitude (V)	2,7V
Frequency Start (GHz)	5,21
Frequency End (GHz)	7,44
Sweep Time (ms)	10,00
m (2piHz/s)	1,40216E+12
Total Frequency Shift (GHz)	2,23
Frequency Difference Between Antennas (Hz)	122,74
Calculated Beam Period (ms)	7,75
Calculated Range Period(km)	2323808,2
Calculated Null to Null interval (ms)	4,07

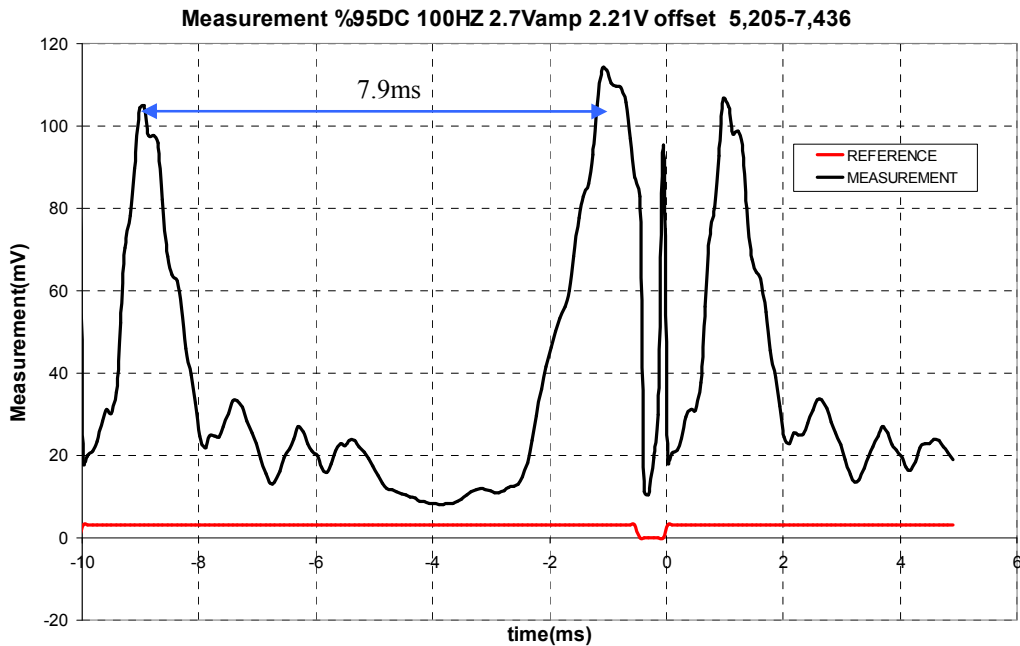


**Figure 4.31: Resulting waveform for measurement 3**

#### 4.3.4.4 Measurement 4

In this measurement, the LFMCW source is arranged such that, the frequency coverage is far outside the spectral width of most of the devices in the line-up. So, during the scan of frequency, no output waveform is expected. Note that the frequency scan is extended up to 5,77GHz and this sector of frequency

scan is in the bandwidth, and a waveform output can be expected at this sector. The resulting waveform is shown in Figure 4.32. Here it can be noted that the side lobes of the resulting waveform is lowered due to out of band scanning.

**Table 4.6: Parameters for fourth measurement**

Voltage Offset (V)	0V
Voltage Amplitude (V)	3V
Frequency Start (GHz)	4,32
Frequency End (GHz)	5,77
Sweep Time (ms)	10,00
m (2piHz/s)	9,08549E+11
Total Frequency Shift (GHz)	1,446
Frequency Difference Between Antennas (Hz)	79,53
Calculated Beam Period (ms)	11,95
Calculated Range Period(km)	3586314,2
Calculated Null to Null interval (ms)	6,29

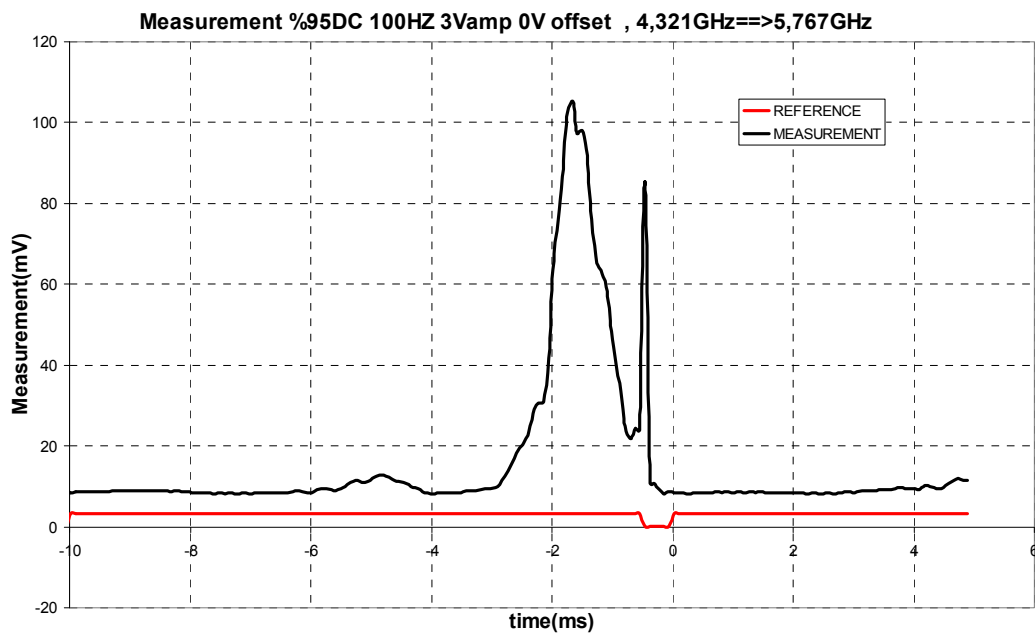


**Figure 4.32 Resulting waveform for measurement 4**

#### 4.3.4.5 Measurement 5 – The effect of center frequency on the positioning of the peak points

Several measurements are performed in the anechoic chamber for justification of the parameters. The effect of center frequency on the positioning of beams in time domain is an important check parameter. Before getting into the details of measurement some points need to be cleared by mathematical expressions.

Equation (3.45) is rewritten below for convenience.

$$\varphi(n, t) = \frac{mT}{c} R_0 + \left( \frac{\omega_0 + mt}{c} \right) (d \sin(\theta) - cT) - \delta \quad (4.1)$$

As mentioned in 3.2.3, the points where  $\frac{\varphi}{2} = p\pi$ ,  $p \in \mathbb{N}$ , the peaks of the waveform can be found.

$$t_p = \frac{\left( 2p\pi - \frac{mTR_0}{c} + \delta \right) c}{m(d \sin(\theta) - cT)} - \frac{\omega_0}{m}, p \in \mathbb{N} \quad (4.2)$$

Rearranging (4.2) using (3.51) and (3.56),

$$t_p = \frac{\left( 2p\pi - \frac{mTR_0}{c} + \delta \right)}{\Delta\omega \left( \frac{\sin(\theta)}{s} - 1 \right)} - \frac{\omega_0}{m}, p \in \mathbb{N} \quad (4.3)$$

In this equation  $\omega_0$  is the starting frequency and the change in the peak point is directly related to the starting point of frequency. In the measurements the reference is not taken to be the starting frequency but the center frequency (assuming no change in the slope of the waveform). A shift in center frequency by  $\Delta\omega$  will shift the beam peak point by  $\frac{\Delta\omega}{m}$ .

In Figure 4.33, three measurements are shown on the same graph. In Table 4.7, the variables regarding the measurements of Figure 4.33 are presented. In all cases the voltage amplitude of the controlling waveform is set to be constant at 2,7V, but the offset voltage is changed. The aim here is to fix the slope of

frequency span but change the center frequency of frequency scan at the LFMCW source. Unfortunately, in all three cases, even though the offset voltage is changed only, both the slopes and center frequencies are affected. Looking at Table 4.7, the results for Cases I and II are close to each other but for Case III the slope and center frequency has changed dramatically. So, comparison using only Case I and Case II would have more meaning than comparing Case III with others. Throughout the demonstration of the results, the arguments will be clearer.

**Table 4.7: Test variables for effect of center frequency on the positioning of beam peaks**

	Case I	Case II	Case III
Voltage Offset (V)	4	4,34	5
Voltage Amplitude (V)	2,7	2,7	2,7
Frequency Start (GHz)	6,73	7,00	7,5
Frequency End (GHz)	8,63	8,83	8,805
Sweep Time (ms)	10,00	10,00	10,00
m (2piHz/s)	1,20E+12	1,15E+12	8,20E11
Total Frequency Shift (GHz)	1,906	1,83	1,305
Frequency Difference Between Antennas (Hz)	104,8	100,7	71,5
Calculated Beam Period (ms)	9,1	9,4	13,3
Calculated Range Period(km)	2720782	2833776	3989084
Calculated Null to Null interval (ms)	4,8	5	7

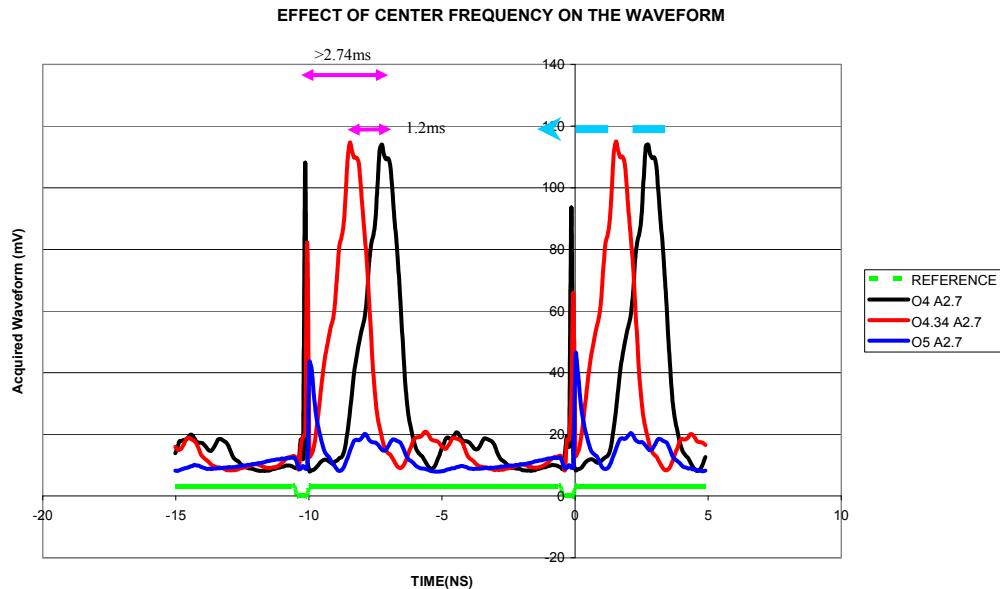


**Figure 4.33: Effect of center frequency on beam shift**

The shift in position of the peak is measured to 1,2 ms when the offset voltage is changed to 4,34 volts (from 4V). Table 4.7 indicates that the center frequency has shifted from 7,678GHz to 7,913GHz by 235MHz. The mean slope of Case I and II is  $1,1737 \cdot 10^{12} \text{ Hz}^2$ . So, calculated shift is expected to be 1,26ms very close to measured value. The difference is mainly due to change of slope of LFMCW frequency regime due to control waveform settings. As mentioned before, this case can be more pronounced for the third case in Table 4.7. In this measurement, the amplitude of the controlling waveform is same but the offset voltage to the waveform generator is changed. The change in frequencies does not follow waveform changes linearly. So, the time shift is calculated to be 3ms but the shift is measured to be 3,4ms, more than ten percent error is visible.

Despite the errors due to nonlinearities, the results are valuable in justifying the dependency on center frequency. In the next measurement, the effect of slope on the positioning of peak points will be demonstrated.

#### 4.3.4.6 Measurement 6 - Effect of Frequency Span

Frequency span is directly related to the slope of the LFMCW frequency regime and the properties (and positioning) of the beams are directly related to the slope by (4.3). For convenience this equation is repeated here.

$$t_p = \frac{\left(2p\pi - \frac{mTR_0}{c} + \delta\right)}{\Delta\omega\left(\frac{\sin(\theta)}{s} - 1\right)} - \frac{\omega_0}{m}, p \in \mathbb{N} \quad (4.4)$$

According to (4.4), the dependency on  $m$  is seen at two places of (4.4). The  $\frac{mTR_0}{c}$  term is a very small (the measurements are performed in anechoic chamber and this term can be ignored) and its effect on beam position can be ignored. The important part of the equation in (4.4) is the last term,  $\frac{\omega_0}{m}$  affecting the properties of the beam. The starting frequency  $\omega_0$  will affect the position of the beam peak but, as the slope of the frequency characteristic of the source is changed, a scaling should be seen in time domain according to (4.4). To see the scaling in time domain, null-to-null beam widths of observations can be observed. Especially the

ratio between null to null measurements of two sample data should be equal to the ratio of the slopes. Table 4.8 includes two measurements for this observation. In Case I, the slope is found to be  $1,3 \cdot 10^{12} \text{ Hz}^2$  while in Case II, the slope is calculated as  $2,82 \cdot 10^{12} \text{ Hz}^2$ . So the scaling in time should be expected to be around 2,17. In Figure 4.34, the resulting waveforms for Case I and Case II are shown with the null-to-null beam widths. Note that the ratio of the null-to-null beam widths is 2,13, very close to the predicted value above. In this measurement, the change of the center frequency and the nonlinear control of LFMCW source at Case II cause discrepancies between the measured and calculated values.

**Table 4.8: Test variables for effect of frequency span**

	Case I	Case II
Voltage Offset (V)	5	5
Voltage Amplitude (V)	4,36	9,5
Frequency Start (GHz)	6,85	4,78
Frequency End (GHz)	8,92	9,27
Sweep Time (ms)	10,00	10,00
m (2piHz/s)	1,30E+12	2,82E+12
Total Frequency Shift (GHz)	2,07	4,5
Frequency Difference Between Antennas (Hz)	113,6	246,6
Beam Period (ms)	8,4	3,9
Range Period(km)	2511288	1156514
Null to Null interval (ms)	4,4	2,03

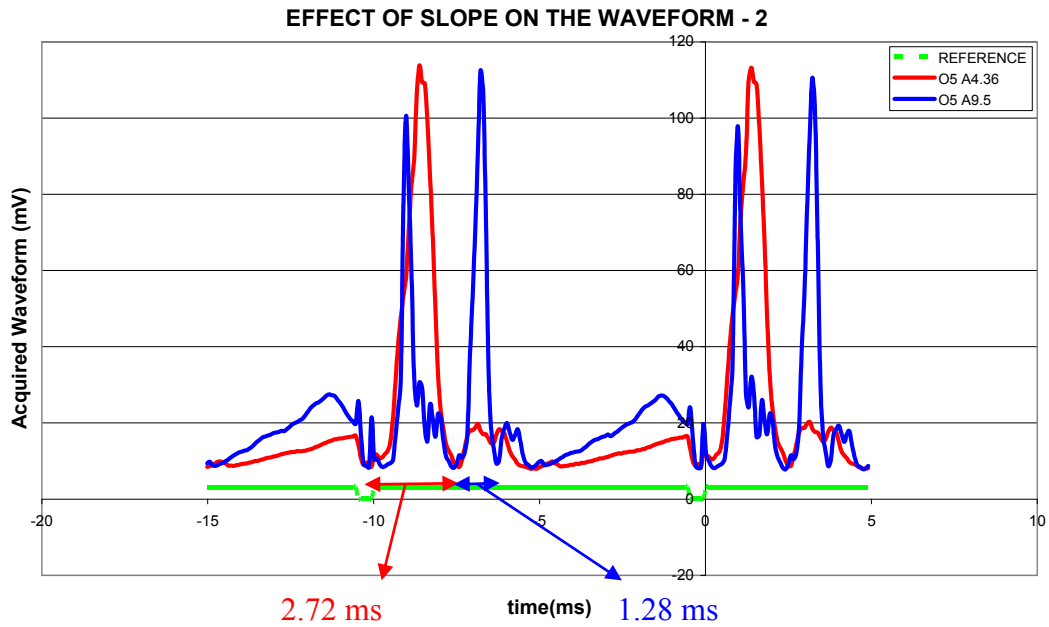


**Figure 4.34: Effect of frequency slope on the time scaling**

Another way to change the slope is to change the scanning period of the saw-tooth waveform controlling the LFM CW source. Here there is no example for this case, but as the period of the LFM CW source is changed, the slope will change and the waveform will scale according to this change. The difference of Figure 4.34 is the fact that in the same period, more frequency points are scanned by the source and two beams in one period at the same observation point are created as shown in the aforementioned figure (blue trace).

## 4.4 RESULTS AND DISCUSSIONS

In this chapter, an implementation of the LFM CW based FDA is presented and measured waveforms are demonstrated. The properties of the waveforms are analyzed comparing to calculated values. The results are found to be consistent with the theoretical findings with some differences (null-to-null beam width, minor deviations from the expected values in some measurements) due to:

- Non-linear scanning regime due to nonlinear control behavior of the oscillator, especially at the frequency extremes.

- Non-ideal spectral properties of implementation parts (antennas, divider, amplifier, detector etc.) being used in the line up.

Despite the measurement non-idealities, some practical advantages and disadvantages of using LFMCW based FDA for beam scanning can be described as:

- Easy handling of beam by just controlling the LFMCW source control waveform is possible. By changing the slope or extents of LFMCW frequency regime, scanning a point in space with more than one beam (due to extra frequency components) in one period of scan, provides frequency agility.
- Implementation of the beam forming network is easier and cheaper as compared to conventional FDA and even conventional scanning phased array structures. This property of the concept can make it an attractive solution in search and track systems as well as telecommunication applications.
- The array can be converted into a more complex form by utilizing T/R modules at each antenna with phase shifters. Although implementations of this chapter do not use phase shifters, it can be used elegantly for solving angular ambiguities (Chapters 6 and 7).
- LFMCW waveform frequency regime should be linear for proper timing. More complex waveforms may be required to control the source. Advancements in digital technologies and increasing clock frequencies would make it possible to create non-linear waveforms in time domain to control the LFMCW source frequencies in a linear fashion.
- The antenna bandwidth is directly related to inter-element delay for efficient usage of FDA. This may require very wide band antennas in the array.
- Similar to the previous point, the oscillator bandwidth is also related to the inter-element delay. Small delays between the

antenna elements may lead to impractical oscillator bandwidths; caution should be taken during the design.

In the following chapters, more information on the properties of LFM CW based FDA will be presented.

## CHAPTER 5

### ANALYSIS OF LFMCW BASED FDA IN A TRANSCEIVER CONFIGURATION

In this chapter, the derivations presented in Chapter 3 is extended to a more practical case where the transmitted fields are received by a similar FDA or an omni-directional antenna element and the amplitude modulations in these cases are analyzed. Also, for the omni-directional receiving antenna case, the analysis is extended into the radar context and some practical parameters are extracted from the formulations. Finally, frequency diversity aspect of the LFMCW based FDA concept is presented with three proposals for the technique.

#### 5.1 TRANSMITTING FDA – RECEIVING FDA CASE

##### 5.1.1 Problem Definition

For the derivations of transmitting FDA – receiving FDA case, two FDA structures with the parameters shown in Figure 5.1 and Figure 5.2 would be defined.

The FDA in Figure 5.1 is the transmitter with the first antenna element at the origin. The inter-element spacing is defined to be  $d$  and inter-element delay is  $T$ . Since this array is the transmitter, the LFMCW source is placed at this site and the array is radiating according to the so-defined parameters of the structure and LFMCW source.

Similar to the transmitter site, the receiver site is also shown in Figure 5.2. According to the figure, primed coordinates and indexes are defined for the

physical parameters of the array; the inter-element distance is  $d'$  and inter-element delay is  $T'$ . In the derivations, it is also assumed that the first antenna in both the transmitting and receiving FDA are placed at the same location in space. This criterion will ease the derivations, but note that the formulations can be easily extended to bi-static case (The reason for this configuration will be clearer in following sections.). Placing the FDA at the same location in space makes  $R_0' = R_0$  as defined in Figure 5.1 and Figure 5.2. In the following paragraphs the range convention will change a little due to placement.

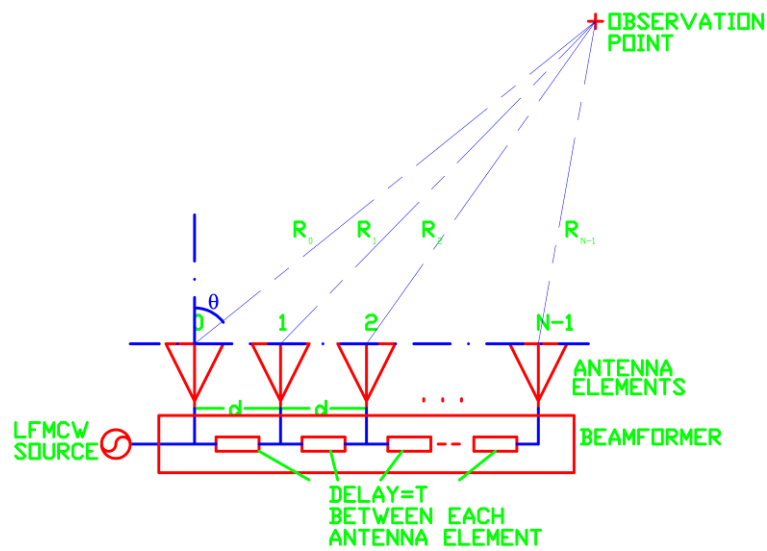


**Figure 5.1: Transmitter Configuration**

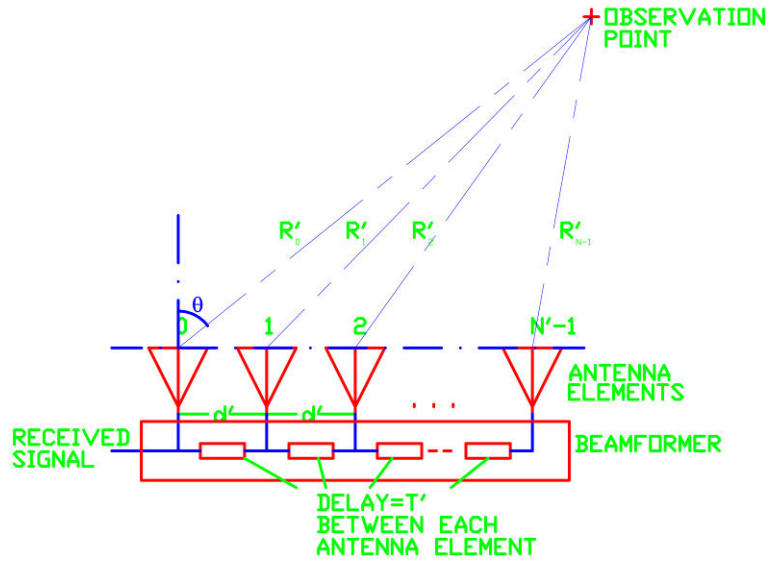


Figure 5.2: Receiver Configuration

The next point to note about is the LFM CW source shown in Figure 5.1. The frequency regime of the source was presented in Figure 3.7 but it is repeated in Figure 5.3 for convenience with the frequency regime given by (3.27) and (5.1) (The equation is repeated here for convenience).

$$\omega = \omega_0 + mt \quad (5.1)$$

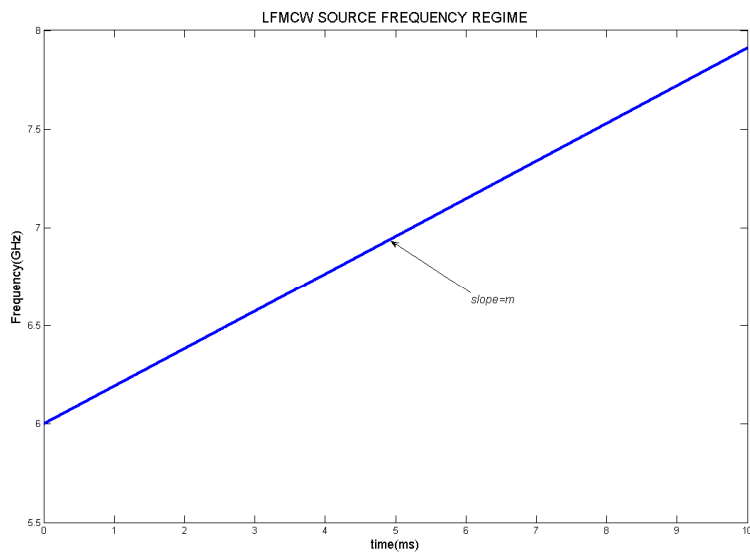


Figure 5.3: LFM CW source frequency regime

The placement of the transmitter and the receiver sites is shown in Figure 5.4. The observation point in Figure 5.4 is  $R'$  away from both arrays (the origin point of the arrays, the first element) and it is at an angle of  $\theta'$  off broadside. The equations of Chapter 3 will be extensively used throughout the derivations but with the parameter name changes according to Figure 5.4.

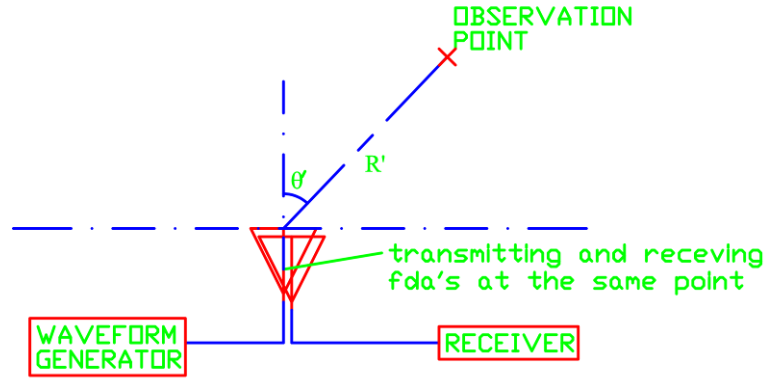


Figure 5.4: The placement of transmitter and the receiver sites in the space

### 5.1.2 Analysis of the Array

Equation (3.47) is the key point in starting the new derivations. In the aforementioned equation the far field array factor was derived which is similar to the transmitting array of this section with  $N$  antenna elements in the array. The equation is repeated below with the parameter changes. Also the inter-element phase shift is assumed to be zero ( $\delta = 0$ ).

$$E_T \cong \frac{1}{R'} e^{j\left(\omega_0 t + \frac{m}{2} t^2 - \frac{\omega_0 R'}{c} - \frac{m R' t}{c}\right)} \sum_{n=0}^{N-1} e^{jn\varphi(R', \theta', t)} \quad (5.2)$$

with

$$\varphi(R', \theta', t) = \left(\frac{\omega_0 + mt}{c}\right) (d \sin(\theta') - cT) + \frac{mTR'}{c} \quad (5.3)$$

Another point to note in (5.2) is that the far field array pattern is named as  $E_t$  to emphasize that this equation belongs to the transmitter site. To ease the above equations further parameter changes can be applied.

$$\Psi_t = \omega_0 t + \frac{mt^2}{2} - \frac{\omega_0 R'}{c} - \frac{mR't}{c} \quad (5.4)$$

Differentiating (5.4) with respect to time, the instantaneous frequency at point  $(R', \theta')$  can be found to be:

$$\omega_t = \omega_0 + mt - \frac{mR'}{c} = \omega_0' + mt \quad (5.5)$$

where

$$\omega_0' = \omega_0 - \frac{mR'}{c} \quad (5.6)$$

and (5.4) can be rewritten as

$$\Psi_t = \omega_0' t + \frac{mt^2}{2} - \frac{\omega_0 R_0}{c} \quad (5.7)$$

Using (5.7) in (5.2),

$$E_t = \frac{1}{R'} e^{j\Psi_t} \sum_{n=0}^{N-1} e^{jn\phi(R', \theta', t)} \quad (5.8)$$

can be reached. Equation (5.8) is a compact form to be used in further analysis. In this equation, as mentioned before, the amplitude modulation at  $(R', \theta')$  is hidden in the summation term and it will not be extended further. Besides  $e^{j\Psi_t}$  term constitutes the linear frequency modulation according to (5.7) at  $(R', \theta')$ . So, the far field array factor (in time domain) can be thought as the LFMCW source displaced from the transmitter site to the  $(R', \theta')$  point, whose amplitude is modulated and the frequency is shifted due to FDA.

Now the attention can be turned into the receiver site. Here a small trick would ease the derivations. As mentioned in the previous paragraph, the waveform at  $(R', \theta')$  is a displaced version of the original LFMCW source, so what is needed is to use reciprocity [2], [46] and make the receiver behave like transmitter whose

fictitious LFMCW source is derived from (5.8). Assume that each antenna in Figure 5.2 has a weighting defined by (5.9).

$$w_{n'} = a_{n'}(\theta', R', t - t_{n'}) e^{j\Psi_t(R', t - t_{n'})} \quad (5.9)$$

In this equation  $n'$  coordinates are reserved for receiver antennas and the index of antennas are arranged between 0 and  $N'-1$ . Another point to note is  $t'_{n'}$ , the delay from the fictitious LFMCW source to the  $n'^{\text{th}}$  receiving FDA antenna element. The far field radiation pattern associated with the receiving FDA can be defined as:

$$E_r = \sum_{n'=0}^{N'-1} \frac{1}{R_{n'}} w_{n'}(t - t_{n'}) f_e(\omega_t(t - t_{n'})) e^{-jk_{n'}(t - t_{n'})R_{n'}} \quad (5.10)$$

In this equation,

$E_r$ : The far field array pattern of receiving FDA in which the far field transmitter FDA array pattern is implicitly utilized.

$R_{n'}$ : The range of observation point to the  $n'^{\text{th}}$  antenna element of the receiving FDA.

$w_{n'}$ : The weighting of  $n'^{\text{th}}$  antenna element as defined in (5.10)

$\omega_t(t - t_{n'})$ : Instantaneous radial frequency at  $n'^{\text{th}}$  antenna element, where  $\omega_t$  is defined in (5.5).

$k_{n'}(t - t_{n'})$ : Instantaneous wavenumber defined at  $n'^{\text{th}}$  antenna element derived from  $\omega_t(t - t_{n'})$ .

$f_e(\omega_t(t - t_{n'}))$ : Element pattern of  $n^{\text{th}}$  antenna element. Take as unity.

Now, the elements of (5.10) can be viewed in mathematical means. The range of observation point to each antenna element in the receiver can be viewed as

$$R_n' = R' - n' d' \sin(\theta') \quad (5.11)$$

Equation (5.11) can be equated to  $R'$  in amplitude terms but should be used as is in phase terms.

$$a_{n'} = \frac{\sqrt{\sigma}}{R'} e^{j\Psi_t(t-t_{n'})} \sum_{n=0}^{N-1} e^{jn\varphi(R',\theta',t-t_{n'})} \quad (5.12)$$

In equation (5.12),  $\sqrt{\sigma}$  is assumed to be the RCS of the target at the observation point. Throughout the derivations, the details about the target reflectivity properties will not be analyzed but this term is used for convenience. The next parameter is the instantaneous wave number explained in (5.13).

$$k_{n'}(t-t_{n'}) = \frac{\omega_0' + m(t-t_{n'})}{c} \quad (5.13)$$

Note that the properties of the fictitious source at the receiver site (in the reciprocal transmitting case) are totally defined by (5.8) as seen in (5.9) through (5.13). Now, (5.11) – (5.13) can be used in (5.10);

$$E_r = \frac{\sqrt{\sigma}}{R'^2} \sum_{n=0}^{N-1} e^{j\Psi_t(t-t_{n'})} \left( \sum_{n=0}^{N-1} e^{jn\varphi(R',\theta',t-t_{n'})} \right) e^{-j\frac{\omega_0' + m(t-t_{n'})}{c}(R' - n'd'\sin(\theta'))} \quad (5.14)$$

Further assume that the inter-element delay in the receiving antenna is  $T'$  as defined in Figure 5.2.

$$t_{n'} = n' T' \quad (5.15)$$

Now, details of (5.14) can be assessed.

$$\begin{aligned} \Psi_t(t-t_{n'}) &= \Psi_t(t-n'T') = \omega_0'(t-n'T') + \frac{m}{2}(t-n'T')^2 - \Delta \\ &= \omega_0't - \omega_0'n'T' + \frac{mt^2}{2} + \frac{mn'^2 T'^2}{2} - mtn'T' - \Delta \end{aligned} \quad (5.16)$$

Where

$$\Delta = \frac{\omega_0 R_0}{c} \quad (5.17)$$

So, using (5.16) in the respective places in (5.14),

$$E_r = \frac{\sqrt{\sigma}}{R'^2} \sum_{n=0}^{N-1} e^{j\left(\omega_0't - \omega_0'n'T' + \frac{mt^2}{2} + \frac{mn'^2 T'^2}{2} - mtn'T' - \Delta\right)} \left( \sum_{n=0}^{N-1} e^{jn\varphi(R',\theta',t-t_{n'})} \right) e^{-j\frac{\omega_0' + m(t-t_{n'})}{c}(R' - n'd'\sin(\theta'))} \quad (5.18)$$

Next,  $\varphi(R', \theta', t - t_{n'})$  term in (5.18) can be written as

$$\varphi(R', \theta', t - t_{n'}) = \varphi(R', \theta', t) - \frac{mn'T'}{c}(d \sin(\theta') - cT) \quad (5.19)$$

Thus, (5.18) becomes;

$$E_r = \frac{\sqrt{\sigma}}{R'^2} \sum_{n'=0}^{N'-1} \left( \begin{array}{c} e^{j\left(\omega_0't - \omega_0'n'T' + \frac{m^2}{2} + \frac{mn'^2T'^2}{2} - mn'T' - \Delta\right)} \\ \sum_{n=0}^{N-1} e^{jn\varphi(R', \theta', t - t_{n'})} e^{-j\frac{mn'T'}{c}(d \sin(\theta') - cT)} \\ e^{-j\frac{\omega_0' + m(t - t_{n'})}{c}(R' - n'd \sin(\theta'))} \end{array} \right) \quad (5.20)$$

The terms in (5.20) can be regrouped;

$$E_r = \frac{\sqrt{\sigma}}{R'^2} \sum_{n'=0}^{N'-1} e^{j\left(\omega_0't + \frac{m^2}{2} - \Delta - \frac{\omega_0'R'}{c} - \frac{mR't}{c}\right)} e^{jn\varphi(R', \theta', t)} \\ e^{jn\left(-\omega_0'T' + \frac{mn'T'^2}{2} - mT' + \frac{\omega_0'd \sin(\theta')}{c} + \frac{mR'T'}{c} + \frac{md \sin(\theta')t}{c} - \frac{mn'd \sin(\theta')T'}{c}\right)} \\ e^{-\frac{jn'nT'}{c}(d \sin(\theta') - cT)} \quad (5.21)$$

In (5.21), a term  $\varphi'(n', t)$  can be defined similar to (3.40); the parameters of this term is defined to be  $n'$  and  $t$ ; but in reality the phase term is also dependent on the position of the observation point. For the context of derivations at this point, the parameters of  $\varphi'$  is assumed to be  $n'$  and  $t$  only:

$$\varphi'(n', t) = -\omega_0'T' + \frac{mn'T'^2}{2} - mT' + \frac{\omega_0'd \sin(\theta')}{c} + \frac{mR'T'}{c} + \frac{md \sin(\theta')t}{c} - \frac{mn'd \sin(\theta')T'}{c} \quad (5.22)$$

Here some assumptions need to be made similar to the ones in 3.2.2. First, note that  $R' \gg \frac{n'cT'}{2}$ , so  $\frac{mn'T'^2}{2}$  term can be ignored in (3.22). This term is a phase term but it is constant. The next assumption can be reached by gathering the phase terms in (5.22) together:

$$\varphi_{\theta'}(n',t) = \sin(\theta') \frac{d'}{c} (\omega_0' + m(t - n'T')) \quad (5.23)$$

In (5.23),  $n'T'$  term is constant term depending on the physical constants of the array. Ignoring this term will cause deformation in the pulse shapes for larger observation point angles (since  $\sin(\theta')$  term is multiplying it) and a shift in the timings. But the deformation can be ignored in analytical derivations. So,  $\frac{mn'd'\sin(\theta')T'}{c}$  term in (5.22) can be ignored throughout the derivations. In summary;

$$\begin{aligned} e^{jn' \left( -\omega_0'T' + \frac{mn'T'^2}{2} - mT' + \frac{\omega_0'd'\sin(\theta')}{c} + \frac{mR'T'}{c} + \frac{md'\sin(\theta')t}{c} - \frac{mn'd'\sin(\theta')T'}{c} \right)} = \\ e^{jn' \left( -\omega_0'T' - mT' + \frac{\omega_0'd'\sin(\theta')}{c} + \frac{mR'T'}{c} + \frac{md'\sin(\theta')t}{c} \right)} = e^{jn'(\varphi'(R',\theta',t))} \end{aligned} \quad (5.24)$$

In (5.24), the phase effect of the receive part turns into a more compact form. Note that the parameters of the phase are announced to be composed of only time and position of the observation point as opposed to the  $\varphi'$  definition in (5.22), but both definitions refer to the same parameter in (5.21). Now a new symbol can be defined as in (5.17),

$$\Delta' = \frac{\omega_0'R'}{c} \quad (5.25)$$

So (5.21) can be rewritten as

$$\begin{aligned} E_r = \frac{\sqrt{\sigma}}{R'^2} \\ \sum_{n'=0}^{N'-1} \sum_{n=0}^{N-1} e^{j \left( \omega_0't + \frac{mt^2}{2} - \Delta - \Delta' - \frac{mR't}{c} \right)} e^{jn'\varphi(R',\theta',t)} e^{jn'\varphi'(R',\theta',t)} e^{-\frac{jnn'mT'}{c}(d\sin(\theta') - cT)} \end{aligned} \quad (5.26)$$

Further let's make another change of parameter;

$$\omega_0'' = \omega_0' - \frac{mR'}{c} = \omega_0 - \frac{2mR'}{c} \quad (5.27)$$

At this point, (5.26) can be rearranged,

$$E_r = \frac{\sqrt{\sigma}}{R'^2} e^{j \left( \omega_0''t + \frac{mt^2}{2} - \Delta - \Delta' \right)} \sum_{n'=0}^{N'-1} \sum_{n=0}^{N-1} e^{jn'\varphi(R',\theta',t)} e^{jn'\varphi'(R',\theta',t)} e^{-\frac{jnn'mT'}{c}(d\sin(\theta') - cT)} \quad (5.28)$$

The last term in (5.28) can be ignored by using similar arguments as in derivation of (5.23). The exponent in the summation can be written as:

$$\varphi_{tot} = n' \varphi'(R', \theta', t) + n \left( \frac{mTR'}{c} + (d \sin(\theta') - cT) \left( \frac{\omega_0 + m(t - n'T')}{c} \right) \right) \quad (5.29)$$

In (5.29),  $n'T'$  term represents the time shift in the exponent and ignoring this term will cause minor deformations in the beam shapes (especially at the null points and beam positions). Ignoring the last term in (5.28) and rearranging the sum terms in the same equation,

$$E_r = \frac{\sqrt{\sigma}}{R'^2} e^{j \left( \omega_0 t + \frac{m^2 t^2}{2} - \Delta - \Delta' \right)} \sum_{n'=0}^{N'-1} e^{jn' \varphi'(R', \theta', t)} \sum_{n=0}^{N-1} e^{jn \varphi(R', \theta', t)} \quad (5.30)$$

can be reached. In this equation

$$\varphi(R', \theta', t) = \frac{\omega_0 + mt}{c} (d \sin(\theta') - cT) + \left( \frac{mTR'}{c} \right) \quad (5.31)$$

$$\varphi'(R', \theta', t) = \frac{\omega_0' + mt}{c} (d' \sin(\theta') - cT') + \left( \frac{mT'R'}{c} \right) \quad (5.32)$$

The last two summations in (5.30) represent the amplitude modulation effect due to the configurations of transmitting FDA, receiving FDA and the LFMCW source. The exponential term outside the summation section represents the incoming LFMCW waveform at the receiver, which has valuable information regarding the range of the target and the time of arrival.

The derivations shown are very basic and can be easily extended to bistatic case where the transmitter and receiver sites are not at the same point, but the equations will be somewhat more complex. Also, if the transmitter site and receiver site are at different positions in space, the receiver cannot benefit from the original LFMCW waveform in detecting the beat term present in the carrier term of (5.30). These considerations will be discussed in further sections.

### 5.1.3 Physical Explanation of the Mechanism

The amplitude modulation shown in (5.30) is an important property of the array since an observation point in space can be focused due to the double

summation term in the aforementioned equation. The peak points of the resulting beam will be defined as:

$$\varphi(R', \theta', t) = 2p\pi, p \in N \quad (5.33)$$

$$\varphi'(R', \theta', t) = 2q\pi, q \in N \quad (5.34)$$

The simultaneous solution of these two equations is hard to compute and require numerical techniques to find the solution (at this point no numerical computation will be performed, but a basic demonstration will be presented in the next chapter using measurements). The main point here is that specific points (derived by calculations) in space can be scanned using two arrays, causing focusing. The points can be shifted by changing the inter-element delays or distances of the FDA antennas (in reality this is impossible), LFMCW source parameters (minimum and maximum frequencies, the slope of the LFMCW source frequency regime, scanning time etc.), configurations of FDA antennas (positions of FDA antennas with respect to each other, and angular bearing of both with respect to each other etc.) and even utilizing phase shifters at the transmitter or receiver (although during derivations, the phases of the transmitting and receiving FDA were assumed to be zero, (5.31) and (5.32) can employ the phase shift values in respective FDA structures directly).

In (5.30), outside the summation terms (i.e. the amplitude modulation term), there exists the carrier term. The carrier at the receiver is again an LFMCW signal, a modified version of the original LFMCW source output. This term has the required information about the position of the target that is observed (FMCW radar concept can be applied and will be analyzed in this chapter for a special case).

#### **5.1.4 Discussion on the Array Design**

The array design requirements for transmitter or receiver are very similar to the ones presented in Chapter 3 but in this case care should be taken in the design, since scanning dynamics now depend on both transmitter and receiver arrays due to (5.33) and (5.34).

As mentioned before, the scanning dynamics of the arrays can be manipulated by changing the frequency scanning regime. In (5.31) and (5.32), the

slope of frequency regime and extents of scanning have direct effect on the solutions of (5.33) and (5.34). The aforementioned change is easy to apply at the source and the system can be adapted for increased scanning range by just adjustment of the LFMCW source.

The physical properties of the FDA transmitter and receiver systems can also be modified for increased scanning range. Especially by modifying the broadside direction of one of the arrays (in this case the range of observation point to the arrays will be different and the derivations of this section will not apply to the case), the solution range of amplitude modulation can be increased. Another clever solution is to turn one of the arrays by 180 degrees without changing the broadside direction of the array. This solution can also be beneficial in optimum placement of the arrays at the same point in space.

During design, phase shifters or switched delay lines at each antenna element of transmitter or receiver or both can be accompanied. Phase shifters can be benefited in (5.31) and (5.32), since the solution points of (5.33) and (5.34) will be broadened to increase the focused scanning range of the system, at the expense of increased costs.

In the next section, a special case will be analyzed where FDA transmitter and omni-Directional receiver is placed at the same point in space. Although there is no focusing effect in this case (focusing through an angular sector is still possible just by arranging for a limited frequency scan at the LFMCW source), it is helpful in viewing the array structure as a part of a radar system.

## **5.2 ANALYSIS OF A SPECIAL CASE: TRANSMITTING FDA – RECEIVING OMNI DIRECTIONAL ANTENNA**

In this section, the analysis will focus on the special case of the first section where the receiving FDA is turned into a single omni-directional antenna. The aim of the analysis is to observe the performance of the system by gathering data from the space and find techniques to investigate the targets.

### 5.2.1 Problem Definition

In the problem, the transmitting FDA shown in Figure 5.1 is used but a single antenna is used for receiving. The problem geometry is sketched in Figure 5.5. In the analysis, it will be assumed that the first antenna of the FDA and the receiving omni-directional antenna are at the same point in space. The other parameters are same as the one shown in Figure 5.4.

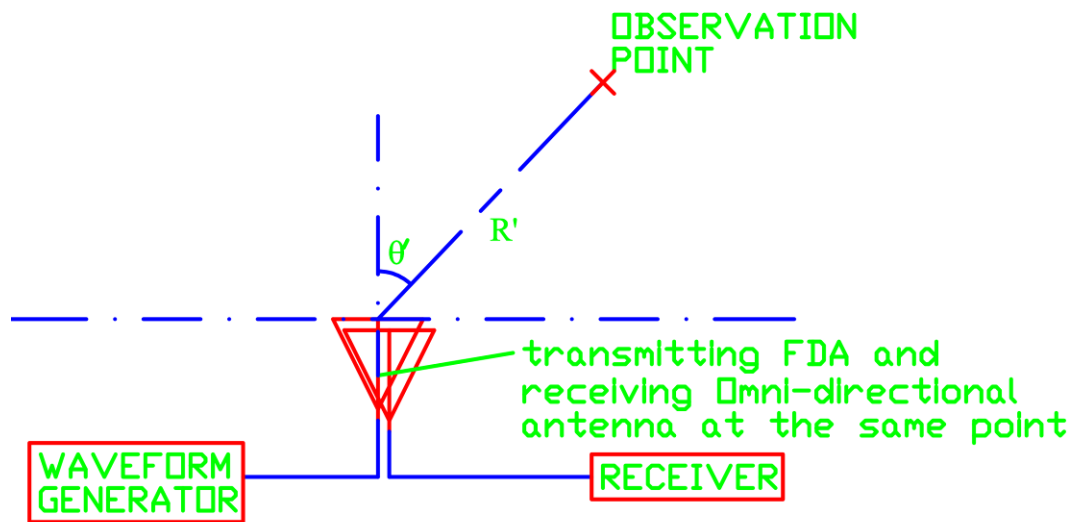


Figure 5.5: Problem sketch for Transmitting FDA-Receiving Omni-directional antenna

### 5.2.2 Analysis of the Fields

The analysis of the case is simple, because what is needed is to modify (5.30) such that the receiving FDA antenna is composed of a single antenna. Also note that the single antenna of the receive array is placed at the origin with the first antenna of the transmitting FDA as assumed before.

Now, assume that  $N^2=1$  in (5.30);

$$E_r = \frac{\sqrt{\sigma}}{R'^2} e^{j\left(\omega_0 t + \frac{mt^2}{2} - \Delta - \Delta'\right)} \sum_{n=0}^{N-1} e^{jn\phi(R', \theta', t)} \quad (5.35)$$

The effect of single antenna at the receiver is not felt at the amplitude modulation but at the carrier phase. Since the waves experience delay while travelling from the target back to the receiving antenna.

In the following subsection, the incoming wave from the target will be investigated in the radar context and important parameters regarding the radar performance will be derived.

### 5.2.3 Analysis of the Case in RADAR Context and Extraction of Design Parameters

#### 5.2.3.1 Beat and Doppler Frequency Derivations

For the analysis in the radar context, the range and velocity of the target should be taken into account in the derivations. Expanding (5.35) using (5.27);

$$E_r = \frac{\sqrt{\sigma}}{R'^2} e^{j\left(\omega_0 t + \frac{mt^2}{2} - \frac{2mR't}{c} - \Delta - \Delta'\right)} \sum_{n=0}^{N-1} e^{jn\phi(R', \theta', t)} \quad (5.36)$$

can be reached. Assume that the velocity of the target is  $v$ , so the range of the target can be expressed as  $R' - vt$ . In (5.36), the range expressions in the equation would be replaced with the last expression for the derivations. Now, let's define a new symbol for the phase expression of the carrier:

$$\phi = \left( \omega_0 t + \frac{mt^2}{2} - \frac{2mR't}{c} - \Delta - \Delta' \right) \quad (5.37)$$

Expanding the last equation

$$\phi = \omega_0 t + \frac{mt^2}{2} - \frac{2mR't}{c} - \frac{2\omega_0 R'}{c} + \frac{mR'^2}{c^2} \quad (5.38)$$

Now,  $R' - vt$  can be placed into (5.38) instead of  $R'$

$$\phi = \omega_0 t + \frac{mt^2}{2} - \frac{2m(R' - vt)t}{c} - \frac{2\omega_0(R' - vt)}{c} + \frac{m(R' - vt)^2}{c^2} \quad (5.39)$$

or

$$\phi = \omega_0 t + \frac{mt^2}{2} - \frac{2mR't}{c} + \frac{2mvt^2}{c} - \frac{2\omega_0 R'}{c} + \frac{2\omega_0 vt}{c} + \frac{mR'^2}{c^2} + \frac{mv^2 t^2}{c^2} - \frac{2mR'vt}{c^2} \quad (5.40)$$

Regrouping the terms in (5.40)

$$\phi = \omega_0 t + \frac{mt^2}{2} + t \left( -\frac{2mR'}{c} + \frac{2\omega_0 v}{c} - \frac{2mR'v}{c^2} \right) + t^2 \left( \frac{2mv}{c} + \frac{mv^2}{c^2} \right) - \frac{2\omega_0 R'}{c} + \frac{mR'^2}{c^2} \quad (5.41)$$

In (5.41),  $\frac{2mR'v}{c^2}$  is very small compared to  $\frac{2mR'}{c}$  term. Although it is in the exponential term, both terms are being multiplied by time, and  $\frac{2mR'v}{c^2}$  can be dropped from the equation. Same considerations also apply to  $\frac{mv^2}{c^2}$  term multiplying  $t^2$ . This term is much smaller than  $\frac{2mv}{c}$  and can be dropped. So, (5.41) becomes;

$$\phi = \omega_0 t + \frac{mt^2}{2} + t \left( -\frac{2mR'}{c} + \frac{2\omega_0 v}{c} \right) + t^2 \frac{2mv}{c} - \frac{2\omega_0 R'}{c} + \frac{mR'^2}{c^2} \quad (5.42)$$

Using (5.42) in (5.36);

$$E_r = \frac{\sqrt{\sigma}}{R'^2} e^{j \left( \omega_0 t + \frac{mt^2}{2} + t \left( -\frac{2mR'}{c} + \frac{2\omega_0 v}{c} \right) + t^2 \left( \frac{2mv}{c} - \frac{2\omega_0 R'}{c} + \frac{mR'^2}{c^2} \right) \right)} \sum_{n=0}^{N-1} e^{jn\phi(R'-vt, \theta', t)} \quad (5.43)$$

In (5.43), the amplitude modulation terms are also affected by the velocity of the target. Now, let's look at the exponential in the summation term.

$$\begin{aligned}
\varphi(R'-vt, \theta, t) &= \frac{\omega_0 + mt}{c} (d \sin(\theta') - cT) + \left( \frac{mT(R'-vt)}{c} \right) \\
&= \frac{\omega_0}{c} (d \sin(\theta') - cT) + t \left( \frac{m}{c} d \sin(\theta') - mT - mT \left( \frac{v}{c} \right) \right) + \frac{mTR'}{c} \quad (5.44)
\end{aligned}$$

In (5.44),  $\frac{v}{c}$  term (doppler) is also affecting the amplitude modulation term.

Remember that at any time in space, only at specific points the pulses form. The effect of this Doppler term is to shift these points, since for a constant velocity target, this term will be constant. For the time being it can be ignored since it is much smaller than 1. So (5.44) can be written as

$$\varphi(R'-vt, \theta, t) = \frac{\omega_0}{c} (d \sin(\theta') - cT) + t \left( \frac{m}{c} d \sin(\theta') - mT \right) + \frac{mTR'}{c} \quad (5.45)$$

So, the velocity and range information regarding the target would be fetched from the carrier [5, 47, 48, and 49]. Multiplying the incoming signal from the target with the original carrier,  $e^{j\left(\omega_0 t + \frac{mt^2}{2}\right)}$  of the LFM CW source, the beat and the Doppler information about the target can be directly found [49]. The carrier after mixing is (target reflectivity and range coefficients ignored):

$$E_{r,carrier} = e^{j\left(t\left(\frac{-2mR'}{c} + \frac{2\omega_0 v}{c}\right) + t^2\left(\frac{2mv}{c} - \frac{2\omega_0 R'}{c} + \frac{mR'^2}{c^2}\right)\right)} \quad (5.46)$$

The phase term in (5.46) is (down-converted signal):

$$\phi_{dc} = t\left(-\frac{2mR'}{c} + \frac{2\omega_0 v}{c}\right) + t^2 \frac{2mv}{c} - \frac{2\omega_0 R'}{c} + \frac{mR'^2}{c^2} \quad (5.47)$$

And the frequency is just the time derivative;

$$\omega_{dc} = \left(-\frac{2mR'}{c} + \frac{2\omega_0 v}{c}\right) + t \frac{4mv}{c} \quad (5.48)$$

In this term,  $\frac{2\omega_0 v}{c}$  part is much smaller than  $\frac{-2mR'}{c}$  (beat) and constitutes the doppler frequency. In one pulse, the range information can be fetched but the doppler frequency can be found by dwelling on the target with more than one pulse [49], with slow time variation. The beat frequency in (5.48) is:

$$\omega_{beat} = \frac{2mR'}{c} \quad (5.49)$$

$$f_{beat} = \frac{mR'}{\pi c} \quad (5.50)$$

and the doppler frequency is (in conventional LFMCW radar analysis, the frequency scan is assumed to be much smaller than the center frequency of operation and according to [49], the Doppler frequency is derived to be dependent on the center frequency. In LFMCW fed FDA, unfortunately the LFMCW frequency scan bandwidth may be such large that center frequency approximation cannot hold):

$$\omega_{doppler} = 2\omega_{inst} \frac{v}{c} = 2(\omega_0 + 2mt) \frac{v}{c} \quad (5.51)$$

$$f_{doppler} = (\omega_0 + 2mt) \frac{v}{c\pi} \quad (5.52)$$

As mentioned before, for Doppler processing slow time variation should be taken into account. The Fourier Transform in each pulse period, results in a spectrum related to ranges according to (5.50), and for each range a number of pulse returns should be collected, whose Fourier Transform (in a range cell, i.e. frequency point) would give the Doppler frequency of the target due to phase component coming from (5.52). Details of LFMCW radar processing can be found in [49].

### 5.2.3.2 Further Derivations and Heuristic Methods for Processing

In the previous paragraph, a new term for the LFMCW based FDA analysis was defined, pulse period. In Figure 3.7, LFMCW source frequency regime was presented but in this figure, the frequency is assumed to be increasing indefinitely. Throughout the measurements, the period of the saw-tooth waveform was defined, which is in fact the pulse period. In this section this concept will be cleared first. In Figure 5.6 a realistic frequency regime for the LFMCW source is shown. According to Figure 5.6, the period of the LFMCW source is shown to be  $T_r$ . The starting frequency of scan is  $\omega_0$  and the maximum frequency in a period is  $\omega_{\max} = \omega_0 + mT_r$ .

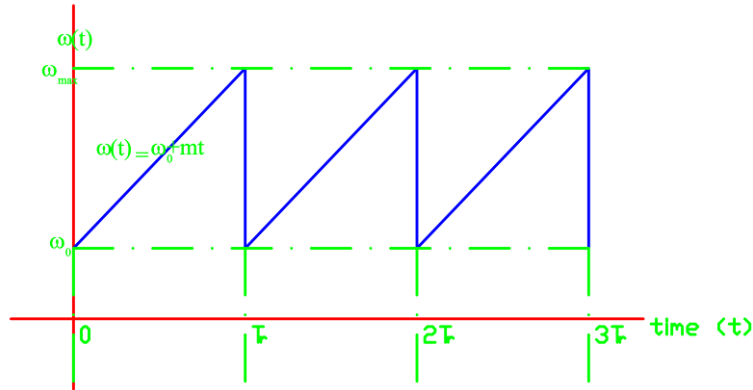


Figure 5.6: A realistic LFMCW frequency regime plot

Remember from (3.58) that there was also the pulse period, which is due to source frequency scanning dynamics. The equation for pulse period is repeated in (5.53).

$$\Delta t = \frac{2\pi}{mT \left( \frac{\sin(\theta)}{s} - 1 \right)} \cong \frac{1}{\Delta f} \quad (5.53)$$

The pulse period,  $\Delta t$  found in (5.53) can be smaller or larger than  $T_r$  depending on the frequency extent of scan. If  $\Delta t$  is larger than  $T_r$ , the period of scan turns out to be  $T_r$  of Figure 5.6, otherwise staggered PRI is attained where different frequency components are used to scan a point in space during a period

of the source (this property can be used for frequency diversity as will be demonstrated in following sections).

Now, let's turn the attention toward baseband waveform.

$$E_{r,baseband} = \frac{\sqrt{\sigma}}{R'^2} e^{j(t\omega_{beat} + \phi_{doppler}(t) - \phi_{const})} \sum_{n=0}^{N-1} e^{jn\varphi(R',\theta',t)} \quad (5.54)$$

where  $\omega_{beat}$  is given by (5.49), the amplitude modulation term was analyzed in Chapter 3, while  $\phi_{doppler}(t)$  and  $\phi_{const}$  are

$$\phi_{doppler}(t) = \frac{2v}{c} (\omega_0 t + mt^2) \quad (5.55)$$

$$\phi_{const} = \frac{mR'^2}{c^2} - \frac{2\omega_0 R'}{c} \quad (5.56)$$

In (5.54), assume that the Doppler frequency is much smaller than the beat frequency. The maximum range of interest during the operation can be defined as  $R_{max}$ , and this range makes the maximum beat frequency to be

$$\omega_{beat,max} = \frac{2mR_{max}}{c} \quad (5.57)$$

According to the maximum beat defined in (5.57), sampling rate in each period shown in Figure 5.6 should be decided assuming that  $\Delta t \geq T_r$ . Now, assume that in each period M samples are gathered from the incoming waveform making;

$$\frac{M}{T_r} \geq \frac{2\omega_{beat,max}}{2\pi} = \frac{\omega_{beat,max}}{\pi} \quad (5.58)$$

Using (5.57) in (5.58) and rearranging (5.58);

$$\frac{M}{T_r} \geq \frac{2mR_{max}}{c\pi} \quad (5.59)$$

or

$$M \geq \frac{2mT_r R_{max}}{c\pi} \quad (5.60)$$

Now assume that  $\Delta t = T_r$ , so

$$M \geq \frac{4R_{\max}}{cT} \quad (5.61)$$

is required. The returning pulses from the target are amplitude modulated as shown in (5.54) and the pulses are sinc-type. Similar to (3.62), the null-to-null interval of the pulses is

$$\Delta t_{\text{null-to-null}} = \frac{4\pi}{mNT} \quad (5.62)$$

and the modulated pulse is filled with signal at beat frequency. The number of samples in the null-to-null interval of the pulses is

$$M' \geq \frac{8R_{\max}}{cNT} \quad (5.63)$$

Equation (5.63) is independent of PRI selection or slope of LFMCW source frequency slope, depending on the number antenna elements, inter-element delay and the maximum range of interest.

The range information of the pulses can be fetched from the frequency spectrum using FFT algorithms. The Fourier transform of the amplitude modulation (5.54) is shown theoretically in Figure 5.7 with amplitude of unity is assumed in (5.54). Figure 5.7 also defines the range resolution to be:

$$R_{\text{res}} = \frac{N(d \sin(\theta') - cT)}{4} \quad (5.64)$$

In (5.64) if  $cT \gg d \sin(\theta')$ , it can be further simplified to be

$$R_{\text{res}} = \frac{NcT}{4} \quad (5.65)$$

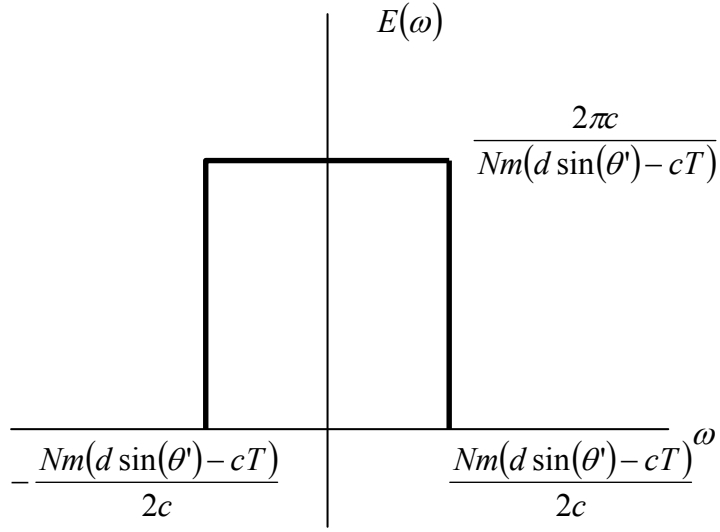


**Figure 5.7: Fourier Transform of (5.54) with unity amplitude assumption**

In (5.65), the range resolution is dependent on the inter-element delay and the number of antennas in the array. Increasing the number of antennas in the array, the null-to-null interval of the pulses decrease and it causes the spectral width of the Fourier transform of the pulses to increase. So the range resolution decreases. Similar concern is also true for the inter-element delay due to (5.62). Summing up, as the total delay over the aperture of the array is increased (instantaneous bandwidth over the aperture of the array is increased), the range resolution is improved.

Next, the time resolution of the pulses will be found. Before getting into time resolution derivation, the amplitude modulation term in (5.54) can be revisited.

$$\begin{aligned}
 E_{r,baseband\_AM} &= \sum_{n=0}^{N-1} e^{jn\varphi(R',\theta',t)} \\
 &= e^{j\left(\frac{N-1}{2}\varphi\right)} \frac{\sin\left(\frac{N\varphi}{2}\right)}{\sin\left(\frac{\varphi}{2}\right)}
 \end{aligned} \tag{5.66}$$

The 3dB points can be formulated as (Appendix 2)

$$\frac{N\varphi}{2} \approx 1.414 \quad (5.67)$$

And the 3dB beam width is found as

$$\Delta\varphi = \frac{5.636}{N} \cong \frac{1.8\pi}{N} \quad (5.68)$$

Figure 5.8 shows a normalized incoming pulse from a target in space. The resolution in time can be defined to be the interval between the 3dB points using (5.68) and (3.51) assuming that the range and angular bearing of the target are known.

$$\Delta t_{3db} \approx \left| \frac{1.8\pi}{NmT \left( \frac{\sin(\theta)}{s} - 1 \right)} \right| \quad (5.69)$$

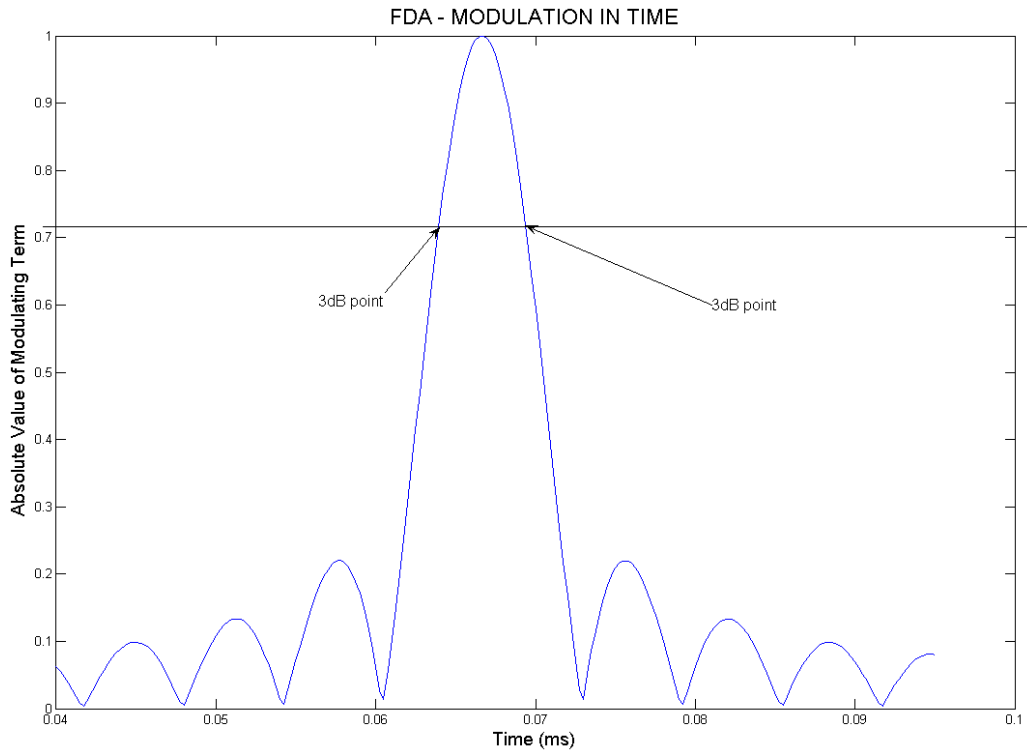


**Figure 5.8: Incoming pulses in time domain and 3dB points. The simulation is made for an 32 element antenna array with inter-element spacing of 25mm and delay of 0.55ns. Also the starting frequency is 6GHz with 2GHz scan in 1ms.**

Equation (5.69) can be simplified assuming that  $cT \gg d \sin(\theta)$ ;

$$\Delta t_{3db} \approx \frac{1.8\pi}{NmT} \quad (5.70)$$

In (5.70), as the total instantaneous bandwidth of the array,  $NmT$ , is increased (total frequency shift on the aperture of the array), the time resolution is improved as expected.

Next, angular resolution should be found. In the derivation of angular resolution it will be assumed that the range of the target is known and the time of arrival of the pulses be known with a resolution presented in (5.70). So the time of arrival of the pulses can be measured to be at the leftmost 3dB point or rightmost 3dB point shown in Figure 5.8. Now assume that the leftmost 3dB point is at  $t_0$  and that of the rightmost is at  $t_1 = t_0 + \Delta t_{3dB}$ . Also assume that  $\theta_0$  measurement is made for  $t_0$  and  $\theta_1 = \theta_0 + \Delta\theta$  measurement is made for  $t_1$ . So two equations from (3.45) can be produced regarding these two solutions (assume  $\delta = 0$  in (3.45)):

$$\varphi_1 = \frac{mT}{c} R' + \left( \frac{\omega_0 + mt_0}{c} \right) (d \sin(\theta_0) - cT) \quad (5.71)$$

$$\varphi_2 = \frac{mT}{c} R' + \left( \frac{\omega_0 + mt_1}{c} \right) (d \sin(\theta_1) - cT) \quad (5.72)$$

The difference between the phase terms in (5.72) and (5.71) is shown in (5.68);

$$\varphi_2 - \varphi_1 = \Delta\varphi = \frac{1.8\pi}{N} \quad (5.73)$$

Expanding  $t_1$  in (5.72) and using (5.71) and (5.72) in (5.73);

$$\frac{1.8\pi}{N} = \left( \frac{\omega_0 + mt_0}{c} \right) d(\sin(\theta_1) - \sin(\theta_0)) + \frac{m\Delta t}{c} (d \sin(\theta_1) - cT) \quad (5.74)$$

In (5.74), assume that  $d \sin(\theta_1) \ll cT$  (according to 3.51,  $s$  can be designed to be larger than 1);

$$\frac{1.8\pi}{N} = \left( \frac{\omega_0 + mt_0}{c} \right) d(\sin(\theta_1) - \sin(\theta_0)) + \frac{m\Delta t}{c} (-cT) \quad (5.75)$$

Using (5.70) in (5.75),

$$\frac{1.8\pi}{N} = \left( \frac{\omega_0 + mt_0}{c} \right) d(\sin(\theta_1) - \sin(\theta_0)) - \frac{1.8\pi}{N} \quad (5.76)$$

or

$$\frac{3.6\pi}{N} = \left( \frac{\omega_0 + mt_0}{c} \right) d(\sin(\theta_1) - \sin(\theta_0)) \quad (5.77)$$

and the difference between the sines can be found as

$$\frac{3.6\pi c}{Nd(\omega_0 + mt_0)} = \sin(\theta_1) - \sin(\theta_0) \quad (5.78)$$

For  $\theta_1 = \theta_0 + \Delta\theta$ , (5.78) can be turned into a more handy form to deal with;

$$\sin(\theta_0)(\cos(\Delta\theta) - 1) + \cos(\theta_0)\sin(\Delta\theta) = \frac{3.6\pi c}{Nd(\omega_0 + mt_0)} \quad (5.79)$$

Continuing the simplifications;

$$\sin(\theta_0)(\cos(\Delta\theta) - 1) + \cos(\theta_0)\sin(\Delta\theta) = \frac{3.6\pi}{Nd \frac{\omega_{inst}(t_0)}{c}} \quad (5.80)$$

where,  $\omega_{inst}(t_0)$  is the instantaneous frequency output of the LFM CW source at  $t_0$ .

In (5.79), the angular resolution seems to depend on the angle of arrival, the number of antennas and the time of arrival or the instantaneous frequency of the waveform on the target. The instantaneous frequency of waveform or wavelength changes the effective aperture length of the array and directly affects the angular resolution. Similar arguments are also true for the number of antennas, since it directly affects the effective aperture of the array. The angle of arrival can be defined using Figure 5.9 for analysis. According to the figure, three different targets at three distinct angles are defined. The effective aperture of the array looking at these three points will be different, so does the angular resolution. Especially, the third point has a very low effective aperture such that the angular resolution may not be found at this point.



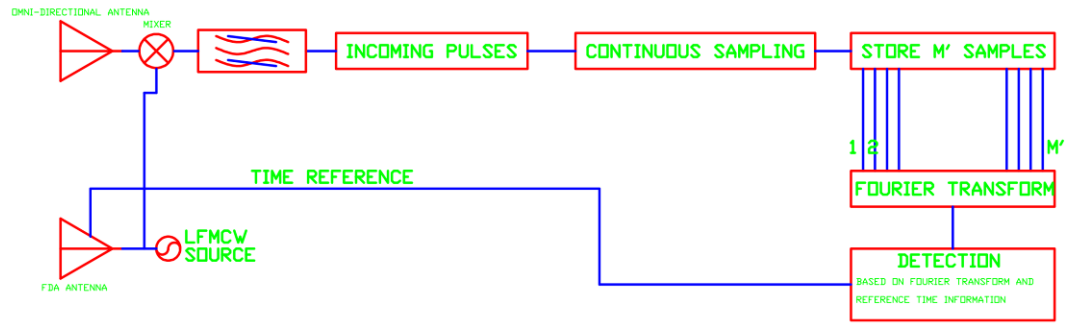


**Figure 5.10: A proposal for FDA processing. Pipelined structure is used where the FFT at each step would provide possible target ranges. Using the time reference from the transmitter, other information about the target can be collected.**

The received pulses from space are multiplied with signal from the source and at the output of the mixer, baseband waveform is produced. After filtering, the baseband waveform is sampled continuously (pipelining). At each known time, the Fourier transform outputs of the samples are checked for range information from a possible target (details about the Fourier transform and frequency resolution are not analyzed). With the time information, spectral output and reference time from the transmitter side, angular bearing of the target can be fetched using (3.45). By making observations on a target over multiple source periods, Doppler information can be gathered as mentioned before [47], [49]. Further analysis is not performed for this application but in Chapter 7 various simulations of FDA and FDA radar will be demonstrated.

#### 5.2.4 A Typical Example

A basic example for the analyzed radar parameters is shown in Table 5.1. In this example, FDA array contains 64 antenna elements and the inter-element distance is designated as 25mm. Inter-element delay is 0,5ns and the corresponding frequency scan extent is 2GHz starting from 6GHz. The period of scan is 5ms and the maximum range of interest is assumed to be 0,5km.

**Table 5.1: An example for a radar structure using FDA for transmit and Omni-directional antenna for receive**

Number of antennas in the system	64
Inter-element spacing(mm)	25,00
Inter-element delay(ns)	0,50
Starting Frequency(GHz)	6,00
Total Frequency Change(GHz)	2,00
Tr (period of the LFM CW frequency regime) (us)	5000,00
Rmax (km) (assumed)	0,50
m (slope of the LFM CW frequency regime) (Hz <sup>2</sup> )	2,51E+12
Frequency Difference Between Antennas (Hz)	200,00
delta-t (FDA period) (us)	5000,00
PRI(us)	5000,00
Null-to-Null interval of the pulses(ms)	0,16
Duty Cycle of the Pulses (%)	3,13
Instantaneous Bandwidth of the pulses (kHz)	80,42
Unambiguous Range (km)	750,00
$f_{beat,max}$ (MHz)	1,33
Sampling Frequency >= (MHz)	2,67
M(number of samples in null-to-null interval)>=	417
M(number of samples in one period)>=	13333,33
Number of samples in a single pulse	416,67
Time Resolution(us)	70,32
Range Resolution (m)	2,40
Time step in the processing (us)	0,38

According to Table 5.1, the frequency difference between the antenna elements is calculated as 200 Hz and the corresponding beam period becomes 5ms; which is equal to the LFM CW source period (this is a flexible parameter and can be utilized for waveform diversity as explained in next section). The null-to-null interval of the pulses is 0,16ms, making the duty cycle 3,2%. As mentioned before the maximum range of interest is assumed to be 0,5km and the corresponding beat frequency is 1,33MHz. The sampling frequency is chosen according to the so-said maximum beat frequency, making the number of samples in one period larger than 13333. Similarly, the number of samples in the pulse is minimum 416. The resulting time resolution is 70us while the range resolution is 2,4m.

For the angular resolution, the time of arrival of pulses is important in the calculations (5.80). For the current example Figure 5.11 shows the time of travel of pulses from the FDA to the target (since from the target back to antenna wave would travel as a packet, it will not be taken into account here) versus the look angle for  $p=1$  in 3.2.3 (where  $\varphi = 2p\pi$ ). In this figure, three different ranges are checked and the other points are for higher ranges. The dependency of time of arrival on the angle of arrival becomes sharper near the bore-sight and as the angle of arrival goes through the end-fire directions, the sensitivity decreases.

Table 5.2 shows the time-of arrivals  $\varphi = 2p\pi, p=1$  and angular resolution for a target at 250 m and various angular bearings. The angular resolution of targets is not symmetric about zero degrees (like the time of arrival) due to increasing frequency of operation at the source, i.e. increasing electrical length of the array.

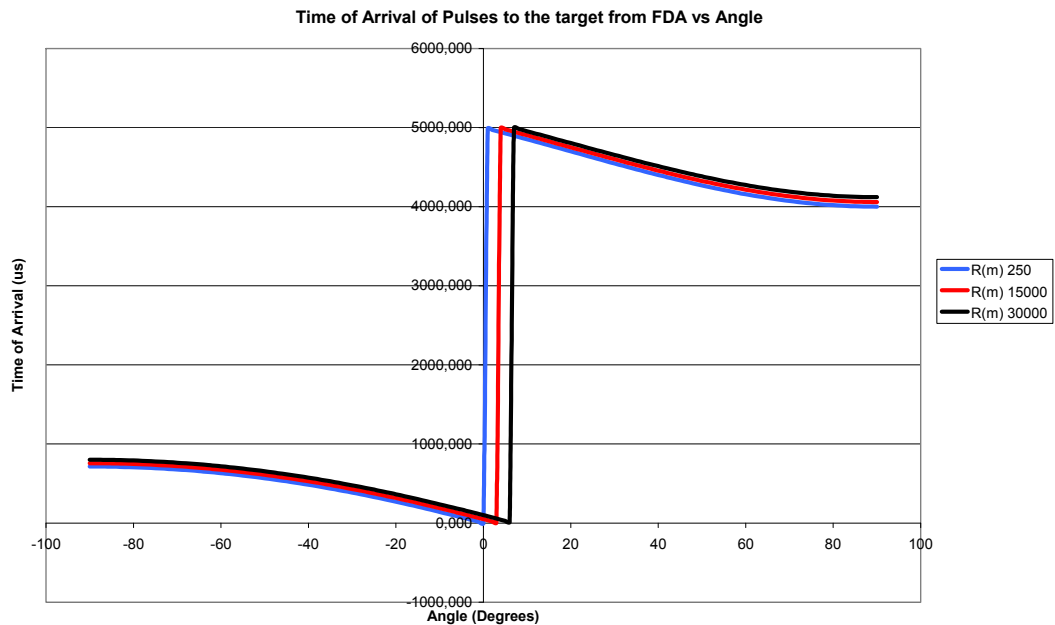


Figure 5.11: Dependency of time-of-arrival on the target angle,  $\varphi = 2p\pi, p = 1$

**Table 5.2: Time of arrivals and angular resolution for a target at 250m range and various angles for  $\varphi = 2p\pi, p = 1$  .**

R(m)	$\theta$ (degrees)	Arrival Time(us) (superimposed into one period)	$\Delta\theta$ , (degrees)
250	-60	631,388	5,7
250	-55	601,359	5,1
250	-50	566,834	4,6
250	-45	527,878	4,4
250	-40	484,576	4,2
250	-35	437,035	3,7
250	-30	385,385	3,6
250	-25	329,786	3,4
250	-20	270,434	3,3
250	-15	207,562	3,3
250	-10	141,446	3,2
250	-5	72,411	3,2
250	0	0,833	3,2
250	5	4927,145	2,4
250	10	4851,839	2,5
250	15	4775,465	2,5
250	20	4698,638	2,6
250	25	4622,029	2,8
250	30	4546,364	2,9
250	35	4472,418	3,1
250	40	4401,006	3,3
250	45	4332,967	3,7
250	50	4269,153	4,1
250	55	4210,407	4,7
250	60	4157,548	5,5

Likewise, Table 5.3 shows a similar case for 450 m.

**Table 5.3: Time of arrivals and angular resolution for a target at 250m range and various angles for  $\varphi = 2p\pi, p = 1$**

<b>R(m)</b>	<b><math>\theta</math> (degrees)</b>	<b>Arrival Time(us) (superimposed into one period)</b>	<b><math>\Delta\theta</math>, (degrees)</b>
450	-45	528,474	4,2
450	-25	330,409	3,4
450	-15	208,201	3,3
450	-5	73,068	3,2
450	0	1500	3,2
450	5	4927,822	2,4
450	15	4776,162	2,5
450	25	4622, 746	2,8
450	45	4333,723	3,7

Up to this point basic radar parameters of the array are analyzed but the analysis can be extended to more sophisticated points like waveform design, Doppler processing etc. In this thesis, these points are not investigated but left for future research on the subject (Chapter 8 deals with the proposals for the future research on LFMCW based FDA).

### **5.3 FREQUENCY DIVERSITY ASPECT OF LFMCW BASED FDA**

In FDA mechanism, the main reason for the beam formation is the interference of waves with different frequencies from the antennas of the array. The interference points in space continually change and at a fixed setting of parameters, each point in space is scanned by a single group of frequency. The continuous scanning characteristic of LFMCW source and the flexible properties of FDA structure can be beneficial in scanning space with different frequencies (frequency diversity). This property of the array increases the resistance of the application of array against interferences like multi-path returns.

Frequency Diversity is explained in various sources in literature. In [7], a detailed treatment of diversity is presented. According to [7], a target with radial length of  $L_r$ , will have a correlation frequency;

$$f_c = \frac{c}{2L_r} \quad (5.83)$$

and the number of independent target samples for a bandwidth of  $\Delta f$  would be

$$n_e = 1 + \frac{\Delta f}{f_c} \quad (5.84)$$

So increasing the total bandwidth of scan increases the number of independent pulses, solving the fluctuation loss problems encountered in radar applications [7].

In this section three methods to accomplish frequency diversity will be explained.

### 5.3.1 How to Benefit from Frequency Diversity – Proposal 1

In this technique at every antenna in the array, a phase shifter / delay line is placed as shown in Figure 5.12. Assume that for  $n$ th antenna, the phase shifter setting is  $\delta_n = n\delta$ . So, (3.45) can be rewritten below for further analysis.

$$\varphi(n, t) = \frac{mT}{c} R_0 + \left( \frac{\omega_0 + mt}{c} \right) (d \sin(\theta) - cT) - \delta \quad (5.85)$$

As mentioned before, the points where

$$\frac{\varphi}{2} = p\pi, \quad p \in \mathbb{N} \quad (5.86)$$

In the analysis throughout the thesis  $\delta = 0$  were assumed, but if it were not, the points in space where (5.74) is satisfied can be shifted (disturbance by phase setting) in time by just changing the phase shifter setting at each antenna element (progressive phase between the antenna elements). The solution can be seen as follows: Since the time of interference at a point in space is shifted by the added incremental phase at each antenna element, the LFM CW source output frequency at this point should be shifted.

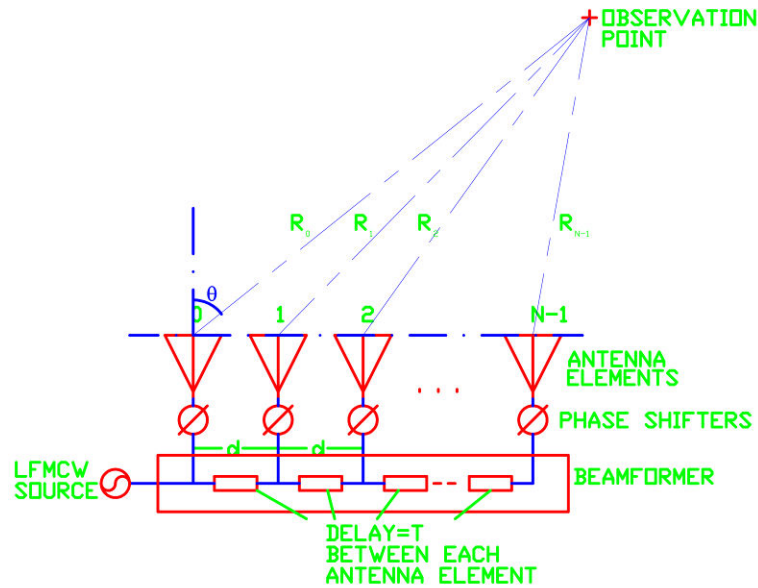


Figure 5.12: Adding a phase shifter can be beneficial for frequency diversity

The bandwidth of scan is dependent on the phase shifter steps, but it can be arranged to be the full scan bandwidth of the source.

### 5.3.2 How to Benefit from Frequency Diversity – Proposal 2

Now, assume that no phase shifter is used at the antenna elements. Another way of achieving the frequency diversity is to let the FDA scan the space more than once throughout the period of the source. The most basic way of achieving this is to change the slope of the frequency regime of the source by changing the frequency extent of scan. The reason is implicit in (5.73). By changing the total extent of the frequency scan in one period, the number of solutions to (5.74) for a point in space increases. Each solution exists for a different scan point in the frequency regime of the source. In this case, the beam period would be smaller than the source period and staggered PRF is achieved.

An example of the case is clearly visible in the measurements of Figure 4.29 and Figure 4.30. In the first figure two beams are formed in one period of scan at the receiving antenna, while in the latter only one. The difference between the two measurements is the extent of frequency scan.

The bandwidth in this case can be increased to up to bandwidth of operation of the system. Since the controls of LFMCW source are flexible, this is possible.

### **5.3.3 How to Benefit from Frequency Diversity – Proposal 3**

This proposal is similar to the one in proposal 2. In this case, without changing the slope of the source, the center frequency of scan can be shifted. This technique is similar to proposal 1 but instead of disturbing (5.75) by phase shifters,  $\omega_0$  is changed to create diversity. Here the bandwidth can be increased up to the bandwidth of system similar to Proposal 2, but the superiority of proposal 2 is the reception of multiple pulses from the same point in space in one period of scan. Third technique can be combined with the technique in proposal 1 to make the technique more flexible.

## CHAPTER 6

### SECOND IMPLEMENTATION OF LFMCW BASED

### FDA

#### 6.1 MOTIVATION AND REQUIREMENTS

In the new implementation, the main aim is to design hardware with much better transmission characteristics. Although most of the hardware from the first measurement set is used for the implementation, some of the critical hardware is redesigned for the FDA structure.

First, the number of antennas is increased from four to eight. This is done to see the FDA performance with higher number of antennas and increase the resolution of measurements. The array is fabricated with ten antennas, two antennas at the edges loaded with system impedance.

The beam former required attention during design since in the first implementation the instantaneous amplitude balance was worse than  $\pm 1.5\text{dB}$  at some points in the bandwidth. The reason for this severe amplitude imbalance is the utilization of T-junctions in the implementation. The multiple reflections at various points in the divider is an expected result with the T-junctions. In the new design of the beam former, instead of using T-junctions, Wilkinson dividers are designed for better transmission characteristics, with increased isolation between the output arms of the beam former.

For higher signal power levels, extra amplification is used at the output of the beam former. Also, an amplitude equalizer is utilized in the line-up to

compensate for the slope in transmission characteristics (slope with respect to frequency).

Besides, extra cables are used to provide interconnection between the array elements. The same cables are also used for tuning of inter-element delays at some points of the array.

The requirements for the implementation are very similar to the ones in the first implementation presented in Chapter 4. They are as follows:

- Array size is 8x1 for higher resolution
- Total frequency band of 6-10GHz; with inter-element distance of 25mm
- Inter-element delay of 0.5ns
- LFMCW source covering the frequency range of interest (Tested in the first measurement setup).
- A wide-band detector (Tested in the first measurement setup).
- The antenna array should cover the whole frequency band of interest (Tested in the first measurement setup).

In the following sections, the new hardware for the implementation will be presented first. Next, some discussions about the implementation will come and lastly, the measurements will be presented with comments on the results.

## **6.2 NEW HARDWARE FOR IMPLEMENTATION**

In this section, the new hardware designed for the second implementation will be presented. Most of the hardware is reconfigured for eight antenna FDA and important details in terms of FDA mechanism will be demonstrated.

### **6.2.1 Proposed Structure**

The structure of the array in the new implementation is shown in Figure 6.1. According to the figure, the beam forming section is formed by three parts; a two way Wilkinson divider with low amplitude and phase imbalance between the output arms, two identical 4way delayed beam formers, an antenna array with ten antenna elements. The inter-element delay in the array is arranged at the 4-way

beam forming networks and the interconnection cables between the 2-way divider and the 4-way beam forming networks. The other interconnection cables are assumed to be identical to each other.

The antenna is designed to be composed of ten antennas with two of them connected to loads. These antennas are designated to be dummy antennas, so the internal antennas will behave identically (the effect of inter-element couplings will be seen at all internal antennas identically).

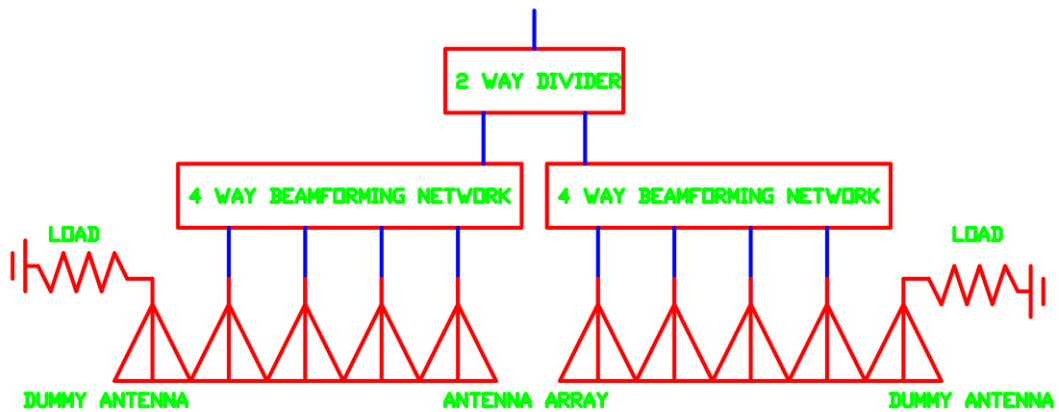


Figure 6.1: General structure of the FDA

### 6.2.2 2-way Divider

The two-way divider is a ceramic type divider built on alumina substrate (More information on alumina can be found in Appendix 1). The thickness of the substrate is 10 mils. Divider is manufactured in ATC (Advanced Technical Ceramics) and packaged here. A photograph of the divider is shown in Figure 6.2.

The divider is placed on a carrier and the connections of the divider to the edges of the carrier are accomplished with alumina micro strip lines. The carrier is attached to the outer housing made of aluminum and plated with nickel. The connections of carrier to the outer interface are done using SMA connectors.

Some of the measurements of the divider are shown in Figure 6.3. The bandwidth of the divider is between 6GHz and 18GHz as required by the specifications. Also, the amplitude imbalance of the divider is better than +/-0.2dB

and around  $\pm 2^\circ$  in the band of interest (6-10GHz) (no stepped delay is given at this divider).

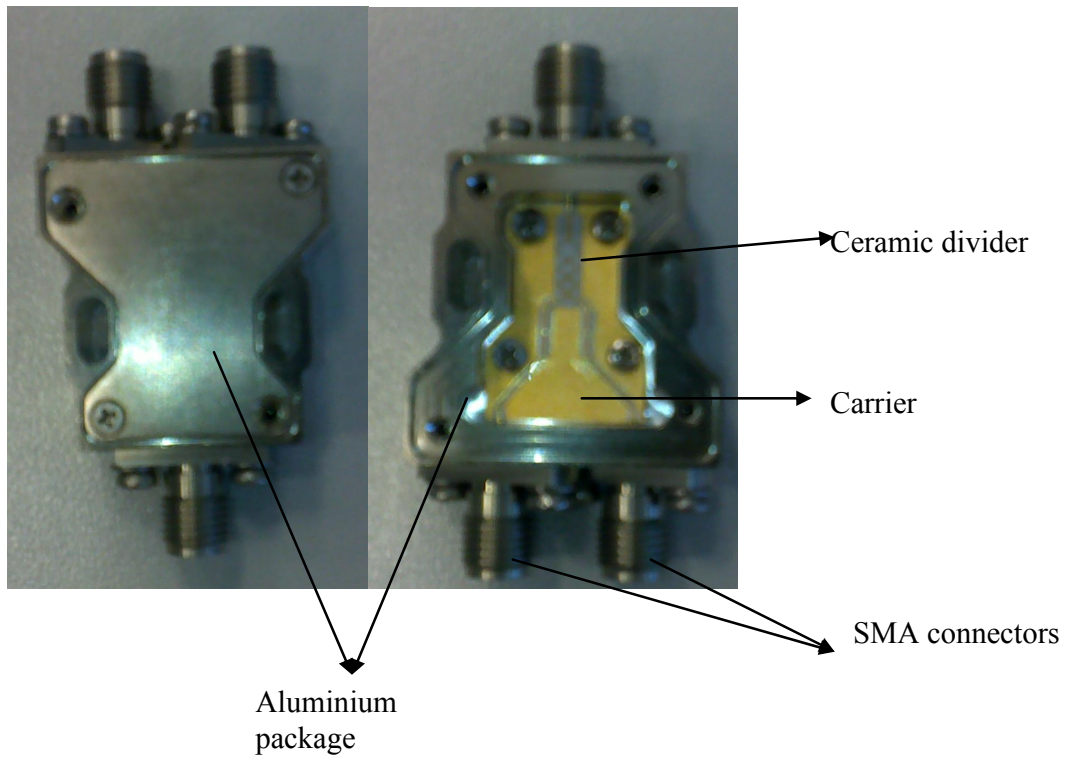


**Figure 6.2: 2-way equal amplitude/ equal phase divider**

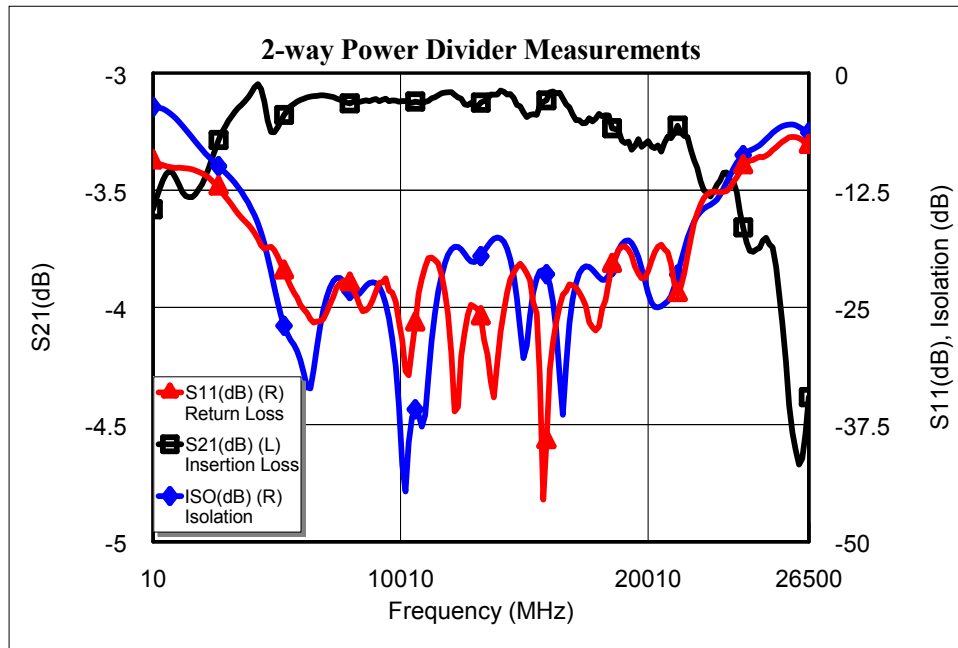
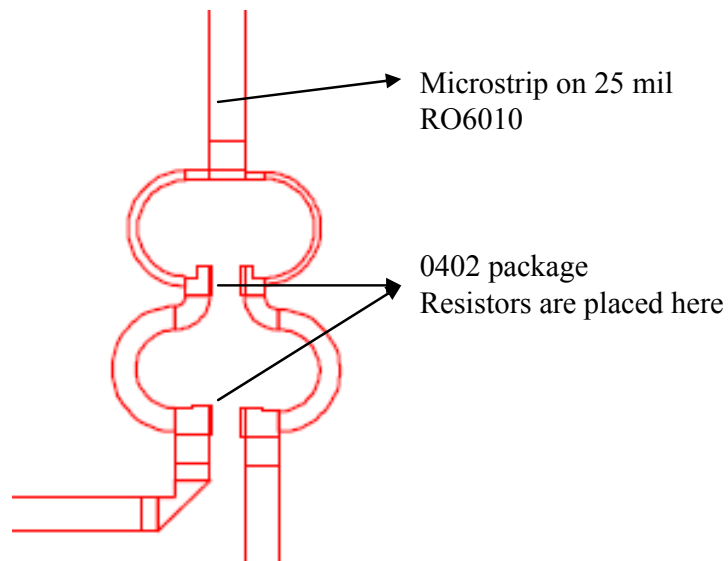


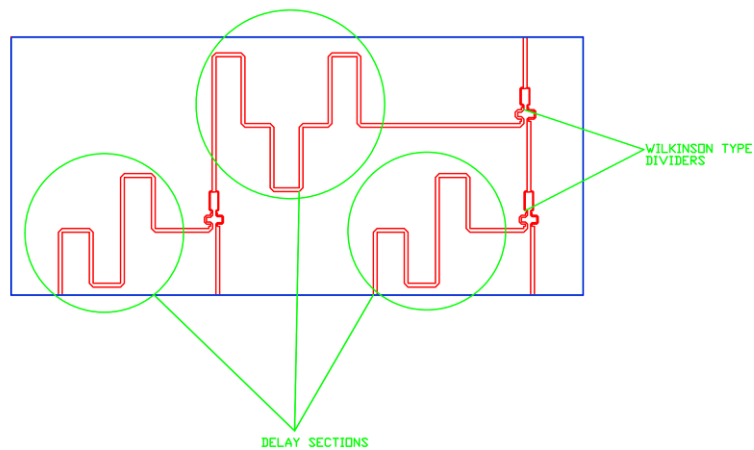
Figure 6.3: Measurements of 2-way divider

### 6.2.3 Four-Way Beam-former

The most critical part of the FDA is the four-way beam former. This part is similar to the 4way divider of Chapter 4, but this time Wilkinson type dividers are used at the junctions. A sample of the junction is shown in Figure 6.4. The junctions are designed to be built with micro-strip technology on 25 mil RO6010 substrate. The odd-mode absorbing resistors are 0402 package resistors with the pads shown in the same figure. In this figure, the lines are curved but in the final design straightened lines are used.

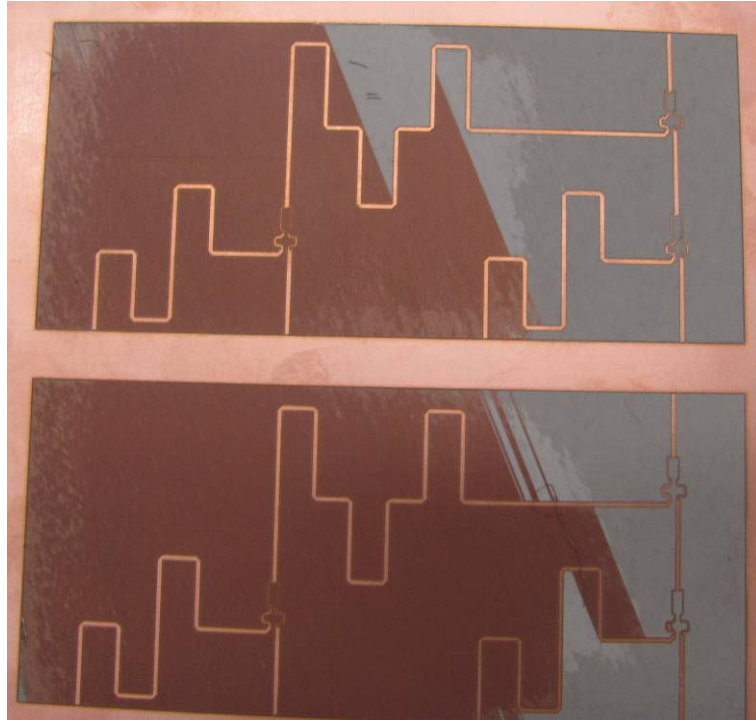


**Figure 6.4: A Wilkinson divider junction on a 25 mil RO6010 substrate**



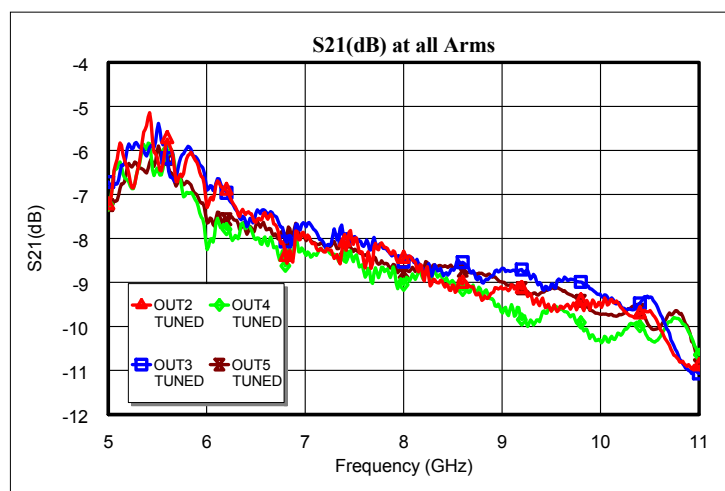
**Figure 6.5: Drawing of the beam former from CAD software.**

Figure 6.5 shows the drawing of the beam forming network. The inter-arm delays are arranged to be 0.5ns and the network is matched to system impedance at all ports. The delay lines are meandered lines and interconnecting the divider sections. A photograph of the divider during production is shown in Figure 6.6.



**Figure 6.6: Photograph of the divider during production**

After production, the divider is measured and tuned for increased performance. The  $S_{21}$  (dB) measurement of the divider is shown in Figure 6.7. Note that the inter-arm amplitude distortion is minimized (better than  $\pm 0,5$ dB), but there is a slope with frequency, which will be adjusted with an equalizer.



**Figure 6.7: S21 (dB) measurements at all arms of the divider**

The return losses of the divider at all arms are better than 15dB at all frequencies while the isolation is better than 20dB throughout the band of interest. The graphs regarding these measurements will not be shown here.

Group delay of each arm is also analyzed with checking the phase of each arm. For the group delay estimation, a stepped delay element is theoretically added to the S-parameter measurement of each arm and the phase is checked as shown in Figure 6.8. Note that there are discrepancies at the edges of the band but the error is on the order of 10 picoseconds.

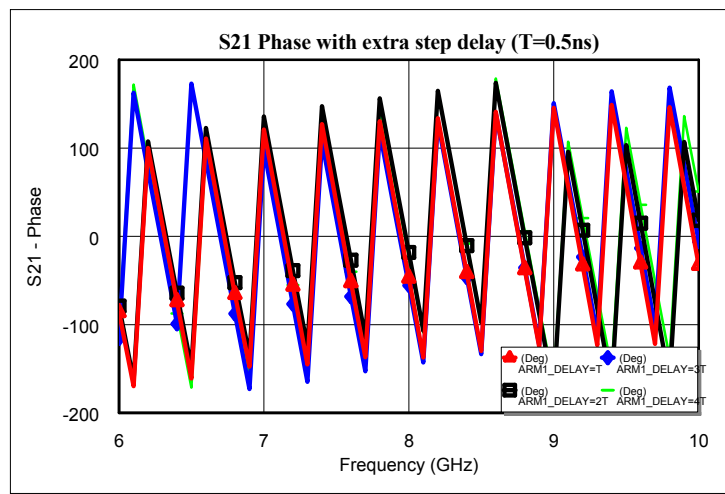


Figure 6.8: Phase measurement at each arm with 0.5ns inter-arm delay

## 6.2.4 Antenna Array

The antenna array is similar to the one in Figure 4.18, but this time it is not connected to the beam former directly due to manufacturing capabilities. Same antenna type (Antipodal Vivaldi) with inter-element distance of 25mm is designed. Also there are two dummy antennas at the edges for identical responses from the middle antennas (as explained in 6.2.1).

In Figure 6.9, a photograph of the manufactured array is demonstrated. All input ports of the antenna array are connected with SMA connectors. The rightmost and leftmost antenna elements are dummy elements which will be loaded with system impedance.



**Figure 6.9: Photograph of 10 element Antipodal Vivaldi Array**

The results of the measurements on the array is similar to the one found in the first measurement setup (4.2).

### **6.2.5 Cables as tuners**

As mentioned before, the antenna array, two 4-way beam formers and 2-way power divider are not connected directly to each other, but RF cables are used instead. Especially the cables connecting the 2-way power divider to the 4-way beam-former are also responsible for the inter element delay. According to Figure 6.1, the length of the cable on the left-side of the two way divider is arranged such that the delay of this is  $2\text{ns}$  higher than that on the right. Besides, the length of wires connecting the 4-way dividers to antenna elements is picked up to be equal. After group measurements on the array (with all parts connected), some tuning is applied to the cables and 4-way beam formers to accomplish stepped group delay ( $0.5\text{ ns}$ ) between the antenna elements.

The cables are RG-216 type whose data sheet is presented in the Appendix 1.

### **6.2.6 Other Parts**

For the proper operation of the structure, some extra parts are added to the line up of FDA.

An amplifier is used at the input to increase the signal level for detector. The amplifier is TGA2513 from Triquint Semiconductor Inc. The gain of this amplifier is around 15dB in 6GHz-10GHz bandwidth with  $P_{1dB}$  point better than 15dBm and NF better than 4dB. The amplifier is packaged in a suitable housing and connected to other parts via SMA connectors and cables. It can be used in receive or transmit configuration according to measurement needs. Detailed information about the amplifier can be found in Appendix 1.

The next device is the amplitude equalizer. This part is for compensating the slope in the transmission characteristics of the dividers, amplifier and other parts in the FDA structure. A schematic of lumped implementation of the structure is shown in Figure 6.10. The structure is typically an attenuator but the resonance frequencies of resonators are arranged in such a way to create an inverted slope in the transmission.

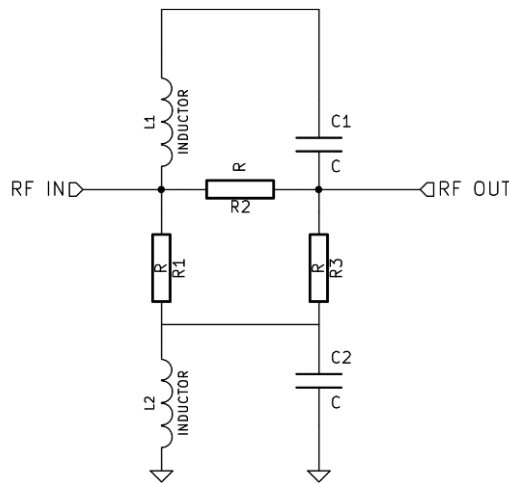


**Figure 6.10: Lumped equalizer structure. The equalizer in the line-up use distributed version where the resonators are replaced with stubs and bond-wires.**

The equalizer used in the setup is distributed type (stubs are utilized instead of resonators). The slope of the equalizer is 4dB between 6GHz and 11GHz with better than 20 dB reflection in band. This device is also packaged and connected using SMA connections and interconnects cables.

Other parts are the same as in the first measurement configuration. These parts are LFMCW source, detector and other parts, and information regarding these devices can be found in 4.2 and Appendix 1.

### 6.3 FULL STRUCTURE AND MEASUREMENTS

In Figure 6.11, schematic view of the FDA structure can be observed. As mentioned before, the parts are connected using RF cables in between. The photograph of the structure is also shown in Figure 6.12.

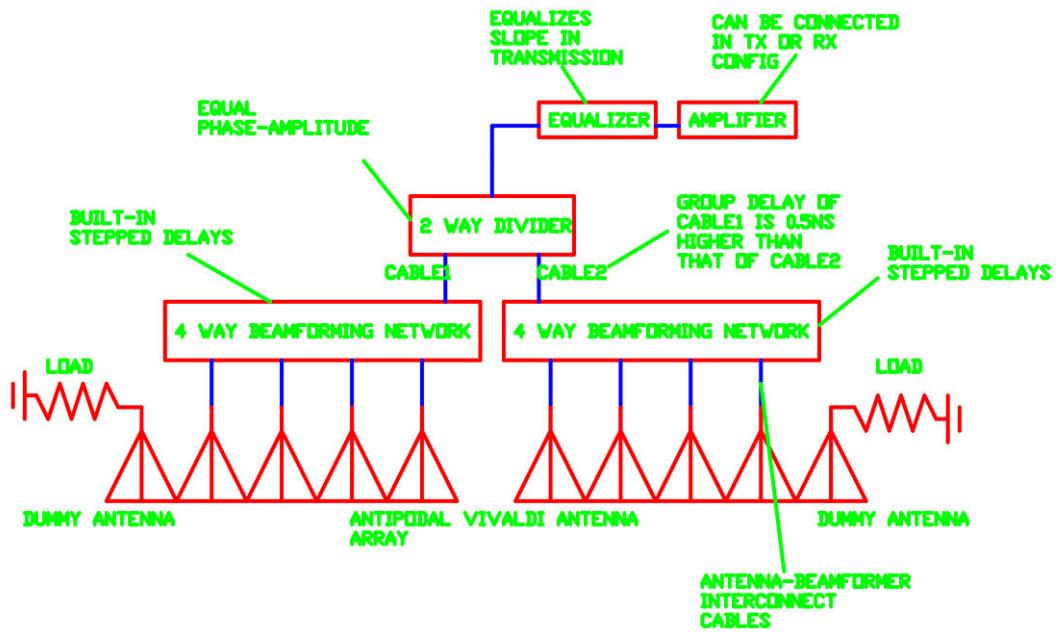
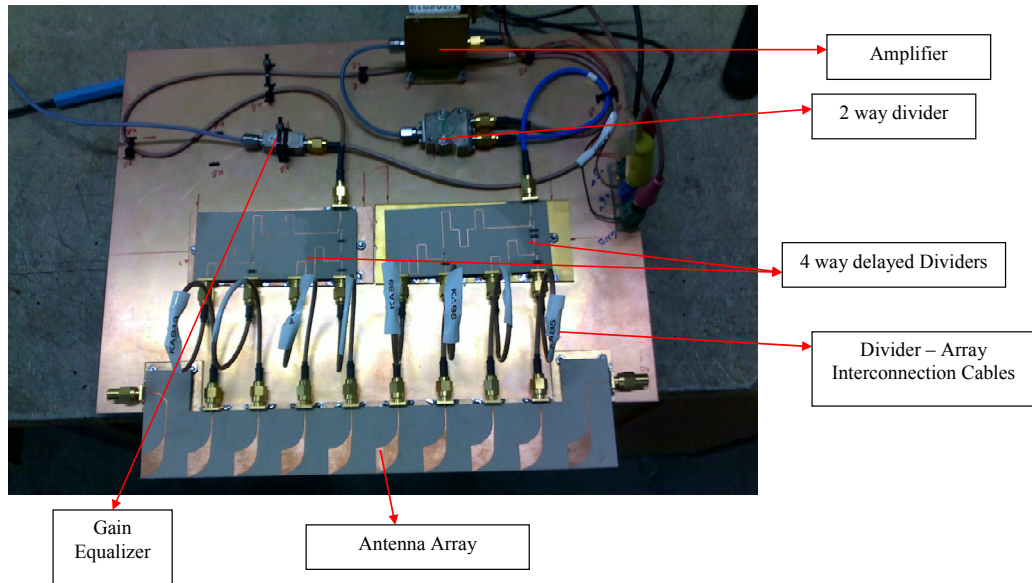


Figure 6.11: Schematic view of the built FDA structure



**Figure 6.12: Photograph of the built FDA structure**

The  $S_{21}$  (dB) measurement at all output ports of the beam former (including the cables between the dividers and the antenna array) is shown in Figure 6.13. The amplitude distortion at any frequency is better than  $\pm 0,75$ dB throughout the band. Similarly, in Figure 6.14, the delay between the antennas is found to be 0,5ns.

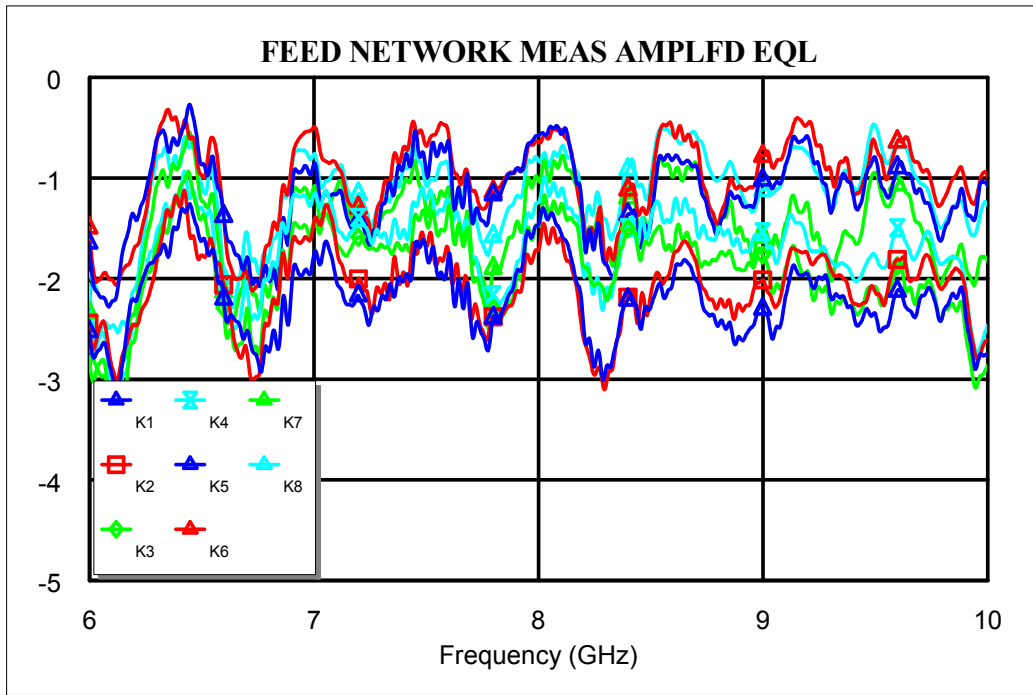


Figure 6.13: S21 (dB) measurement at all ports of the beam former

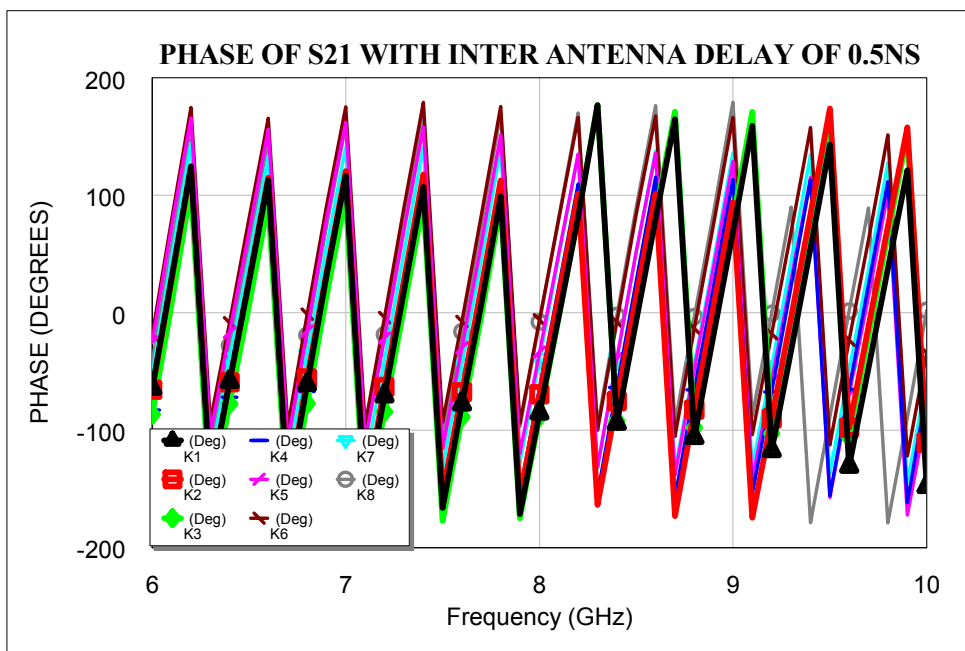


Figure 6.14: S21 Phase measurement with added inter-element delay (0.5ns)

Although the structure is working in this way, another and much easier method is to implement the structure on a single PCB instead of using interconnect cables. In the next section, these subjects will be addressed.

## 6.4 DISCUSSIONS ON IMPLEMENTATION

In this implementation, as shown in Figure 6.12, all parts are designed, tested and integrated to the structure using interconnections between the parts. The implementation can also be made on a single PCB but there are some limitations to this.

First, integration on a single PCB requires a larger area on the substrate and current capabilities on LPKF do not let this PCB to be manufactured. This is the main limitation to the implementation.

Another and more interesting problem was seen at the beam former supplying the delays to each antenna. In the first trial, all divider structure was manufactured on a single PCB as shown in Figure 6.15. This beam former did not work due to the radiation experienced at the delay lines interconnecting the dividers. To overcome this effect, there should be housing around the delay lines and the divider, but this can be an expensive solution for the study. So, the aforementioned structure is built.

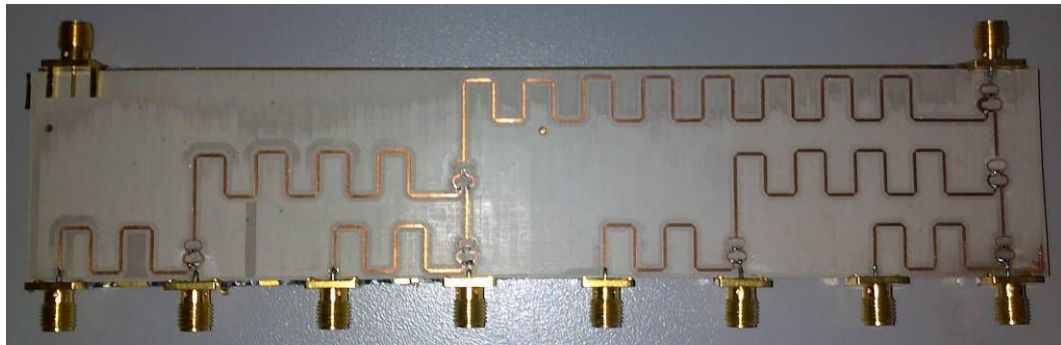


**Figure 6.15: First trial of implementation**

The losses experienced from the common port to the output ports with highest delay are found to be very large, so design of unequal power dividers at the

junctions are in avoidable. Some of the unequal power ratios force the use of very narrow transmission lines. LASER LPKF is unavoidable for these dividers.

## 6.5 MEASUREMENT SETUPS AND TESTS

The aim of this implementation was to observe the LFMCW based FDA concept and scanning mechanism with a higher performance array and to justify the first measurements. This time, the first built FDA is also used in the measurements to demonstrate the bi-static case. All measurements are performed in the anechoic chamber similar to the previous measurements.

### 6.5.1 Measurement Configuration – 1

The first configuration is similar to the one shown in Figure 4.28. A wideband horn antenna is used to transmit the LFMCW waveform in the anechoic chamber and the output of FDA is amplified and detected. The detected waveform from the detector is input to an oscilloscope together with trigger signal coming from the arbitrary waveform generator feeding the oscillator. The configuration is shown in Figure 6.16.

In the following sections resulting waveforms and comments about the results will be presented briefly.

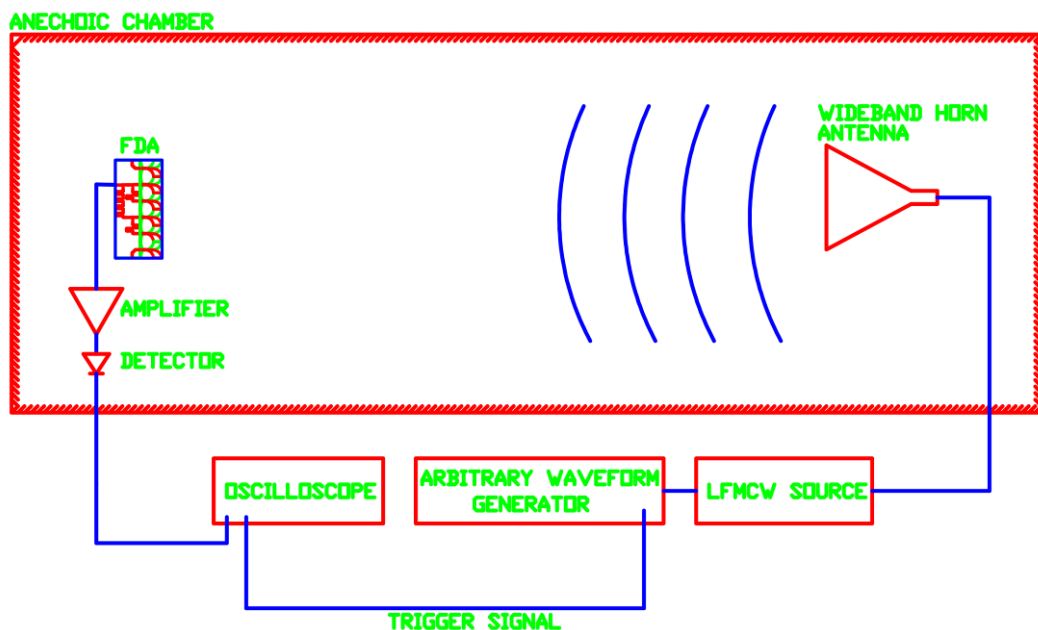


Figure 6.16: First Configuration- same as the configuration of Figure 4.28.

## 6.5.2 Sample Measurements with Configuration – 1

In this section samples from the measurements performed using the designed FDA will be demonstrated. The measurement constants are shown in Table 6.1.

**Table 6.1: Measurement Constants**

Inter element distance (mm)	25
Inter element delay (ns)	0,55
s	6,6

### 6.5.2.1 Measurement 1

In this demonstration scaling in time due to slope change will be shown. The parameters related to the measurements are shown in Table 6.2. The only change between the parameters is the voltage amplitude causing the frequency extent of scan, the slope of scan to change. The resulting time domain waveforms can be viewed in Figure 6.17.

According to the figure, the beam widths for the two cases are measured to be 1,7 ms and 2,2 ms which are very consistent with the calculations shown in Table 6.2. The scaling between the two cases can be calculated from the beam width change to be 1,3 and the value found from the ratio of slopes is 1,34. These values are also close to each other justifying the derivations of FDA concept. Also, note that, the beam period in case 1 is measured to be 6,7 ms very close to the calculated value and visible in one period of 10ms, whereas in the second case this value is calculated to be 8.96ms outside the measurement range.

**Table 6.2: Measurement 1 parameters**

PARAMETERS	CASE 1	CASE 2
Voltage Offset (V)	3,5	3,5
Voltage Amplitude (V)	3,5	3
Look Angle (deg)	0	0,00
Frequency Start (GHz)	5,96	6,18
Frequency End (GHz)	8,6	8,41
Sweep Time (ms)	10	10,00
m (2piHz/s)	1,88E+12	1,40E+12
Total Frequency Shift (GHz)	3	2,23
Frequency Difference Between Antennas (Hz)	150	111,55
Beam Period (ms)	6,67	8,96
Range Period(km)	2000000	2689376,96
Null to Null interval (ms)	1,67	2,24

It can be noted from the measurements that the results are better compared to the previous measurements due to superior performance of the devices utilized in the FDA. In fact, the implementation of the second FDA was to visualize this result in real life. The small discrepancies between the measured and calculated values seem to be caused by the non-linear control response of the LFMCW waveform generator. The next measurement will demonstrate the effect of offset change – center frequency change.

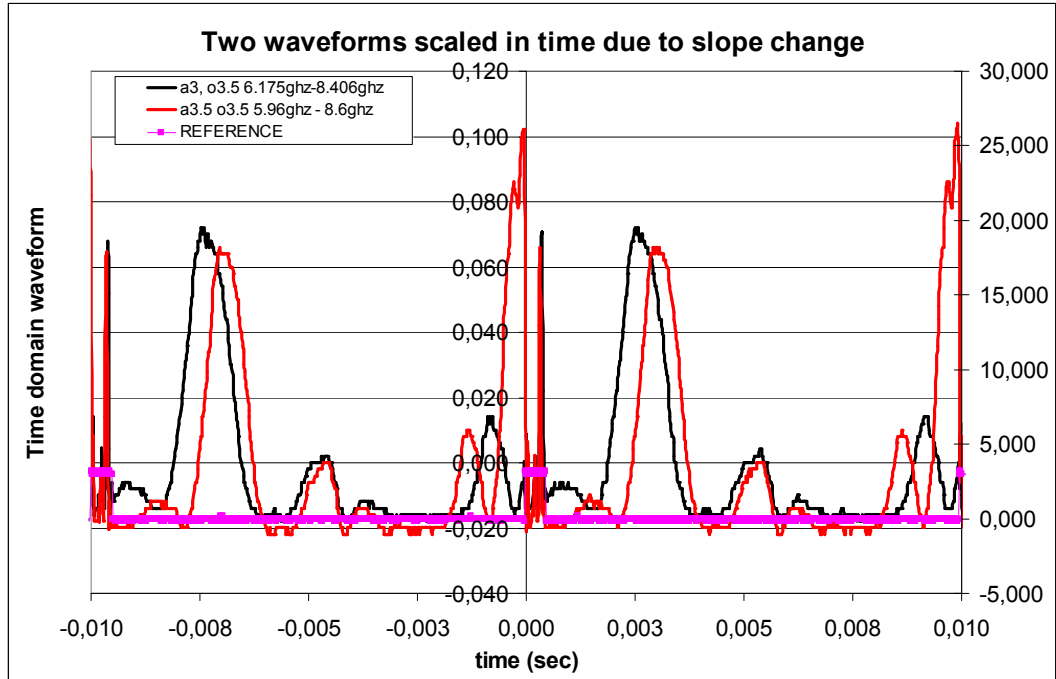


Figure 6.17: Resulting waveforms for measurement 1 - effect of slope change on the time domain waveforms

### 6.5.2.2 Measurement 2

In this measurement, the effect of center frequency change on the positioning of beams will be demonstrated. Again two cases will be of concern during the section. The cases are shown in Table 6.3. The difference between the two cases is the offset voltage affecting the center frequency of operation. So beam position should shift as discussed earlier in Chapter 4.

The results are shown in Figure 6.18. Note that the shift is measured to be 2,1 ms and the calculations using Table 6.3 and (4.3) would result in the same value. The null-to-null beam widths are also in good agreement with theory.

**Table 6.3: Measurement 2 Parameters**

PARAMETERS	CASE 1	CASE 2
Voltage Offset (V)	4,2	4,40
Voltage Amplitude (V)	1	1,00
Look Angle (deg)	0	0,00
Frequency Start (GHz)	7,58	7,73
Frequency End (GHz)	8,27	8,4
Sweep Time (ms)	10	10,00
m (2piHz/s)	4,37E+11	4,21E+11
Total Frequency Shift (GHz)	0,69	0,67
Frequency Difference Between Antennas (Hz)	34,75	33,5
Beam Period (ms)	28,78	29,85
Range Period(km)	8633093,53	8955223,53
Null to Null interval (ms)	7,19	7,46

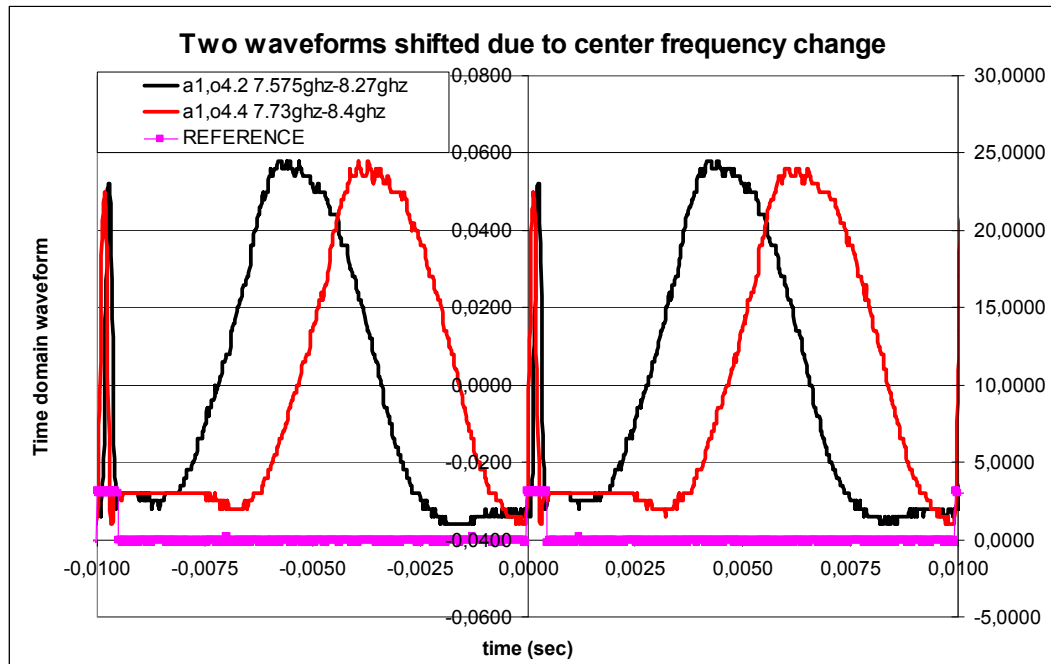


**Figure 6.18: Measurement 2 results**

### 6.5.2.3 Measurement 3

In this measurement, the look angle of FDA with respect to the horn transmitter is changed. The measurements are gathered for three look angles:  $+15^\circ$ ,  $-15^\circ$ ,  $0^\circ$ . In fact, in the anechoic chamber, reference horn antenna is

near the FDA and the dependency on look angle is hard to formulize but the measurements are shown in Figure 6.19 and the variables are presented in

Table 6.4.

Equation (4.8) is rewritten below for convenience.

$$t_p = \frac{\left(2p\pi - \frac{mTR_0}{c} + \delta\right)}{\Delta\omega\left(\frac{\sin(\theta)}{s} - 1\right)} - \frac{\omega_0}{m}, p \in \mathbb{N} \quad (6.1)$$

**Table 6.4: Measurement 3 variables**

PARAMETERS	CASE 1	CASE 2	CASE 3
Voltage Offset (V)	4,00	4,00	4,00
Voltage Amplitude (V)	3,10	3,10	3,10
Look Angle (deg)	0,00	15,00	-15,00
Frequency Start (GHz)	5,31	5,31	5,31
Frequency End (GHz)	8,47	8,47	8,47
Sweep Time (ms)	10,00	10,00	10,00
m (2piHz/s)	1,99E+12	1,99E+12	1,99E+12
Total Frequency Shift (GHz)	3,16	3,16	3,16
s constant	6,00	6,00	6,00
Inter-element distance(mm)	25,00	25,00	25,00
Inter-element delay (ns)	0,50	0,50	0,50
Frequency Difference Between Antennas (Hz)	158,15	158,15	158,15
Beam Period (ms)	6,32	6,61	6,06
Range Period(km)	1896933,29	1982449,23	1818489,98
Null to Null interval (ms)	1,58	1,58	1,58

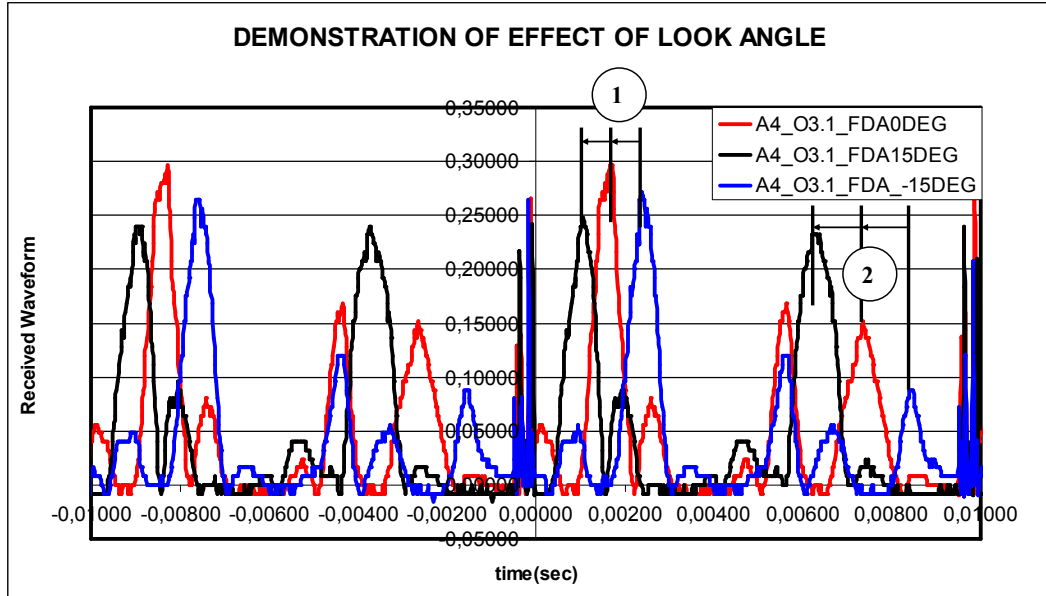


**Figure 6.19: Demonstration of effect of look angle on the positioning of beam peaks**

According to (6.1), the waveform receive times are affected by the look angle shown in the first term of equation. Ignoring  $\frac{mTR_0}{c}$  (since the measurements are performed in anechoic chamber) and inter-element phase difference, the receive times would be;

$$t_p = \frac{p}{\Delta f \left( \frac{\sin(\theta)}{s} - 1 \right)} - \frac{\omega_0}{m}, p \in \mathbb{N} \quad (6.2)$$

In the last equation the second term is constant in all terms. During a scan in space, by changing the FDA direction, the received beams would be shifted due to (6.2).

The result of this experiment is shown in Figure 6.19 with two points in one period; (1) and (2). In both points the effect of changing the direction of FDA from  $15^\circ$  to  $-15^\circ$  is clearly visible. The shift in time at point (1) is 1,4 ms, while at point (2) the measured value is 2,05ms. So the difference between the shifts is 0.65 ms. The calculated shift difference from (6.2) is 0,55ms close to the measured value.

The discrepancy is mainly due to the non-linear control behavior of FMCW source as discussed before. Also note from the measurements that the antenna behavior is different for different angles and frequencies causing discrepancies.

### 6.5.3 Measurement Configuration – 2

In this case the transmitting horn is replaced with the FDA mentioned in Chapter 4. The configuration in this case is shown in Figure 6.20.

According to the analysis presented in Chapter 5, the arrangements and physical constants required for justification is hard to deal with and a more advanced setups are required. In (5.30), for the formation of beams at the receiver, the exponents in the summations should be equal to an integer multiple of  $2\pi$  simultaneously and it is hard to arrange for this setup (In fact that equation were for the case with the receiver and the transmitter at the same point in space, now the case is totally bi-static).

In the measurements of this section, reliable data for the justification of theory were not gathered but the measurements are for demonstration of the case.

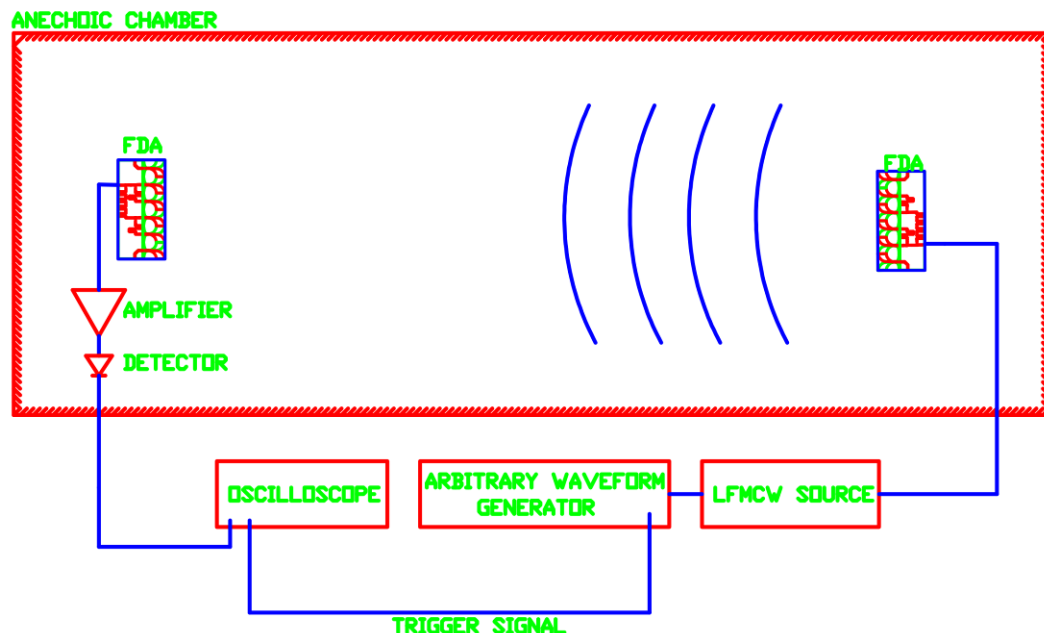


Figure 6.20: FDA transmitter - FDA receiver configuration

### 6.5.3.1 Sample Measurement with Second Configuration

A measurement for the case is shown in Figure 6.21. The variables of measurement are shown in Table 6.5. Here there are two cases to investigate. The source characteristics are same but the source antenna orientation is tilted to  $10^\circ$  in case 2 to see the effect on the waveform parameters. The results are demonstrated in Figure 6.21. Note that the frequency range lets two beams to be formed throughout one period of scan but in tilted antenna case, both main beams correspond to the null of one of the arrays and nullified (the product in 5.30).

**Table 6.5: Parameters for FDA Transmitter – FDA Receiver sample measurements**

PARAMETER	CASE 1	CASE 2
Voltage Offset (V)	4,00	4,00
Voltage Amplitude (V)	3,30	3,30
Look Angle (deg)	0,00	10,00
Frequency Start (GHz)	5,48	5,48
Frequency End (GHz)	8,59	8,59
Sweep Time (ms)	10,00	10,00
m (2piHz/s)	1,96E+12	1,96E+12
Total Frequency Shift (GHz)	3,12	3,12
Frequency Difference Between Antennas (Hz)	155,95	155,95
Beam Period (ms)	6,41	6,60
Range Period(km)	1923693,49	1981027,12
Null to Null interval (ms)	1,60	1,60

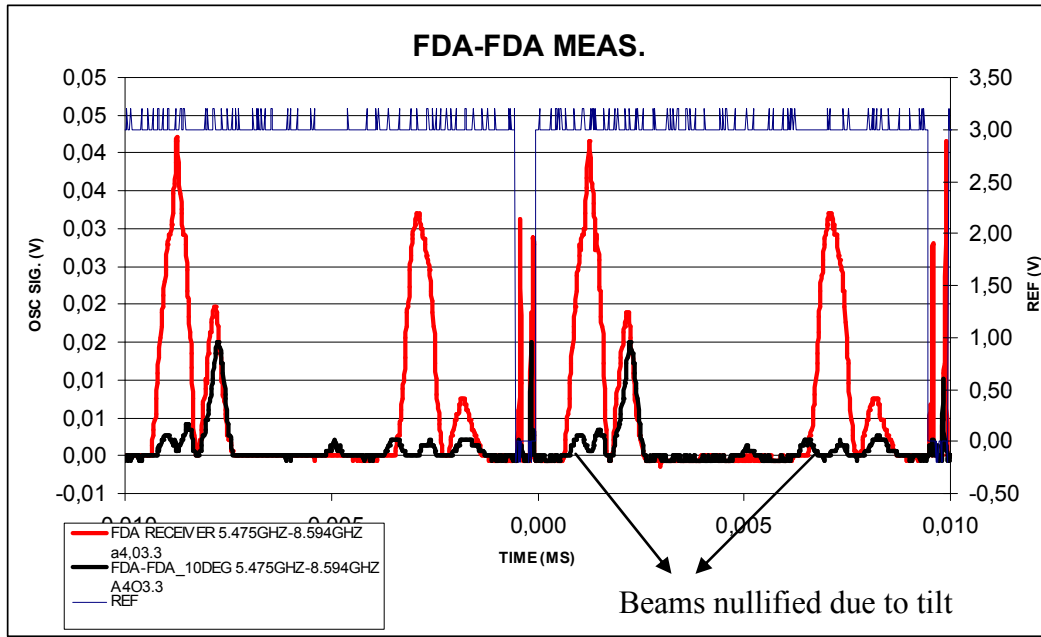


Figure 6.21: A sample measurement for FDA transmitter – FDA receiver case

## **CHAPTER 7**

### **SIMULATIONS OF LFMCW BASED FDA**

#### **STRUCTURE**

In this chapter, simulations of the LFMCW based FDA will be demonstrated. Although some numerical simulations were performed in MATLAB environment before, the simulations demonstrated in this chapter will not only present the performance of array concept but also the properties of the array as a part of radar. Transmitting FDA – Receiving Omni-Directional antenna logic (Chapter 5) is the core throughout the simulations.

#### **7.1 BASIC INFORMATION ABOUT THE SIMULATION ENVIRONMENTS**

For the simulation of the structure, two software were utilized. MATLAB is the main simulation tool for the data analysis. The other software is Microwave Office (MWO) from Advanced Wave Research (AWR). This tool allows simulation at system level while offering basic microwave elements to be modeled [50]. Since the amplitude modulation is formed due to interactions between the distinct frequency waveforms from each antenna element, time domain simulation is preferred despite the long simulation times (For a high precision simulation, the time steps in the simulation should be much lower than the period of lowest frequency component. Some of the anomalies in the simulation are due to insufficient steps).

The output waveforms extracted from MWO is exported to a text file and used in MATLAB to analyze spectral properties of the returns.

Although simulations can be performed using only MATLAB, user-friendly structure of MWO (selection of measurement points just by using test points) is the main factor in selecting this environment as the main simulation tool.

## **7.2 INFRASTRUCTURES OF SIMULATION**

### **7.2.1 LFMCW Source**

LFMCW source is modeled as an FM modulator where the controller waveform is fed from a saw-tooth generator as demonstrated in Figure 7.1. The period of LFMCW source is designated by the period of saw-tooth waveform generator whose value is input as a variable,  $T_r$ . The starting frequency of the FM generator is accepted from a microwave tone generator to be  $f_0$ . Frequency sensitivity of modulator is defined as  $df(Hz/V)$ , and the instantaneous output frequency from the modulator is calculated by the instantaneous amplitude of the saw-tooth waveform. The output is taken from the first port of the structure.

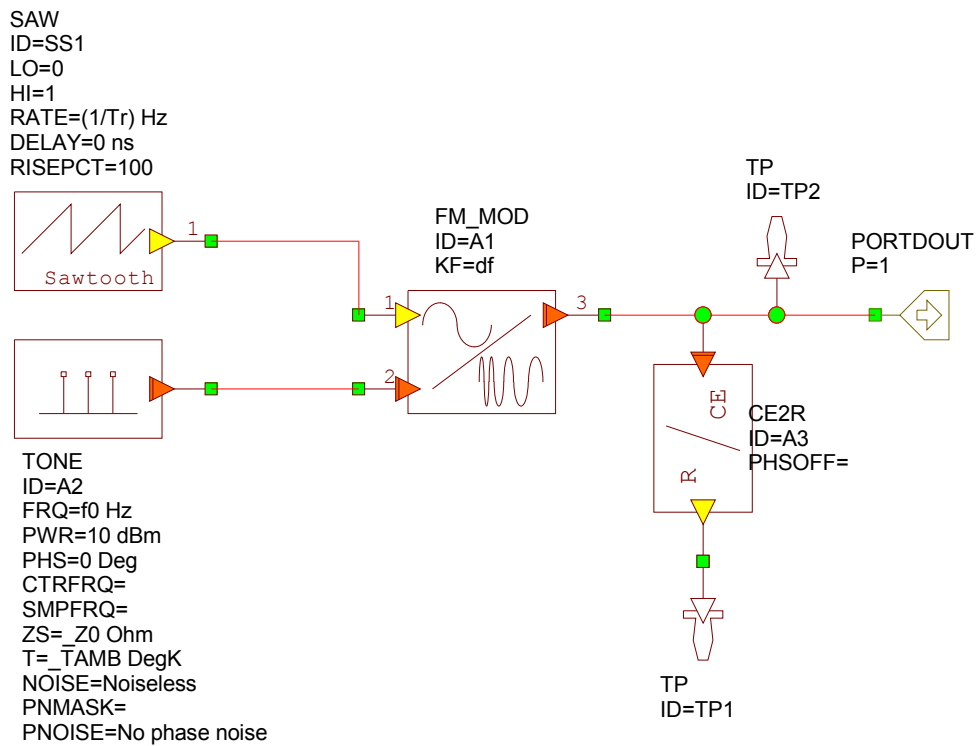


Figure 7.1: LFM CW source and the constituting parts

Note from Figure 7.1 that to view the output waveform, the complex envelope from the FM source is converted to real waveform.

## 7.2.2 FDA and an Approach to Propagation Implementation

This part is the main part of the simulation. The output of the LFM CW source part is taken directly to this point. The structure is shown in Figure 7.2.

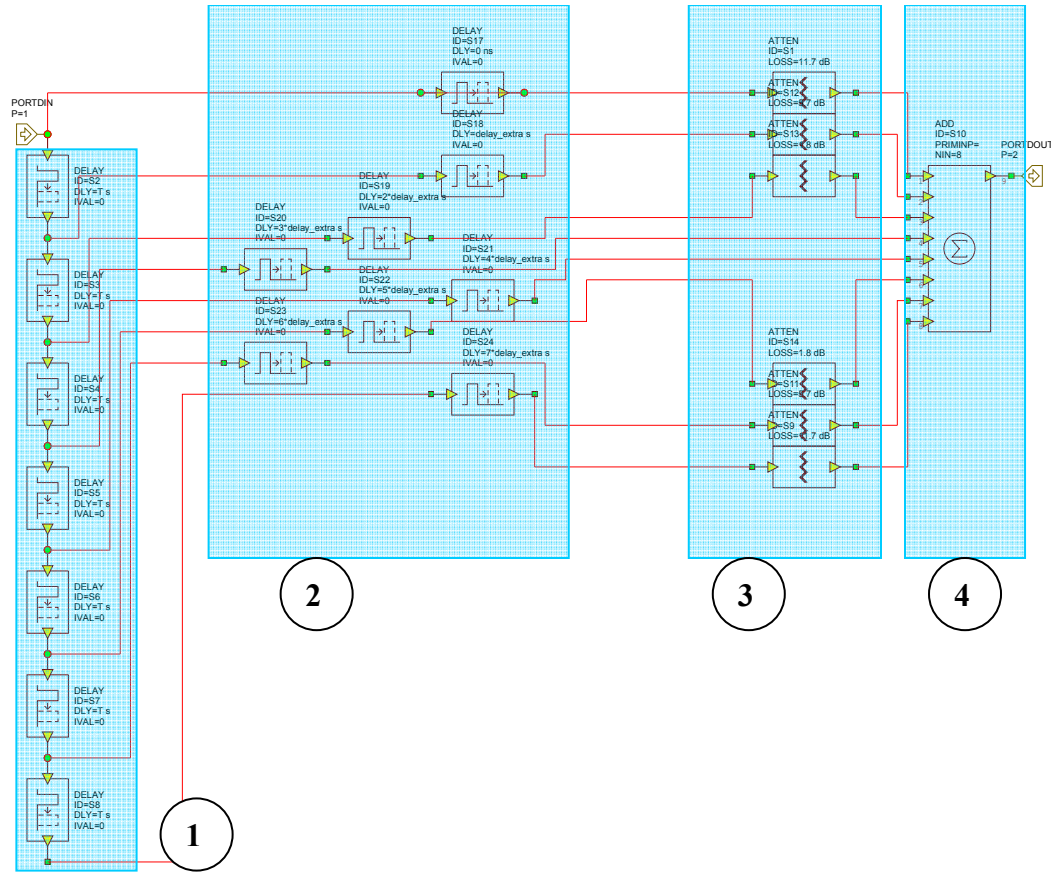


Figure 7.2: FDA part of the simulation

FDA part is formed by four building blocks. In the first part the inter-element delays are arranged and inter-element delay is input to the simulation as a parameter,  $T$ . Remember that this part is the core in the concept and kept as a constant for the simulations. The second building block in Figure 7.2 is mainly a trick to steer the antenna through a predetermined direction (or a target). The delay experienced at  $i^{\text{th}}$  antenna element is  $i * \text{delay\_extra}$ , where

$$\text{delay\_extra} = \frac{d \sin(\theta)}{c} \quad (7.1)$$

Here  $d$  is the inter-element distance in the array and  $\theta$  is the angular bearing of the target (and  $c$ , the speed of light in vacuum). Stepping this delay value between antenna elements, antenna steering can be accomplished mathematically. Note that, this steering mechanism assumes the range of the target to be much larger than the length of the aperture [2].

The third part in the simulation is composed of attenuators and with the aim of creating amplitude tapering between the antenna elements for lowered side-lobes. Lastly an eight input adder is adapted for addition of waves from each antenna through the predetermined direction and the output is directed to output port.

Here no antenna pattern deterioration is assumed. Also the peak value of the output waveform will be the number of antennas (eight for this example) and no normalization is done.

After FDA, the output waveform is transferred to a lossless delay line, which would serve as the propagation environment. In reality space spread loss and atmospheric losses will dominate but for the sake of simulation and FDA demonstration the medium is assumed to be a lossless one as shown in Figure 7.3. Again there is no normalization here. Note that the delay is  $\frac{2R}{3e8}$ , showing the propagation of waves from FDA to source and back to the origin where it is taken into a receiver for further processing.

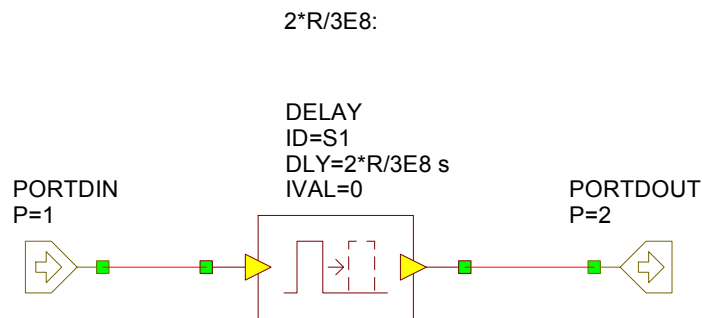


Figure 7.3: Lossless delay element as propagation environment

### 7.2.3 Processing on Incoming Waveform

After propagation of waves, the incoming waves are fed to a mixer from the first port as shown in Figure 7.4. The third port of the structure inputs the original LFM waveform and the output of the multiplier is further high-pass filtered (with an eleventh degree filter) at this stage to remove the DC components from the waveform. The output waveform is taken into the second port.

In the simulation, the mixer is not selected as a realistic mixer but a multiplier to extract the baseband waveform. This is because the output of a realistic mixer would be polluted by the various products of local oscillator and the main tone preventing the understanding of the concept. Note that all operations are performed in real number domain.

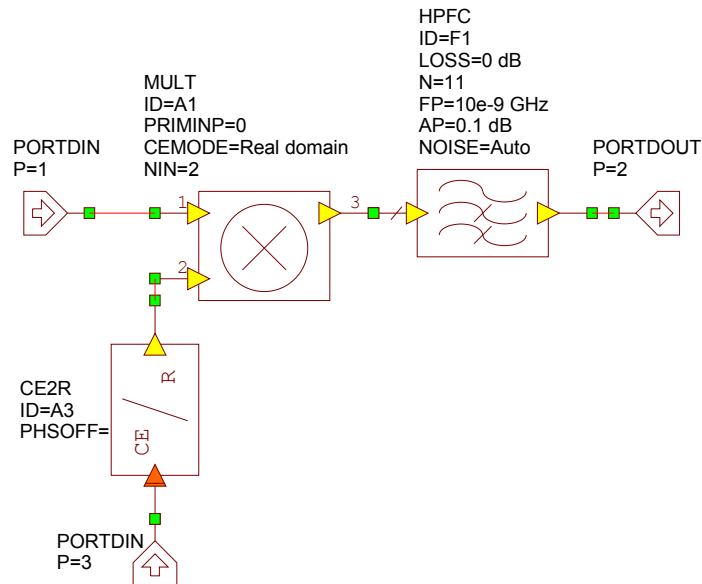
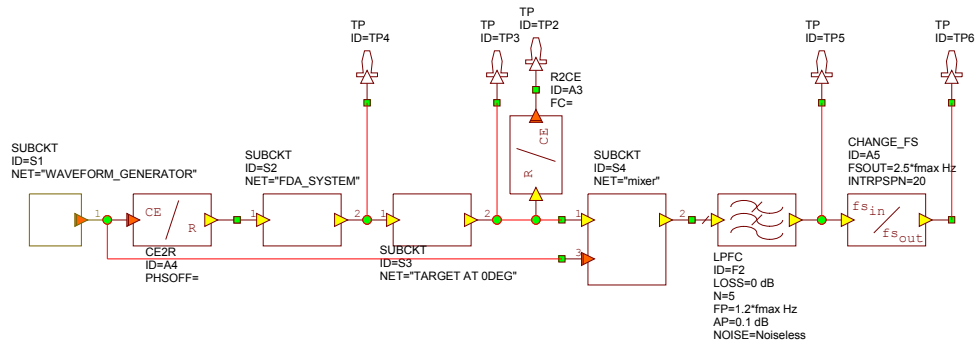


Figure 7.4: Mixing the original LFM waveform and the target return

## 7.2.4 Further Processing

The building blocks of the structure are arranged as shown in Figure 7.5. There are several test points in the aforementioned figure and the sub structures to visualize the resulting waveforms (will be shown in further sections).



**Figure 7.5: All structure arranged for the basic simulations**

According to Figure 7.5, the LFM CW from the source is fed both to the FDA and to the mixer block. The output of the mixer block is further low-pass filtered with cut-off at  $1.2f_{\max}$  and re-sampled at  $2.5f_{\max}$ , where  $f_{\max}$  is the expected maximum beat frequency from (5.57).

The output waveform in Figure 7.5 is the baseband term, whose frequency is related to the range of target, and the angular bearing to be extracted from the time-of-arrival of the pulses (due to amplitude modulation).

The waveform at this stage is extracted from MWO to a text file, whose content is the baseband waveform in time domain. The returns from the targets are gathered and analyzed in MATLAB for further processing.

### 7.2.5 Discussion on the simulations

The ease of implementation of the structure on the computer is the most attractive property of MWO as a simulation tool as evidenced from the figures of the current chapter. Just implementing the basic blocks, placing the test points at critical points and gathering measurements from these points and transfer of data to MATLAB is clearly easier than writing dedicated codes for long simulations.

As mentioned before, the simulation is performed in time domain where the time steps are selected as much lower than the period of highest frequency. In the simulations the upper frequency is assumed to be 10GHz, for which the period becomes 100ps. In the simulation, the steps are selected to be 25ps and even for a

LFMCW source period of 50 us, two million steps should be employed causing long calculation times. So to save time, limited simulations focusing on realistic examples are performed. Also, the large steps in the simulation cause waveform impairing and decreasing the sampling period decreases anomalies at the expense of long solution times (0.5 hrs to 4 hrs). Since the concept utilizes the time-domain relations, this is the only way for simulation.

In following sections, the results from the working simulator and the output waveforms will be shown with various discussions on the results.

### 7.3 WAVEFORMS AT DISTINCT POINTS AND DISCUSSIONS

For the examination of the waveforms at distinct points in the simulation, some simulation constants are to be defined as shown in Table 7.1.

**Table 7.1: Parameters of simulation**

VARIABLES	VALUES
Number of antennas in the system	8
Inter element spacing(mm)	25,00
Inter element delay(ns)	0,50
Starting Frequency(GHz)	6,00
Total Frequency Change(GHz)	2,00
Tr (period of the LFMCW frequency regime) (us)	2,50
Rmax (km) (assumed)	0,08
m (slope of the LFMCW frequency regime) (hz <sup>2</sup> )	5,03E+15
Frequency Difference Between Antennas (Hz)	400000,00
delta-t (FDA period) (us)	2,50
PRI(us)	2,50
Null-to-Null interval of the pulses(ms)	0,00063
Duty Cycle of the Pulses (%)	25,00
Instantaneous Bandwidth of the pulses (kHz)	20106,19
Unambiguous Range (km)	0,38
$f_{\max \text{ beat}}$ (MHz)	266,67
Sampling Frequency $\geq$ (MHz)	533,33
M'(number of samples in null-to-null interval) $\geq$	333
M(number of samples in one period) $\geq$	1333
Number of samples in a single pulse	333
Time Resolution(us)	0,28
Range Resolution (m)	0,30
Time step in the processing (us)	0,0002

The number of antennas is taken to be 8 and period of simulation as 2,5us to decrease the simulation time. Besides, the antennas are uniformly fed, so a sinc-type waveform with increased side lobes is to be expected in time domain. Inter-element spacing and delay, frequency span are selected according to already implemented structure. Besides, maximum range is selected by selecting the maximum beat frequency to be around 5 percent of the total frequency span.

The other parameters calculated from the basic variables are readily demonstrated in Table 7.1. Throughout basic simulations, there would be opportunity to check the results against the calculations of Table 7.1.

The first check point is to be made at the LFM CW source, since the dynamics of the waveform is crucial to the operation of the concept. In Figure 7.6, the controlling waveform and the corresponding frequency is shown for just one period of simulation.

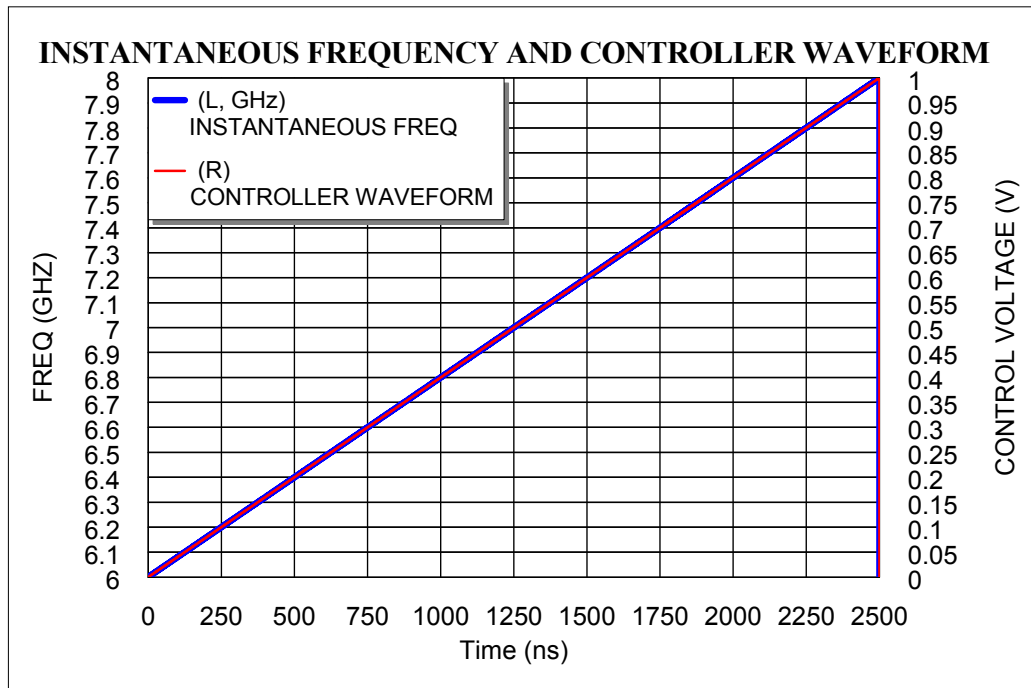
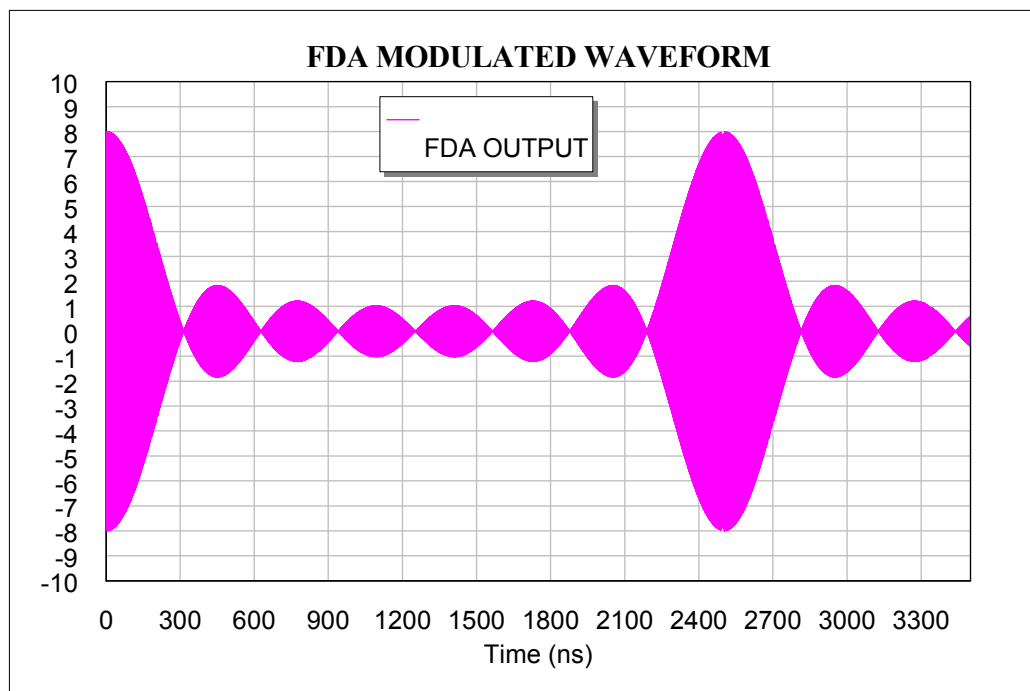


Figure 7.6: Controlling waveform (left) and output frequency (right) as a function of time

The left axis of the graph belongs to the output voltage from the controller and the axis on the right to the instantaneous frequency output from the generator.

Note that the waveform is shown for one period, but in fact the waveform is a saw-tooth waveform. The instantaneous time domain waveform is hard to visualize, so it will not be shown here.

The next waveform should be visualized just at the output of FDA. The carrier at this point is again hard to visualize but the amplitude modulation is clearly visible in the graph shown in Figure 7.7. The null to null period of the simulated waveform is compliant with the analytical findings as expected (0.625 us). The side lobes are 13 dB below the main lobe due to uniform excitation of the antenna elements. Since the measurement is observed just at the output of the antenna array, at the beginning, the waveform does not reach to all antenna elements and the peaks of the waveform are expected to deteriorate at these instants. Besides, since the period of the controller waveform and FDA are same, the second pulse is seen as a full pulse. Also note that the peak voltage is at 8 volts due to the number of antennas.



**Figure 7.7: Time domain waveform at the output of the FDA**

After creation of amplitude modulated waveform at FDA, the waveform is propagated through the target and the return from the target is collected back at the source by an omni-directional antenna. As mentioned before, assume that no loss is associated with the propagation but the delay from the source to target and back to source (for a clear understanding of the concept). The source waveform together with the returned waveform is shown in Figure 7.8. In the simulation it is assumed that the target is at 150m and the associated delay with the target can be calculated to be 1 us as also evidenced in Figure 7.8.

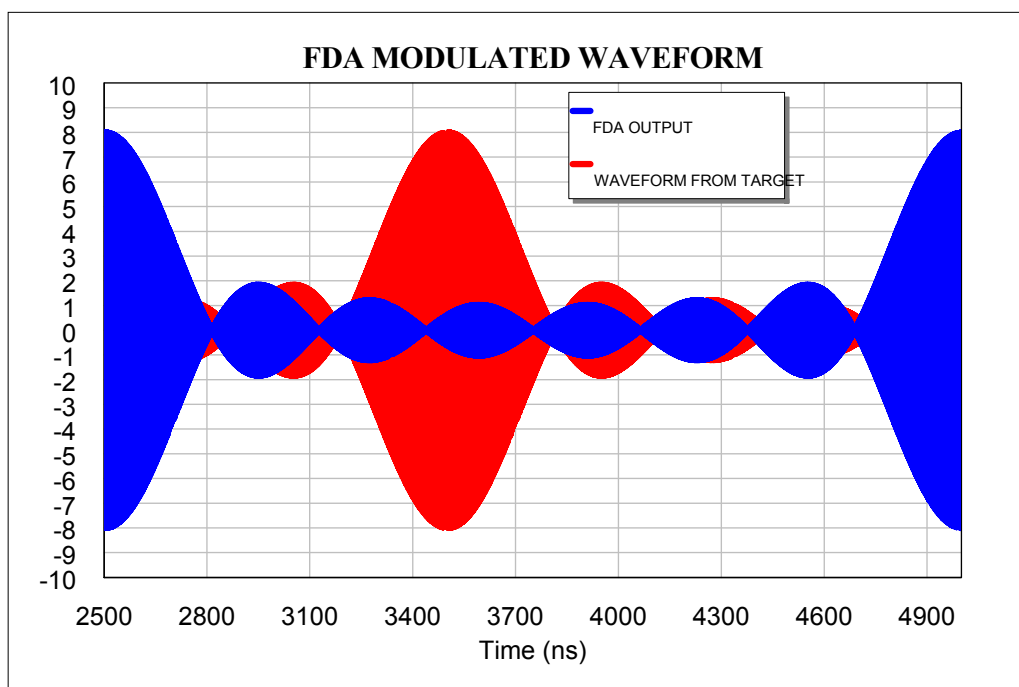


**Figure 7.8: Transmitted and received waveforms, assuming no amplitude change during propagation and return**

After this stage, the original LFMCW and the returned wave are multiplied at mixer and the resulting waveform is low pass filtered. The resulting waveform is the beat signal whose frequency is proportional to the range of the target. In Figure 7.9, the instantaneous frequencies of the source and the returned wave can be viewed for a target at 70m and  $0^\circ$ .

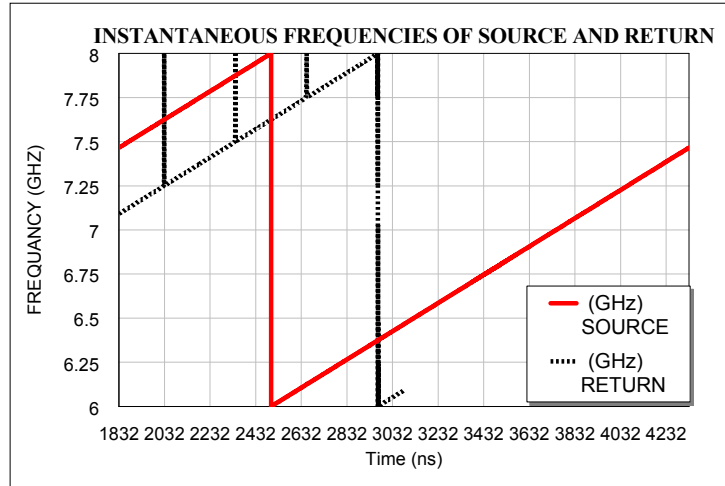


**Figure 7.9: Instantaneous frequency of the source and the returned waveform**

In Figure 7.10 the resulting waveform is shown for a small time interval to visualize the beat frequency.

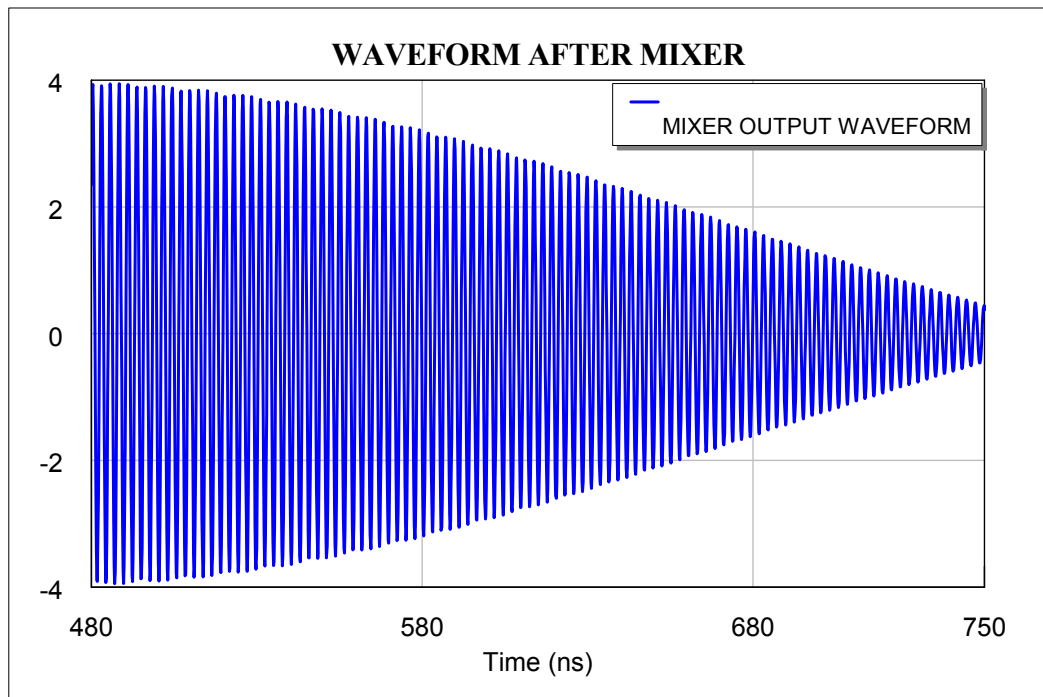


**Figure 7.10: Demonstration of waveform after mixer**

In the last step, the down converted signal is resampled at a rate designated by the maximum range of interest ((5.57)). The resulting waveform will not be shown here since it is the same as the one shown in Figure 7.10.

## **7.4 SIMULATION OF A RADAR**

In this section, a basic simulation of radar with sample targets will be performed using the implemented simulation in the current chapter. For the simulation, a realistic scenario is selected and the resulting returns from various targets will be presented. Also, returns from multiple targets and relevant difficulties in detection will be demonstrated with some analytical derivations. Finally, the performance of the simulated radar will be discussed and various proposals for increasing the performance will be shown.

### **7.4.1 Requirements**

In the realistic scenario first assume that the maximum range of surveillance is 500m and the corresponding range resolution is 0.3m. According to (5.65) an FDA with inter-element delay of 0,5ns would require at most eight antennas for the required resolution. Besides, according to (5.62), the maximum range is such that the sampling frequency of the structure is at nominal values. Bounding to the already designed array, assume that the array is designed to be scanning between 6GHz and 8GHz with a slope dictated by the period of scanning regime (to scan whole space once for each scanning period, the slope is selected to make beam period equal to scanning period).

The time resolution associated with the variable selections can be calculated from (5.70) to be 5,63us. Using (5.80), the minimum angular resolution can be calculated to be 21 degrees (in other directions, the resolution becomes worse), which may be unacceptable in sensitive applications. Nevertheless, design can proceed with these values. In the following chapters, the proposals for improvements will be demonstrated also.

The variables of simulated case and the results of resolution calculations can be viewed in Table 7.2.

**Table 7.2: The variables of structure used for the simulation**

VARIABLES	VALUES
Number of antennas in the system	8
Inter element spacing(mm)	25,00
Inter element delay(ns)	0,50
Starting Frequency(GHz)	6,00
Total Frequency Change(GHz)	2,00
Tr (period of the LFM CW frequency regime) (us)	50,00
Rmax (km) (assumed)	0,50
m (slope of the LFM CW frequency regime) (hz 2)	2,51E+14
Frequency Difference Between Antennas (Hz)	20000,00
delta-t (FDA period) (us)	50,00
PRI(us)	50,00
Null-to-Null interval of the pulses(ms)	0,013
Duty Cycle of the Pulses (%)	25,00
Instantaneous Bandwidth of the pulses (kHz)	1005,31
Unambiguous Range (km)	7,50
fmax_beat (MHz)	133,33
Sampling Frequency >= (MHz)	266,67
M'(number of samples in null-to-null interval)>=	3333
M(number of samples in one period)>=	13333
Number of samples in a single pulse	3333,33
Time Resolution(us)	5,63
Range Resolution (m)	0,30
Time step in the processing (us)	0,0038

Besides, the time-of-arrival and angular resolution results for a target at 300m are demonstrated in Table 7.3 (for  $\varphi = 2p\pi, p = 1$ ).

**Table 7.3: Time of arrival and angular resolution calculations for  $\varphi = 2p\pi, p = 1$**

R(m)	$\theta$ (degrees)	Arrival time(us)	$\Delta\theta$ (degrees)
300	-45	6,166	29
300	-40	5,741	27,9
300	-35	5,275	27
300	-30	4,769	26,3
300	-25	4,224	25,9
300	-20	3,643	25,6
300	-15	3,026	25,5
300	-10	2,378	25,6
300	-5	1,702	26
300	-4	1,563	26,1
300	-3	1,424	26,2

300	-2	1,283	26,3
300	-1	1,142	26,4
300	0	1,000	26,6
300	1	0,857	26,7
300	2	0,713	26,9
300	3	0,569	27
300	4	0,424	27,2
300	5	0,278	27,4
300	10	49,540	20,8
300	15	48,791	21,8
300	20	48,038	23,1
300	25	47,287	24,9
300	30	46,545	27,5
300	35	45,821	31,7
300	40	45,121	41,4
300	45	44,454	na

In Table 7.3, note that minimum resolution is not at the bore-sight but shifted by ten degrees due to beam bending. The minimum resolution is 20 degrees and increases with the angular bearing of the target.

The minimum resolution is also affected by the range of the target. This is because of the dependency of time, range and angular bearing in creating the interference. For example, if the target is at 100m, the minimum resolution is the same but it is at three degrees off broadside.

In the simulations, to decrease the effect of side-lobes, Chebyshev weighting is applied to the antenna elements with 20dB side-lobe. This level of tapering does not create considerable discrepancies from the calculated values.

#### **7.4.2 Sample Target Returns and Multiple Target Cases**

The sample target returns are extracted from MWO and analyzed in MATLAB. In this section returns from several targets are demonstrated. The resulting waveforms are not normalized.

The first target is at 90m and +30° off-broadside. The resulting waveforms and the Fourier Transform of the waveforms are shown in Figure 7.11. The plots in the figure show the magnitude, phase and group delay of Fourier transform, and the time domain waveform for one period. From the plots, the beat frequency is clear by just looking at the magnitude of the transform. The change of

phase and the group delay is also clear at the beat frequency. Note from the last figure that the beam is a wide beam which would have lower time and angular resolution as predicted before.

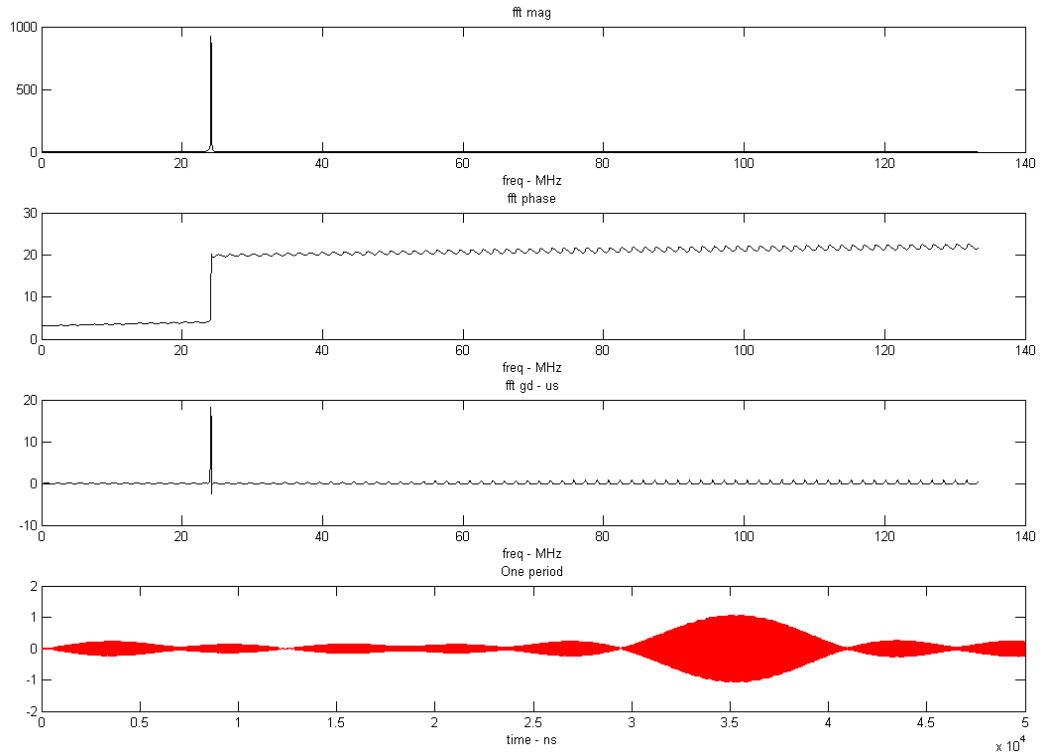


**Figure 7.11: The returning waveform from a target at 90 m and 30 degrees and the Fourier transform of the waveform**

In another simulation the results for a target with same range but at 20 degrees can be viewed. The results are shown in Figure 7.12. Note that the beam is shifted by 5 us.

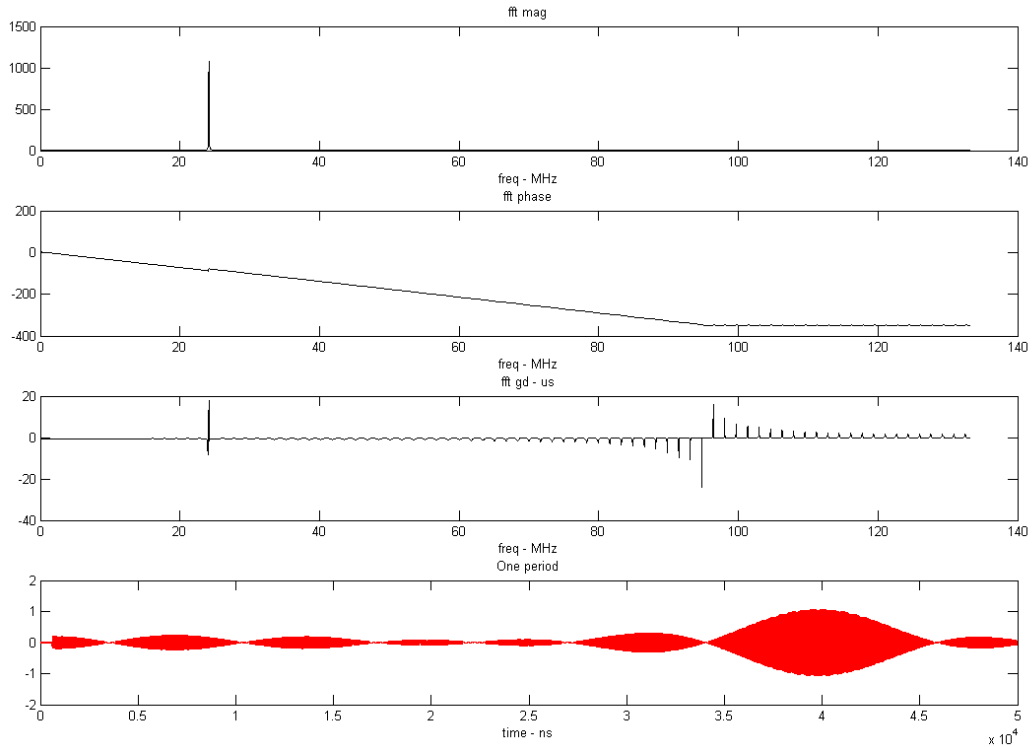


**Figure 7.12: The returning waveform from a target at 90 m and 20 degrees and the Fourier transform of the waveform**

If both targets were present at the same time, the return would be as shown in Figure 7.13. In time domain the returns from the targets interfere but they can be discriminated in time domain. In frequency domain, the beat frequency of the targets would be the same and indistinguishable by just looking at the magnitude of Fourier transform. The phase and group delay properties of the target returns may be helpful but require some analytical derivations. The phase and group delay of the Fourier transform for a single target can be expressed using the phase of the down-converted signal. From (5.56) and the phase terms coming from amplitude modulation terms of (5.54), the phase of the down-converted signal becomes:

$$\phi_{baseband} = \frac{-2\omega_0 R'}{c} + \frac{mR'^2}{c^2} + \frac{N-1}{2} \frac{\omega_0}{c} (d \sin(\theta') - cT) + \frac{mTR' N-1}{c \cdot 2} \quad (7.2)$$

Here

- $N$  : Number of antennas in the array
- $\omega_0$  : The starting frequency of scan
- $m$  : Slope of frequency scanning regime
- $(R', \theta')$  : Position of the target
- $T$  : Inter-element delay
- $d$  : Inter element distance

In equation (7.2), (5.49) can be used to get ( $\omega_b$ , the beat frequency)

$$\phi_{baseband} = \frac{\omega_0 \omega_b}{m} + \frac{\omega_b^2}{4m} + \frac{N-1}{2} \frac{\omega_0}{c} (d \sin(\theta') - cT) - \frac{\omega_b T N-1}{2 \cdot 2} \quad (7.3)$$

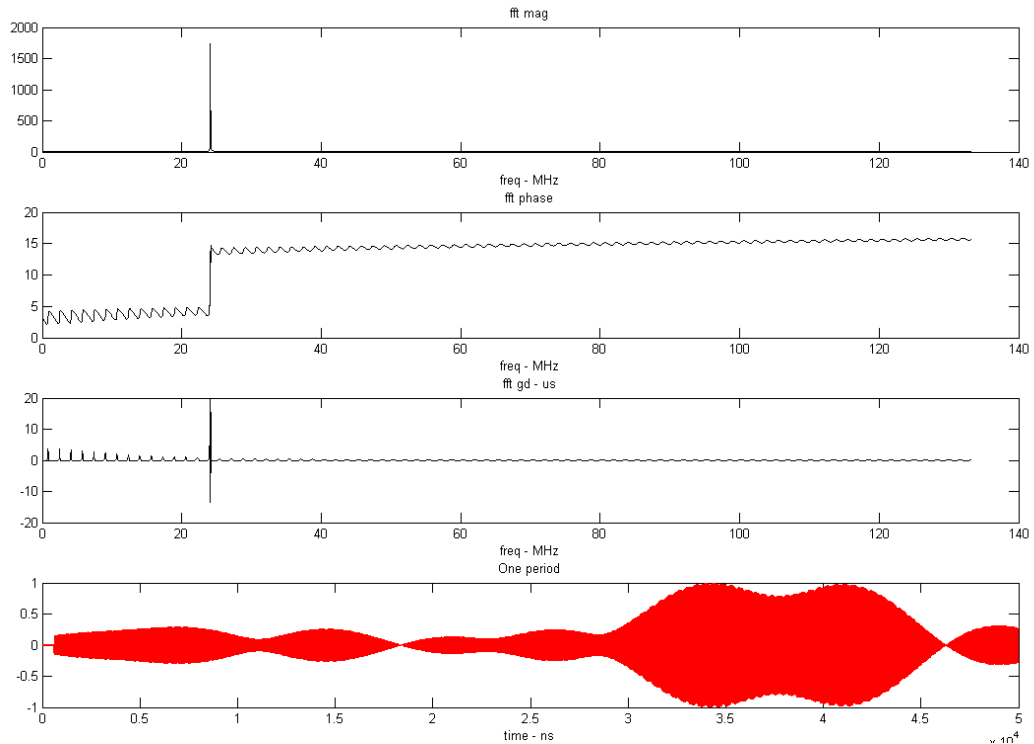


**Figure 7.13 The returning waveform from targets at 90 m and 20 degrees and 30 degrees and the Fourier transform of the waveform**

Here the third term does not depend on the beat frequency but according to this term, the angular position of the target affects the phase of baseband signal. But, this term is much smaller than the effect of the first term in the expression (where this linear term is much more effective than the quadratic term, the increase of phase with beat at target frequencies is clearly visible in the plots) and it is hard to determine the angle of target from the phase of the beat signal.

In another case, the range of the target can be shifted but with the same angle. In Figure 7.14, two targets at 50m and 90m with an angular bearing of  $30^\circ$  is shown. The targets can be easily distinguishable in the first graph, the magnitude of Fourier transform. In time domain, it is hard to distinguish between the targets. Also note from the phase of Fourier transform that at the respective frequencies, the phase of return shows a linear change as evidenced from (7.3) (This effect can also be observed in the following plots also. The angular position of the targets affects the phase but the effect is minimal).

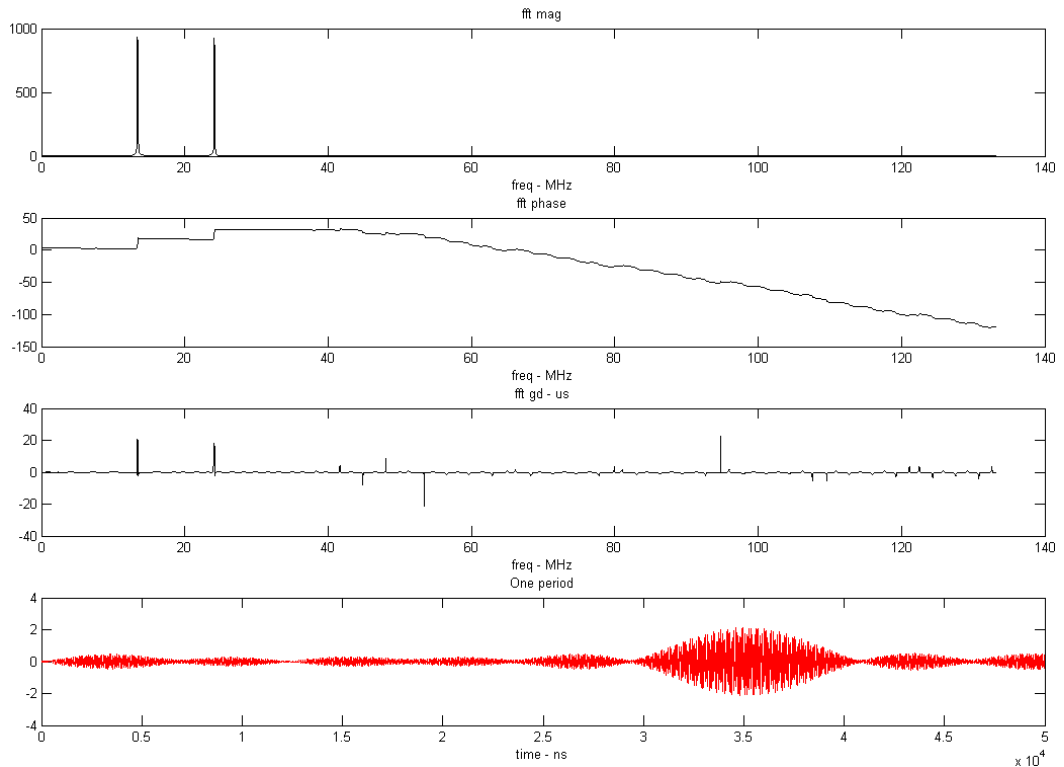


**Figure 7.14: The returning waveform from targets at 90 m and 50m with 30 degrees of angular bearing and the Fourier transform of the waveform**

In another case assume that both the range and the angular bearing of the target are changed. The case is demonstrated in Figure 7.15 for two targets at  $50m, 10^\circ$  and  $80m, 30^\circ$ . The targets are easily distinguishable from the magnitude of Fourier transform. Likewise, the time domain waveform in the fourth plot shows the distinction between the targets. Since the time of arrival and the ranges of targets are distinguishable, the angular positions can be easily detected.

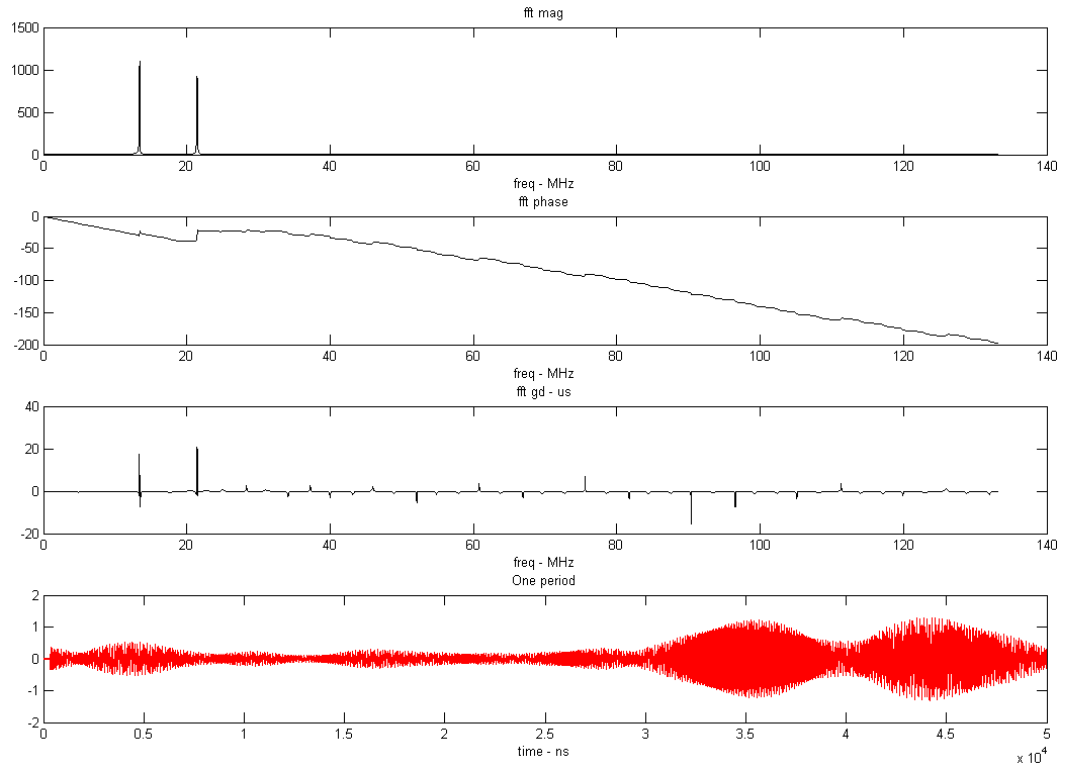


**Figure 7.15: Two targets at  $50m,10^\circ$  and  $80m,30^\circ$**

In a harder case, the angular positions of targets can be made close to each other. The case is demonstrated in Figure 7.16 for two targets at  $50m,10^\circ$  and  $80m,15^\circ$ . Again the distinction between the targets can be easily made looking at the magnitude of the Fourier transform, but the time domain waveforms almost coincide making the distinction between the targets impossible. If the target at 50m is shifted to  $5^\circ$ , the distinction between the targets in time domain would be possible somewhat. This case is demonstrated in Figure 7.17. In this case the targets can be again distinguished using the Fourier transform of the incoming waveform and in time domain the main beam of the returns is widened due to two targets.

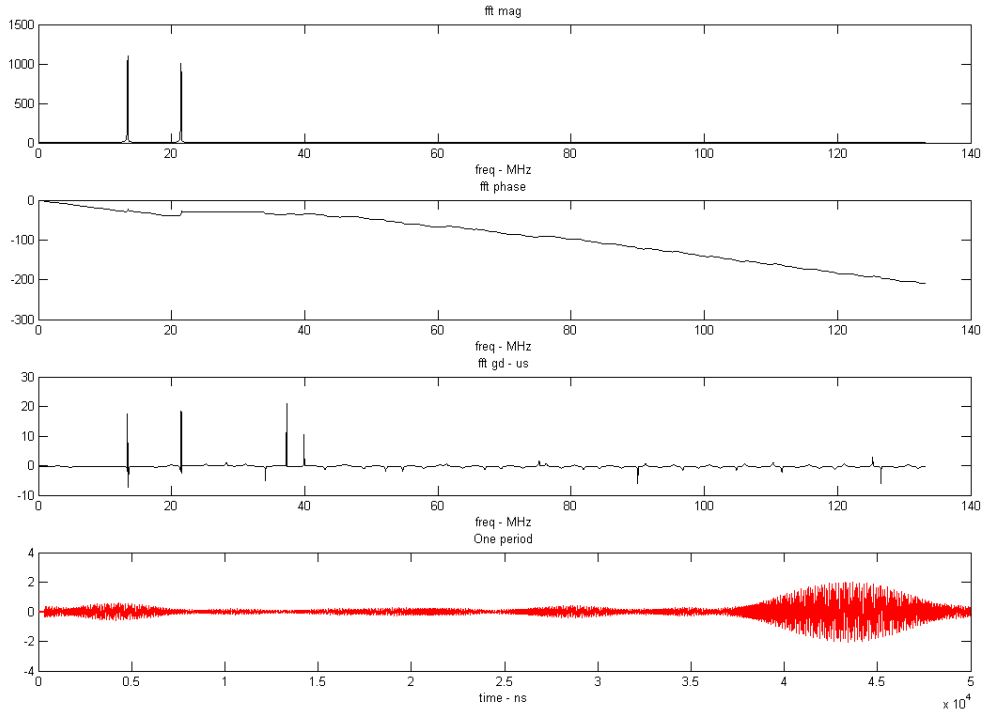


Figure 7.16: Two targets at  $50m, 10^\circ$  and  $80m, 15^\circ$

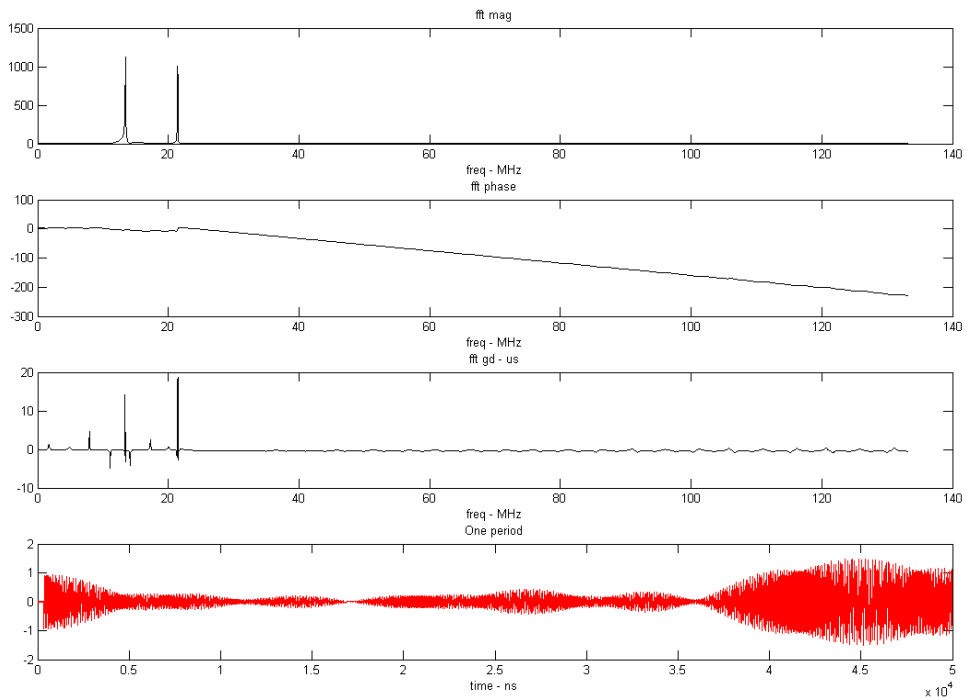


Figure 7.17: Two targets at  $50m, 5^\circ$  and  $80m, 15^\circ$

The simulations can be performed for more targets and more scenarios, but the results would be similar in these cases also. Also the detection process is another area of research and out of scope of this thesis. In the next section the performance of the FDA and proposals for better performance will be discussed.

### **7.4.3 Discussions on the Performance of the Structure – Proposals for Better Performance**

The dilemma between the angle and range resolution is the main problem in FDA radar scenarios. The detection of range relies on the Fourier transform of the incoming waveform while the detection of angular position requires the detection time of the waveform. The number of antennas put a limit on the resolutions but there are ways to increase the resolution by means of the slope of LFMCW source regime.

According to (5.65), the range resolution does not depend on the slope of the waveform. The slope term in (5.70) can increase the resolution in time, also increasing the resolution in angle. Slope change should be achieved by changing the frequency extent of the system, since changing the period of scan would not change the duty cycle of the main beams (in one period of scan), leaving the resolution same. But, increasing the slope of LFMCW frequency regime would require higher sampling rates and lowered unambiguous range (equations 5.57, 5.59, 3.54, 3.58). Nevertheless switching to higher slopes can increase the resolution somewhat at the expense of increased sampling frequency.

Another way of increasing the angular resolution is to add a dummy antenna to the array as shown in Figure 7.18. In this structure a dummy antenna is placed at a distance of  $zd, z \in \mathbb{N}$  and with an extra delay of  $zT, z \in \mathbb{N}$ , (where  $d$  is the inter-element distance and  $T$  is the inter-element delay). After detection of a target in range by Fourier transform, this antenna can be switched momentarily on to create a narrower beam on the target to increase the angular resolution. This interferometer technique can be a powerful solution to the angular resolution problem. A drawback of the technique is the creation of multiple beams in one period (grating lobes), but all returns would be from the targets and the ranges of the targets are already calculated from the Fourier transform.

Increasing the size of FDA antenna is in fact the basic solution to the angular resolution problem but the range resolution would also get worse. So designing an FDA system with switchable sub-matrices can solve the problem. In this case a sub-array of FDA is used to detect the range of the target while the whole array for detection of the angular bearing of the target. The difference of this technique from the before-mentioned dummy antenna technique is the cost of designing whole array and grating lobe free scan period.

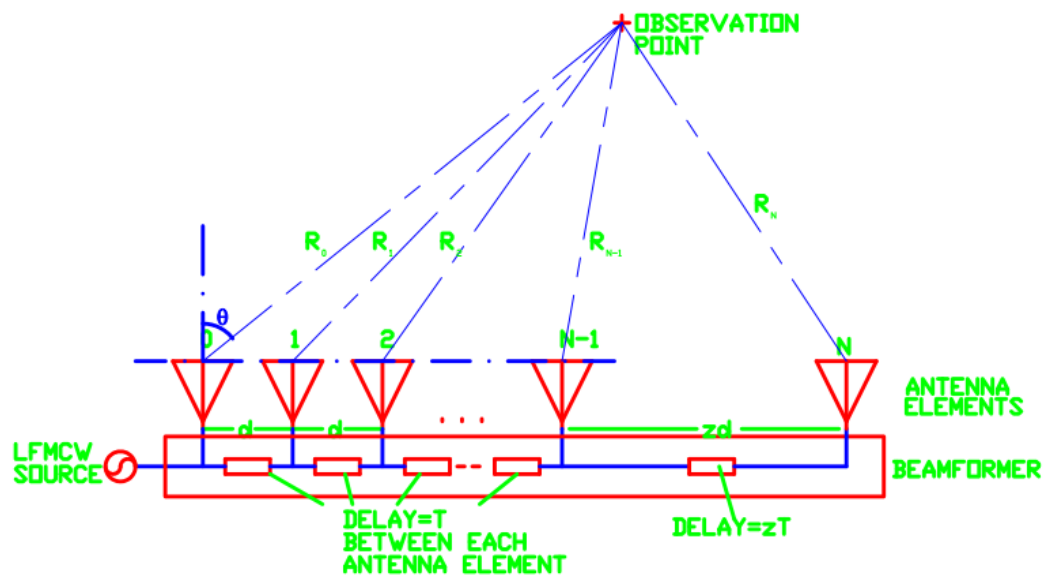


**Figure 7.18: Adding a dummy element to the array and using interferometry principles can help in solving angular resolution problems**

An advanced proposal for solving the problem is to change the linearity of the LFM CW source by control voltage. In this scheme, the point of target in space is illuminated by a group of frequencies and by control of the instantaneous slope of LFM CW waveform at those frequencies, higher resolutions can be achieved (with possible scanning improvements of the array). With the advancements in digital technologies for higher clock rates, adaptive rate change of control voltage can be possible. Detailed analysis of this case is not undertaken throughout this study, but left as a proposal.

Throughout simulations, some side-lobes seem to deteriorate due to sampling rate of the simulator. Increasing the sampling rate of the simulator

prevents the anomalies in the simulation but unfortunately it takes much longer time to calculate the returns in this case. Nevertheless the resulting waveforms were as expected.

## CHAPTER 8

### CONCLUSIONS AND FUTURE STUDIES

LFMCW based FDA technique is a novel concept and presents a new proposal for the implementation of FDA. The virtue of the concept lies in the ease of implementation and low costs compared to the other implementation schemes proposed in literature. The technique takes the advantage of dynamic scanning behavior of LFMCW source and the specialized property of a beam former in which special inter-element delay is utilized. It is this delay causing inter-element frequency steps and continuous steering of the main beam.

The technique is generally confused with the traditional frequency scanning concept where the array antenna is willingly tilted by a change in the working frequency. In LFMCW based FDA, continuous frequency scanning is utilized in the array, so the instantaneous frequency in the array is always changing, and each antenna receives a distinct frequency at any time during scanning as opposed to frequency scanning case.

In this study, various mathematical derivations are performed starting from basic FDA concept through LFMCW based FDA. The LFMCW based FDA derivations are also extended to more applicable radar scenarios. Finally several simulations are performed on the computer to visualize the performance of the array in a radar environment. Besides, implementation of the array is performed. In the implementations, based on a typical system design, several hardware are designed, tested individually and integrated to the larger picture. Utilizing the implementations, various measurements are conducted for comparison of the theory and the real life results. The results were as expected by the derivations.

During research, some applicable cases for the array were determined. Those include short range radars, security systems and even telecommunications.

In all implementations and simulations, the analysis is mainly focused on 6-10GHz bandwidth due to the frequency bandwidth of designed hardware but the design and the analysis can be brought to other frequencies for further research. This can also help in quantifying the practical properties of the array with respect to the main operating frequency range.

The next step in the analysis is the detailed derivations of the array for radar applications. In this thesis, some derivations are performed but the mathematical analysis needs to go further for more general cases. A more complex implementation of the concept should be required for a radar application. The theoretical analysis and the application of the technique would expose the benefits and drawbacks of the array and direct the studies toward advanced concepts about the array.

The dilemma between the angular resolution and the range resolution is another point of research and various proposals about the solution were mentioned in Section 7.4.3. These points (and maybe other new solutions) require detailed mathematical analysis for clarification, and sample implementations may be required for justification of proposed solutions.

Another point to note about the array is the frequency scanning regime of the source. Up to this point in the study, the frequency regime of the source is assumed to be linear. Nonlinear control of the source waveform is another area of research in the study and adds more flexibility to the scanning behavior of the array. Digital techniques are more suitable for the scanning control of source but care should be taken during the design as mentioned in Section 3.3.

During implementations, the inter-element delay is accomplished using TEM transmission lines and high dielectric constant materials. Some other means for delay devices can be adapted to the array. A more advanced case will be adjustable delay lines between antenna elements creating flexible scanning options with the LFMCW source.

The instantaneous diverse waveform property of the LFM CW based FDA is another interesting property of the array. The dynamic scanning feature of the source and the delay between antenna elements would create diversity between the antenna elements. Especially the nonlinear control of the source can be helpful in the diversity as devised in [17], making the array suitable for radar imaging application.

## REFERENCES

- [1] Fourikis, Nicholas., Chang, Kai, eds. "Phased Array-Based Systems and Applications". New York: Wiley, 1997.
- [2] Balanis, Constantine A., "Antenna Theory Analysis and Design". New York: John Wiley and Sons, 1997.
- [3] Skolnik, Merrill I., "Radar Handbook". Boston: McGraw Hill, 1990.
- [4] Brookner, Eli., "Practical Phased Array Antenna Systems". Boston: WINTER/SPRING 2003 Lecture Series Boston IEEE AESS, 2003.
- [5] Stimson, George W. "Introduction to Airborne Radar". Mendham New Jersey: Scitech Publishing Inc., 1998.
- [6] A. J. Parish, "Electronically Steerable Arrays: Current and Future Technology and Applications", Msc. Project Report, Loughborough University of Technology and Royal Airforce College, Cranwell, UK, 1989.
- [7] Barton, David K. "Modern Radar System Analysis", Norwood MA: Artech House Inc., 1988.
- [8] Simon Remo, John R. Whinnery, Theodore Van Duzer, "Field and Waves in Telecommunication Electronics", New York: John Wiley & Sons Inc., 1993.
- [9] W. Ng et al. "Wide-band Fiber-Optic Delay Network for Phased Array Antenna Steering", Electronics Letters, 25, (21), 1456, October 1989.
- [10] D. K. Paul, "Optical Beamforming and Steering for Phased Array Antenna". IEEE Proc. Natl. Telesyst. Conf. 1993.
- [11] R. Benjamin. "Optical Techniques for Generating Multiple Agile Antenna Beams". IEE Colloq. Multiple Beam Antennas Beamformers, 1989, p11/1.

- [12] E. Ackerman, S. Wanuga, and D. Kasemset. "Integrated 6-bit Photonic True Time Delay for Lightweight 3-6GHz Radar Beamformer". IEEE MTT-S Int. Microwave Symp. Digest, p681, 1992.
- [13] D. D. Curtis and R. J. Mailloux, "A Critical Look at the Photonics for Phased Array Systems". IEEE AP-S Int. Symp./ URSI Radio Sci. Meet. Nucl. EMP Meet., 1992 Dig., Vol. 2, p717.
- [14] H. Steyskal, "Digital Beamforming Antennas: An Introduction". Microwave Journal, January, p107, 1987.
- [15] H. Steyskal and J. F. Rose. "Digital Beamforming for Radar Systems". Microwave Journal., January 1989.
- [16] J. F. Rose. "Digital Beamforming Receiver Technology". IEEE AP-S International Symposium., Vol.1, p380., 1990.
- [17] Antonik, P., Wicks, Michael C., Griffiths Hugh D., Baker Cristopher J., "Frequency Diverse Array Radars". Proc. 2006 IEEE Radar Conference, pp. 215-217, Verona NY, April 2006.
- [18] Secmen M., Demir S., Hizal A., and Eker T., "Frequency Diverse Array Antenna with Periodic Time Modulated Pattern in Range and Angle". Proc. IEEE Radar Conference, pp. 427-430, April 2007.
- [19] W. H. Kummer, A. T. Villeneuve, T. S. Fong, F. G. Terrio. "Ultra-Low Sidelobes from Time-Modulated Arrays". IEEE Trans. On Antennas And Propagation, vol. 11, pp.633-639, November 1963.
- [20] P. Baizert, T. B. Hale, M. A. Temple and M. C. Wicks. "Forward Looking Radar GMTI Benefits Using a Linear Frequency Diverse Array". Electronics Letters, Vol. 42, No. 22, October 2006.
- [21] P. Antonik, M. C. Wicks, H. D. Griffiths, C. J. Baker, "Multi-Mission Multi-Mode Waveform Diversity", Proc. 2006 IEEE Radar Conference, pp. 580-582, Verona NY, April 2006.
- [22] Jingjing Huang, Kin-Fai Tong, C. J. Baker, "Frequency Diverse Array with Beam Scanning Feature". Proc. IEEE 2008 Antennas and Propagation Society International Symposium, 5-11 July 2008, pp. 1-4.

- [23] F. Jawad, Temple Michael A., Saville Michael A., "Exploiting Frequency Diverse Array Processing to Improve SAR Image Resolution", IEEE Radar Conference 2008, pp1-5, May 2008.
- [24] P. F. Sammartino, C. Baker, "The Frequency Diverse Bistatic System", Proc. 4<sup>th</sup> Intl. Waveform Diversity & Design Conf., Orlando, FL, 8-13 Feb. 2009.
- [25] T. Higgins and S. Blunt, "Analysis of Range-Angle Coupled Beamforming with Frequency-Diverse Chirps", Proc. 4<sup>th</sup> Intl. Waveform Diversity & Design Conf., Orlando, FL, 8-13 Feb. 2009.
- [26] P. F. Sammartino and C. J. Baker, "Developments in the Frequency Diverse Bistatic Systems", Radar Conference, 2009 IEEE, May 2009.
- [27] Wicks Michael C., "A Brief History of Waveform Diversity", IEEE Radar Conference 2009, pp1-6, May 2009.
- [28] Huang J., Baker C., "Frequency Diverse Array: Simulation and Design", IEEE Radar Conference 2009, pp427-430, May 2009.
- [29] Sammartino P.F., Baker C.J., Griffiths H.D., "Range-Angle Dependent Waveform", IEEE Radar Conference 2010, pp511-515, May 2010.
- [30] Chen Y., Li Y., Wu Y., Chen H., "Research on the Linear Frequency Diverse Array Performance", IEEE ICSP 2010, pp2324-2327, Oct 2010.
- [31] J. Farooq, M.A. Temple, M.A. Saville, "Application of Frequency Diverse Arrays to Synthetic Aperture Radar Imaging", International Conference on Electromagnetics in Advanced Applications 2007, pp447-449, Sept. 2007.
- [32] Zhuang L., Xingzhao L., Wenxian Y., "Precisely Beam Steering for Frequency Diverse Arrays Based on Frequency Offset Selection", International Radar Conference-Surveillance for a Safer World, pp1-4, Oct 2009.
- [33] Wicks Michael C., Antonik P. "Frequency Diverse Array with Independent Modulation of Frequency, Amplitude and Phase", US Patent 7319427, Jan. 2008.

- [34] Kurt S. "Range Resolution Improvement of FMCW Radars", MSc Thesis, The Graduate School of Natural and Applied Sciences of Middle East Technical University, September 2007.
- [35] Pozar, David M., "Microwave Engineering". NY: John Wiley & Sons Inc. 1998.
- [36] Hittite Corporation Official Web Page, <<http://www.hittite.com> >, August 2011.
- [37] Zhang C., Kuhn M., Mahfouz M., Fathy Aly E., "Planar Antipodal Vivaldi Antenna Array Configuration for Low Cross-Polarization and Reduced Mutual Coupling Performance", IEEE Antennas and Propagation Society International Symposium 2007, pp725-728, June 2007.
- [38] Tianming Li, Yuping Rao, Zhongxia Niu. "Analysis and Design of UWB Vivaldi Antenna", IEEE 2007 International Symposium on Microwave, Antenna, Propagation, and EMC Technologies for Wireless Communications, 2007.
- [39] D.A. Burrell, J.T. Aberle, "Characterization of Vivaldi Antennas Utilizing a Microstrip-to-Slotline Transition", IEEE Antennas and Propagation Society International Symposium 1993 Digest, pp1212-1215, July 1993.
- [40] Kim S., Chang K., "Ultra Wideband Exponentially-Tapered Antipodal Vivaldi Antennas", IEEE Antennas and Propagation Society International Symposium 2004, pp2273-2276, Vol3, 2004.
- [41] Ehud Gazit, "Improved Design of the Vivaldi Antenna", IEE Proceedings, Vol. 135, Pt. H, No. 2, April 1988.
- [42] Wang S., Chen X. D., Parini C. G., "Analysis of Ultra Wideband Antipodal Vivaldi Antenna Design", Loughborough Antennas and Propagation Conference, April 2007.
- [43] Hood A. Z., Karacolak T., Topsakal E., "A Small Antipodal Vivaldi Antenna for Ultra Wide Band Applications", IEEE Antenna and Wireless Propagation Letters 2008, pp. 656-660.

- [44] Maas, Stephen A. "The RF and Microwave Circuit Design Cookbook", Boston: Artech House, 1998.
- [45] Maas, Stephen A., "Nonlinear Microwave and RF Circuits", Boston: Artech House, 2003.
- [46] Kraus J. D., Marhefka R. J., "Antennas for All Applications", Boston: McGraw Hill, 2002.
- [47] Wojtkiewicz A., Misiurewicz J., Nalecz M., Jedrzejewski K., Kulpa K., "Two-dimensional Signal Processing in FMCW Radars", Instytut Podstaw Elektroniki, Polytechnika Warszawska, Warszawa.
- [48] Meta, Adriano. "Signal Processing of FMCW Synthetic Aperture Radar Data", Dissertation at Delft University of Technology, 2006.
- [49] Barrick, Donald E. "FM/CW Radar Signals and Digital Processing", Technical Report, U.S. Department of Commerce, National Oceanic and Atmospheric Administration, Environmental Research Laboratories, July 1973.
- [50] Advanced Wave Research (AWR) Official Web Page, <<http://web.awrcorp.com>>, August 2011
- [51] Bao J., Tsui yen., "Microwave Receivers and Related Components", Air Force Avionics Labs. Wright Patterson AFB, Ohio, 1983.

## APPENDIX A – SPECIFICATIONS OF HARWARE

In this part, the specifications of various devices utilized in the implementations will be summarized. The data shown are mostly gathered from the official datasheets of the devices and the name of the manufacturer can be referred as the reference of the data presented.

### A.1 TGA2513

TGA2513 is used for general amplification of the signals in the rf line-up. The basic specifications for the amplifier and a photograph of it are shown in Table A.1 and Figure A.1. The amplifier is in chip form and packaged for use.

**Table A.1: Specifications for TGA2513**

Manufacturer	Triquint Semiconductor
Frequency Range	2-23GHz
Nominal Gain	17dB
Nominal Output P1	16 dBm
OIP3	>25dBm for f<18GHz
Noise Figure	< 2dB Mid-band noise figure
Power Supply Specifications	Vdd = 5V, Id = 75mA

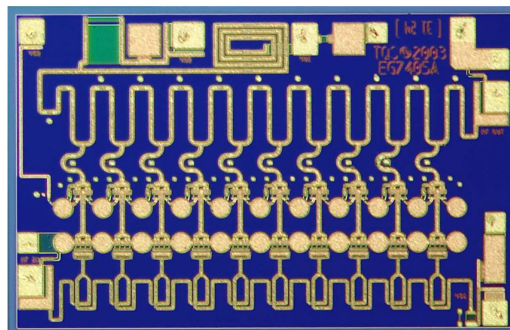


**Figure A.1: TGA2513 chip photograph**

## A.2 NARDA 3326B-2 POWER DIVIDER

This power divider is used for the initial tests of the LFMCW based FDA concept. It simulates the power combination effect in space at  $0^\circ$  bearing. The specifications of the divider are shown in Table A.2. Also shown in figure is a photograph of the divider. The connections of the divider are made with SMA connectors to the outside world. Note that the divider is wide bandwidth device and we use only a small portion of the bandwidth resulting in much better specifications.

**Table A.2: Specifications of NARDA 3326B-2**

Manufacturer	NARDA
Frequency Range	6-18GHz
VSWR,IN MAX	1.6
VSWR,OUT MAX	1.5
Insertion Loss	1dB max
Minimum Isolation	16dB
Amplitude Balance (max)	0.3dB
Phase Balance (max)	3.6 degrees

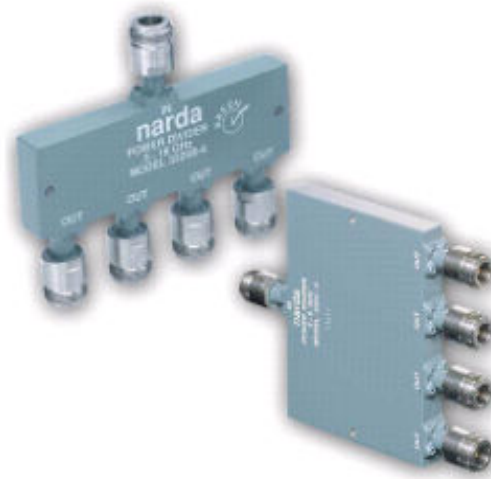


**Figure A.2 Photograph of the NARDA divider (33 series)**

### **A.3 DETECTOR NARDA-4506**

The detector is an important part in the measurements since it is the last element in the rf-line up and detects the instantaneous power of the incoming waveform. Simply it is used as the detector of the receiving section. The specifications of the detector are shown in Table A.3.

**Table A.3: Specifications of the detector**

Manufacturer	NARDA
Model Number	4506
Frequency Range	0.01-18GHz
VSWR,IN MAX	1.5
Sensitivity	0.5mV/mW
Flatness	+/-0.5dB
Output Capacitance	30pF

### **A.4 HMC587LC4B, VCO**

This is another important part of the implementations. VCO creates the required LFMCW waveform at the output by a control waveform from a waveform generator. The specifications for the VCO are shown in Table A.4. Besides, a sketch of the VCO is shown in fig, where the pin functions are visible from the mentioned figure.

**Table A.4: Specifications for HMC487LC4B**

Manufacturer	HITTITE
Frequency Range	5-10GHz
Output Power Range	0-5dBm
Tuning voltage range	0-18V
Output Return Loss	7 dB
2 <sup>nd</sup> Harmonic	-15dBc
Pulling in to VSWR=2	4MHz pp
Pushing at $V_{tune}=+5V$	15MHz/V
Frequency Drift Rate	0.8MHz/°C

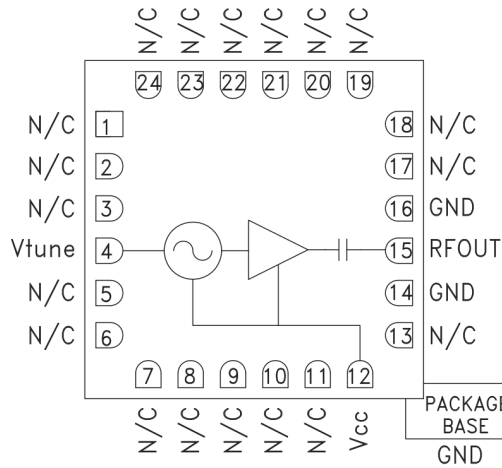


**Figure A.3: Pin functions of HMC487LC4B**

## A.6 RO6010 SUBSTRATE MATERIAL

RO6010 is extensively used as the substrate material due to the high dielectric constant (For easy adjustment of inter-element delay, high dielectric constant material is an appropriate solution). The beamformer and antenna elements are built on this substrate for integration. The electrical specifications for the substrate are shown in Table A.5. More information about the substrate can be found at the web page of the manufacturer.

**Table A.5: Some electrical properties of RO6010**

Manufacturer	ROGERS CORPORATION
Dielectric Constant	10.2 +/- 0.25
Dissipation Factor, $\tan \delta$	0.0023
Thermal coefficient of $\epsilon_r$	-425 ppm/ $^{\circ}C$

## **A.7 ALUMINA (AL<sub>2</sub>O<sub>3</sub>) SUBSTRATE**

Alumina is the most common substrate material utilized in microwave industry. Its high dielectric constant and low dissipative properties make it an excellent candidate for microwave circuitry [51]. The electrical and thermal properties of this material are shown in Table A.6[51]. Thin film manufacturers (ATC, ATP etc.) utilize this substrate extensively.

**Table A.6: Properties of alumina**

Dielectric Constant	10 +/- 0.25
Dissipation Factor, $\tan \delta$	0.0002
Thermal conductivity	0.3 (W/cm $^{\circ}C$ )

## **A.8 MINIBEND CABLES**

Minibend cables are produced by Astrolab Inc. and solve the RF interconnection requirements in a practical manner. It has various lengths and various rf interfaces. In the studies, SMA format is utilized. Some of the specifications of a 4" cable are shown in Table A.7. Another point to note about these cables is that they are very repeatable in terms of the insertion loss and phase.

**Table A.7: Specifications of a 4" minibend cable**

Manufacturer	Astrolab Inc.
12.4GHz VSWR	1.25
12.4GHz IL	0.48dB
2GHz VSWR	1.20
2GHz IL	0.23dB

## **A.9 RG316 SINGLE BRAID SHIELD COAXIAL CABLE**

RG316 is used for interconnection between the beam former and the antenna array. It is also used for tuning the delay distortions. This cable is an industry standard and manufactured by various suppliers. The specifications of the cable can be viewed in Table A.8.

**Table A.8: RG316 Specifications**

Inner Conductor Diameter	0.53mm, Silver plated annealed copper wire
Outer Conductor Diameter	1.53 mm, Silver plated annealed copper wire
Nom. Impedance	50 Ohms
Nom. Capacitance	95.8 pF/m
VSWR (0-6GHz)	Max 1.3
Attenuation (dB/100m)	6GHz →263, 8GHz →319, 10GHz →480

## APPENDIX B - SIN(X)/X TABLE

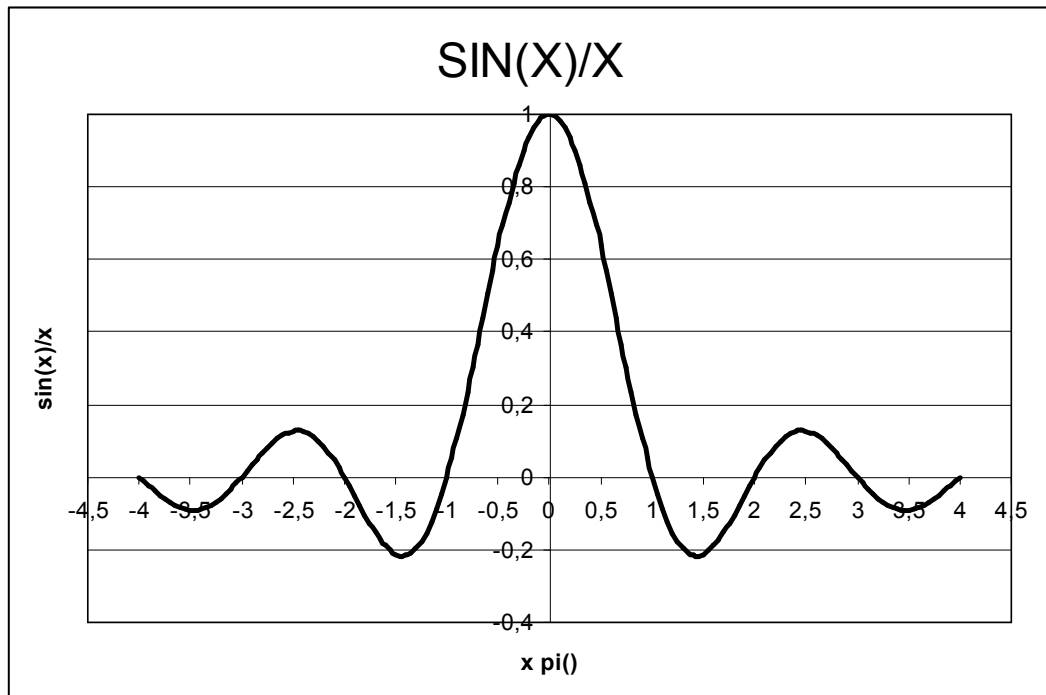


Figure B.1: SIN(X)/X plot

**Table B.1: SIN(X) / X values**

x	sin(x)/x	x	sin(x)/x	x	sin(x)/x	x	sin(x)/x
-12,57	0,00	-6,13	-0,03	0,31	0,98	6,75	0,07
-12,41	-0,01	-5,97	-0,05	0,47	0,96	6,91	0,09
-12,25	-0,03	-5,81	-0,08	0,63	0,94	7,07	0,10
-12,10	-0,04	-5,65	-0,10	0,79	0,90	7,23	0,11
-11,94	-0,05	-5,50	-0,13	0,94	0,86	7,38	0,12
-11,78	-0,06	-5,34	-0,15	1,10	0,81	7,54	0,13
-11,62	-0,07	-5,18	-0,17	1,26	0,76	7,70	0,13
-11,47	-0,08	-5,03	-0,19	1,41	0,70	7,85	0,13
-11,31	-0,08	-4,87	-0,20	1,57	0,64	8,01	0,12
-11,15	-0,09	-4,71	-0,21	1,73	0,57	8,17	0,12
-11,00	-0,09	-4,56	-0,22	1,88	0,50	8,33	0,11
-10,84	-0,09	-4,40	-0,22	2,04	0,44	8,48	0,10
-10,68	-0,09	-4,24	-0,21	2,20	0,37	8,64	0,08
-10,52	-0,08	-4,08	-0,20	2,36	0,30	8,80	0,07
-10,37	-0,08	-3,93	-0,18	2,51	0,23	8,95	0,05
-10,21	-0,07	-3,77	-0,16	2,67	0,17	9,11	0,03
-10,05	-0,06	-3,61	-0,13	2,83	0,11	9,27	0,02
-9,90	-0,05	-3,46	-0,09	2,98	0,05	9,42	0,00
-9,74	-0,03	-3,30	-0,05	3,14	0,00	9,58	-0,02
-9,58	-0,02	-3,14	0,00	3,30	-0,05	9,74	-0,03
-9,42	0,00	-2,98	0,05	3,46	-0,09	9,90	-0,05
-9,27	0,02	-2,83	0,11	3,61	-0,13	10,05	-0,06
-9,11	0,03	-2,67	0,17	3,77	-0,16	10,21	-0,07
-8,95	0,05	-2,51	0,23	3,93	-0,18	10,37	-0,08
-8,80	0,07	-2,36	0,30	4,08	-0,20	10,52	-0,08
-8,64	0,08	-2,20	0,37	4,24	-0,21	10,68	-0,09
-8,48	0,10	-2,04	0,44	4,40	-0,22	10,84	-0,09
-8,33	0,11	-1,88	0,50	4,56	-0,22	11,00	-0,09
-8,17	0,12	-1,73	0,57	4,71	-0,21	11,15	-0,09
-8,01	0,12	-1,57	0,64	4,87	-0,20	11,31	-0,08
-7,85	0,13	-1,41	0,70	5,03	-0,19	11,47	-0,08
-7,70	0,13	-1,26	0,76	5,18	-0,17	11,62	-0,07
-7,54	0,13	-1,10	0,81	5,34	-0,15	11,78	-0,06
-7,38	0,12	-0,94	0,86	5,50	-0,13	11,94	-0,05
-7,23	0,11	-0,79	0,90	5,65	-0,10	12,10	-0,04
-7,07	0,10	-0,63	0,94	5,81	-0,08	12,25	-0,03
-6,91	0,09	-0,47	0,96	5,97	-0,05	12,41	-0,01
-6,75	0,07	-0,31	0,98	6,13	-0,03	12,57	0,00
-6,60	0,05	-0,16	1,00	6,28	0,00		
-6,44	0,02	0,00	1,00	6,44	0,02		
-6,28	0,00	0,16	1,00	6,60	0,05		

# CURRICULUM VITAE

## PERSONAL INFORMATION

Surname, Name: EKER, Taylan

Nationality: Turkish (TC)

Date and Place of Birth: 03.08.1980, İZMİR

Marital Status: Single

Phone: +905073634239

## EDUCATION

Degree	Institution	Year of Graduation
MS	Bilkent Univ. Electrical and Electronics Engineering	2005
BS	Bilkent Univ. Electrical and Electronics Engineering	2002
High School	Şehit Temel Cingöz High School	1998

## WORK EXPERIENCE

Year	Place	Enrollment
2000 (summer)	ASELSAN A.Ş.	Intern Engineering Student
2001 (summer)	ELİMKO A.Ş.	Intern Engineering Student
2002 - present	ASELSAN A.Ş.	Design Engineer

## FOREIGN LANGUAGES

Advanced English, Intermediate German, Basic Japanese

## PUBLICATIONS

- [1] Akram R., EKER T., Bozbey A., Fardmanesh M., Schubert J., Banzet M., "Study of Correlation between the flux to voltage transfer function signal of

rf-SQUID and the rf pumping frequency and power", Ulusal Yüksek Sıcaklık Superiletkenler Sempozyumu, 20-22 June 2005.

- [2] EKER T., Inal M. E., Demir Ş., "Xband 20 Yollu, Es Fazlı, Genlik Dağılımlı, Kayıpsız Güç Bölücüsünün Mikroserit Teknolojisi ile Tasarımı", URSI Ulusal Konferansı 2006 Hacettepe ANKARA, Türkiye
- [3] Akram R., EKER T., Bozbey A., Fardmanesh M., Schubert J., Banzet M., "Effect of rf-bias frequency, rf-pumped power and fabrication process on the rf-SQUID signal characteristics", Applied Superconductivity Conference, Seattle WA- USA, Sep 2006.
- [4] Akram R., EKER T., Bozbey A., Fardmanesh M., Schubert J., Banzet M., "Effect of rf pumping frequency and rf input power on the flux to voltage transfer function of rf-SQUIDs", IEEE Trans. Appl. Supercond. Vol. 17, pp 676-679.
- [5] Secmen M., Demir Ş., Hızal A., Eker T., "Frequency Diverse Array Antenna with Periodic Time Modulated Pattern in Range and Angle", IEEE Radar Conference 2007.
- [6] Eker T., Demir Ş., Hızal A., "Exploitation of Linear Frequency Modulated Waveform (LFMCW) for Frequency Diverse Arrays", submitted to IEEE Trans. On Antennas & Propagation.
- [7] Eker, T., Demir, S., Hızal A., "Design and Implementation of Frequency Diverse Array (FDA) using Linear Frequency Modulated Continuous Waveform (LFMCW)", ISMOT 2009, India, Dec. 2009.

## **SPECIAL INTERESTS**

Electronic Warfare Receiver Design, Phased Array Design, Microwave Components.